Molecular Characterisation of PDIp: the pancreas-specific isoform of PDI

Kelly L. Walker

A thesis submitted in partial fulfilment

of the requirements for the degree of

Doctor of Philosophy

School of Life Sciences

The University of Warwick

July 2013

THE UNIVERSITY OF
WARWICK

Library Declaration and Deposit Agreement

1. STUDENT DETAILS

Please complete the following:

Full name: Kelly Lucas Walker

University ID number: 0630232

2. THESIS DEPOSIT

2.1 I understand that under my registration at the University, I am required to deposit my thesis with the University in BOTH hard copy and in digital format. The digital version should normally be saved as a single pdf file.

2.2 The hard copy will be housed in the University Library. The digital version will be deposited in the University's Institutional Repository (WRAP). Unless otherwise indicated (see 2.3 below) this will be made openly accessible on the Internet and will be supplied to the British Library to be made available online via its Electronic Theses Online Service (EThOS) service.
[At present, theses submitted for a Master's degree by Research (MA, MSc, LLM, MS or MMedSci) are not being deposited in WRAP and not being made available via EthOS. This may change in future.]

2.3 In exceptional circumstances, the Chair of the Board of Graduate Studies may grant permission for an embargo to be placed on public access to the hard copy thesis for a limited period. It is also possible to apply separately for an embargo on the digital version. (Further information is available in the *Guide to Examinations for Higher Degrees by Research.*)

2.4 *If you are depositing a thesis for a Master's degree by Research, please complete section (a) below. For all other research degrees, please complete both sections (a) and (b) below:*

(a) Hard Copy

I hereby deposit a hard copy of my thesis in the University Library to be made publicly available to readers (please delete as appropriate) EITHER immediately ~~OR after an embargo period of ..... months/years as agreed by the Chair of the Board of Graduate Studies~~.

I agree that my thesis may be photocopied. (YES) / NO (*Please delete as appropriate*)

(b) Digital Copy

I hereby deposit a digital copy of my thesis to be held in WRAP and made available via EThOS.

Please choose one of the following options:

~~EITHER My thesis can be made publicly available online. YES / NO (Please delete as appropriate).~~

OR My thesis can be made publicly available only after.....[date] 1/11/2015 (Please give date)
YES / NO (*Please delete as appropriate*)

~~OR My full thesis cannot be made publicly available online but I am submitting a separately identified additional, abridged version that can be made available online.~~
~~YES / NO (Please delete as appropriate)~~

~~OR My thesis cannot be made publicly available online. YES / NO (Please delete as appropriate)~~

3. **GRANTING OF NON-EXCLUSIVE RIGHTS**

Whether I deposit my Work personally or through an assistant or other agent, I agree to the following:

Rights granted to the University of Warwick and the British Library and the user of the thesis through this agreement are non-exclusive. I retain all rights in the thesis in its present version or future versions. I agree that the institutional repository administrators and the British Library or their agents may, without changing content, digitise and migrate the thesis to any medium or format for the purpose of future preservation and accessibility.

4. **DECLARATIONS**

(a) I DECLARE THAT:

- I am the author and owner of the copyright in the thesis and/or I have the authority of the authors and owners of the copyright in the thesis to make this agreement. Reproduction of any part of this thesis for teaching or in academic or other forms of publication is subject to the normal limitations on the use of copyrighted materials and to the proper and full acknowledgement of its source.
- The digital version of the thesis I am supplying is the same version as the final, hard-bound copy submitted in completion of my degree, once any minor corrections have been completed.
- I have exercised reasonable care to ensure that the thesis is original, and does not to the best of my knowledge break any UK law or other Intellectual Property Right, or contain any confidential material.
- I understand that, through the medium of the Internet, files will be available to automated agents, and may be searched and copied by, for example, text mining and plagiarism detection software.

(b) IF I HAVE AGREED (in Section 2 above) TO MAKE MY THESIS PUBLICLY AVAILABLE DIGITALLY, I ALSO DECLARE THAT:

- I grant the University of Warwick and the British Library a licence to make available on the Internet the thesis in digitised format through the Institutional Repository and through the British Library via the EThOS service.
- If my thesis does include any substantial subsidiary material owned by third-party copyright holders, I have sought and obtained permission to include it in any version of my thesis available in digital format and that this permission encompasses the rights that I have granted to the University of Warwick and to the British Library.

5. **LEGAL INFRINGEMENTS**

I understand that neither the University of Warwick nor the British Library have any obligation to take legal action on behalf of myself, or other rights holders, in the event of infringement of intellectual property rights, breach of contract or of any other right, in the thesis.

Please sign this agreement and return it to the Graduate School Office when you submit your thesis.

Student's signature: K Wauer Date: 18-10-13

Contents

List of Figures

List of Tables

For my dad and Fen

Acknowledgements

Foremost, I would like to express my sincere gratitude to Professor Robert Freedman for his continuous support and generosity. His guidance has enabled me to reach and surpass my potential. It is impossible to imagine a better advisor and mentor.

Special thanks must go to Dr. Katrine Wallis who has been a never-ending source of advice and has been pivotal to my scientific and personal development. In addition I must thank past and present members of the Structural Biology laboratory for making the last four years so enjoyable.

Further thanks go to Professor Lloyd Ruddock (University of Oulu) and his group for being so accommodating and making me feel welcome during my research trip. Also to our collaborators from the University of Kent who have provided invaluable advice over the years.

I am grateful to the Medical Research Council (MRC) for funding this work and also providing financial support for my research trip to the University of Oulu.

I must also thank my partner Jason, who has stood by me through thick and thin. His unconditional love has given me the confidence to believe in myself.

Finally, I would like to thank my dad and step-mother Fenella who are probably my biggest fans. They have been an endless source of support, guidance and inspiration. I am lucky to have such amazing people so close to me.

Declaration

I hereby declare that the research submitted in this thesis is my own and was performed under the supervision of Professor R. B. Freedman at the School of Life Sciences, University of Warwick.

No part of this work has previously been submitted to be considered for a degree or other qualification. All sources of information have been specifically acknowledged in the form of references.

Abstract

PDIp is a close homolog of the well known protein folding catalyst PDI. Unlike PDI however, PDIp exhibits restricted protein expression and is found predominantly in the exocrine pancreas. Currently, the physiological function of PDIp is unknown but previous work has shown a clear specificity for substrates containing a hydroxyaryl group. Again this is in contrast to PDI which exhibits more general specificity. This work to investigate the *in vitro* activities of PDIp, was stimulated by the hypothesis that PDIp has an essential role in folding a specific subset of secretory proteins. The identity of these proteins is currently unknown.

In this work, the redox-mediated conformational changes of PDIp have been studied and compared using far UV CD, dynamic light scattering and limited proteolysis. Compared to PDI, these changes are conservative in PDIp. Also, unlike PDI for which **b'xa'c** is the minimal redox-active cassette, the PDIp **a** and **b** domains seem to be involved in modulating these conformational changes. This may indicate that PDIp has a unique substrate binding mechanism that may work synergistically with its restricted substrate specificity.

Using the insulin reduction assay, PDIp was shown to have ~50% of the oxido-reductase activity of PDI and this was not due to the aberrant threonine residue in the **a'** domain active site motif (CTHC). Further investigation by stopped flow kinetic studies showed that the low activity could be due to the abnormally high pK_a for the PDIp **a** domain N-terminal catalytic cysteine. This result was unexpected because PDI and PDIp **a** share the same catalytic active site motif (CGHC) indicating that nearby residues may act as mediators of activity. Future work to clarify this will be essential.

This is the first study of the structure of PDIp and its molecular basis for activity. Through investigation of these two areas, it is hoped that the general understanding of the role of PDIp and its contribution to oxidative folding in secretory tissues will be improved.

Abbreviations

ANS	8-anilinonaphthalene-1-sulphonate
BPTI	bovine pancreatic trypsin inhibitor
CD	circular dichroism
CV	column volume
E. coli	*Escherichia coli*
EDTA	ethylenediaminetetraacetic acid
ER	endoplasmic reticulum
Ero1	endoplasmic reticulum oxidoreductin 1
ESI	electrospray ionisation
DLS	Dynamic light scattering
DNTB	5,5'-dithiobis-(2-nitrobenzoic acid)
DTT	dithiothreitol
FAD	Flavin Adenine Dinucleotide
GAPDH	glyceraldehyde-3-phosphate dehydrogenase
Gpx	Glutathione peroxidase
GSH	glutathione
GSSG	glutathione disulphide
UGGT	UDP-glucose: glycoprotein glucosyltransferase
His-tag	hexa-histidine tag
HSQC	heteronuclear single quantum coherence
IEC	ion exchange chromotography
IMAC	immobilised metal affinity chromatography
IPTG	isopropyl-β-D-thiogalactopyranoside
LB	Luria-Bertani
LMW	low molecular weight
MWCO	molecular weight cut-off
MRE	mean residue ellipticity
MS	mass spectrometry
OD	optical density
ORF	open reading frame
PAGE	polyacrylamide gel electrophoresis
PCR	polymerase chain reaction
PDB	protein data bank
PDI	protein disulphide isomerase
PMSF	phenylmethanesulphonylfluoride
Prx	peroxiredoxin
RFU	relative fluorescence unit
SDS	sodium dodecyl sulphate
SEC	size exclusion chromatography
TOF	time of flight
UPR	unfolded protein response

Amino Acids:

Alanine	Ala, A
Arginine	Arg, R
Asparagine	Asn, N
Aspartic acid	Asp, D
Cysteine	Cys, C
Glutamic acid	Glu, E
Glutamine	Gln, Q
Glycine	Gly, G
Histidine	His, H
Isoleucine	Ile, I
Leucine	Leu, L
Lysine	Lys, K
Methionine	Met, M
Phenylalanine	Phe, F
Proline	Pro, P
Serine	Ser, S
Threonine	Thr, T
Tryptophan	Trp, W
Tyrosine	Tyr, Y
Valine	Val, V

Chapter 1. Introduction

This chapter introduces the area of protein folding with particular emphasis on the roles taken by members of the protein disulphide isomerase (PDI) family. These proteins are catalysts of protein folding and typically exhibit oxido-reductase and isomerase activity. PDI, the archetypal family member, is very well characterised and a high resolution X-ray crystal structure of the human protein has recently been published (Wang *et al.* 2012). This chapter describes in detail the catalytic activities and redox-mediated conformational changes associated with the physiological role of PDI.

In addition to PDI, the pancreas-specific PDI family member, PDIp is also discussed. Unlike PDI, there is very little data for PDIp in terms of structure and activity but it is known to have restricted substrate binding specificity. In this chapter, the current understanding of PDIp is reviewed. This includes its cellular and physiological location, potential activity and also probable role in disease pathogenesis.

Finally the aims of this study will be specified, indicating any possible implications for the structure, activity or physiological role of PDIp.

1.1. Protein Folding and the role of molecular chaperones in the cell

1.1.1. Protein folding in the Endoplasmic reticulum

1.1.1.1. Oxidative protein folding

Oxidative protein folding occurs in the endoplasmic reticulum (ER) of eukaryotic cells and is a fundamental cellular process essential for the function of approximately one third of all eukaryotic proteins (Chen *et al.* 2005). Although occurring predominantly in the ER, some folding can take place co-translationally and begins when the nascent chain emerges from the ribosome and starts to translocate across the ER membrane (for review see Kolb, 2001). It is not until translocation and entry into the oxidising environment of the ER that the newly synthesised protein can become post-translationally modified; examples of which are N and O glycosylation and disulphide bond formation. Furthermore, before proteins leave the ER, it is crucial that they are correctly folded. It is the role of molecular chaperones and also the unfolded protein response (UPR) to regulate this (see figure 1.1).

Protein folding is highly complex and can be illustrated by Levinthal's paradox which states that there is a huge number of possible conformations for any given polypeptide chain (Levinthal, 1968). For example, a 100 amino acid polypeptide can have up to 3^{198} different conformations. The 'paradox' is that most proteins reach their native state much quicker than would be expected if each possible conformation was sampled. Therefore protein folding must be guided by rapid formation of local interactions which subsequently allow further folding of the polypeptide to occur. This mechanism of protein folding (by way of partially folded intermediates) has been clearly defined for bovine pancreatic trypsin inhibitor (BPTI) (Creighton *et al.* 1995).

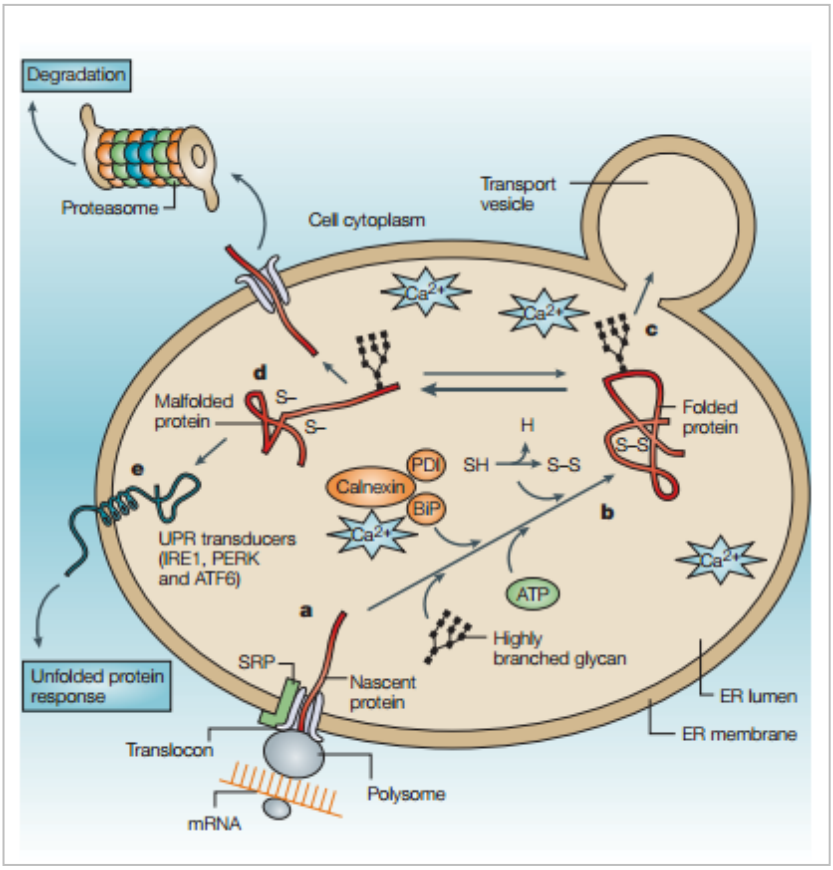

Figure 1.1: Protein folding and degradation pathways in the ER (figure from Ma and Hendershot, 2004). a) The nascent chain enters the ER via protein channels called translocons. b) Protein folding occurs in the presence of molecular chaperones e.g. BiP and PDI. Post-translational modifications also take place including the formation of disulphide bonds. c) If correctly folded, the protein leaves the ER via transport vesicles. d) Misfolded proteins are targeted back to the cell cytosol where they will be degraded by the proteasome. e) As unfolded proteins accumulate, stress sensors IRE1, PERK and ATF6 are activated and initiate the unfolded protein response (UPR).

1.1.1.2. The fully characterised folding pathway of BPTI

BPTI is a small protein containing only 58 residues and 3 disulphide bonds in its' native structure (30-51, 5-55 and 14-38). Although only small, the formation of BPTI involves 5 major intermediate stages (characterised by a disulphide bond) between the unfolded and the fully folded state of the protein (see figure 1.2). These intermediates 'funnel' BPTI via oxidation (S-S formation), reduction (S-S breaking)

and isomerisation (S-S rearrangement) reactions towards the correct fully folded state (Arolas *et al.* 2006).

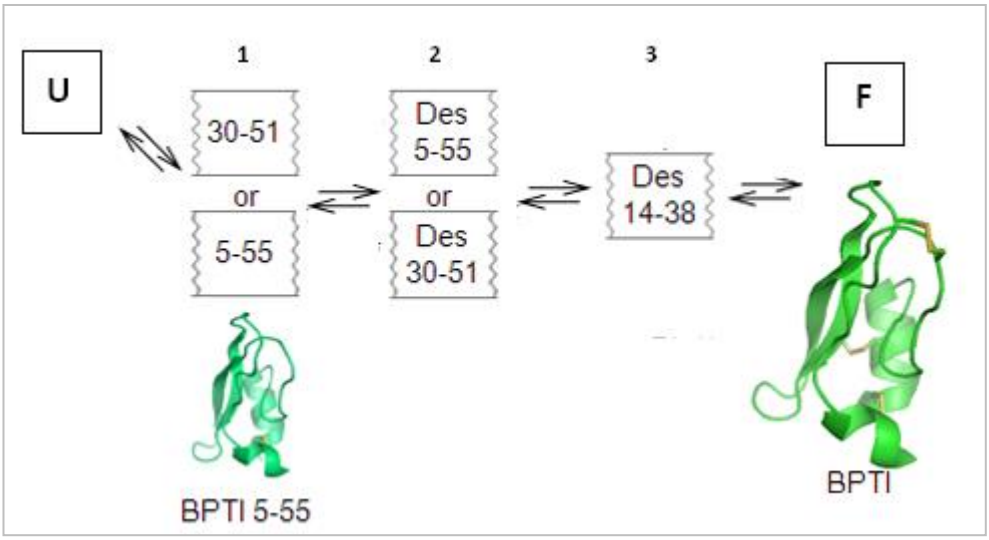

Figure 1.2: BPTI folding pathway (adapted from Wallis and Freedman, 2011). Shown is the kinetically favourable folding pathway of BPTI including 3 intermediate stages between the unfolded (U) and folded (F) state. 1) The first disulphide forms quickly and efficiently giving rise to 1S 30-51 (major product) and 1S 5-55. 2) These species are constrained by the newly formed disulphide bond and the second disulphide bond 14-38, is made (missing disulphides between steps are indicated by the prefix 'Des'). 3) Progression from Des 5-55 and Des 30-51 requires both unfolding and isomerisation of the 14-38 bond as all free thiols are buried and unreactive. This is the rate limiting step. Once Des 14-38 is made the full-folded state can be reached easily.

The final, native state of BPTI is obtained following isomerisation of the 14-38 disulphide bond. This is the rate limiting step of the folding process and can be catalysed by PDI. In the absence of a protein folding catalyst such as PDI, disulphide bond isomerisation can occur spontaneously but the time scale is not biologically feasible. Kinetically trapped species such as BPTI Des 30-51, are common in the folding pathways of many proteins and consequently protein folding catalysts and molecular chaperones are often indispensable.

1.1.2. Protein misfolding in the endoplasmic reticulum (ER)

1.1.2.1. Implications of protein misfolding for the cell

Protein misfolding can be quite common, and unfolded or partially folded proteins in the overcrowded ER can very quickly begin to aggregate. The role of molecular chaperones is to identify proteins that are susceptible to aggregation and prevent it from occurring. However, if a protein does become misfolded and is not noticed by various cellular 'check points' (such as the UPR) or corrected by molecular chaperones it can become cytotoxic (Elgaard and Helenius, 2003).

There are many well known protein misfolding diseases such as cystic fibrosis (misfolded CFTR protein), Gaucher's disease (misfolded β-glucocerebrodisase) and Fabry disease (misfolded α-galactosidase). Additionally, there are diseases caused by the accumulation of misfolded proteins: Alzheimer's disease (deposits of amyloid, beta and tau), Type II diabetes (deposits of amylin) and Creutzfeldt-Jakob disease (deposits of prion protein). The latter class of disease can often be caused later in life if a reduction in molecular chaperone number/ efficacy is seen (Dobson, 2003).

1.1.2.2. The Unfolded Protein Response (UPR)

Under periods of ER stress the unfolded protein response (UPR) is activated (for schematic see figure 1.3. The UPR attempts to regulate cellular stress by: 1) targeting misfolded proteins to the proteasome for degradation, 2) increasing expression of foldases and molecular chaperones and 3) reducing translation (Yoshida, 2007). As misfolded protein accumulates, three ER stress sensors located in the ER membrane become activated: 1) IRE-1 (inositol-requiring enzyme 1), 2) PERK (pancreatic ER kinase (PKR)-like ER kinase) and 3) ATF6 (activated transcription factor 6). If stress is prolonged, these molecules are also able to enable apoptotic pathways (Lin *et al*. 2008).

In response to ER stress, IRE-1 becomes oligomerised. This activates both its kinase and endoribonuclease functions allowing it to perform specific splicing of XBP-1

mRNA. Once sliced, this encodes a potent transcription factor of the basic leucine zipper (B-ZIP) family which can enter the nucleus of the cell and enhance the transcription of a select group of genes, so increasing the protein-folding capacity of the ER and degradation of misfolded proteins (Lin *et al*. 2008).

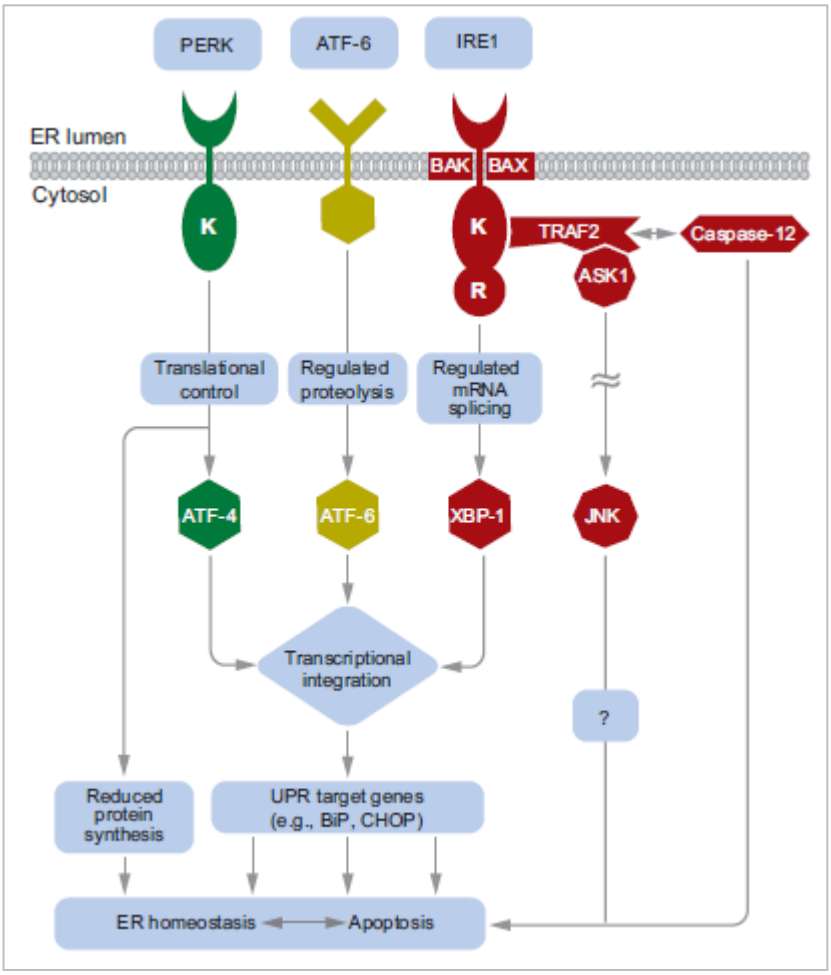

Figure 1.3: The mammalian UPR (taken from Lin *et al*. 2008). PERK, ATF-6 and IRE-1 proteins found transversing the ER membrane are essential for sensing ER stress. Upon activation each invokes signalling cascades which reduce stress and/or promote apoptosis.

In higher eukaryotes, IRE-1 binds to adaptor protein TRAF2 via its kinase domain. This activates the apoptosis signal regulating kinase 1 (ASK1). The activation of ASK1 causes phosphorylation and activation of c-Jun N-terminal kinase (JNK)

which induces apoptosis. Incidentally, binding of TRAF2 by IRE-1 can also lead to displacement of pro-caspase 12 and its conversion into the active enzyme (Lin *et al*. 2008).

The ER lumenal domain of PERK is homologous to that of IRE-1 and becomes oligomerised in response to ER stress (Lin *et al.* 2008). Once activated, PERK phosphorylates eukaryotic initiation factor 2α (eIF2α), a molecule involved in the assembly of 80S ribosomes at the intiation codon. Phosphorylation of eIF2α by PERK leads to inhibition of this function and therefore attenuates protein synthesis. As some protein synthesis is essential, GADD34 mediates the phosphorylation of eIF2α by PERK to ensure that protein synthesis is able to sustain vital functions (Novoa *et al.* 2001). Interestingly however, when ribosomal assembly is impaired by the interaction of PERK and eIF2α there is increased enhancement of ATF-4 translation (Lin *et al*. 2008). ATF-4 is another B-ZIP transcription factor and reduces stress by targeting molecular chaperones. It also increases transcription/translation of CHOP a B-ZIP transcription factor involved in regulating cell death by increasing GADD34 expression.

ATF-6α consists of an ER-stress sensing lumenal anchor coupled to a transmembrane domain and a cytosolic B-ZIP transcription factor domain (Haze *et al*. 1999). In periods of ER stress, ATF-6α travels from the ER to the Golgi where the transmembrane domain is cleaved allowing the liberated transcription factor domain to travel to the nucleus. Following entry to the nucleus, ATF-6α upregulates various genes some of which overlap with those activated by XBP-1 and ATF-4 e.g. BiP and CHOP and also others that are known to be connected to ER-associated degradation (ERAD) (Lin *et al*. 2008).

1.1.2.3. ERAD

Incorrectly folded proteins are targeted to ERAD to prevent their accumulation in the cell. This process is split into 3 main stages: 1) recognition, 2) retrotranslocation and 3) degradation which are shown in figure 1.4 (Vembar and Brodsky, 2008).

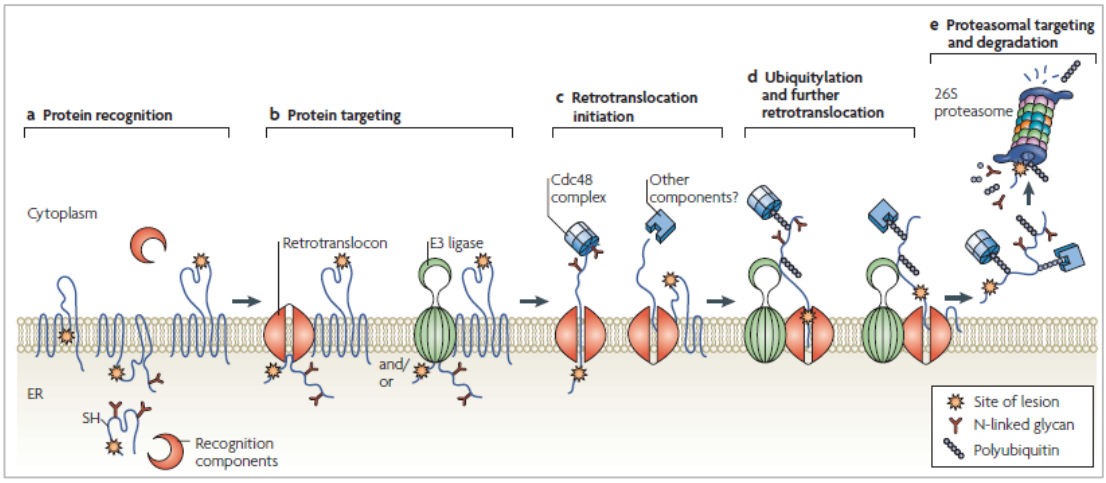

Figure 1.4: ERAD (adapted from Vembar and Brodsky, 2008). a) Misfolded proteins are recognised by various chaperones including: Hsp70 family members, calnexin, calreticulin and the protein disulphide isomerases. b) ERAD substrates are targeted to the retrotranslocation machinery and/or E3 ligases. c) Substrate retrotranslocation may be initiated by the cell-division cycle-48 (Cdc48). The molecular chaperones or the proteasome may also be required for this step. d) As proteins exit the retrotranslocon they are polyubiquitinated by the E3 ubiquitin ligases. This promotes further retrotranslocation and is aided by cytoplasmic ubiquitin binding protein complexes. e) Having entered the cytoplasm, polyubiquitinated ERAD substrates are recognised by receptors in the 19S subunit of the proteasome. Once the polyubiquitin tag has been removed, the substrate can enter the 26S core of the proteasome where it is degraded. Ubiquitin generated in this process is then recycled for further rounds of modification.

In stage one, unfolded proteins are recognised by the ERAD machinery. This can occur via interaction with molecular chaperones or via the calnexin-calreticulin cycle. The latter relies on the fact that during co-translational translocation into the ER, many proteins are glycosylated. The presence of an N-glycan itself increases the hydrophilicity of the protein and encourages it to fold correctly (Daniels *et al.* 2003).

If the protein is folded correctly, 3 glucose molecules are removed by ER-resident glucosidases, it is released from calnexin/calreticulin and then it can exit the ER

(Wang and Hebert, 2003). If the protein is unfolded however (has exposed hydrophobic surfaces etc) it is recognised by UDP-glucose: glycoprotein glucosyltransferase (UGGT) which re-adds a single glucose molecule. The misfolded monoglycosylated protein then re-enters the calnexin-calreticulin cycle where aggregation is prevented and hopefully the correct protein conformation is achieved. Incidentally it is at this stage that ERp57 is able to interact with calnexin thereby promoting oxidative protein folding (Ellgaard and Frickel, 2003).

After recognition, unfolded proteins are extracted from the calreticulin/calnexin cycle and targeted for retrotranslocation by the ER degradation-enhancing α-mannosidase-like lectins (EDEMS) (Wang and Hebert, 2003). During exit from the retrotranslocon, the ERAD substrates are polyubiquitinated by E3 ubiquitin ligases which are embedded in the ER membrane (Mehnert *et al.* 2010). These ligases work alongside accessory proteins involved in substrate recognition (described previously) and their activities are specific to the substrate class in question (Hirsch *et al.* 2009). Once polyubiquitinated, misfolded protein binds to ubiquitin receptors on the 19S proteasome and in doing so drives the unfolded protein into the proteasome core for degradation.

1.1.2.4. Molecular chaperones as protection against protein misfolding

Somewhat unsurprisingly, molecular chaperones rank among the most highly abundant proteins in cells and are found in most cellular compartments (cytosol, ER, mitochondria and chloroplasts) (Saibil, 2008). The major role of molecular chaperones in the cell is to assist protein folding i.e. correct any mistakes that are made along the way and reduce external pressure opposing the folding reaction. In doing this, molecular chaperones improve the efficiency and thus increase the speed of protein folding allowing the folding event to occur on a biologically feasible timescale. Additionally, many chaperones (including the Heat shock family of proteins; Hsps) also function to target misfolded protein out of the cell to the proteasome (see figure 1.1) or by directing the cell to apoptosis (Saibil, 2008).

There are a huge number of different molecular chaperones in both eukaryotic and prokaryotic cells which all have 3 common properties: 1) they recognise structural elements that are in the unfolded protein such as hydrophobic surfaces, 2) they do not bind to proteins that are correctly folded and 3) they exhibit very little substrate specificity (Hartl *et al*. 1994).

1.1.2.5. BiP

BiP is an abundant and ubiquitous ER-resident molecular chaperone and a member of the Hsp70 family. It exhibits broad substrate specificity for newly synthesised, unfolded proteins, but does not bind to native proteins (Gething, 1999). Once nascent protein is bound, BiP promotes folding and prevents the formation of insoluble aggregates. Examples of well characterised, natural substrates of BiP are antibodies (Hendershot *et al.* 1996).

Like other members of the Hsp70 family, BiP has 2 domains: an N-terminal domain and a C-terminal domain. The N-terminal domain has ATPase activity and the C-terminal domain contains the substrate binding site (Gething, 1992). Thus the interaction between BiP and its protein substrates is coupled to ATP-dependent conformational change (Mayer *et al.* 2003).

1.1.3. PDI and the oxidative protein folding pathway

1.1.3.1. Oxidative protein folding in the ER and the role of Ero1

PDI is a molecular chaperone and protein folding catalyst essential for the *in vivo* formation of disulphide bonds. This process (i.e the oxidation of dithiols) requires that oxidising equivalents are passed from molecular oxygen to PDI and then to the reduced protein substrate. Contributors to this include oxidised/reduced glutathione (GSSG/GSH), hydrogen peroxide (H_2O_2), ER oxidoreductins and various peroxiredoxins and peroxidases (Ruddock, 2012).

Unlike many of the molecules mentioned previously, the role of glutathione in disulphide bond formation is probably more indirect. Although initially thought to be pivotal to the process, it is now known that a major source of oxidising equivalents comes from ER oxidoreductin 1 (Ero1) (Appenzellor *et al*. 2010). The role of glutathione therefore seems to be maintaining the redox potential of a variety of intracellular compartments including the ER, where a high GSSG: GSH ratio gives rise to its characteristic, oxidising environment and consequently promotes oxidative protein folding. Currently the exact role of glutathione in disulphide bond formation is poorly understood although it is possible that GSH is responsible for maintaining the oxido-reductases in a reduced state and therefore allowing catalysis of reduction and isomerisation reactions (Chakravarthi and Bulleid, 2004). For a comprehensive review of glutathione see Appenzellor, (2011).

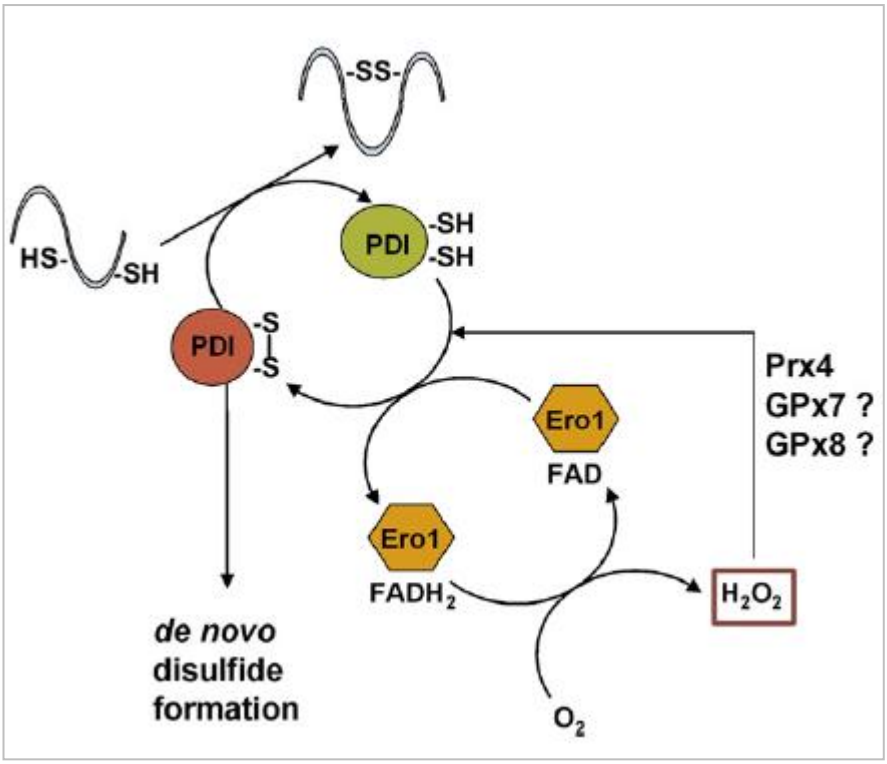

Figure 1.5: Oxidative protein folding (taken from Flohé and Maiorino, 2013). Disulphide bond formation in newly synthesised protein is catalysed by PDI. Reduced PDI is re-oxidised by Ero1 in a reaction that generates H_2O_2. Peroxide made in this way can then be used by peroxiredoxin 4 (Prx4) or the glutathione peroxidases, GPx7 and Gpx8 as an additional mechanism for the re-oxidation of PDI.

Although often regarded as a potentially dangerous by-product of disulphide bond formation, peroxide itself may be important for oxidative folding. H_2O_2 is made by sulphydryl peroxidases such as Ero1 *in vitro* (see later) and work by Karala *et al.* (2009) shows that it is more efficient than a glutathione redox buffer in refolding non-native proteins *in vitro*. Additionally, hydrogen peroxide can be metabolised by peroxiredoxin 4 (Prx4) and glutathione peroxidases, Gpx7 and Gpx8 (also discussed later). In this way the ER is able to regulate the accumulation of potentially dangerous hydrogen peroxide while also promoting the efficient oxidative folding of non-native proteins (Tavender *et al.* 2010, Nguyen *et al.* 2011).

As mentioned previously, a major source of oxidising equivalents comes from the ER oxidoreductins (Ero's). In mammalian cells there are two Ero proteins: Ero1α and Ero1β (Dias-Gunasekara *et al.* 2005). Ero1α is a flavin dependent oxidase located on the ER membrane that is able to transfer oxidising equivalents from molecular oxygen to the **a'** domain of PDI. This activity is not specific to the **a'** domain but is position dependent and in PDI **a'bb'a** mutants, **a** rather than **a'** is oxidised (Wang *et al.* 2009). Preferential oxidation at the C-terminus of PDI is likely to be due to specific binding of Ero1α at the **b'** domain and similarly, the minimal requirement for oxidation by Ero1α is PDI **b'xa'** (Wang *et al.* 2010) (see figure 1.6).

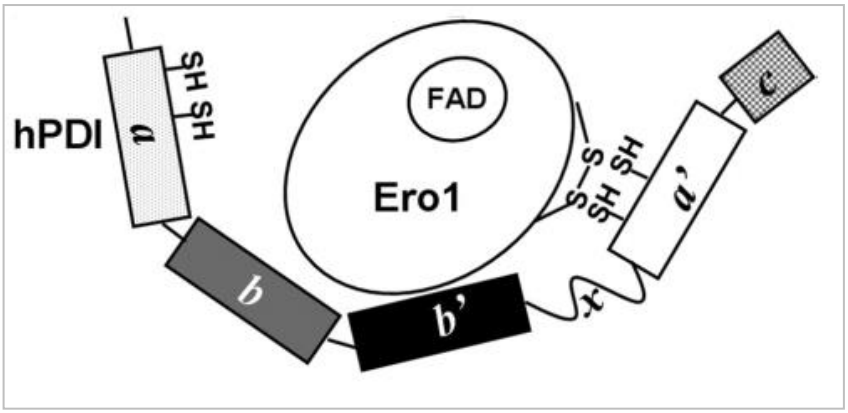

Figure 1.6: Mechanism for Ero1α mediated oxidation of the PDI a' domain (adapted from Wang *et al.* 2009). Ero1 binds to the **b'** domain of PDI positioning itself in such a way that its active site is in proximity of the catalytic site of the **a'** domain.

The implication of this for PDI is that substrate binding at **b'** cannot occur while Ero1α is still bound, and therefore substrate cannot bind until the reaction cycle has been completed and PDI is in the oxidised state (Wang *et. al* 2008). Incidentally, despite having identical domain architecture, Ero1α is unable to oxidise ERp57 (Inaba *et al.* 2010). This indicates that the reaction between Ero1α and PDI is specific (Wang *et al.* 2011).

Unlike Ero1α, Ero1β is constitutively expressed in the chief cells of the stomach and the islet cells of the pancreas (Dias-Gunasekara *et al*. 2005). Interestingly, its expression does not correlate with expression of PDI or PDIp and therefore its physiological role is unknown. It does however form homo and heterodimers with other Ero1 proteins and it is the complex form that predominates in the stomach and pancreas (Dias-Gunasekara *et al.* 2005). Authors suggest that this work indicates a possible role for Ero1β in passing oxidising equivalents to Ero1α within these highly secretory tissues.

1.1.3.2. Alternative mechanisms for re-oxidation of PDI

The role of Ero1 as an oxidant of PDI is not unique and in its absence, mammalian cells retain some degree of thiol oxidation activity (Appenzellor-Herzog *et al.* 2010). Alternative oxidants of PDI include: quiescin sulphydryl oxidases, glutathione peroxidases, and also certain peroxiredoxins (Tavender *et al*. 2010).

One of the attractive features of peroxiredoxin 4 (Prx4) mediated PDI oxidation is that it can metabolise H_2O_2 created by Ero1 mediated oxidation (see figure 1.6). This is important because although H_2O_2 is able to oxidise PDI itself, it can also be harmful to the cell (Tavender *et al*. 2010, Karala *et al.* 2011). The activity of Prx4 relies on the reduction of an active site disulphide bond. Some PDI family members are able to directly reduce Prx4 themselves becoming oxidised in the process and leaving Prx4 in a position to oxidise other family members (Tavender *et al.* 2010). Therefore it is probable that oxidation of PDI by Prx4 increases the efficiency of EroI mediated disulphide formation and subsequently allows disulphide formation via alternative sources of H_2O_2.

An additional mechanism to reduce the concentration of H_2O_2 is via two ER-resident glutathione peroxidases, Gpx7 and Gpx8. Similar to Prx4, these proteins can use H_2O_2 to transfer oxidising equivalents to PDI family members while at the same time reducing intracellular peroxide levels (Nguyen *et al.* 2011). Perhaps more interesting is that both Gpx7 and Gpx8 have also been shown to interact with Ero1 *in vivo* and that *in vitro,* Gpx7 can increase oxygen consumption by Ero1α. The net consequence of the presence of the glutathione peroxidases and the peroxiredoxins in the ER is that high intracellular H_2O_2 concentrations are avoided despite its constant production via Ero1 mediated oxidation of PDI (Nguyen *et al*. 2011). In this way, the ER has evolved to protect itself from the side effects of oxidative folding.

1.2. The protein disulphide isomerases

1.2.1. The PDI family

1.2.1.1. The domain architecture of hPDI family members

One very large molecular chaperone family found in eukaryotic cells is the protein disulphide isomerase (PDI) family.

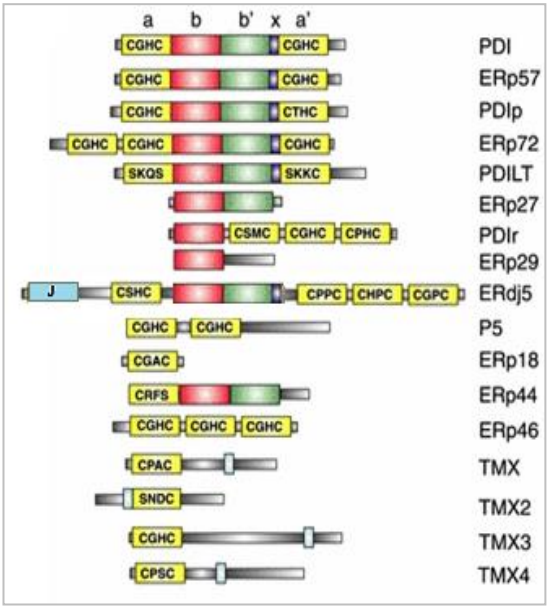

Figure 1.7: The domain structure of the human protein disulphide isomerase (PDI) family (adapted from Hatahet and Ruddock, 2007). PDI, ERp57 and PDIp share identical domain architecture although the **a'** active site motif of PDIp is slightly different.

The human PDI family has been extensively studied and ~17 members have now been identified (Hatahet and Ruddock, 2007). Although the domain architecture of the PDI family members varies considerably (see figure 1.7) each has at least one domain with the thioredoxin fold, αβ-fold and mixed β sheet core (Ferrari and Söling 1999).

In addition to domain architecture, figure 1.7 also shows the catalytic active sites of various PDI family members. Of the 17 shown, figure 1.7 indicates that 5 of the PDI family members (PDILT, ERp27, ERp29, ERp44 and TMX2) lack a CXXC catalytic active site and therefore may not be able to perform thiol: disulphide exchange (Hatahet and Ruddock, 2007). For these proteins, their place in the PDI family is defined by their ER residency and structural homology to thioredoxin rather than their catalytic activity (Hatahet and Ruddock, 2007).

1.2.1.2. The Thioredoxin fold

As mentioned previously, human PDI family members have at least one thioredoxin-like domain (Hatahet and Ruddock, 2007). The thioredoxin (TRX) fold was first identified in the small (12kDa) *E.coli* protein thioredoxin (for review see Holmgren and Bjornstedt, 1981) but has since been observed in both eukaryotes and prokaryotes. Furthermore, the thioredoxin super-family incorporates protein families such as the protein disulphide isomerases, DsbAs and glutaredoxins all of which are known to be involved in thiol-disulphide exchange.

In the 1.6 Å X-ray crystal structure of oxidised *E.coli* TRX, there is a central (hydrophobic) core of five β-strands surrounded by four α-helices (see figure 1.8). Typically however, the TRX fold consists of four β-strands and three α-helices (Katti *et al*. 1990). The structure can be separated further into an N-terminal βαβ motif (parallel β- strands) containing the CGPC active site and a C-terminal ββα motif (anti-parallel β- strands). The two are connected by a loop incorporating the third helix (see figure 1.8) and of the two, the N-terminal motif is the least conserved within PDI family members whereas the C-terminal motif indicates the most highly conserved region (Ferrari and Söling, 1999).

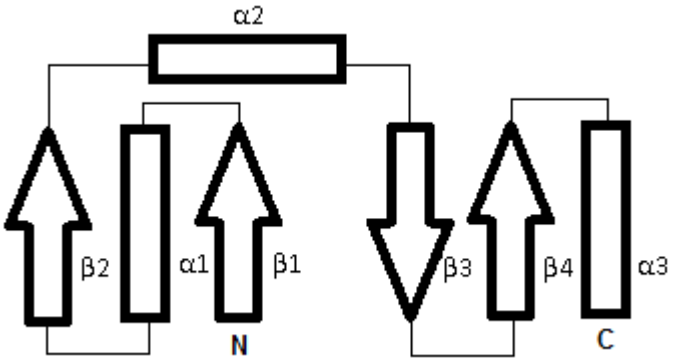

Figure 1.8: Schematic of the thioredoxin fold. Arrows indicate β-sheet structures and rectangles α-helices.

In the catalytic domains, the active site motif (CGPC) is located at the N-terminus of α2 and allows catalysis of the thiol: disulphide exchange (Hatahet and Ruddock, 2007). When reduced, (two reactive thiols in active site) TRX binds target proteins via its hydrophobic surface before subjecting their disulphide bonds (now in close proximity of the reactive thiols) to nucleophilic attack. Ultimately this leads to a disulphide bond being formed between active site cysteines and the reduction of a disulphide bond in the target protein. Subsequently the activity of TRX is restored by reduction with thioredoxin reductase.

1.2.1.3. PDI

PDI is probably the best characterised member of the PDI family and also the most abundant being found ubiquitously in all eukaryotes. It is both a molecular chaperone and a general folding catalyst aiding the formation (oxidation), breakage (reduction) and rearrangement (isomerisation) of disulphide bonds in a wide range of protein substrates.

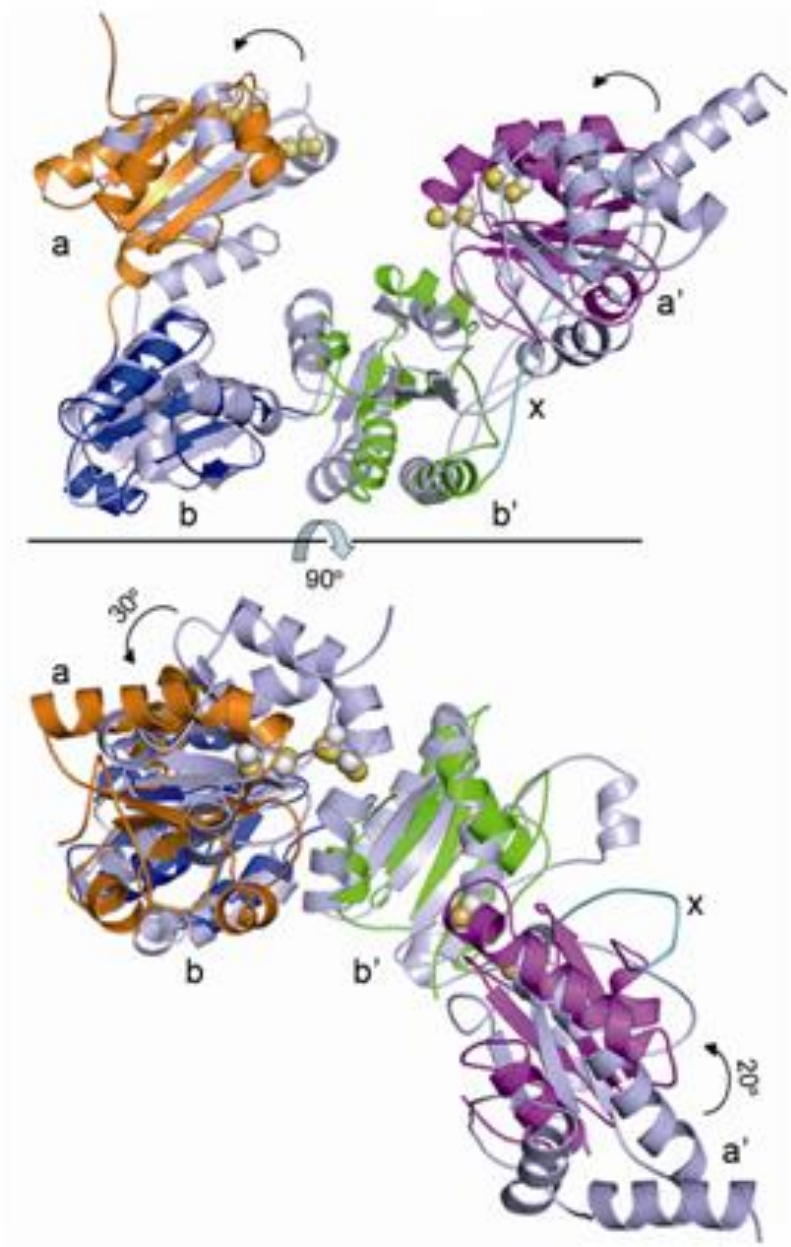

Figure 1.9: Superimposition of the yPDI and hPDI X-ray crystal structures (adapted from Wang *et al.* 2012). The two structures are superimposed based on alignment of the **b** and **b'** domains. hPDI is shown in multi-colour and yPDI in light blue. The rotations associated with the **a** domain (yPDI) and **a'** domain (hPDI) are shown).

High resolution X-ray crystal structures for both yeast PDI (yPDI) and human PDI (hPDI) are now available (Tian *et al*. 2005, Tian *et al.* 2008, Wang *et al.* 2012). These proteins share ~30% sequence identity and significant structural homology (see figure 1.9).

Despite structural similarities, yPDI and hPDI clearly undergo different mechanisms of conformational change. For yPDI, the two published full-length structures (obtained at 4ºC and 22ºC) show that conformational change is centred on the **a** and **b** domains (Tian *et al.* 2005 and Tian *et al.* 2008 respectively). However molecular dynamic simulations of yPDI, performed by Emilio Jiminez-Roldan (data currently unpublished) show that it has flexibility at both the N and C-terminus i.e. **ab** and **b'xa'c**.

Published data for hPDI which includes: fluorescence experiments, limited proteolysis, a solution structure of **bb'** and full length X-ray crystal structures indicates that its flexibility is centred on the x-linker region (Wang *et al.* 2010, Denisov *et al*. 2008, Wang *et al.* 2012). Furthermore the major redox-active cassette is defined as **b'xa'c** (Wang *et al* 2011, Wang *et al.* 2012). Differences between hPDI and yPDI in terms of conformational change are probably indicative of the two proteins having different protein substrates and catalytic activity.

In yeast, the *PDI1* gene is essential for viability (Farquhar *et al*. 1991). This is not the case for human PDI however which can be compensated for by other PDI family members including ERp57, ERp72 and P5 (Rutkevich *et al.* 2010).

1.2.1.4. PDIp

PDIp is a pancreas-specific homolog of PDI (Desilva *et al.* 1996, Desilva *et al.* 1997). It is also a glycoprotein and has 3 glycan chains (Desilva *et al*. 1996, Walker *et al*. 2012). Like PDI, PDIp has the **abb'a'** domain architecture and they share ~45% sequence identity. Unlike PDI however, PDIp is very poorly characterised and currently little is known about its domains: isolated or domain constructs/full length protein. Furthermore there are a considerable number of papers on PDIp that use an incorrect construct. This construct incorporates part of the signal peptide into the

mature protein (Desilva *et al.* 1996). The correct construct has now been published (Walker *et al.* 2012). Consequently studies of the activities of PDIp now need to be reviewed.

1.2.1.5. ERp57

ERp57 is another close homolog of PDI sharing ~33% sequence identity (Frickel *et al.* (2004). Unlike many of the PDI family members however, a specific physiological role has been determined. ERp57 interacts with calreticulin and calnexin and therefore is important for the oxidative folding of glycoproteins (Oliver *et al*. 1999). ERp57 has also been implicated as an important component of the major histocompatability complex (MHC) class I peptide loading complex and in the folding of influenza hemagglutinin (Bouvier 2003, Daniels *et al.* 2003).

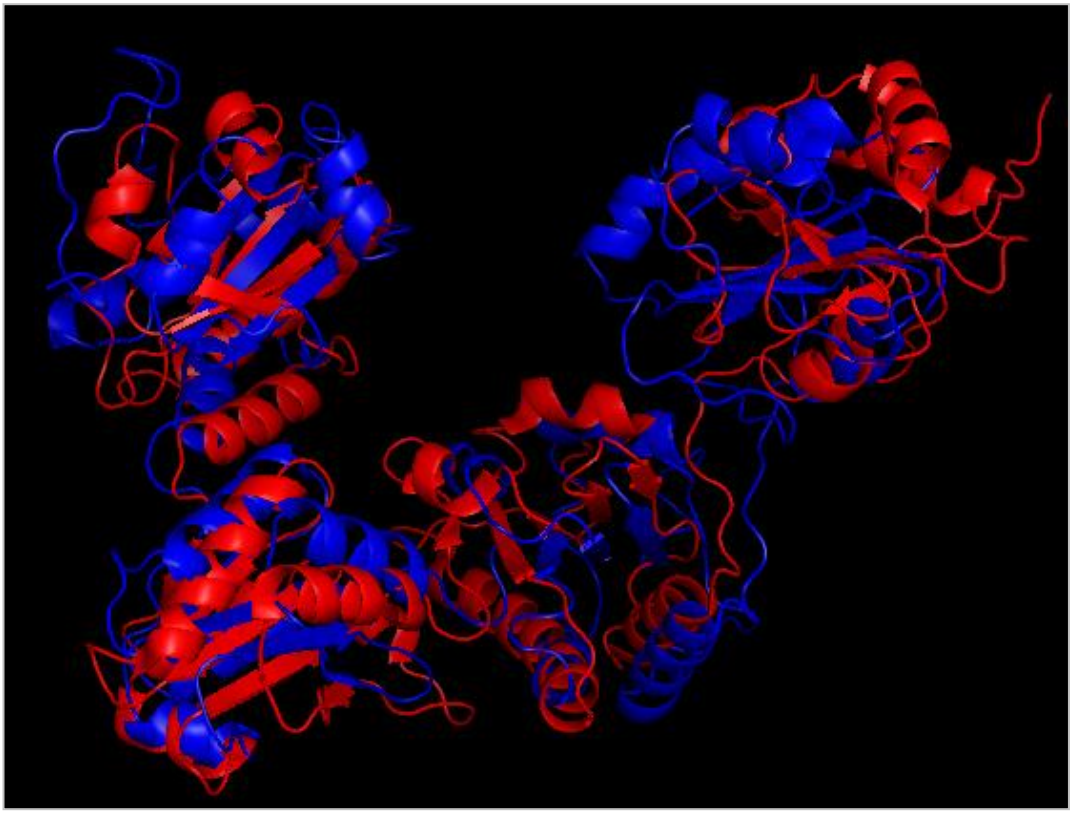

Figure 1.10: PyMOL alignment of PDI and ERp57. PDB structures 4EKZ (reduced PDI) and 3F8U (ERp57) were aligned in PyMOL and shown in blue and red respectively. Tapasin, which was co-crystallised with ERp57, has been deleted from the alignment for clarity.

The crystal structure of ERp57 complexed with tapasin, has been determined to 2.6Å (Dong *et al.* 2009). It shows remarkable similarity to the recently determined structure of hPDI (see figure 1.10) (Wang *et al*. 2012). The greatest region of difference between the two proteins is seen at the C-terminus but this may be due to the presence of tapasin, because in PDI the C-terminus is the greatest region of flexibility (Wang *et al.* 2011, Wang *et al.* 2012). The structure of ERp57 with tapasin bound is useful because it provides information about substrate binding in the PDI family.

1.2.1.6. ERp72

Unlike PDI, ERp72 has 3 catalytic domains and the domain architecture **a^0abb'a'** (Hatahet and Ruddock, 2007). Also unlike PDI but similar to ERp57, ERp72 does not have a hydrophobic surface in **bb'** that is associated with substrate binding (Kozlov *et al.* 2010). This is particularly interesting because this region is structurally homologous to the **bb'** domains of ERp57 in terms of the isolated domain and domain orientation (Kozlov *et al.* 2009).

The catalytic domains of ERp72 are unequal in their contribution to activity in the insulin reduction assay (Satoh *et al.* 2005). ERp72 **a^0** seems to act predominantly as a catalyst of oxido-reductase activity, **a** has an intermediate role in both catalysis and substrate binding and the **a'** domain is involved in substrate binding (Satoh *et al.* 2005). Molecular modelling of ERp72 using crystal structures of **a^0a** and **bb'** domains and aligning to the structure of ERp57, indicate that in correlation with the activity data described above and in total contrast to other PDI family members, the **a^0**, **a** and **a'** domains make up the substrate binding site (Kozlov *et al.* 2010).

1.2.1.7. P5

P5 is another poorly characterised member of the PDI family. It is unlike PDI in that it has just two domains, both of which are catalytic and contain a PDI-like active site motif (Hatahet and Ruddock 2007). Unsurprisingly therefore, PDI and P5 share only 11% sequence identity (Kikuchi *et al.* 2002).

Currently the function of P5 is unknown but it has been shown to have ~45% isomerase activity and ~50-60% chaperone activity relative to PDI (Kikuchi *et al.* 2002). These relative percentages are high considering that P5 has no obvious substrate binding domain like PDI. It is thus likely that P5 exhibits more restricted substrate specificity than PDI and that this is also limited by size. Like PDI however, P5 shows asymmetry of activity and the first catalytic domain of P5 seems to be more important for isomerase activity than the second domain (Kikuchi *et al*. 2002, Wang *et al.* 2008).

1.2.1.8. PDILT

PDILT, like PDIp is also tissue specific and is found in the testes (van Lith *et al.* 2005). Also like PDIp, PDILT is an ER-resident glycoprotein. This is an unusual trait for PDI family members and is probably linked to its unique physiological role in the quality control of sperm membrane protein ADAM3 and male infertility (Tokuhiro *et al.* 2012). Unlike both PDI and PDIp however, PDILT has only one catalytic cysteine: in its **a'** domain SXXC motif (see figure 1.7). This is sufficient for interaction with Ero1α indicating that binding of PDI family members is not dependent of the N-terminal cysteine of the CXXC motif (van Lith *et al.* 2005).

1.2.1.9. Functional redundancy of PDI family members

PDI1 is essential for viability in yeast indicating that it is unique in its role as a protein folding catalyst in these cells (Farquhar *et al*. 1991). This does not appear to be the case in human cells however, and PDI depletion from human hepatoma cells has only a minimal effect on the secretion of selected proteins; giving rise to a delay in oxidative folding rather than causing arrest (Rutkevich *et al*. 2010). The combination of PDI and ERp57 depletion causes a more significant phenotype: slower export of secretory proteins from the ER, slower rate of oxidative folding and accumulation of misfolded protein (Rutkevich *et al.* 2010). This therefore suggests that *in vivo*, ERp57 may well be able to compensate for loss of PDI (and vice versa)

and is in agreement with previous work that showed that an ERp57 knockout had minimalistic implications (Solda *et al.* 2006).

The effect of depletion of either P5 or ERp72 on the secretory properties of the hepatoma cells was negligible and no significant difference was seen for combinations including P5 and PDI, P5 and ERp57 etc, relative to PDI and ERp57 depletion alone (Rutkevich *et al*. 2010). Again this is indicative of PDI and ERp57 being able to compensate for one another in the cell. This is interesting because if the roles of the PDI family members are able to interconvert, it is difficult to explain why so many (~17) have been conserved.

1.3. PDI- structure and activity

1.3.1. Structural elucidation of full length hPDI and implications for activity

1.3.1.1. The domain architecture of PDI

Despite having been studied for many years previous, PDI cDNA was first isolated from rat liver and characterised just 30 years ago (Edman *et al.* 1985). It encoded a 508 amino acid protein that had both a signal peptide and a C-terminal ER-retrieval signal. In addition, this protein was shown to have two distinct regions of homology (**a** and **a'**) with ~ 47% sequence identity and homology to thioredoxin, and two further regions (**b** and **b'**) that shared ~28% sequence identity (Edman *et al.* 1985).

In total, PDI genomic DNA has 11 exons and 10 introns (Tasanen *et al.* 1998). On account of this, it was suggested that the domain boundaries of PDI could be defined using the exon patterns. The **a** and **a'** domains were found to be encoded by exon 1-2 and 8-9 respectively and exon 3 was thought to encode the **e** domain as it shared sequence homology to oestrogen receptors (Tsibris *et al.* 1989). This was not the case and the **e** domain was later found to be an artefact when structural studies

showed that this region constituted part of the thioredoxin fold of the **a** domain (Kemmink *et al*. 1997). Additionally, further studies showed that the isolated **e** domain had no independent secondary structure and therefore was more susceptible to proteolysis than other regions of the molecule (Darby *et al*. 1996, Freedman *et al.* 1998).

After many years of collective effort, the current domain boundaries for **abb'a'** were defined in 2003 (Alanen *et al.* 2003, Pirneskoski *et al.* 2003). Figure 1.11 (below) shows a schematic representation of the domain architecture of PDI.

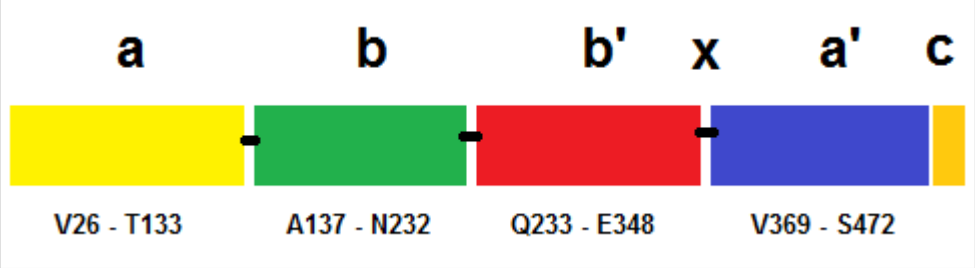

Figure 1.11: The domain architecture of PDI. The **a** and **a'** domains of PDI are catalytically active and share 41% and 32% sequence identity with thioredoxin (respectively). The **b** and **b'** domains do not contain an active site and share low sequence identity with thioredoxin. Nonetheless both **b** and **b'**, display a typical thioredoxin-like fold.

Determination of the correct domain boundaries for PDI was a collaboration of limited proteolysis, studies of recombinant protein expression and NMR (Kemmink *et al.* 1995, Darby *et al.* 1996, Kemmink *et al.* 1997, Freedman *et al*. 1998, Kemmink *et al.* 1999, Darby *et al*. 1999, Alanen *et al*. 2003 and Pirneskoski *et al*. 2003). The domain boundaries of PDI were defined as **a** (V26-T133), **b** (A137-N232), **b'** (Q233-E348) and **a'** (V369-S472). The 19 amino acid linker between **b'** and **a'** and an acidic C-terminal tail of 36 amino acids were also identified (x and C respectively).

1.3.1.2. The catalytic domains of PDI

As described previously, the catalytically active domains of PDI are **a** and **a'**. These share 41% and 32% sequence identity with thioredoxin and exhibit a typical TRX

fold (Kemmink *et al*. 1995, Dijkstra *et al*. 1999, Tochio *et al.* 2005). The **a** and **a'** domains each present a CGHC active site motif and therefore are responsible for both the oxido-reductase and isomerase activities of PDI. The unique active site properties and functional activities of PDI will be discussed later.

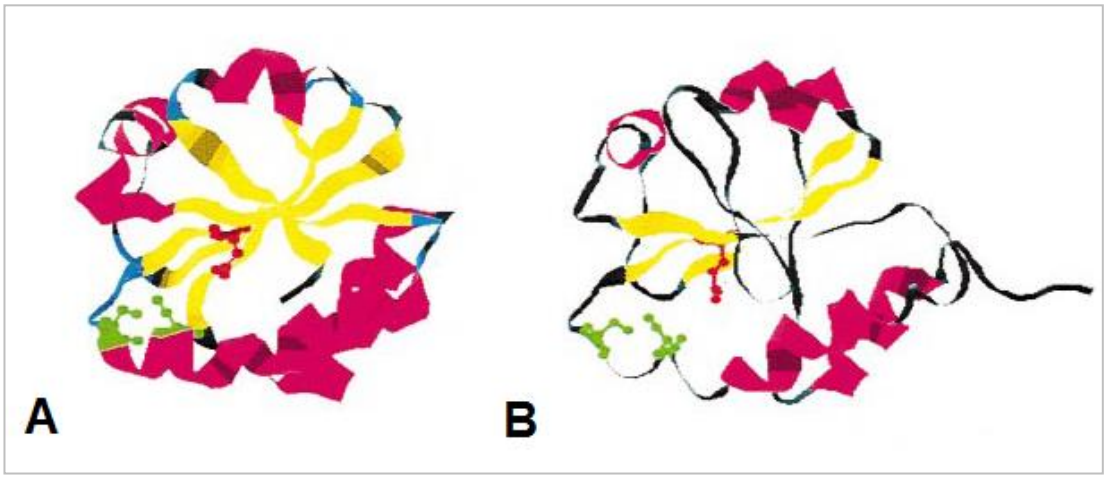

Figure 1.12: Comparison of the structures of *E. coli* thioredoxin and human PDI a (taken from Ferrari and Söling (1999)). A) The structure of thioredoxin as determined by Katti *et al.* (1990). B) The structure for PDI **a** as determined by Kemmink *et al*. (1997). The active site is shown in green, α-helix in red and β-sheet in yellow.

1.3.1.3. The non-catalytic domains of PDI

The **b** and **b'** domains of PDI do not contain an active site and therefore are not catalytically active. Interestingly, despite sharing very little sequence homology to thioredoxin family members, it was shown by NMR that PDI **b**, like the catalytic domains, displayed a thioredoxin-like fold (Kemmink *et al*. 1997, Kemmink *et al.* 1999). Traditionally PDI **b'** has been more difficult to study but the solution NMR structure of PDI **bb'** shows that it too has a thioredoxin-like fold (Denisov *et al*. 2008).

The intransigent nature of **b'** has been blamed for the delay in obtaining a high resolution 3D structure for full length PDI. It is now understood that the **b'** domain is highly dynamic and that this is essential for redox-mediated conformational change (Wang *et al.* 2010, Wang *et al*. 2011, Wang *et al.* 2012). Furthermore **b'** contains the

major ligand binding site and is therefore essential for substrate binding (Klappa *et al.* 1998a, Darby *et al.* 1998, Byrne *et al.* 2009). It is expected that the conformational changes (described previously) enable this (Klappa *et al.* 1998a, Byrne *et al.* 2009, Wang *et al.* 2011).

1.3.1.4. The x-linker region

The **x**-linker is a region of intrinsic flexibility separating the **b'** and **a'** domains. Although poorly understood, it has been identified as a possible modulator of substrate binding and as a contributor to changes in redox conformation (Nguyen *et al.* 2008, Byrne *et al.* 2009, Wang *et al.* 2011, Wang *et al*. 2012).

1.3.1.5. The C-terminal Tail

The C-terminal tail is a 29 amino acid extension comprising predominantly acidic residues and containing an ER-retention signal (Pihlajaniemi *et al.* 1987). Its functional importance remains largely unknown but it has been implicated in sequestration of calcium in the ER (Macer and Koch, 1988). Unlike yeast PDI (yPDI), the C-terminal tail of human PDI (hPDI) does not seem to have any appreciable secondary structure (Tian *et al*. 2006). Furthermore in order to facilitate crystallisation, C-terminal truncates (**abb'xa'**) were used (Wang *et al.* 2012).

1.3.1.6. Full length structures of PDI

The first low resolution full length structure of hPDI was the product of small angle X-ray scattering (SAXs) studies and atomic force microscopy (AFM) (Li *et al.* 2005). Using available NMR structures of the **a** and **b** domains it was possible to determine a structure for PDI (in solution) which showed the **abb'a'** domains aligned in an annular arrangement about a central cavity (Li *et al.* 2005). However, the central cavity was found to be not sufficiently large for binding of all possible substrates so it was postulated that PDI must undergo some degree of conformational flexibility in order to carry out its full range of activities.

The first X-ray structure of yPDI showed that at 4ºC, its 4 domains were ordered in a twisted 'u' conformation. In this structure, the **a** and **a'** domains face each other at either side of the 'u' and the **b** and **b'** domains form the base (Tian *et al.* 2006). Furthermore the inner surface of the 'u' is made up of hydrophobic residues that likely facilitate substrate binding but again the central cavity was found to be too small to accommodate the majority of PDI target proteins.

In hPDI, extensive flexibility has been seen around the **x**-linker region indicating that this is a very dynamic region (Wang *et al.* 2010). Unexpectedly despite similarities with hPDI in this area, the major site of flexibility in yPDI is between **a** and **b** (Tian *et al.* 2008). Consequently, conformational changes that increase cleft size in yeast PDI are probably not mirrored by human PDI as previously postulated (Tian *et al*. 2008). It is likely therefore that many PDI family members use inter-domain flexibility in order to regulate their activity.

The second crystal structure for yPDI at 22ºC indicates the full extent of this motion (see figure 1.13). The **a** domain turns away from **a'** via a 123º rotation of the loop between **a** and **b**. Contact with the **b'** domain is lost and this gives rise to a 'boat-shaped' structure with an increased cleft diameter (Tian *et al*. 2008). When the flexibility of **a** was stabilised with inter-domain disulphide bonds, a reduction in both isomerisation and oxidoreductase activity of ~60-70% was seen. This is in stark contrast to an **a'** stabilised mutant which saw just a 24% reduction in both activities indicating that the domain motion of **a** is essential for the physiological function of yPDI (Tian *et al*. 2008).

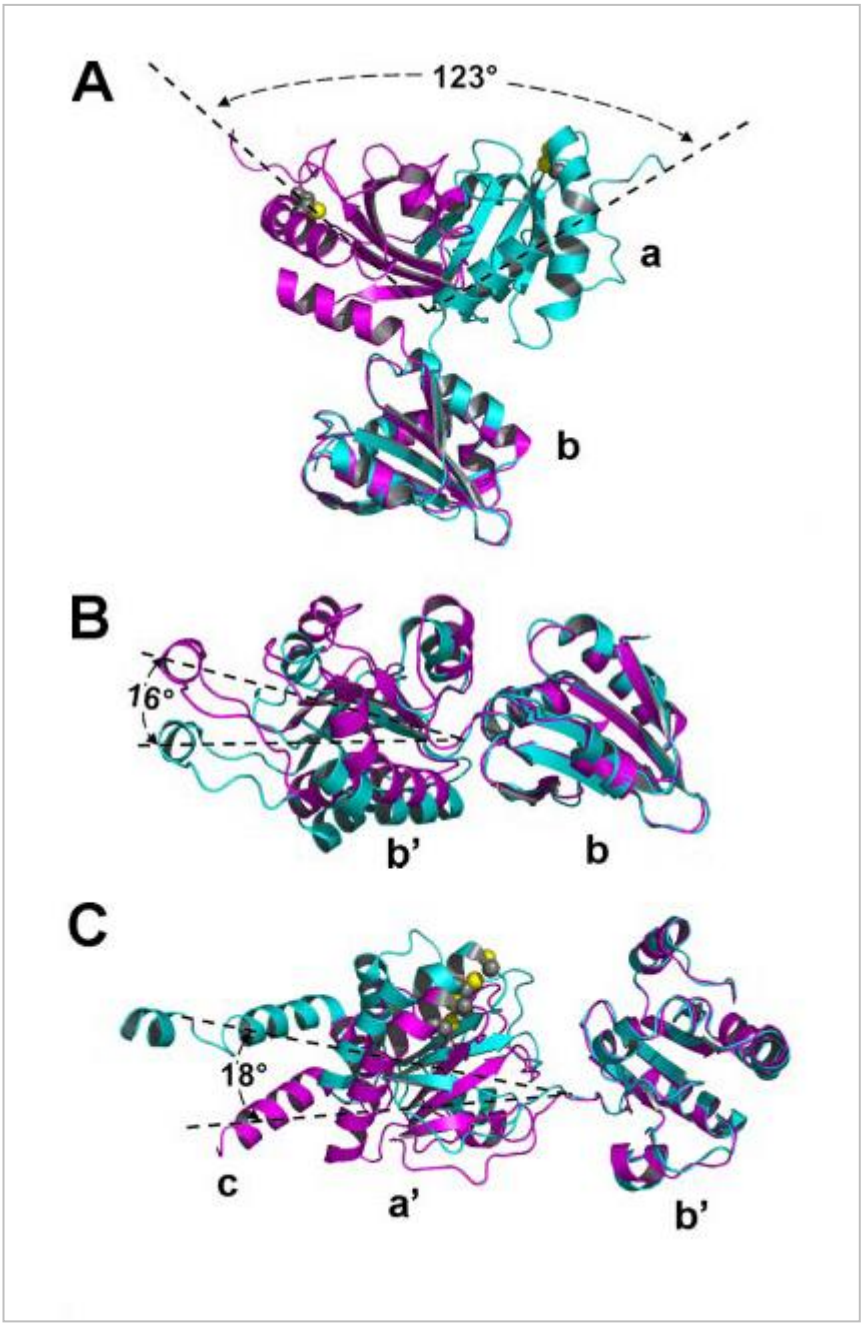

Figure 1.13: Alternate conformations of yPDI associated with changing crystallisation temperature (taken from Tian *et al.* 2008). The structure of yPDI at 4ºC is shown in magenta and 22ºC in cyan. A) change in the position of the **a** domain relative to **b**. B) relative conformation of the **b** and **b'** domains. C) Comparison of the orientation of **b'** and **a'**. Clearly the biggest conformational change is at the **a** domain.

1.3.1.7. X-ray crystal structures of hPDI

Structural elucidation of full length hPDI has revealed that it is an enzyme with alternative conformations. Currently two well resolved conformations have been identified but it is expected that there are still many dynamic structures yet to be observed (see figure 1.14). One such structure shows that in the presence of DTT: a well characterised reductant, PDI exhibits a tight, 'closed' conformation but in another (in the absence of DTT), PDI is 'open' (Wang *et al*. 2012).

The minimal domain requirement for these structural changes is **b'xa'** with position of the x-linker region in relation to these domains being particularly important (Wang *et al.* 2011, Wang *et al.* 2012). In the recent X-ray crystal structure for example, DTT-treated PDI displays tight packing of the **a'** domain upon **b'** with clear interaction between the two domains. In untreated PDI however, **b'** and **a'** are more distinct (Wang *et al.* 2012). It is likely that the plasticity of the **x**-linker region facilitates these movements.

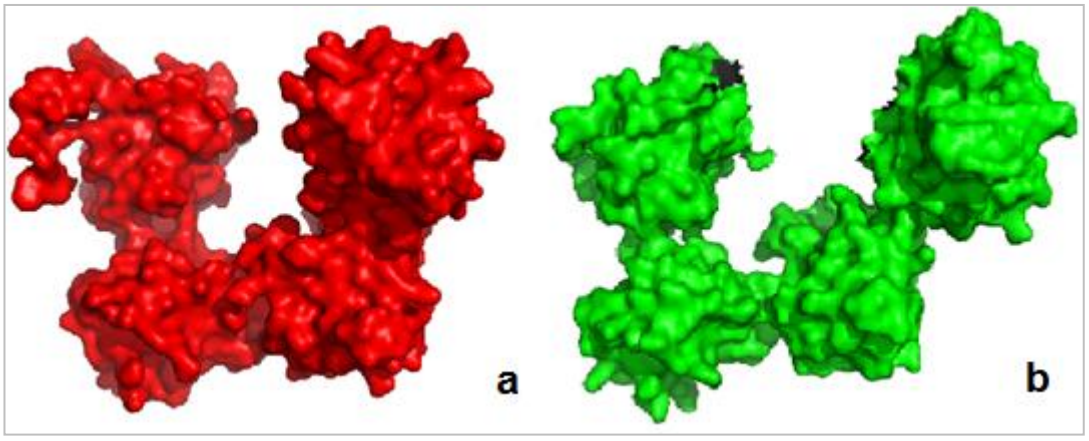

Figure 1.14: X-ray crystal structures of PDI. Domains shown **a-b-b'-a'** (left to right) a) PDI crystallised in the presence of 50mM DTT. Diffraction to 2.5Å. b) PDI crystallised as a) but in the absence of DTT. Diffraction to 2.9Å. (Wang *et al*. 2012).

The 'opening' of PDI gives rise to an increase in cleft diameter from 15Å to 30Å and increases the distance between the catalytic active sites from 27.6Å to 40.3Å (Wang

et al. 2012). Clearly this suggests an attractive mechanism for substrate binding with the 'open' form being far more likely to be able to bind large protein substrates than the 'closed' form. Furthermore, oxidised **bb'xa'** has greater chaperone activity than the reduced form (Wang *et al.* 2011) Examples of substrates that could use these structural changes for association/dissociation with/from PDI have not yet been identified and currently a molecular explanation for these conformational exchanges remains controversial.

One such explanation is that in the presence of DTT, PDI is reduced and therefore tethering interactions between the **b'** and **a'** domains are intact. In the absence of DTT or in the presence of an oxidant however, PDI becomes oxidised and this leads to these linkages being broken. In particular, a cation-π interaction between the **a'** active site adjacent tryptophan (W396) and an arginine (R300) in the **b'** domain is broken in the 'open' structure (Wang *et al.* 2011, Wang *et al.* 2012). As would be expected, an R300A mutant presents a permanently 'open' conformation (Wang *et al.* 2011).

The notion that the activities of PDI may be redox-regulated was highlighted when it was found that the cholera toxin A1 chain (CTA1) would only bind to reduced PDI and not oxidised PDI (Tsai *et al.* 2001, Taylor *et al.* 2011). Consequently it was suggested, that oxidation of PDI would lead to dissociation of the CTA1: PDI complex giving rise to a very pleasing mechanism for redox-regulated substrate binding (Tsai *et al*. 2001, Tsai *et al.* 2002). Recent work however has shown that disassembly of the CTA1: PDI complex occurs spontaneously at physiological temperature (Taylor *et al*. 2011) and therefore examples of substrates that utilise these redox-dependent conformational changes remain to be identified.

An alternative, contrasting explanation is that organic oxidants/reductants (such as DTT, GSH, GSSG etc) are able to bind to PDI and therefore substrate/ligand binding gives rise to changes in conformation rather than redox state. This is not unheard of and GSSG: a common oxidant used in PDI structural studies, has been shown to compete with the α subunit of prolyl-4-hydroxylase for binding to PDI (Lumb and Bulleid, 2002). Furthermore, a recent X-ray structure of human PDI **bb'xa'** shows a molecule of oxidised DTT bound at the **b'** domain (Wang *et al.* 2011) (see figure

1.15). It is thus clear that subsequent work to further understand these conformational changes is required. Investigators must also be aware of the possible implications of using organic molecules to modulate the redox state of PDI and should look for alternatives.

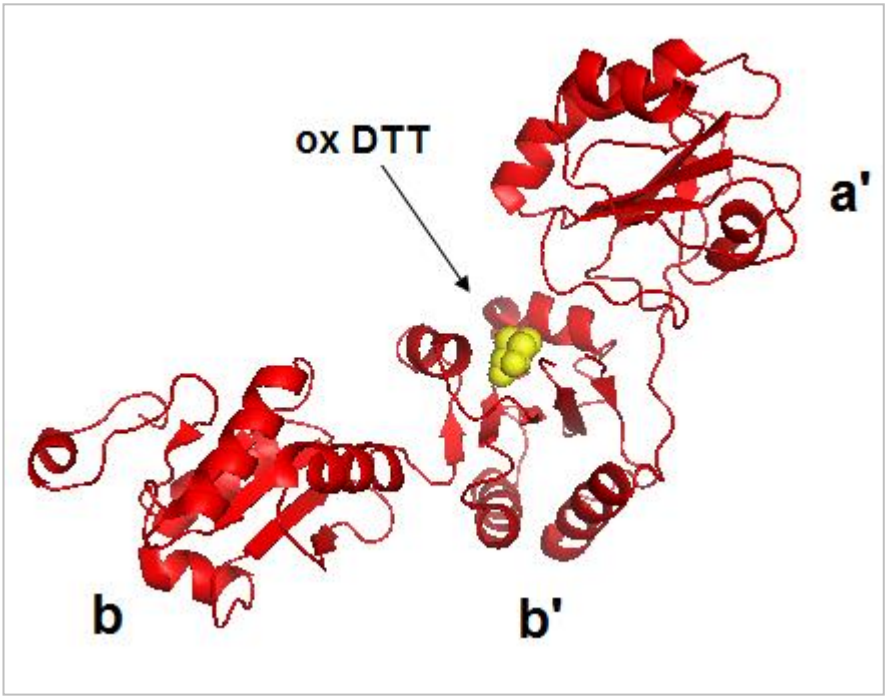

Figure 1.15: PyMOL figure of hPDI bb'xa'. The recent crystal structure of **bb'xa'** (PDB ID: 3UEM. Wang *et al.* 2011), shows that a molecule of oxidised DTT is bound at the **b'** domain (shown in yellow).

1.3.1.8. Structural conformations associated with capping of the **b'** domain

Alternative examples of dynamic movements within the PDI structure have also been identified. The **x**-linker region, shown to be pivotal in the above conformational changes is found in at least two different conformations (Nguyen *et al.* 2008, Byrne *et al.* 2009). In the first species the **b'** substrate binding site is capped by the x-linker but in the second this interaction does not occur, giving rise to the uncapped species (see figure 1.16).

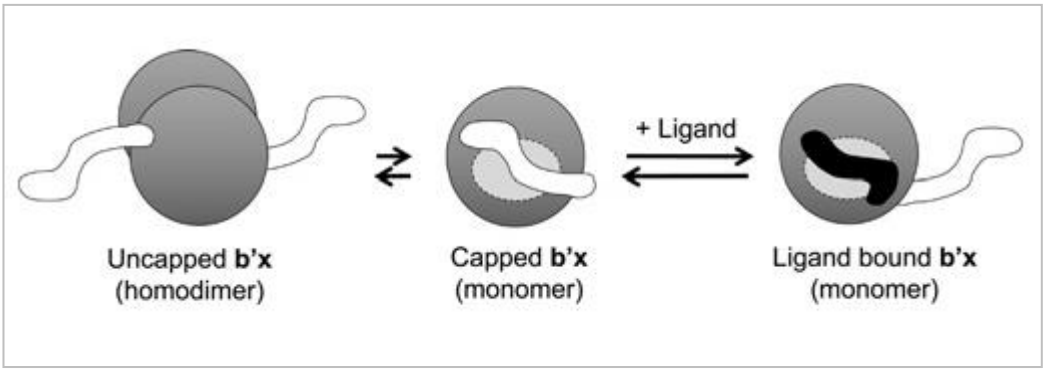

Figure 1.16: Alternative conformations of the x-linker region (taken from Byrne *et al*. 2009). When uncapped, the **b'x** molecule has a natural propensity to dimerise. In the capped form, the x-linker binds to the substrate binding site and this prevents dimerisation from occurring. In the presence of ligand, neither dimerisation nor x-linker binding occurs because the substrate binding site is already occupied.

Interestingly, in the presence of ligand (e.g. somatostatin) equilibrium is shifted towards the uncapped species suggesting a possible mechanism for substrate modulation (Byrne *et al.* 2009). Similar capping events have also been seen for other PDI family members including ERp44 which is capped by its C-terminal tail in a comparable manner (Wang *et al.* 2008).

Unlike the previous structural change there is no evidence to suggest that these capping/uncapping events are redox-regulated (Nguyen *et al.* 2008). In addition when looking at the X-ray structure of DTT-treated PDI it is clear that the majority of the **b'** binding site (defined by Byrne *et al.* 2009) is not in contact with the x-linker region. The same is true for the un-treated PDI structure. This could indicate that the two types of conformational changes described here are unconnected. It might also imply that again molecules like DTT have competed successfully with the x-linker for binding at **b'** supporting a substrate binding induced model for conformational change in PDI.

1.3.2. The functional activities of hPDI

1.3.2.1. Disulphide bond chemistry *in vivo*

Disulphide bond formation is essential for protein folding and occurs in the periplasm of bacteria and the ER of eukaryotic cells. Spontaneous disulphide bond formation however, is very slow and therefore it is the role of oxido-reductases such as PDI and other PDI family members to catalyse this reaction *in vivo* (Anfinsen, 1973). The catalytic activities of PDI that enable this are: oxidation, reduction and isomerisation, i.e. the formation, breakage and rearrangement of disulphide bonds.

1.3.2.2. The catalytic active sites of PDI

Common to all oxido-reductases of the TRX family, the catalytic domains of PDI (**a** and **a'**) contain CXXC active site sequences. For PDI this is CGHC for both, but the exact active site sequence can vary between family members with some not having an active site at all (see figure 1.7). For PDI **a**, the N-terminal cysteine (C53) is essential for activity. Not only is it accessible (unlike the C-terminal cysteine), it also has a pK_a of 4.8 +/- 0.1 (Karala *et al.* 2010). This is particularly low (a typical cysteine residue has a pK_a of ~8.3) and means that at physiological pH (pH~7.3) the reactive thiolate form is stabilised. On account of this, PDI is able to act as an oxido-reductase and isomerase (see figure 1.17).

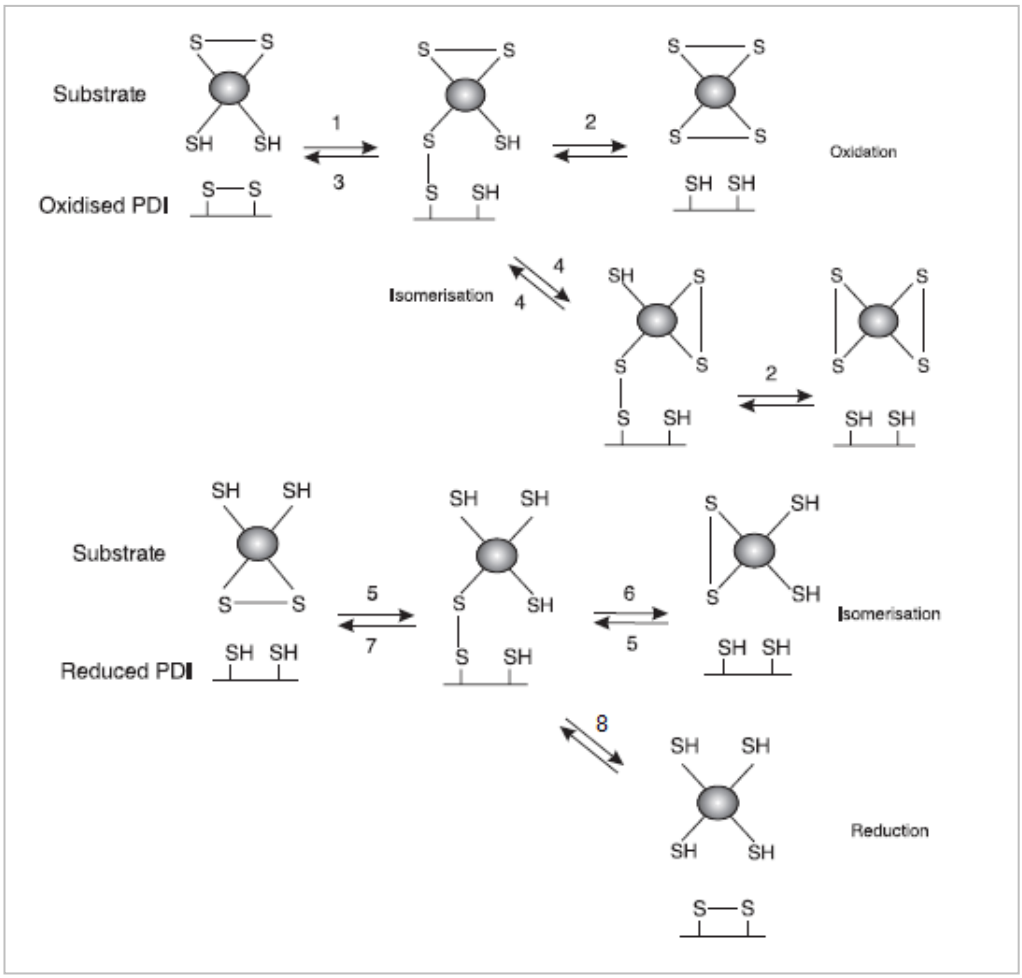

Figure 1.17: Oxidation, reduction and isomerisation reactions of PDI (taken from Hatahet and Ruddock, 2007). When PDI is oxidised: 1) A substrate thiol nucleophilically attacks the active site disulphide bond of PDI forming a mixed disulphide. From here there are 3 possible reactions 2, 3 & 4. 2) The substrate thiol can nucleophilically attack the disulphide bond of the mixed disulphide leading to formation of a disulphide bond in the substrate and reduction of the PDI active site. 3) The C-terminal cysteine could also nucleophillically attack the mixed disulphide leading to re-formation of the PDI active site disulphide bond and leaving the substrate cysteine in the reduced state. 4) Finally a substrate thiol could nucleophilically attack the substrate disulphide i.e. isomerisation. When PDI is reduced: 5) The N-terminal thiol group of PDI nucleophilically attacks the substrate disulphide. This gives rise to formation of a mixed disulphide. Again there are 3 possible reactions 6, 7 & 8. 6) Nucleophilic attack of a different substrate thiol on the mixed disulphide leading to isomerisation in the substrate. 7) Nucleophilic attack by the substrate thiol on the mixed disulphide to give rise to reduced PDI and a disulphide bond in the substrate protein. 8) Or finally, nucleophilic attack by the C-terminal cysteine of PDI on the mixed disulphide leasing to reduction of the substrate thiol and disulphide formation in PDI.

The requirement for the C-terminal cysteine however, is much more complex. While a low pK_a at this position favours reduction and the last step in oxidation, it has an

inhibitory effect on earlier steps in the oxidation pathway and also isomerisation (see figure 1.17). The actual pK_a of the C-terminal cysteine of PDI **a** (C56) is ~8.6 +/-0.0 and so in order to meet the requirements described previously, it must be modulated by nearby residues (Karala *et al*. 2010). Molecular dynamic simulations indicated that the residue most likely to display this activity was R120 and this was supported in later work by the same group (Lappi *et al*. 2004, Karala *et al*. 2010).

R120 is highly conserved in the catalytic domains of PDI family members (PDI, PDIp, ERp57, ERp72, P5 and PDIr) and is located on a loop between β5 and α4 (Lappi *et al*. 2004). *In silico* studies have suggested that in PDI *in vivo*, this loop can have alternative conformations leading to its movement in and out of the active site locale. Consequently, when R120 is in proximity of the active site, it may stabilise the thiolate state of the C-terminal cysteine via electrostatic interactions with its positively charged side chain (Lappi *et al.* 2004). In support of this hypothesis, mutations in R120 lead to a significant increase in pK_a and thus these mutants are also less active in the peptide oxidation assay (Karala *et al*. 2010, Lappi *et al.* 2004).

The two catalytic domains of PDI share high sequence identity, especially around the active site. Therefore, despite the fact that the pK_a's of the **a'** active site cysteines have not been determined, it is likely that they are comparable to the pK_a of C53 and C56. In addition there is no evidence to suggest that the **a'** domain of PDI is any less active as an oxido-reductase than PDI **a**, although clearly there is some positional benefits of being at the C-terminus of the molecule adjacent to the ligand binding **b'** domain (Wang *et al.* 2008).

1.3.2.3. Influences on redox activity

The activity of all thioredoxin family oxido-reductases (including PDI), is determined by the standard redox potential of the disulphide/dithiol pair formed by the two active site cysteines. This is highly variable within the PDI family, and the stability of the active site disulphide can vary by up to 7 kcal/mol, equivalent to a 10^5 fold difference in the equilibrium constant (Kortemme *et al.* 1996). For the **a** and **a'** domains of PDI, the redox potentials are -163mV and -169mV respectively

(Chambers *et al.* 2010). Contributing to these redox potentials and subsequently the –SH/S- equilibria, are the two residues between the active site cysteines i.e. Gly54 and His55.

As the pK_a of the N-terminal cysteine of PDI **a** is very low, its thiolate state must be stabilised by nearby positive charges. As discussed previously, interaction with R120 on the loop between β5 and α4 is probably very important for this but it is likely that the imidazole group of H55, immediately adjacent to the C-terminal cysteine also plays a stabilising role (Lappi *et al.* 2004, Karala *et al.* 2010, Kortemme *et al.* 1996). In support of this, the pK_a of the imidazole group of H55 is altered in the presence and absence of a C53 thiolate ion indicating that when exerting a stabilising effect on the thiolate ion, it too is stabilised (Kortemme *et al*. 1996). Furthermore this histidine residue is conserved in DsbA, confirming that it may be important for stabilising the N-terminal thiolate ion and promoting oxidase activity.

The importance of the residues at positions 2 and 3 in the Cys_1-Xaa_2-Xaa_3-Cys_4 motif can be seen by studying the activities of thioredoxin and DsbA, which have the active site sequences CGPC and CPHC respectively. In both cases, the active site differs from that of PDI by just one amino acid but contributes to pK_a's for the N-terminal cysteines of 6.3+/-0.1 and 3.4+/-0.2 for thioredoxin and DsbA respectively (Forman-Kay *et al.* 1992, Bardwell *et al*. 1991, Grauschopf *et al.* 1995). The net effect of this is that thioredoxin predominantly acts as a reductase and DsbA as an oxidase.

Interestingly, mutation of the thioredoxin active site to that of PDI (CGPC to CGHC) increases the redox potential (from -270mV to -235mV), lowers the pK_a of the N-terminal cysteine, decreases reductase activity and improves isomerase activity (Krause *et al.* 1991, Lundstrom *et al.* 1992). Similarly, mutation of the PDI active site (CGHC to CGPC), increases the pK_a of the N-terminal cysteine and has a negative effect on its oxidase and isomerase activities (Chambers *et al.* 2010). For DsbA however, mutation of its active site (CPHC to CGHC) reduces the reduction potential and increases the pK_a of the N-terminal cysteine, making it less active as an oxidase (Huber-Wunderlich and Glockshuber, 1998). Hence it is clear that the residues between the catalytic cysteines of the active sites of PDI, thioredoxin and

DsbA contribute to maintaining the redox potential and also the catalytic activity of the enzymes. Furthermore a high pK_a value for the N-terminal cysteine promotes reductase activity and a low pK_a value, oxidase activity.

1.3.2.4. Roles of additional regions of PDI in activity

The isolated **a** and **a'** domains have limited catalytic activity of protein substrates; the sum of which does not equal the total activity of PDI. For example, in their studies of the disulphide bond rearrangement of BPTI, Darby *et al.* (1998) saw no/negligible activity for the isolated **a** and **a'** domains despite them being wholly responsible for the isomerase activity in the full-length protein. In the presence of **b'** however, activity is markedly improved suggesting that substrate binding is essential for complicated disulphide isomerisations of larger protein substrates (Darby *et al*. 1998, Klappa *et al*. 1998a). Subsequently the minimal requirement for disulphide bond rearrangement is **b'xa'** and maximal isomerisation efficiency is seen in constructs containing all 4 domains (Darby *et al.* 1998). This work is indicative of synergy between the thioredoxin-like catalytic and ligand binding domains of PDI (Freedman *et al*. 2002).

1.3.2.5. The chaperone activity of PDI

Alongside its activity as a protein folding catalyst, PDI also exhibits molecular chaperone activity. Although this activity complements the catalytic activity of PDI, it is actually independent of it and consequently, PDI is able to prevent the aggregation of proteins that do not have disulphide bonds e.g. D-glyceraldehyde-3-phosphate dehydrogenase (GAPDH) (Cai *et al.* 1994).

Unlike the oxido-reductase and isomerase activities of PDI for which the catalytic sites are fundamental, the **b'** domain has been shown to be essential for chaperone activity. Furthermore the addition of a small peptide substrate that binds to PDI **b'** is able to completely abolish chaperone activity (Quan *et al*. 1995). This is perhaps an over simplification however, and chaperone activity is probably linked to the

interaction of non-native protein with the hydrophobic surface that spans the inside of the 'u' shaped structure of PDI (Wang *et al.* 2012). Certainly it has recently been shown that the oxidised 'open' form of PDI exhibits greater chaperone activity than the reduced form (Wang *et al.* 2011).

1.4. Pancreas-specific PDI (PDIp)

1.4.1. Identification of PDIp and observation of its domain architecture

1.4.1.1. Initial identification of PDIp

PDIp is a relatively newly identified PDI family member having been identified for the first time in 1996 (Desilva *et al.* 1996). Located on chromosome 16p13.3, initial studies of the PDIp gene (Pa-1) suggested that it encoded an ORF of 511 amino acids. As no in-frame stop codon was identified and a typical ER signal sequence was lacking, authors agreed that the assigned ATG start was tentative (Desilva *et al.* 1996). This has now been resolved and it seems that Pa-1 is the product of an aberrant recombination event that led to introduction of an incorrect start codon (Walker *et al.* 2012). Figure 1.18 explains how this may have occurred.

Figure 1.18: Comparison of Pa-1 cDNA with correct PDIp cDNA (taken from Walker *et al.* 2012). The region of reverse homology is shown in red. Direct homology is shown in blue.

Unfortunately, the incorrect Pa-1 construct has been used in a number of published studies of the activities and binding properties of PDIp. It is known that this incorrect form of PDIp has increased propensity to dimerise on account of a cysteine residue in its uncleaved signal peptide (Fu and Zhu, 2009a). Thus, recently published studies on the activity and binding properties of PDIp (that use the Pa-1 construct) must be considered with caution.

1.4.1.2. The domain architecture and unusual **a'** active site sequence of PDIp

Like PDI and ERp57, PDIp has 4 thioredoxin-like domains and **abb'a'** domain architecture (Hatahet and Ruddock 2007). It shares 45% sequence identity with PDI and despite a distinct lack of structural information available, is anticipated to have a similar 3-dimensional structure (Ferrari and Söling, 1999). In addition, PDIp has an extended N-terminus which is very negative charged. The implications of this are unknown.

Perhaps one of the most significant differences between PDI and PDIp, is the Gly to Thr substitution seen in the **a'** active site of PDIp (CTHC instead of CGHC). Although seemingly unimportant, changing the dipeptide between active cysteines residues (from CGHC) can have major side effects for the reactivity of the protein (as described previously for DsbA and thioredoxin). Furthermore, the presence of a Thr residue at position 2 in the **a'** active site of PDIp may prevent stabilising interactions between the N-terminal Cys and active site His due to steric hindrance. The net result of this would be that the pK_a of the **a'** domain N-terminal cysteine is increased leading to a reduction in reactivity (relative to the **a** domain that has a CGHC active site).

1.4.2. Localisation of PDIp: cellular and physiological

1.4.2.1. The cellular location of PDIp

Full length PDIp is a 525 amino acid protein with both a 21 amino-acid signal peptide and a KEEL ER-retention signal. Unlike PDI and ERp57, PDIp is found exclusively in the ER (Walker *et al*. 2012). Captivatingly, when expressed in transfected HeLa cells, both wild-type and glycosylation-null PDIp co-localise with calreticulin, an ER marker but not ERGIC53 a marker for the ER-Golgi intermediate compartment. This indicates that none of the 3 N-linked glycans of PDIp (located in **a, b'** and **c)** are modified by Golgi-resident enzymes. This was further confirmed by sensitivity of wild-type PDIp to PNGase F and Endo H (Walker *et al*. 2012).

1.4.2.2. The physiological location of PDIp

The exact location(s) of PDIp expression is disputed in the literature. Early Northern blot studies observed PDIp mRNA in (human) pancreatic acinar cells but not brain, pituitary gland, lymph node, thyroid, thymus, lung, liver, kidney, spleen, testes or stomach (Desilva *et al*. 1996). Furthermore, this restricted expression pattern was later confirmed via Western analysis and also a radio-labelled somatostatin binding assay (Klappa *et al.* 1998b). In contrast to these results, RT-PCR has since been used to identify low levels of PDIp expression in the human brain (Conn *et al.* 2004). It is likely that the increased sensitivity of RT-PCR over blotting techniques (used previously) has made this possible and it would be interesting to determine other tissues exhibiting low level PDIp expression that may have been formerly overlooked.

More recently PDIp expression has also been observed in (mouse): liver, kidney, lung, uterus, stomach, caecum and ileum by Western blot (shown in figure 1.19) (Fu *et al.* 2009). This is opposed to previous data that saw no expression of PDIp in (rat): liver, kidney, lung, reproductive organs or intestinal tract also by Western blot (Klappa *et al.* 1998b). At this time it is not possible to explain these conflicting results but it is interesting that PDIp expression seems to be specific to secretory

cells e.g. pancreatic acinar cells, chief cells in the stomach and paneth cells in the ileum (Fu *et al.* 2009b).

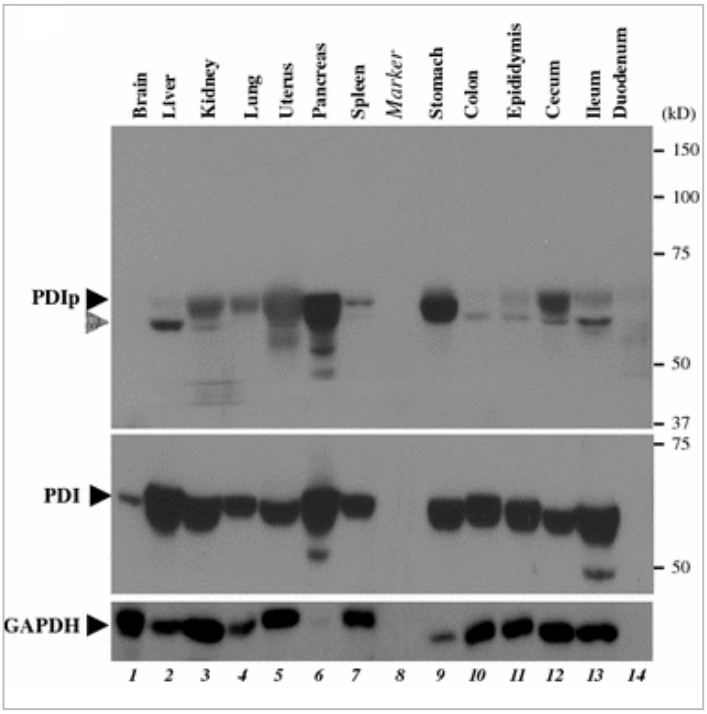

Figure 1.19: Comparison of PDI and PDIp expression in various mouse tissues by Western blot (taken from Fu *et al.* 2009b). Shaded arrow probably indicates unglycosylated PDIp.

Interestingly, Western and Northern blots show that PDIp is expressed (protein and mRNA respectively) in the stomachs of auto-immune regulator (AIRE) deficient NOD mice (Niki *et al.* 2006). NOD mice are typically used as an animal model for Type-1 diabetes and classically exhibit islet cell destruction, but in AIRE-deficient NOD mice, acinar cells are targeted instead. Furthermore PDIp (both from mouse serum and also the recombinant protein) acts as an auto-antigen in these mice (Niki *et al.* 2006). These results may indicate that non-acinar cell expression of PDIp occurs in diseased tissues following induction of the UPR.

Therefore the physiological role of PDIp may be to ensure correct folding of secretory molecules such as zymogens thereby preventing cellular stress and induction of the UPR caused by the heavy work load of the secretory cell (discussed later). Furthermore, this function is likely to be independent of PDI which is

ubiquitously and abundantly expressed in all tissues including the exocrine pancreas as it is improbable that PDIp would have been evolutionarily conserved otherwise.

1.4.2.3. PDIp expression during *Xenopus* development

Pancreatic development is highly conserved in vertebrates and is regulated by signals from adjacent tissues such as the mesenchyme (Sogame *et al.* 2003, Golosow and Grobstein, 1962).

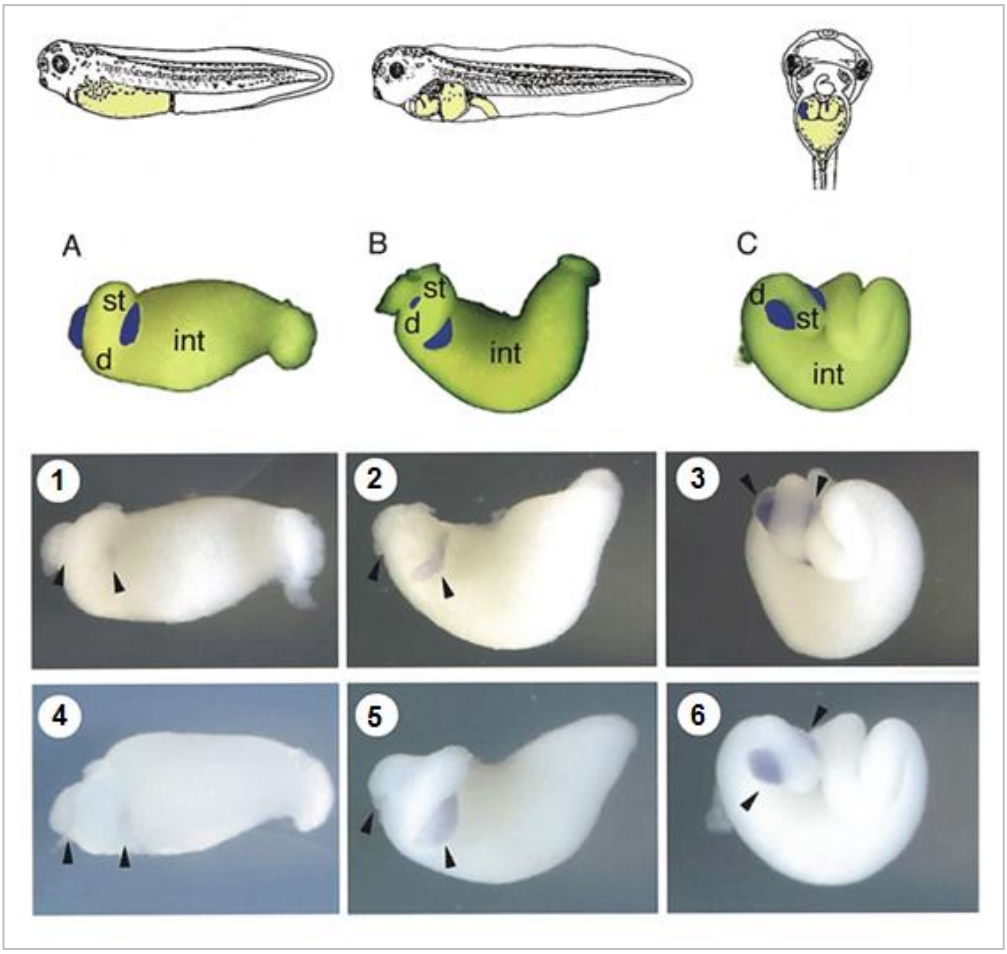

Figure 1.20: Development of the pancreas and expression patterns for *PE2* and *PDIp* (adapted from Sogame *et al*. 2003). A-C: Schematic diagrams of gut tubes taken from tadpoles. All associated endodermal organs except the pancreas have been removed for clarity. The developing pancreas is shown in blue. A) Stage 40 embryo, B) stage 42 embryo and C) stage 44 embryo. 1-6: Expression patterns of *PE2* and *PDIp* in the gut tubes of tadpoles; examined by *in situ* hybridisation. 1) *PE2* expression, stage 40, 2) *PE2* expression, stage 42, 3) *PE2* expression, stage 44, 4) *PDIp* expression, stage 40, 5) *PDIp* expression, stage 42 and 6) *PDIp* expression, stage 44.

During pancreatic development, PDIp cDNA is first detected at embryonic stage 40 and is much stronger by stage 42 (see figure 1.20). This coincides with the development and finally the fusing of the ventral buds and overlaps significantly with the expression of pancreatic elastase 2 (PE2) cDNA (Sogame *et al.* 2003).

This work indicates that expression of both *PDIp* and *PE2* occurs during the late stages of pancreatic development. This is consistent with studies showing that transcription of exocrine enzymes occurs later than that of endocrine hormones (Debas, 1997). The co-expression of *PDIp* and *PE2* may indicate that as hypothesised, the physiological role of PDIp is to ensure the correct folding of pancreatic zymogens (Klappa *et al.* 1998b).

1.4.3. PDIp, cellular stress and disease

1.4.3.1. PDIp and the Unfolded Protein Response (UPR)

Despite the preferential expression of PDIp in the pancreatic acinar cells, there is increasing evidence for its role in the UPR in other tissues. For example, expression of PDIp mRNA is up-regulated following MPP^+ treatment of retinoic acid differentiated SH-SY5Y neuroblastoma cells whereas that of other PDI family members (PDI, PDIR, P5, ERp29, ERp44, ERp57 or ERp72) was not (Conn *et al*. 2004). Similar results were seen for two known proteasome inhibitors lactacystin and MG115, but not H_2O_2 or canavanine which cause oxidative stress and the accumulation of misfolded proteins respectively (Conn *et al*. 2004). Furthermore MPP^+ and lactacystin treatment of cell lysates also results in up-regulation of PDIp protein expression although to a lesser extent (shown by Western blot). This is probably due to a reduction in translation caused by ER stress. This work suggests a role for PDIp in proteasomal impairment although currently there is no evidence of PDIp being present in the cytosol (Walker *et. al* 2012).

Immunohistochemistry of diseased human brains (Parkinson's disease, Dementia with Lewy bodies and Altzheimer's Disease) shows the presence of PDIp within

some Lewy bodies (LBs) but not in senile placques or neurofibrillary tangles (Conn *et al*. 2004). Approximately 57% of α-synuclein immunostained LBs also stained positive for PDIp and the two have been shown to co-localise (see figure 1.21). Unpublished data from C.C. Wang (personal communication) shows that PDIp cannot inhibit formation of the α-synuclein fibril. Consequently it is likely that the presence of PDIp within LBs is circumstantial and a result of sequestration after up-regulation and the initial stress response.

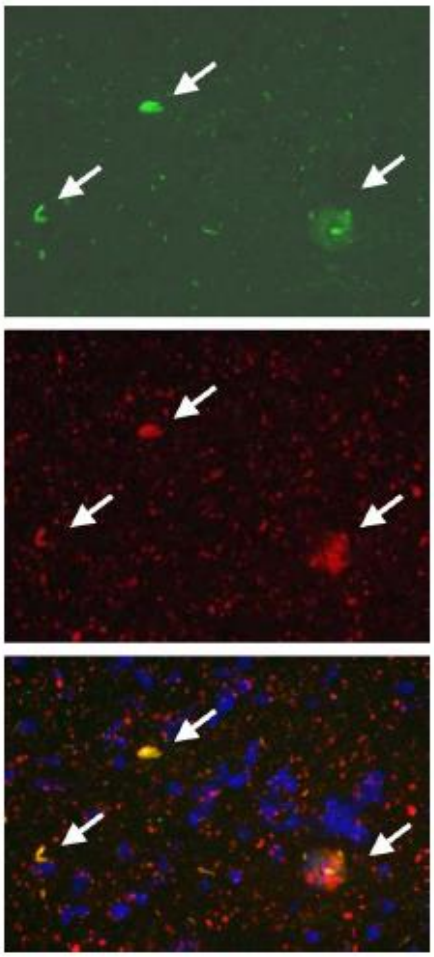

Figure 1.21: Co-localisation of α-synuclein and PDIp expression in human DLB substantia nigra (taken from Conn *et al*. 2004). SN tissue immunostained with PDIp (green) and α-synuclein (red). Overlaying immunoreactivity (yellow).

1.4.3.2. The role of XBP-1 activation in induction of PDIp expression

As described previously, the transcription factor XBP-1 is activated in times of cellular stress. XBP-1$^{-/-}$ Liv^{XBP-1} mice survive the embryonic lethality of XBP-1 deficient mice but exhibit severe abnormalities in secretory organs, particularly pancreatic acinar cells. While islet cells develop normally, acinii are poorly distributed and numbers of zymogen granules are reduced (Lee *et al.* 2005). In addition the ER is also poorly developed. This leads to reduced zymogen production and consequently mice with this phenotype die shortly after birth due to an inability to digest milk (Lee *et al.* 2005). On this basis it is likely that XBP-1 is essential for the development of highly secreting cells.

XBP-1 has previously been shown to induce ER-resident chaperone genes involved in the UPR (Lee *et al*. 2003). RT-PCR studies used to identify genes regulated by XBP-1 in the pancreas identified significantly reduced expression of Sec61α, EDEM, PDI and PDIp mRNAs in XBP-1$^{-/-}$ Liv^{XBP-1} mice (Lee *et al.* 2005). Expression of ERdj5, P5 and Grp58 mRNAs were unaffected and this is probably due to compensation by alternative pathways such as the ATF6 pathway.

Overall this work suggests that PDIp expression may be up-regulated by activation of XBP-1 and the UPR. It could also be evidence of a role for PDIp in zymogen production as postulated previously (Ruddock *et al.* 1998).

1.4.3.3. PDIp and Cancer

Although PDIp is abundantly expressed in pancreatic tissue, its expression is absent from pancreatic tumour cell lines (Fu *et al*. 2009). Furthermore, PDIp expression was not detected in 17 out of 18 human pancreatic duct adenocarcinoma samples and this indicates that the disappearance of PDIp may be associated with the development of disease (Fu *et al.* 2009). Figure 1.22 shows the results of immunohistochemical staining of PDIp in various different human pancreatic tissue samples.

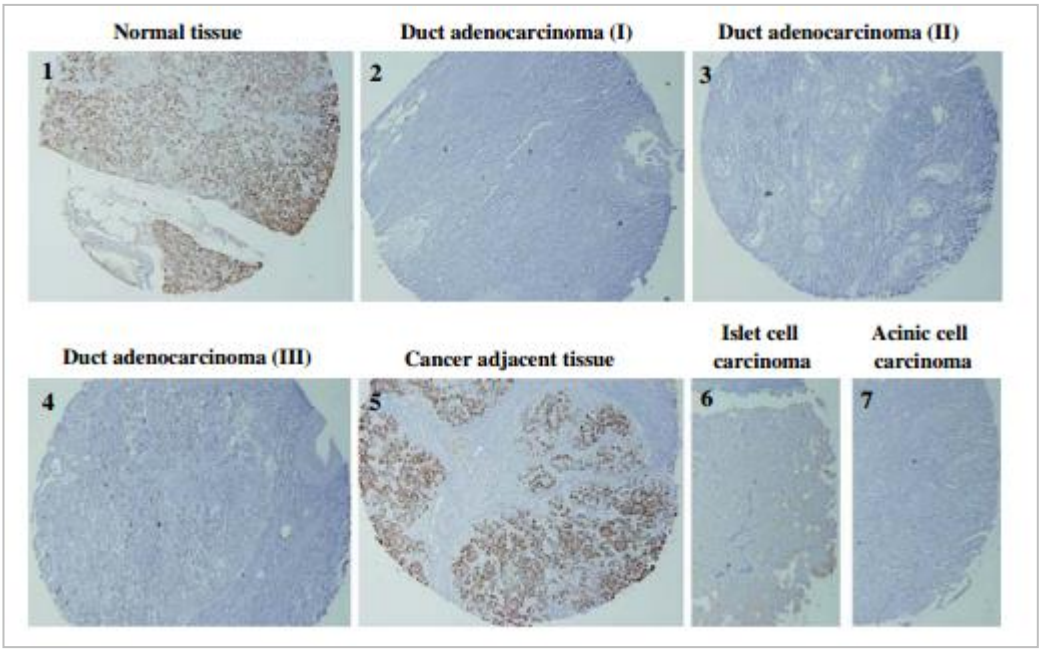

Figure 1.22: Immunohistochemical staining of human pancreatic tissue (taken from Fu *et al.* 2009). Staining of normal tissue indicates high expression of PDI (1). In duct adenocarcinoma, islet cell carcinoma and acinic cell carcinoma there is no staining, indicating that PDIp is not expressed (2, 3, 4, 6 & 7). However PDIp staining is seen in cancer adjacent tissue (5) indicating that loss of PDIp may be indicative of disease onset.

From figure 1.22 it is clear that expression of PDIp was absent from all cancerous tissues tested. Interestingly, PDIp was still expressed in cancer adjacent tissue and authors have suggested therefore that loss of PDIp expression could be used as a biological marker for pancreatic cancer (Fu *et al*. 2009). Currently the relationship between PDIp expression and cancer is poorly understood. Based on the medical implications of this work, it probably warrants further investigation.

1.4.4. The unique substrate binding specificity of PDIp

1.4.4.1. Binding studies of PDIp

Early studies showed that like PDI, PDIp only interacts with non-native proteins. Moreover these reactions are independent of cysteine residues within the ligand or presence of glycans. When ERp57 is inhibited in canine pancreatic microsomes, cross-linking to PDI and PDIp is increased (Elliott *et al.* 1998) indicating that PDI family members exhibit some degree of functional redundancy. Consequently it is difficult to understand the cellular requirement for a pancreas specific-PDI, but determining a natural substrate may aid elucidation of a physiological role.

The substrate binding properties of PDIp have been determined by measuring the ability of various ligands to inhibit Δ-somatostatin binding to PDIp. From these studies it has been possible to define the minimal requirement for ligand binding to PDIp as a hydroxyl-aryl group (Klappa *et al.* 1998b, Ruddock *et al.* 2000, Klappa *et al*. 2001). This is in stark contrast to PDI which exhibits broader substrate specificity linked to its role as a general folding catalyst and could be indicative of an exact role for PDIp that is also related to its unusual expression pattern. It is also clear that the presence of an N-glycan protruding from the putative substrate binding domain (**b'**) has no effect on ligand binding specificity with similar results being reported for both microsomal (rat, sheep and dog) and also recombinant PDIp (Klappa *et al.* 2001). The significance of this is not yet known.

As expected, only pentapeptides containing a tryptophan or tyrosine residue inhibited cross-linking of labelled peptides to PDIp although this was impeded if either residue was adjacent to an acidic amino acid. Similarly, single tryptophan or tyrosine residues could compete for binding but only if the C-terminus was modified (Ruddock *et al*. 2000). In addition compounds lacking a hydroxyl-aryl group and those with a modified hydroxyl-aryl group showed little or no competition for binding to PDIp at any concentration tested (Klappa *et al*. 2001). It is thus clear that PDIp requires only single amino acid recognition for ligand binding but that there is some additional specificity in regards to chemical environment.

In some cases, modification of the aromatic ring (particularly substitutions at the para position to –OH) can lead to reduced inhibition (Klappa *et al.* 2001). It is likely that these modifications decrease ligand binding by destabilising π-π interactions between the aromatic ring of the ligand and an aromatic ring structure in the substrate binding site of PDIp. Conversely, a 2-4C substituent at the para position to –OH improves substrate binding and this becomes further enhanced as alkyl chain length increases (Klappa *et al*. 2001). Clearly hydrophobic interactions are important for binding of substrate to PDIp but currently this is not well understood.

Various compounds containing a hydroxy-aryl group have been tested for their ability to inhibit cross-linker binding including synthetic peptides derived from digestive enzymes and also various oestrogens (Klappa *et al.* 1998b, Klappa *et al.* 2001). All enzyme derived peptides tested (synthetic peptides derived from pancreatic lipase, pancreatic α-amylase, cholesterol esterase etc) interacted with PDIp as did 17β-oestradiol, oestriol and oestrione (see figure 1.23) (Klappa *et al*. 1998b). Binding of 17β-oestradiol to PDIp was particularly tight (approximately stochiometric) and could inhibit the binding of synthetic digestive enzyme derived peptides (Klappa *et al*. 1998b). In this way high oestrogen concentration (i.e. during oestrogen replacement therapy or pregnancy) might modulate the activity of PDIp *in vivo*.

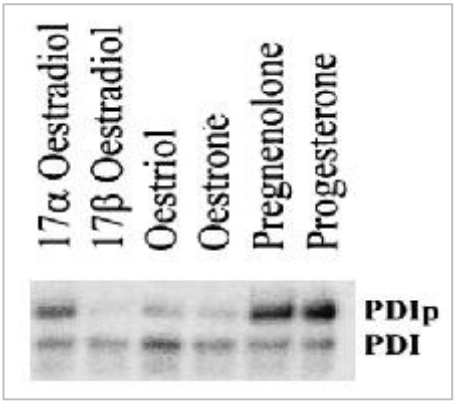

Figure 1.23: Oestrogens inhibit cross-linking of PDIp. Oestrogens were tested for their ability to prevent radiolabeled somatostatin from binding to PDIp (adapted from Klappa *et al.* 1998).

Interestingly, despite the high affinity for 17β-oestradiol, no significant interaction is seen for 17α-oestradiol and PDIp (Klappa *et al*. 1998b). This finding clearly indicates a complexity to substrate binding that is linked to structural and steric requirements rather than specific chemical groups.

1.4.4.2. PDIp as a modulator of intracellular oestrogen

It has been suggested that the physiological role of PDIp may be to act as an intracellular oestrogen modulator (Fu *et al.* 2012). This coincides with previous work that shows that PDIp is able to bind to 17-β-oestradiol *in vitro* (Klappa *et al.* 1998b, Fu and Zhu, 2009b and Fu *et al.* 2011). Further characterisation of this interaction shows that when PDIp and 17-β-oestradiol are separated from a crude pancreatic cell lysate, the apparent K_d for their interaction is ~150nM (Fu *et al.* 2012). There are a number of issues with the hypothesis that PDIp and 17-β-oestradiol would interact *in vivo*: 1) recent data shows that PDIp is exclusively expressed in the ER of the cell (Walker *et al*. 2012). There is currently no data for 17-β-oestradiol in the rough ER, indicating that its concentration may be negligible or insufficient for interaction with PDIp. 2) The normal concentration of 17-β-oestradiol in the blood serum of a fertile woman is <1.5nM. Consequently very little/no interaction would be seen *in vivo* according to the specified K_d (Akerlund *et al.* 1981). 3) No difference in PDIp expression was seen between male and female rats, whereas oestrogen concentration is significantly higher in females (Fu *et al.* 2009).

Although 17-β-oestradiol is probably not the physiological substrate of PDIp itself, it may help to mediate the interactions of PDIp with proteins that are. One suggestion is that PDIp is involved in the folding of acinar cell-specific proteins such as the pancreatic zymogens. This may explain conditions such as hyperemesis (morning sickness) which are associated with an increase in blood serum oestradiol concentration (Baron *et al*. 1993). Presently, the role of molecular chaperones in folding pancreatic zymogens has not been studied but it is clear that for prochymosin (zymogen found in the stomach), refolding efficiency is increased from 2% to 28% in the presence of PDI (Wei *et al*. 2000). Furthermore with the high secretory output

of the acinar cells, chaperones would be essential to ensure correct folding and reduce the toxicity caused by misfolded proteins.

1.4.4.3. The oestradiol binding site of PDIp

Similar to the interaction of PDI and its substrates, binding of oestradiol occurs predominantly at the **b'** domain of PDIp. Unlike for PDI however, some binding also occurs in the **b** domain and it seems that both the **b** and **b'** domains are important for efficient binding of 17-β-oestradiol (Fu *et al*. 2011).

Computational modelling analysis, using the solution structure of PDI **bb'** (Denisov *et al*. 2009), showed that the binding pocket of PDIp was similarly located to that shown for PDI in work by Byrne *et al.* (2009). Furthermore, using a combination of mutagenesis and molecular modelling, authors were able to identify PDIp His278 as a residue essential for the interaction between PDIp and 17-β-oestradiol (Fu *et al*. 2011). Unpublished data by the RBF group however shows that the PDIp H278A mutation is destabilising and therefore suggests that further investigation is required.

1.4.4.4. The functional activities of PDIp

Although the functional activities of PDIp have been studied quite extensively, much of the work has been performed using the incorrect Pa-1 construct. This construct gives rise to protein with an un-cleaved signal peptide: MASCPWG. The presence of an additional cysteine residue at the N-terminus leads to aberrant formation of an inter-subunit disulphide bond and therefore increased dimerisation (Fu and Zhu, 2009a). As a consequence of this, studies of activity that use the incorrect Pa-1 construct must be considered with caution and will not be discussed here.

PDIp is able to bind to scrambled RNAse but not native protein indicating that like PDI, it too has chaperone activity (Klappa *et al*. 1998b, Ruddock *et al.* 1998). This activity was later assigned to the **bb'** domains by Fu and Zhu (2010) having studied the PDIp **bb'** domain construct for its ability to suppress aggregation of GAPDH.

There is very little published data for the oxido-reductase and isomerase activities of wild-type PDIp. In a peptide oxidase assay however, PDIp was ~50% as active as PDI and had unusual pH dependence compared to other PDI family members (Alanen *et al*. 2006). The low activity of PDIp in this assay could be due to the unusual CTHC active site sequence in the **a'** active site. Certainly it is well known from studies of the active sites of thioredoxin and DsbA that the residues between catalytic cysteines are important for defining their reactivity (see previously).

1.5. Aims of this study

This chapter has introduced protein folding and the quality control systems that regulate protein folding in the ER. The role of protein disulphide isomerase (PDI), an abundant ER-resident molecular chaperone has also been discussed. This protein is the most characterised member of the PDI family; a family categorised by their intracellular location and structural homology to thioredoxin. PDIp, a PDI family member with identical domain architecture to PDI, is by comparison, very poorly characterised.

Using comparisons to PDI, this work aims to investigate the redox-mediated conformational changes and oxido-reductase activity of PDIp (*in vitro*) in order to improve understanding of this otherwise poorly characterised PDI family member. This is important because the majority of available data for recombinant PDIp uses an aberrant DNA construct.

The aims of this work can be broken down as follows:

1. Identify suitable conditions for optimal expression, purification and storage of PDIp and PDIp constructs.

2. Characterise the redox-mediated conformational changes and oxido-reductase activity of wild-type PDIp relative to PDI using far UV CD, limited proteolysis, DLS and the insulin reduction assay.
3. Identify regions within PDIp that contribute to its redox-mediated conformational changes and activity using both chimera proteins and active site mutants.
4. Examine the role of the **a** domain in the oxido-reductase activity of PDIp using stopped flow pK_a determination and oxidase/reductase assays.

It is hoped that studying PDIp (as described above) will facilitate understanding of its role within the exocrine pancreas and perhaps enable identification of physiological substrates.

Chapter 2. Materials & Methods

2.1. Molecular Biology

2.1.1. Clone list and primer design

2.1.1.1. The pET 23b vector

All constructs were cloned into a pET 23b vector (Novagen) between the NdeI and SalI sites of the multiple cloning region (see figure 2.1). This vector also has ampicillin resistance, conferred by base pairs 2211-3068.

The vectors used for this work have been modified slightly to add coding for an N-terminal hexa-His tag and also a ribosome binding site between the NdeI and XbaI sites of the multiple coding region (courtesy of Lloyd Ruddock). The His-tag is not removed after protein purification because there is no evidence to suggest that it has a negative effect on the structure/function of any of the proteins tested. All plasmids were stored in DH5α cells and transformed into BL21(DE3)pLysS competent cells for expression.

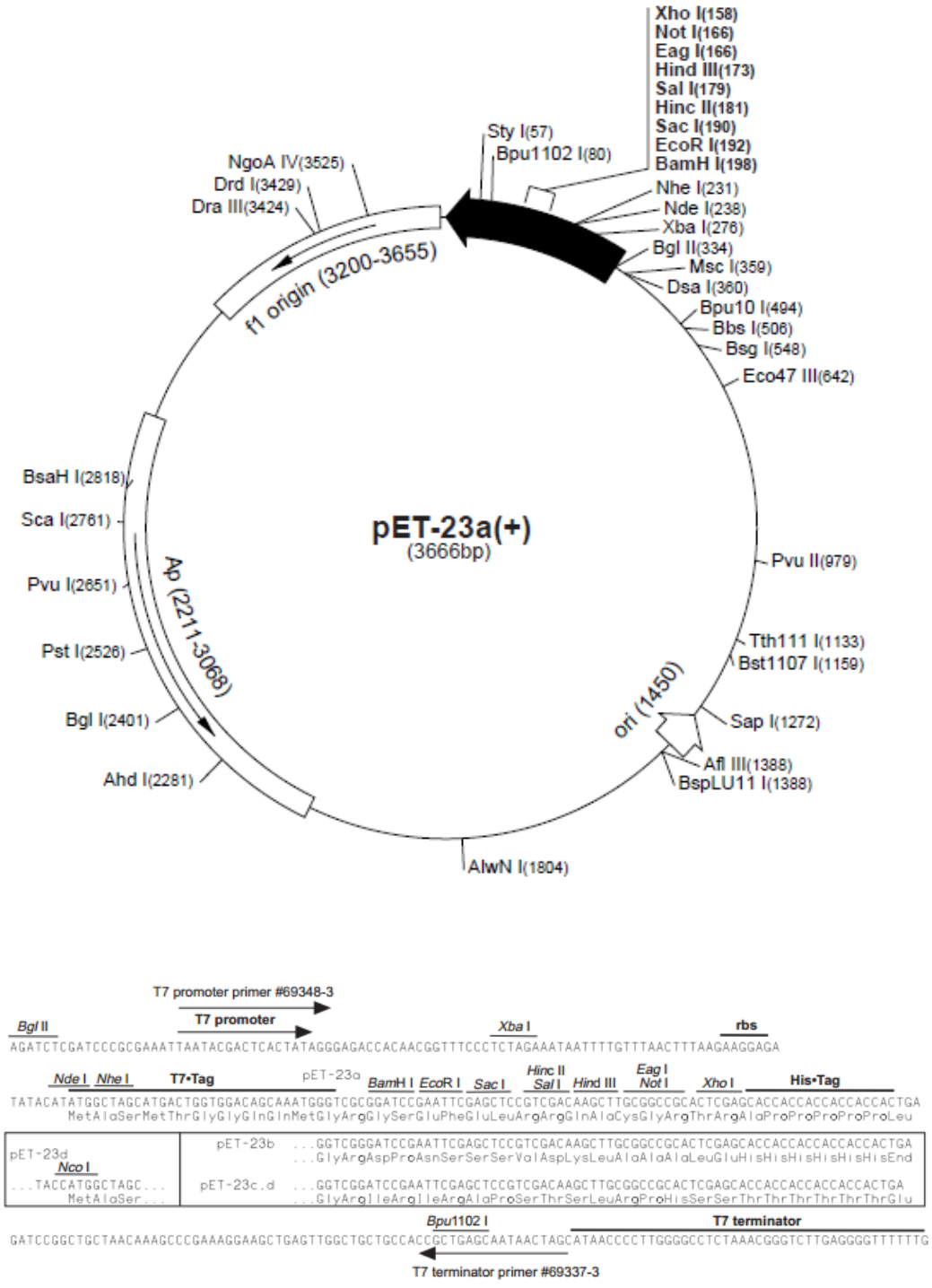

Figure 2.1: Vector map showing pET- 23a (+) vector (Novagen). pET- 23b is identical to pET- 23a except that it lacks a base pair just after the BamHI site (198) making it a 3665bp plasmid. Furthermore the region between NdeI and XbaI contains coding for an N-terminal hexa-Histidine tag and also a ribosome binding site. This alteration has been designed to improve protein expression levels.

2.1.1.2. PDI/PDIp clone list

Table 2.1. lists the PDI/PDIp constructs used in this study. Constructs identified by pKLW were designed and created specifically for this work.

Plasmid	**Protein**	**Donor**
pLR188	PDIp **b'xa'c**	Prof. Lloyd Ruddock
pLR330	PDIp	Prof. Lloyd Ruddock
pRF631	PDI	Prof. Lloyd Ruddock
pLR1368	PDIp **a**	Prof. Lloyd Ruddock
pLR1370	PDIp **a'**	Prof. Lloyd Ruddock
pKLW1	PDIp (K40-L525)	N/A
pKLW2	PDI H256A	N/A
pKLW3	PDIp H278A	N/A
pKLW4	PDIp R300H	N/A
pKLW5	PDIp **a** C71S	N/A
pKLW6	PDIp **a** C74A	N/A
pKLW7	PDIp C71S	N/A
pKLW8	PDIp C418S	N/A
pKLW9	PDIp C421A	N/A
pKLW10	PDIp C71S C74A	N/A
pKLW11	PDIp C71S C74A C364S	N/A

pKLW12	PDIp C71S C74A C418S	N/A
pKLW13	PDIp C71S C74A C421A	N/A
pKLW14	PDIp **a** W146F	N/A
pKLW15	PDIp K40- L525 Q75K	N/A
pKLW16	PDIp **a** Q75K	N/A
pKLW17	PDIp **a** Q75K W146F	N/A
pKLW18	PDIp **a** C71S Q75K	N/A
pKLW19	PDIp **a** C74A Q75K	N/A
pAKW5	PDIp (**ab**) PDI (**b'xa'c**)	Dr. Katrine Wallis
pAKW6	PDIp T419G	Dr. Katrine Wallis
pAKW11	PDIp (**ab**) PDI (**b'x**) PDIp (**a'c**)	Dr. Katrine Wallis
pAKW12	PDIp (**ab**) PDI (**b'x**) PDIp (**a'c**) T419G	Dr. Katrine Wallis

Table 2.1: Description and details of PDI.PDIp constructs used in this study.

2.1.1.3. Primer list

Clone	Mutagenesis Protocol	Forward Primer	Reverse Primer
pKLW1	Truncation PCR	CTGACTACCATATGAAGGAGGATGGGATCTTGGT	GACATGTCGTCGACTTATTACAGTTCCTCC
pKLW2	QuikChange	GGAGGTGAAATCAAGACTGCCATCCTGCTGTTCTTGCCCAAG	CTTGGGCAAGAACAGCAGGATGGCAGTCTTGATTTCACCTCC
pKLW3	QuikChange	CGCGGCCAGGATCCTCAACGCCCTGCTGCTCTTTGTCAACCAG	CTGGTTGACAAACAGCAGCAGGGCGTTGAGGATCCTGGCCGCG
pKLW4	QuikChange	GCCGACAATGAGCGCGTGCTGCAGTACTTTG	CAAAGTACTGCAGCACGCGCTCATTGTCGGC
pKLW5	QuikChange	GAATTCTATGCCCCGTGGAGTGGGCACTGCCAGGCCCTG	CAGGGCCTGGCAGTGCCCACTCCACGGGGCATAGAATTC
pKLW6	QuikChange	GCCCCGTGGTGTGGGCACGCCCAGGCCCTGGCCCCCGAG	CTCGGGGGCCAGGGCCTGGGCGTGCCCACACCACGGGGC
pKLW7	3 step SDM	1. GAATACCATATGCAGGAACAGGGAGCGCGTAGCCCG	1.CAGGGCCTGGCAGTGCCCACTCCACGGGGCATAGAATTC
		2. GAATTCTATGCCCCGTGGAGTGGGCACTGCCAGGCCCTG	2.GTTGACAAACAGCAGCAGGTGGTTGAGGATCCTGGC
		3. GAATACCATATGCAGGAACAGGGAGCGCGTAGCCCG	3.GTTGACAAACAGCAGCAGGTGGTTGAGGATCCTGGC
pKLW8	3 step SDM	1. GCCAGGATCCTCAACCACCTGCTGCTGTTTGTCAAC	1. CATCTCCTTGCAGTGGGTGCTCCACGGGGCATAGAACTT
		2. AAGTTCTATGCCCCGTGGAGCACCCACTGCAAGGAGATG	2.CTAGATGTCGACCTACAGTTCCTCCTTGGACCCCAT
		3. GCCAGGATCCTCAACCACCTGCTGCTGTTTGTCAAC	3.CTAGATGTCGACCTACAGTTCCTCCTTGGACCCCAT
pKLW9	3 step SDM	1. GCCAGGATCCTCAACCACCTGCTGCTGTTTGTCAAC	1. GGCAGGGGCCATCTCCTTGGCGTGGGTGCACCACGGGGC
		2. GCCCCGTGGTGCACCCACGCCAAGGAGATGGCCCCTGCC	2.CTAGATGTCGACCTACAGTTCCTCCTTGGACCCCAT
		3. GCCAGGATCCTCAACCACCTGCTGCTGTTTGTCAAC	3.CTAGATGTCGACCTACAGTTCCTCCTTGGACCCCAT
pKLW10	3 step SDM	1. GAATACCATATGCAGGAACAGGGAGCGCGTAGCCCG	1. GGCCTGGGCGTGCCCACTCCACGGGGCATACAA
		2. TTCTATGCCCCGTGGAGTGGGCACGCCCAGGCC	2.GTTGACAAACAGCAGCAGGTGGTTGAGGATCCTGGC
		3. GAATACCATATGCAGGAACAGGGAGCGCGTAGCCCG	3.GTTGACAAACAGCAGCAGGTGGTTGAGGATCCTGGC
pKLW11	QuikChange	TCCATCACTGCTTTCAGCCATGCAGTCCTCAAC	GTTGAGGACTGCATGGCTGAAAGCAGTGATGGA
pKLW12	Digest & Ligation	N/A	N/A
pKLW13	Digest & Ligation	N/A	N/A
pKLW14	QuikChange	GAGGGCATTGCCGAGTTTCTGCGTCGCCGCGTG	CACGCGGCGACGCAGAAACTCGGCAATGCCCTC
pKLW15	QuikChange	GGTGTGGGCACTGCAAGGCCCTGGCCCCCGAG	CTCGGGGGCCAGGGCCTTGCAGTGCCCACACC
pKLW16	QuikChange	GGTGTGGGCACTGCAAGGCCCTGGCCCCCGAG	CTCGGGGGCCAGGGCCTTGCAGTGCCCACACC
pKLW17	QuikChange	GAGGGCATTGCCGAGTTTCTGCGTCGCCGCGTG	CACGCGGCGACGCAGAAACTCGGCAATGCCCTC
pKLW18	QuikChange	GGAGTGGGCACTGCAAGGCCCTGGCCCCCGAG	CTCGGGGGCCAGGGCCTTGCAGTGCCCACTCC
pKLW19	QuikChange	GGTGTGGGCACGCCCAAGGCCCTGGCCCCCGAG	CTCGGGGGCCAGGGCCTTGGCGTGCCCACACC

Table 2.2. Table of primers used during mutagenesis. The mutagenesis protocol and primers for each clone are shown.

A number of different clones were made for this work. Both the mutagenesis protocol and primers used are shown in table 2.2.

2.1.2. Truncation PCR

2.1.2.1. PCR

This protocol was used for construction of pKLW1 (for primers and construct description see table 2.2.). The forward primer was designed to anneal to the ORF of pLR330 (excluding 54 nucleotides at the 5' end) and contains an NdeI site. The reverse primer was designed to anneal to the ORF at the 3' end and contains a SalI site.

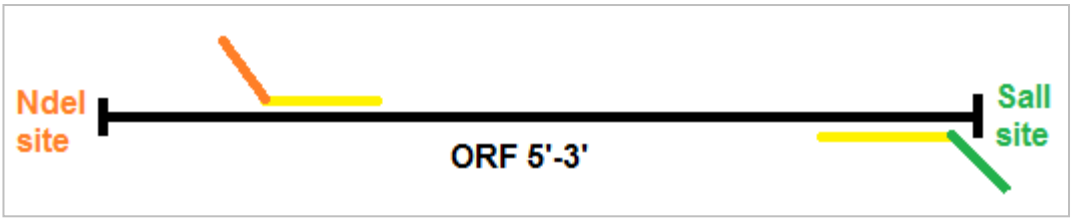

Figure 2.2: Primer annealing for truncation PCR. Primer annealing is shown in yellow. Restriction site sequences are shown in orange and green for NdeI and SalI respectively. Notice that the forward primer does not anneal at the extreme 5' end of the ORF.

PCR was performed using PWO DNA polymerase (Roche Diagnostics) to amplify the ORF situated between primers. 50µl reactions were set up and implemented as described by the manufacturer's guidelines. The DNA template was pLR330 DNA: obtained using a Miniprep kit (QIAGEN).

2.1.2.2. Obtaining insert DNA

DNA gel electrophoresis was performed using a 1% agarose gel stained with SYBR Safe DNA stain (Invitrogen). The PCR product (~1500 bp) was cut from the gel and purified using a Gel Extraction kit (QIAGEN). Following purification, the PCR product was digested using NdeI and SalI (following manufacturer's guidelines, (Fermentas)) and then re-purified by DNA gel electrophoresis and gel extraction (as described previously).

2.1.2.3. Obtaining vector DNA

NdeI and SalI restriction digests were set up (overnight) using the manufacturer's guidelines (Fermentas) and containing 5μg template DNA (pLR330). The vector DNA (~3600 bp) was then purified using DNA gel electrophoresis and gel extraction (as described previously in section 2.1.2.2.).

2.1.2.4. Ligation

Ligation reactions were set up following the manufacturer's guidelines (Fermentas) ensuring an excess of insert to prevent self-ligation. Control reactions (- insert) were also set up.

2.1.3. QuikChange

The QuikChange protocol is a method of site-directed mutagenesis in which a pair of complementary primers are used to amplify an entire plasmid. It is essential that a high fidelity polymerase such as *Pfu* is used for this. The template DNA can then be removed from the mutant plasmid using DpnI, a restriction digest that is specific for methylated DNA. The QuikChange kit is available commercially (Agilent).

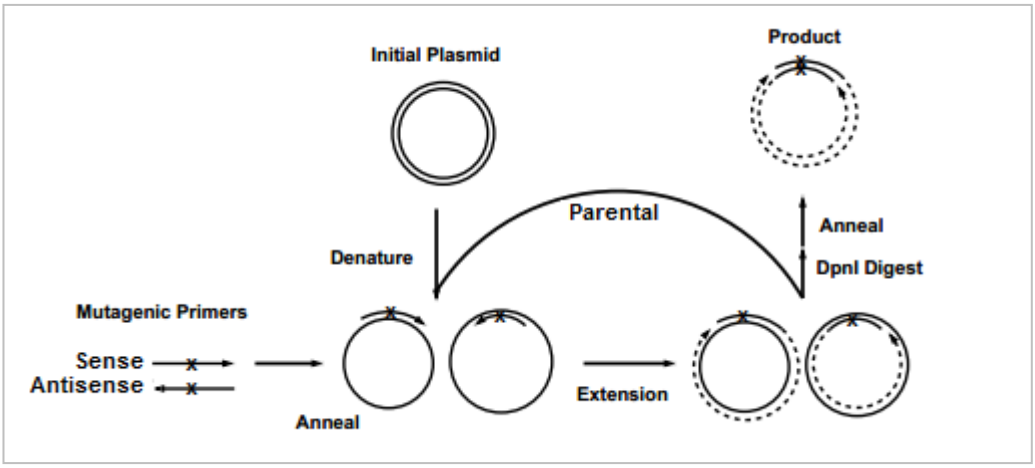

Figure 2.3: Schematic for QuikChange mutagenesis (taken from http://www.stanford.edu/~loening/protocols/Site_Directed_Mutagenesis.pdf). Parental DNA is denatured and mutagenic primers anneal. The whole plasmid is amplified, and parental DNA is digested by Dpn1 which is specific for methylated DNA.

Plasmids: pKLW2-6, pKLW11 and pKLW14-19 were made using the QuikChange protocol and using the primers detailed in table 2.2.

2.1.3.1. Mutagenesis

Primers were designed following the manufacturer's guidelines and are shown in table 1.2. (QuikChange, Agilent). The reaction was set up as described in the QuikChange protocol and using *Pfu* Ultra (Agilent).

2.1.3.2. Dpn1 digest and DNA purification

Following mutagenesis, DNA was incubated with Dpn1 overnight at 37ºC (set-up as described by manufacturer (Fermentas)). Following incubation, the mutagenic DNA was purified by DNA gel electrophoresis and gel extraction (as described in section 2.1.2.2.).

2.1.4. 3 step PCR

The **a** and **a'** domains of PDIp (and also PDI) are very similar to one another on both protein and DNA level. Consequently the QuikChange method of site-directed mutagenesis can be very difficult when trying to mutate either the **a** or **a'** domain because the mutagenic primers can easily mis-align. The 3 step PCR protocol avoids this by focussing on just one domain at a time and is explained in figure 2.4.

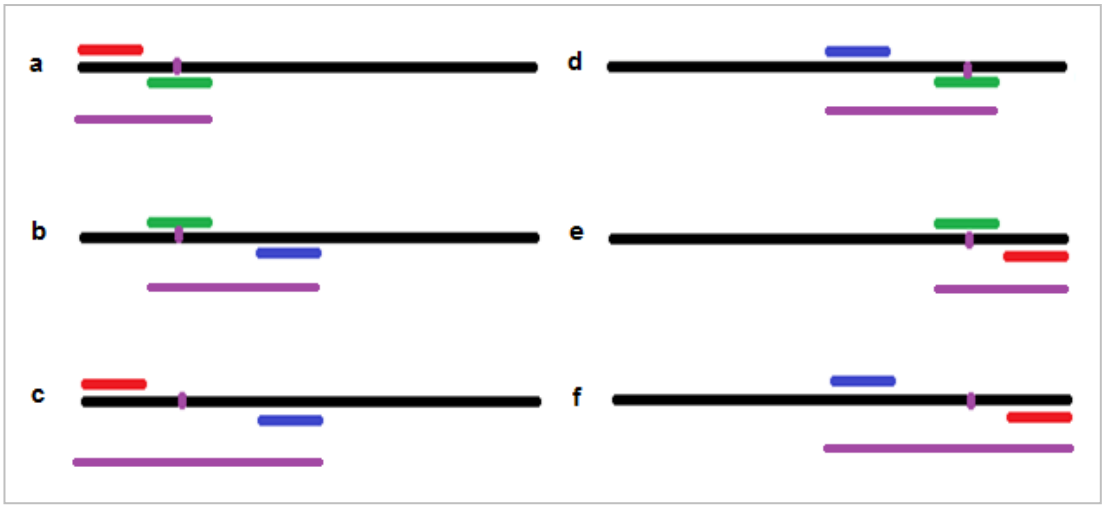

Figure 2.4: 3 step PCR protocol for mutation of the a and a' domains. Flanking primers contain digest sites and are shown in red (start or end) and blue (middle). a) in the first stage of **a** domain mutagenesis, the DNA between the start primer (red) and the reverse mutagenic primer (green) is amplified giving rise to the first PCR product (purple). b) using the forward mutagenic primer (green) and the middle reverse primer (blue) the second PCR product is made (purple). c) using the two PCR products from a & b and the start and middle primers, (red and blue respectively), the full insert is made (purple). d) in the first stage of **a'** domain mutagenesis, the DNA between the middle forward primer (blue) and the reverse mutagenic primer (green) is amplified giving rise to the first PCR product (purple). e) using the forward mutagenic primer (green) and the end reverse primer (red) the second PCR product is made (purple). c) using the two PCR products from d & e and the middle forward and end reverse primers, (blue and red respectively), the full insert is made (purple).

In this protocol, the intrinsic BamHI site of PDIp is used. This is approximately mid-way in the ORF of PDIp and a 'middle' primer incorporating this restriction site was designed. In this way it is possible to split PDIp into two halves and this prevents the difficulties associated with primer mis-aligning.

Plasmids: pKLW7-10 were made using the 3 step PCR protocol and using the primers detailed in table 2.2.

2.1.4.1. PCR

3 step PCR requires 3 different reactions. These are different according to the domain being mutated (either **a** or **a')** and are described in figure 2.4.

For a mutation in the **a** domain, the first reaction amplifies a fragment of the ORF between the start and the mutation and the second reaction amplifies from the mutation to the middle of the ORF (utilising a mid-sequence BamHI site). In the third reaction, the two products of reactions one and two are used as template DNA (purified as described by section 2.1.2.2.), and the start and middle primers are used to amplify the entire insert (~700bp) which now incorporates the required mutation (see figure 2.4.).

To mutate the **a'** domain, the first reaction amplifies between the middle primer and the mutagenic primer and the second reaction amplifies from the mutation to the end of the ORF. In the third reaction, the two products of reaction one and two are used as template DNA (purified as described in section 2.1.2.2.) and the middle and end primers are used to amplify the entire insert (~700bp) which is now mutated.

For this protocol Phusion high fidelity polymerase (New England Biolabs) was used. This enzyme is a fast, accurate and thermostable polymerase. It also comes with specially optimised buffers for amplification of GC rich DNA. As the **a** and **a'** domains are particularly GC rich, mutagenesis can be particularly difficult. Using this system, the required mutations were successfully made.

These PCRs, were set up according to optimal reaction conditions for Phusion high fidelity polymerase (NEB). In this study, the GC buffer (rather than the standard buffer) and 3% DMSO were used (for reasons described previously).

2.1.4.2. Obtaining insert DNA

Following step 3, the full 700bp insert was digested with either NdeI and BamHI or SalI and BamHI (for **a** and **a'** domain mutations respectively). This was done according to manufacturer's guidelines (Fermentas) and creates sticky ends. Inserts were then purified by DNA gel electrophoresis and gel extraction (see section 2.1.2.2.).

2.1.4.3. Obtaining vector DNA

To obtain vector DNA, the parental DNA (pLR330 for KLW7-9 and pKLW6 for pKLW10) was digested with either NdeI and BamHI or BamHI and SalI (for **a** and **a'** domain mutations respectively). This was done overnight according to manufacturer's guidelines (Fermentas). The vectors were then purified by DNA gel electrophoresis and gel extraction (as described previously).

2.1.4.4. Ligation

As described in 2.1.2.4.

2.1.5. Digest and ligation

To make pKLW12 and pKLW13 a restriction digest and ligation strategy was used. For both, the insert DNA was obtained by restriction digest of pKLW8/pKLW9 using BamHI and SalI (according to manufacturer's guidelines (Fermentas)). The inserts were then purified by DNA gel electrophoresis and gel extraction (as described previously).

For the vector, pKLW10 was cut with BamHI and SalI overnight and purified (as before). Vector and insert were then ligated as described in section 2.1.2.4.

2.1.6. Transformation

Super competent cells (DH5α, NEB) were incubated on ice with plasmid for 30 minutes and then subjected to heat shock (42°C) for 30 seconds. After a further 2 minutes on ice, 0.9ml Soc was added and cells were left to grow for 90 minutes at 37°C and 180 rpm. Cells were then plated onto lysogeny broth (LB) + ampicillin (35ng/ml) agar plates and incubated overnight at 37°C.

2.1.7. Screening/checking possible clones

A single colony was used to inoculate 5ml LB (containing 35ng/ml ampicillin) before being incubated overnight at 37°C and 180rpm. The DNA was extracted and purified using a Miniprep kit (QIAGEN). 1hr restriction digests were set up (according to manufacturer's guidelines (Fermentas)) each containing ~100ng of the purified plasmid DNA and the appropriate restriction enzyme. Having visualised the digest products by DNA gel electrophoresis (as before), accurate clones (those that showed the correct size on the gel) were sent for sequencing using a T7 primer pair (Sanger).

2.2. Protein expression

2.2.1. PDI expression protocol

Frozen glycerol stocks of the appropriate plasmid in BL21(DE3)pLysS, were used to streak out cells onto an LB agar plate (containing 100ng/ml chloramphenicol and 35ng/ml ampicillin). Plates were then incubated overnight at 37°C. Following incubation, a single colony was used to inoculate 50ml LB (antibiotics as before) contained in a 250ml conical flask. Again this was incubated overnight at 37°C and

180rpm. Following measurement of the optical density (OD) at 600nM, 1L conical flasks were inoculated such that the final OD_{600} = 0.05 in 400ml LB. Cells were left to grow at 37°C until OD_{600} = 0.5, which takes ~2.5 hours. Expression of protein was induced with a final concentration of 1mM isopropyl-β-galactoside (IPTG) and cells were left to express for 4 hours at 37°C and 180 RPM. Cells were harvested by centrifugation at 5,000 RPM using a Beckman JLA-8.1000 rotor for 15 minutes at 4°C.

2.2.2. PDIp expression protocol

As for PDI, except that when OD_{600} = 0.5, cells were induced with IPTG (final concentration 1mM) and left for 16 hours at 25°C and 180 RPM. Cells were then harvested by centrifugation at 5,000 RPM using a Beckman JLA-8.1000 rotor for 15 minutes at 4°C.

For the expression studies described in section 3.3., the above protocol was altered as indicated in the text.

2.2.3. EnBase expression system

Protein expression in EnBase media was performed exactly as described by the manufacturer (BioSilta).

2.2.4. Cell Lysis

The cell pellet was resuspended in 20mM sodium phosphate, pH 7.3. DNase (final concentration: 10μg/ml), PMSF, leupeptin and pepstatin (final concentration for each: 200μM) were also added at this stage (protease inhibitors only added during cell harvest of PDIp). Cells were lysed by a combination of freeze/thaw and sonification. The latter was perfomed on ice using a Bandelin Sonoplus HD 2070 sonicator for 3 x 30 second bursts of 70% power with 90 second rest intervals.

2.3. Purification

2.3.1. Immobilised metal ion affinity chromatography (IMAC)

Lysed cells were centrifuged at 12,000 RPM for 15 minutes (4°C) to pellet insoluble cell debris. IMAC columns were produced by adding Chelating Sepharose Fast Flow Resin (GE healthcare) to a syringe to produce a column volume (CV) of ~5ml. The column was rinsed with 10 CVs water before adding 2ml 0.2M Nickel chloride. After rinsing with a further 5 CVs of water, 5 CVs 20mM sodium acetate, 0.5M sodium chloride, pH 3.0 was added to remove unbound nickel. The column was then equilibrated with 5 CVs 20mM sodium phosphate, pH 7.3. The supernatant (total soluble portion of cell lysate) was loaded onto the column and loosely bound impurities removed with 2 CVs 25mM Imidazole, 0.5M sodium chloride, 20mM sodium phosphate, pH 7.3. This was followed by 5 CVs of 20mM sodium phosphate, pH 7.3 and finally, protein was eluted using 5 CVs of 50mM EDTA, 20mM sodium phosphate, pH 7.3.

2.3.2. Salt precipitation

Reactions were set up containing 35% saturated ammonium sulphate solution and left for 1hr at 4°C for precipitation to occur. After 1hr, the reaction was centrifuged for 15 minutes at 20,000 rpm. The supernatant was dialysed overnight into 20mM sodium phosphate buffer (pH 7.3) (see 2.3.4.).

2.3.3 Batch purification

5ml High performance chelating sepharose (which already has Ni^{2+} bound (GE Healthcare)) was resuspended in 10 CVs water and centrifuged at 500g for 10 minutes. The supernatant was discarded and the column material resuspended in 5 CVs 20mM sodium acetate, 0.5M sodium chloride, pH3.0 before centrifugation (as before). The supernatant was once again discarded, and the material resuspended in 5

CVs 20mM sodium phosphate, pH 7.3 in order to neutralise the low pH. The column material was centrifuged at 500g for 10 minutes and the supernatant removed.

Cells were lysed and centrifuged as described in 2.4.1 but with the addition of PMSF, pepstatin and leupeptin (final concentration for each = 200μM). 20ml of the cell supernatant (containing soluble proteins) was added to the column material and then left for 1hr at 4°C on rollers to ensure thorough mixing. After this time, the sepharose/supernatant solution was poured into an empty PD-10 column (GE Healthcare) and the flow through discarded.

Unspecifically bound protein was washed from the column material by 2CVs 20mM sodium phosphate, 20mM imidazole, 0.5M sodium chloride (pH 7.3). Finally, protein was eluted with 5CVs 20mM sodium phosphate, 200mM imidazole, 0.5M sodium chloride (pH 7.3). After protein elution, the column material was washed with distilled water and stored in 20% ethanol.

2.3.4. Buffer exchange by dialysis

Unwanted salts were removed by overnight dialysis into sodium phosphate buffer, pH 7.3 (4ºC). The dialysis membrane that was used had a molecular weight cut off (MWCO) of 12 – 14 kDa (Medicell International).

2.3.5. Ion Exchange Chromatography (IEC)

Anion exchange chromatography was performed with a 10ml Source 30Q column (GE Healthcare) connected to an ÄKTA purifier 100 fast protein liquid chromatography (FPLC) system (GE Healthcare). The column was rinsed and equilibrated with 20mM sodium phosphate, pH 7.3. The protein sample was loaded onto the column via an injection loop. A gradient from 0-100% 20mM sodium phosphate, 0.5M sodium chloride, pH 7.3 was used to elute the protein over a total of 10 CVs. 2ml fractions were collected and those corresponding to a peak in the chromatogram were analysed by SDS-PAGE.

2.3.6. Gel filtration

Size exclusion chromatography was performed with a Superdex 200 10/300 GL column (GE Healthcare) connected to an ÄKTA purifier 100 fast protein liquid chromatography (FPLC) system (GE Healthcare). 20mM sodium phosphate, 150mM sodium chloride, pH 7.3 was used as the buffer. The protein sample was loaded onto the column via a 2ml injection loop (protein concentrated previously to volume (and desalted if necessary)). Protein elution was monitored at A_{280} and 5ml fractions were collected until a drop in conductivity was seen corresponding to NaCl being eluted from the column. Fractions were analysed by SDS-PAGE.

2.3.7. Protein concentration

Vivaspin 20 protein concentrators (Sartorius Stedim) with a molecular weight cut off (MWCO) of 10,000 were used to concentrate fractions containing protein from IEC or SEC. During the concentration process, samples were also desalted.

2.3.8. Estimating Protein Concentration

The concentration of PDIp was determined by measuring the A_{280} of the sample using a Jenway 6305 spectrophotometer. The extinction coefficient (ε_{280}) determined using ProtParam (http://www.expasy.ch/tools/protparam.html), can then be used to derive protein concentration using the Beer-lambert Law:

$$\text{Protein Concentration (M)} = A_{280} / (\varepsilon_{280}\,(M^{-1}) \times \text{path length of cuvette (cm)})$$

The extinction coefficients for proteins used in this study are shown in table 2.3 (see over). Single point mutants have the same extinction coefficient as their background proteins.

Protein	Extinction Coefficient (M^{-1} cm^{-1})
PDI	45380
PDIp	43890
PDIp 1/2	42400
PDIp 3/4	42400
PDIp **a**	16960
PDIp **a'**	16960

Table 2.3: Extinction coefficients for PDI, PDIp and PDI.PDIp constructs. The extinction coefficients were calculated using ProtParam. The values provided here are for the reduced proteins.

2.4. Analysis

2.4.1. Polyacrylamide Gel Electrophoresis (PAGE)

SDS-PAGE was used to analyse proteins under denaturing and reducing conditions and was carried out according to the Tris-Glycine buffer system (Laemmli, 1970). Typically, a 12% separation gel (pH 8.8) and 7% resolving gel (pH 6.8) were used and cast using the Mini Protean II gel kit (Bio-Rad). Samples for SDS-PAGE were reduced with loading buffer (1M Tris-HCl pH 6.8, 50% glycerol, 0.8% SDS, 0.1% w/v bromophenol blue and 10% β-mercaptoethanol). Gels were run at 60mV until protein had entered the separation gel and then 180mV for ~60 minutes in a 10% SDS buffer. A low molecular weight marker (GE Healthcare) was used to estimate the molecular weight of protein seen on the gel. Gels were stained with Instant Blue gel stain (Expedeon).

Native-PAGE was performed as for SDS-PAGE but with the complete omission of SDS and β-mercaptoethanol.

2.4.2. Mass Spectrometry

Approximately 1mg of protein was dialysed into 10mM ammonium acetate overnight at 4°C. Samples were then freeze-dried (ScanVac) and sent to Kevin Howland (University of Kent) for high resolution electrospray ionisation (ESI) mass spectrometry.

2.4.3. Circular Dichroism (CD)

Far UV CD was performed on all constructs using a Jasco J-815 CD spectropolarimeter at various different temperatures (controlled by a Peltier thermostat controller). Samples containing 0.1mg/ml protein in 5mM sodium phosphate buffer (pH 7.3) were prepared. Data were recorded using 0.1mm cuvette, 260nm-190nm, step resolution 0.2nm, response 0.25s, bandwidth 1nm, scan speed 20nm/min, average of 16 scans. All data was corrected against a buffer blank and analysed using DichroWeb (Whitmore and Wallace, 2008).

Mean residue ellipticity was calculated using the following equation taken from Kelly *et al*. (2005):

$$[\theta]_{mrw,\lambda} = (MRW \times \theta\lambda) / (10 \times d \times c)$$

Where MRW = M/ (N-1) and M is the molecular mass of the polypeptide (in Da) and N is the number of amino acids in the chain. $\theta\lambda$ is the observed ellipticity (degrees), d is the pathlength (nm) and c is the concentration (g/ml).

2.5. Structural studies

2.5.1. Intrinsic fluorescence

The intrinsic fluorescence of samples containing 10μM protein in 20mM sodium phosphate buffer (pH 7.3.), was measured using a Perkin/Elmer LS50 fluorimeter. Excitation wavelength 280nm, emission 290-400nm, slit width 2nm, scan speed 100nm/min, an average of 3 scans and temperature, 25ºC.

2.5.2. ANS fluorescence

An ANS saturation curve for both PDI and PDIp was determined using 1μM PDI/ PDIp in 20mM sodium phosphate buffer (pH 7.3) and increasing concentrations (0-200μM) of anilino naphthalene sulphonate (ANS) (Sigma). For these measurements a Perkin/Elmer LS50 fluorimeter was used, excitation wavelength 390nm, emission 400-600nm, slit width 2nm, scan speed 100nm/min, an average of 3 scans and temperature 25ºC. The relative fluorescence unit (R.F.U.) at λ_{max} was then plotted against [ANS] to produce a saturation curve.

For ANS enhancement, 10μM protein (reduced or oxidised) was incubated with 100μM ANS for 30 minutes at 37ºC before measurements were taken (as described above). The ANS enhancement factor was calculated as follows:

$$\text{ANS enhancement factor at } \lambda_{max} = (F_{protein + ANS)} / F_{ANS}$$

Where F = fluorescence.

2.5.3. Thermal denaturation

Thermal denaturation was monitored using far UV CD. The secondary structure of samples containing 0.1mg/ml protein in 20mM sodium phosphate buffer (pH 7.3) was measured at 222nm on a Jasco J-815 CD spectropolarimeter and in 0.1mm cuvettes. Temperature was increased in 4ºC steps from 20-80ºC, controlled by a Peltier thermostat controller. Samples were allowed to equilibrate for 10 minutes at each temperature before data collection (2 minutes). All data was corrected against a buffer blank (measured at the same temperature) and the mean residue ellipticity for each temperature was calculated as described previously (see section 2.4.3.)

2.5.4. Thermal re-naturation

Thermal re-folding was measured described in section 2.5.3. but with temperature decreasing from 80-20ºC.

2.5.5. Preparation of oxidised and reduced samples

For studies of redox-state dependent structural change, samples were oxidised or reduced. Sample preparation is described below but otherwise the method is unchanged from the un-redox controlled protocol.

Buffer stocks were prepared to contain 20mM sodium phosphate (5mM for far UV CD samples) and in addition 0.5M DTT/diamide stocks were also made (Sigma) (pH 7.3). Protein samples were treated with a 10x molar excess of the DTT/diamide stock and incubated for 15 minutes at room temperature. Samples were desalted into 20mM (or 5mM for CD samples) sodium phosphate buffer (pH 7.3) using a PD-10 column (GE Healthcare) following the manufacturer's standard gravity based protocol. If required, samples were then concentrated as described in section 2.3.7.

2.5.6. Limited proteolysis

For each protein, a 200µl sample containing 15µM protein and 50mM sodium phosphate buffer, 10mM DTT/diamide, 10mM $CaCl_2$ (pH 7.6) was prepared (as described in Wang *et al*. 2010). Chymotrypsin (Worthington) was then added to a final concentration of 75nM and the stock solution incubated at 37°C. After 0, 5, 10, 20, 40, 60, 90 and 120 minutes, an aliquot was removed from the stock and the reaction stopped with SDS-loading buffer and boiling at 95°C for 5 minutes. A sample of each aliquot was then run on a 12% SDS-gel (see section 2.4.1) and the results visualised.

For further analysis, the required band was cut from the SDS-PAGE gel and subjected to tryptic digest using the manufacturers recommended protocol on the MassPrep robotic protein handling system. The resulting peptides from each sample were analysed by nanoliquid chromatography (LC) - electrospray ionisation –

MS/MS using a 45 minute LC gradient. All data collected was corrected for mass drift using reference data collected from human [Glu^1]-fibrinopeptide B (Sigma). Finally the amino acid sequence of the protein was used to determine percentage sequence coverage of the peptides present.

Alternatively, samples were prepared as described above but no aliquots were taken and the reaction was incubated for the full 120 minutes. After this time, the reaction was stopped with a 10x molar excess of PMSF and samples were dialysed into 10mM ammonium acetate overnight (4°C). Samples were freeze-dried (ScanVac) and sent to Kevin Howland (University of Kent) for ESI mass spectrometry.

2.5.7. Dynamic Light Scattering (DLS)

DLS was performed using a Malvern Zetasizer Nano instrument. Samples contained 10μM protein (oxidised or reduced as described in section 2.5.5.) and 20mM sodium phosphate (pH 7.3). A minimum of 5 measurements were taken, at 25ºC and using the dispersant/solvent properties of water for comparison.

2.5.8. Nuclear Magnetic Resonance (NMR) sample preparation

PDIp **a** was expressed using identical conditions to PDIp but in minimal media instead of LB (see section 2.2.). NMR measurements of PDIp **a** were taken at the University of Kent by Michelle Rowe using a 4-channel Varian Unity INOVA 600 MHz NMR spectrometer.

2.6. Activity studies

2.6.1. Insulin assay

In the insulin assay, the reduction of insulin disulphides by GSH, catalysed by PDI, generates GSSG and this is coupled to the reduction of GSSG by NADPH, catalysed by glutathione reductase. The latter process is monitored by a decrease in A_{340} (see figure 2.5.)

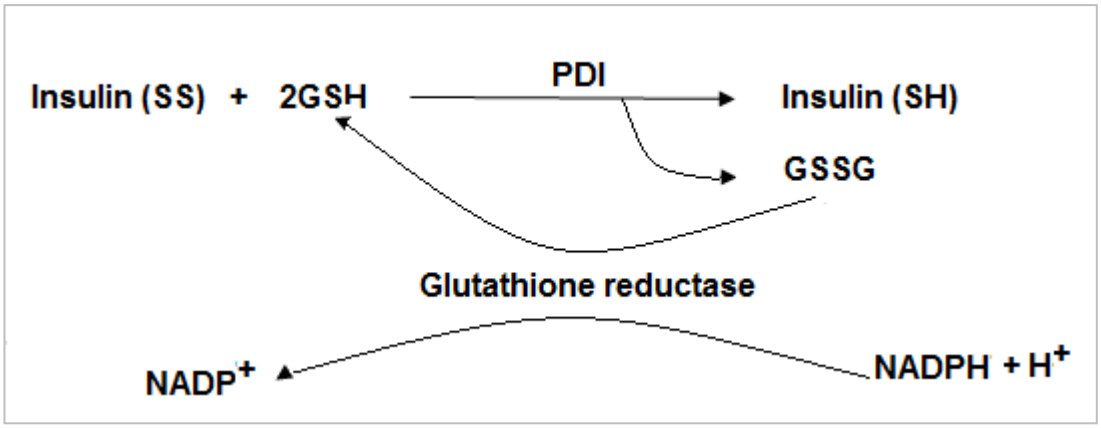

Figure 2.5: Reaction scheme for insulin oxido-reductase assay.

Samples containing 120µM NADPH, 8mM GSH, 1 unit of glutathione reductase and 0.5-2µM protein were prepared and 200mM sodium phosphate, 5mM EDTA buffer (pH 7.5) was then added to give a total volume of 1ml. Measurements were taken using a Cary UV-Vis spectrophotometer (Agilent), absorbance: 340nm and temperature, 37ºC. The sample was equilibrated at 37ºC before starting sample measurement. After a background rate has been obtained, 15µM insulin was added and the consequent change in A_{340} recorded as a function of time. All reagents (except the protein) were obtained from Sigma.

2.6.2. Oxidation/reduction stopped flow assay

The rates of oxidation by GSSG and reduction by GSH of the **a** domain active site of PDI **a** W128F and PDIp **a** W146F mutants were determined by a change in fluorescence of the active site adjacent tryptophan using a method similar to that of Lappi and Ruddock (2011). This was measured using a KinTek SF-2004 stopped flow fluorimeter (KinTek), excitation 280nm and band-pass emission >320nm at 25ºC. PDI/PDIp **a** concentration was 10μM, GSSG concentration 1-20mM and GSH concentration 1-50mM. Enzyme samples were reduced/oxidised and desalted as described in section 2.5.5 but using the assay buffer (100mM disodium hydrogen phosphate, 100mM boric acid buffer (pH 7)) instead of 20mM sodium phosphate.

2.6.3. Stopped flow pK_a calculations

The pH dependence of the reactions of 25μM PDIp **a** C71S and PDIp **a** C74A with 0.073 mg/ml 5,5-dithio-bis(2-nitrobenzoic acid) (DNTB) (Sigma) was measured using KinTek SF-2004 equipment, absorbance wavelength 412nm and temperature 25ºC (as described by Karala *et al.* 2010). Sample buffers (pH 6.5 - 10.0) were 100mM disodium hydrogen phosphate, 100mM boric acid buffer, pH corrected with 5M NaOH.

Chapter 3. Optimisation of expression & purification

3.1. Introduction

Prior to this work, PDIp had not been studied by the RBF group and therefore protocols for the expression and purification of recombinant PDIp were not yet optimised. Standard expression and purification conventions for PDI were not compatible with PDIp and gave rise to low yields of relatively unstable protein.

This aim of this work was to identify conditions suitable for obtaining a maximal yield of PDIp and PDIp constructs, in order to facilitate future studies of their structure and activity.

3.2. Preliminary work

3.2.1. Expression, Purification and Stability of PDIp

When PDIp was expressed and purified using standard PDI protocols (see methods) the total yield obtained was ~2μg/ml culture: 10 fold less than the average yield for PDI. The problem was associated with both a low level of expression and a poor

protein recovery from expression (see below) In addition, purified PDIp was found to be very unstable under conventional storage conditions (see figure 3.1).

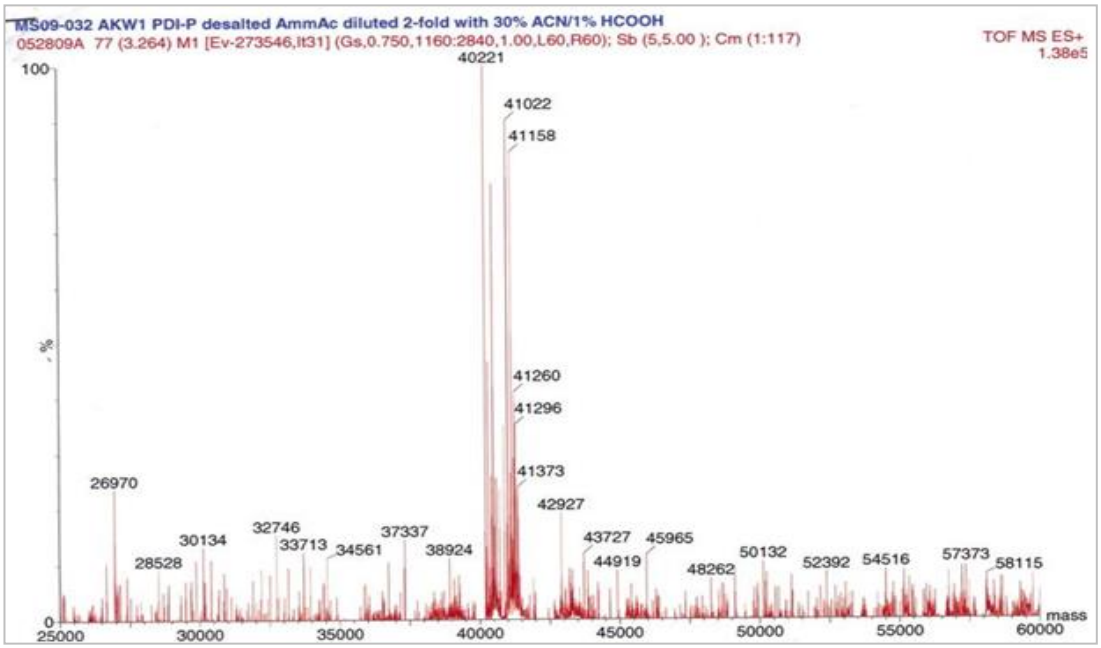

Figure 3.1: High resolution electrospray ionisation (ESI) MS spectra for PDIp after 4 weeks storage at -20°C. There is no peak corresponding to hexa-His tagged full length PDIp (M_w: 56919 Da) indicating that the sample is significantly degraded.

Figure 3.1 shows the absence of full-length PDIp (M_w: 56919 Da) and the extent of degradation after 4 weeks at -20ºC. The most abundant species is a ~40kDa fragment probably corresponding to His-tagged PDIp **abb'x** (M_w: 42kDa, ProtParam). This indicates that like PDI, PDIp may also have intrinsic flexibility centred on the x-linker region (Wang *et al.* (2010).

3.3. Optimisation of Expression

3.3.1. Varying host, temperature and expression period

Initial studies to improve the expression of PDIp involved comparing total soluble protein produced by 5 different host cell-strains, 4 different expression times and 3

different temperatures. The results of this were visualised by SDS-PAGE and are shown in figure 3.2.

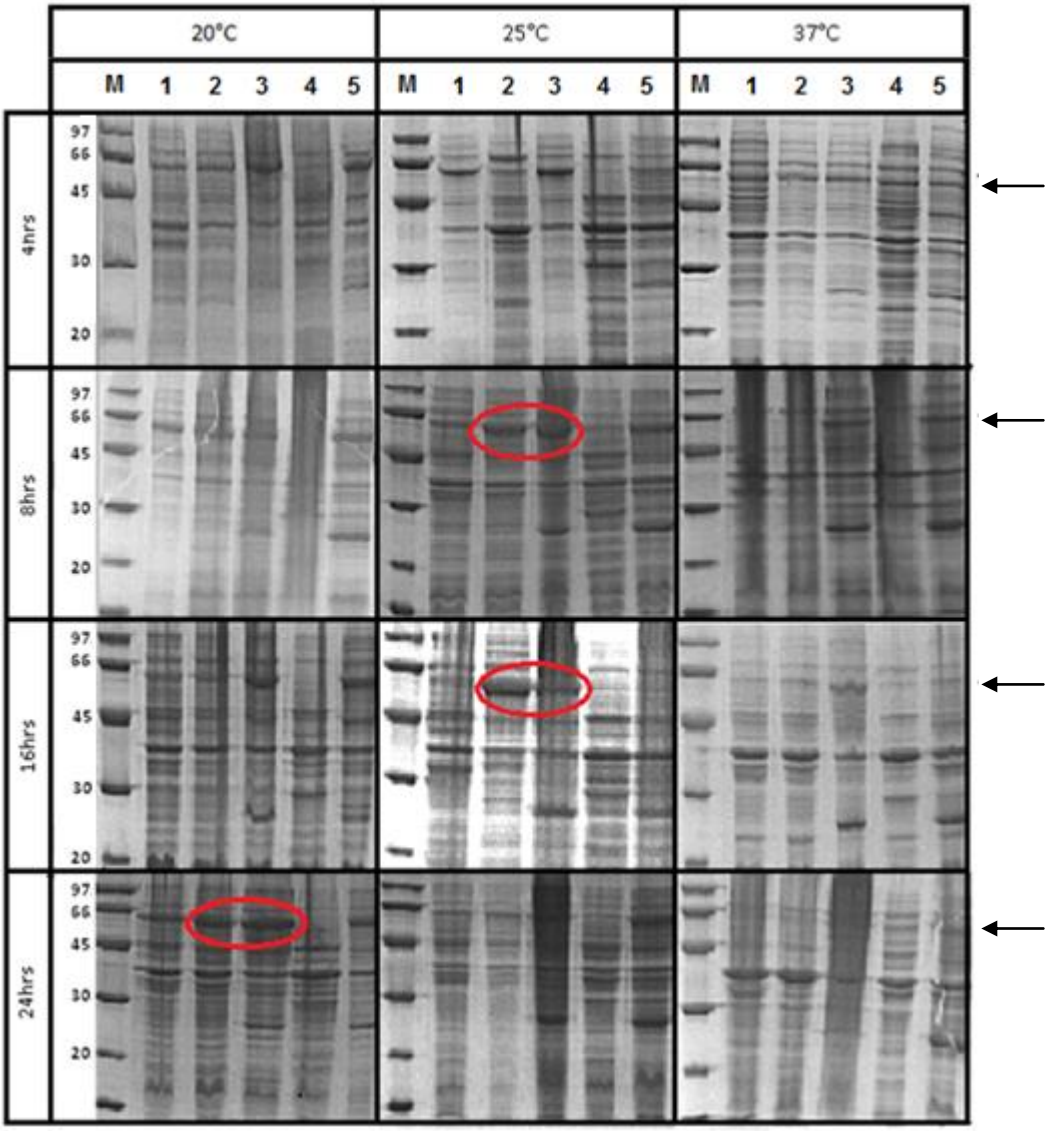

Figure 3.2: Recombinant expression of PDIp. SDS-PAGE showing total soluble proteins produced during expression of PDIp. 5 different competent cell strains were studied: 1) B834(DE3), 2) BL21(DE3), 3) BL21(DE3)pLysS, 4) C41(DE3) and 5) Rosetta Star (DE3) (marker depicted by M). Cells were grown at 37°C to A_{600} = 0.5 and then induced with 1mM IPTG and incubated at 20, 25 or 37°C for 4, 8, 16 or 24 hours. Arrow indicates expected position of PDIp on the gel (M_w = ~ 57kDa) and highest yields are circled.

Figure 3.2 shows that in each instance tested, cells incubated at 37°C post-induction expressed less PDIp than their counterparts at lower temperatures. This is not

uncommon in recombinant protein expression where high and non-physiological rates of protein production give rise to accumulation of misfolded/partially folded protein which leads to cellular stress, formation of insoluble aggregates and proteolysis. The benefits of reducing expression temperature as a solution to reducing cellular stress are widely discussed in the literature (For review see Gasser *et. al* 2008).

Supporting the suggestion that cellular stress is affecting total yield, figure 3.2 shows that optimal induction time is temperature dependent i.e. that optimal expression time increases as temperature decreases. This means that while cells induced at 20ºC benefit from a 24 hour expression period, those induced at 25°C have optimal expression after 8-16 hours. Furthermore in the latter, expression times of >16 hours lead to a reduction in yield probably due to formation of insoluble aggregates and/or proteolysis (unconfirmed). It is thus clear that when expressing PDIp recombinantly, measures must be taken to balance both protein production and cellular stress.

Perhaps surprisingly, C41(DE3) cells were consistently the least successful cell-type tested despite being designed to resist expression-derived toxicity. Rosetta Star (DE3) cells also showed poor expression yields for the majority of conditions tested. This was also unexpected because these cells have optimised translation efficiency conferred by an additional plasmid (pRARE). B834(DE3) cells did produce a fair yield in most conditions tested but not enough to outweigh the disadvantage of them being methionine auxotrophs. BL21(DE3) and BL21(DE3)pLysS were consistently the best cell-strains tested in terms of yield but also grew quickly prior to induction making them more user-friendly. Consequently further study was performed on BL21(DE3) and BL21(DE3)pLysS only (see figure 3.3).

3.3.2. Varying IPTG concentration

Sevastsyanovich *et al.* (2009) suggested that induction of recombinant protein expression using high concentrations of IPTG could lead to increased cellular stress and reduce total yield. Figure 3.3 shows that expression of PDIp by BL21(DE3) cells is not dependent on IPTG concentration at either 25ºC or 37°C. At 25ºC however

there is no appreciable yield of PDIp at any concentration of IPTG implying a fault of the experiment as previous work had shown that good yields of PDIp could be obtained in these conditions with induction by 1mM IPTG (see figure 3.2).

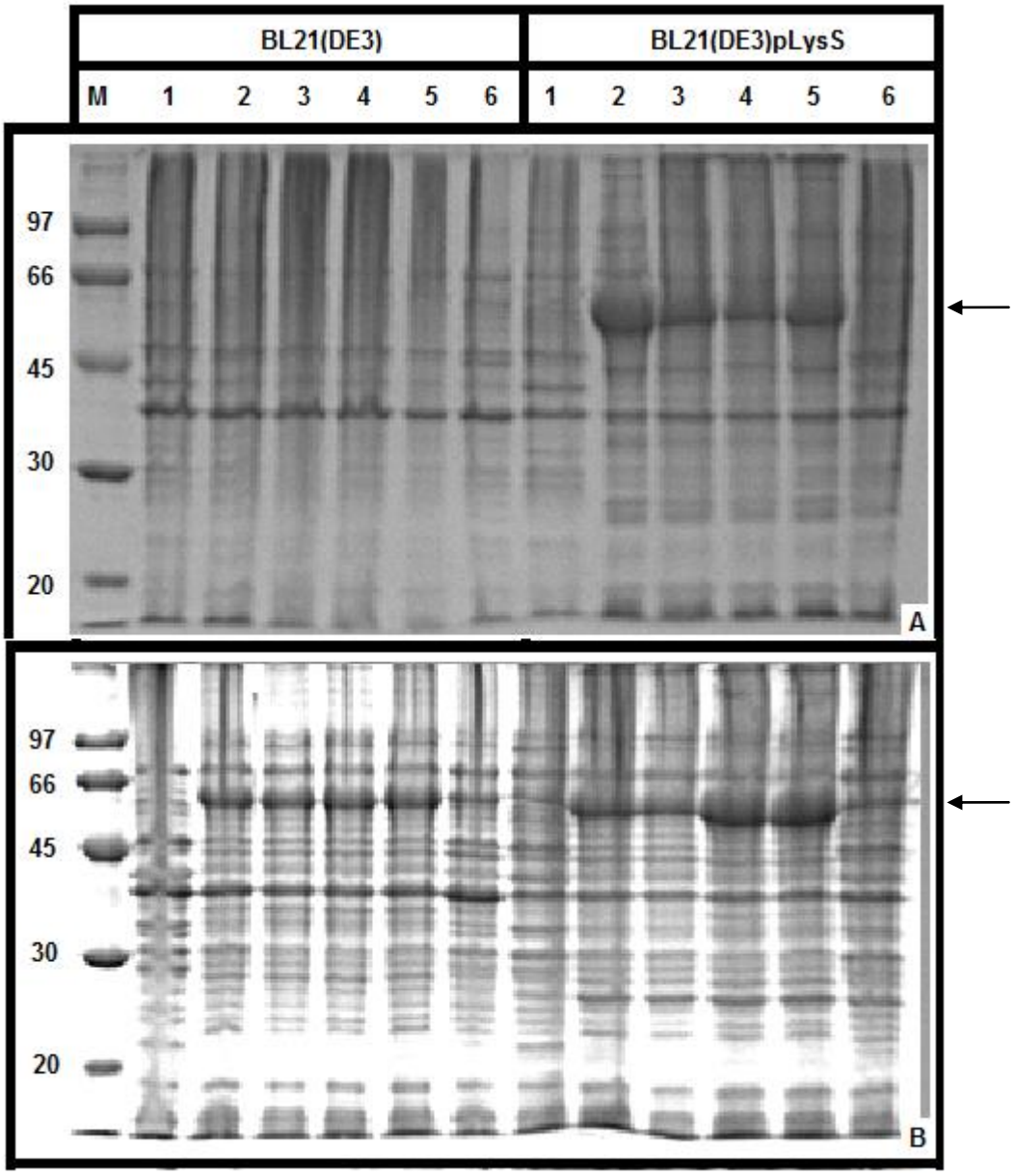

Figure 3.3: Recombinant PDIp expression after induction by varying [IPTG]. SDS-PAGE showing PDIp expression using BL21(DE3) and BL21(DE3)pLysS competent cells. 5 different concentrations of IPTG were studied for each cell line: 1) 0mM, 2) 1mM, 3) 0.5mM, 4) 0.25mM, 5) 0.1mM and 6) 10µM. M indicates marker. Cells were grown at A) 25°C or B) 37°C and then left to express at 25°C for 8 hours. Arrow indicates expected position of PDIp on the gel (Mw= ~ 57kDa).

At 37°C total yield of PDIp was roughly equivalent for all cultures induced with 1mM, 0.5mM, 0.25mM or 0.1mM IPTG. Surprisingly, a total IPTG concentration of 10μM was sufficient to induce BL21(DE3) cells at 37°C although yield was far reduced compared to at higher IPTG concentrations.

Expression of PDIp by BL21(DE3)pLysS is dependent on IPTG concentration and this seems to be linked also to expression temperature. At 25°C, yield decreases as IPTG concentration decreases but at 37ºC, yield increases as IPTG concentration decreases. This implies that the combination of high IPTG concentration and high temperature leads to an increase in cellular stress. Again it is clear that in order to achieve optimal yields of PDIp, cellular stress must be controlled. This correlates well to published work by Sevastsyanovich *et al*. (2009) which shows that optimal protein expression occurs when cellular stress is kept to a minimum.

3.3.3. Conclusions of Expression Studies

Expression of PDIp clearly promotes cellular stress to a greater extent than PDI. Therefore in order to improve total yield of PDIp, cellular stress must be controlled.

The optimal conditions for the recombinant expression of PDIp are:

1. BL21(DE3)pLysS host cell: although little difference was observed between yields of PDIp obtained from BL21(DE3)pLysS or BL21(DE3) cells, BL21(DE3)pLysS cells were chosen as expression vector because they have the advantage of having a pLysS plamid which prevents background expression.

2. Temperature (growth and expression) 25ºC: an expression temperature of 25ºC allows a shorter expression time than at 20°C and benefits from reduced cellular stress compared to expression at 37ºC.

3. Expression time 8-16 hrs: at 25ºC, expression times of >16 hours led to an increase in cellular stress and a reduction in total protein.

4. IPTG concentration 1mM: at 25°C and using BL21(DE3)pLysS host cells, highest yields of PDIp were obtained following induction with 1mM IPTG. Decreasing IPTG concentration led to a reduction in yield.

3.3.4. EnBase Expression Trials

EnBase is an expression system that uses enzymatic digestion of a synthetic substrate to slowly feed bacterial cells glucose. This means that much higher cell densities can be achieved prior to induction and subsequently higher yields of protein can be obtained.

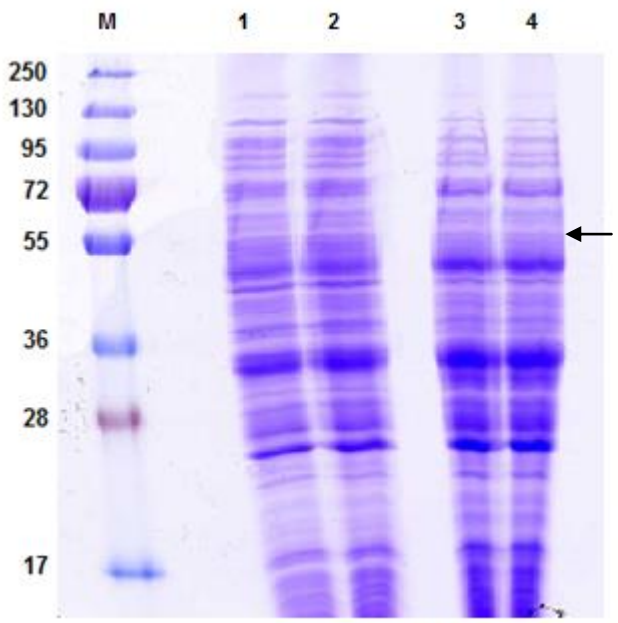

Figure 3.4: Recombinant PDIp expression using EnBase system. SDS-PAGE showing total soluble protein obtained using BL21(DE3)pLysS competent cells and EnBase media. Protocol as described by manufacturer. Gel shows products of two separate expression batches in duplicate (batch 1 (1-2) and batch 2(3-4) Arrows shows expected position of PDIp.

Figure 3.4 shows that the total yield of PDIp obtained using the the EnBase system is very low. Although unconfirmed it is possible that the long expression time (~24 hours) may be inducing cellular stress and giving rise to formation of inclusion bodies and proteolysis. Consequently a low yield would be obtained. Clearly recombinant expression of PDIp is prone to induction of cellular stress in both LB and EnBase media.

Although found to be unsuitable for expressing PDIp, the EnBase system was used to produce very high yields (~0.1mg/ml culture) of recombinant single domain constructs, specifically PDIp **a,** PDI **a** and also mutant forms of both proteins. Figure 3.5 shows the quantity of PDIp **a** C71S found in 10µl samples of fractions corresponding to the elution peak after IEC (data not shown). Clearly the gel is very overloaded indicating that a large yield of protein was obtained and this explains why PDIp **a** C71S appears to have a M_w of ~16kDa instead of 14.5 kDa. Total yield was 10x more than typically expected from standard expression in LB (described previously).

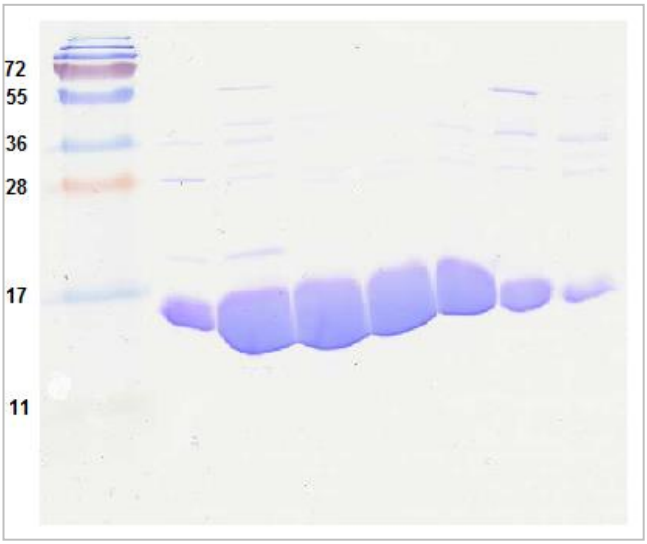

Figure 3.5: IEC of PDIp a C71S. 10µl samples were taken from fractions corresponding to major peak of IEC chromatogram (not shown) and analysed by 12% SDS-PAGE. M_w of hexa-His tagged PDIp **a**: 14552 Da (ProtParam)

3.4. Optimisation of Purification

3.4.1. Standard IMAC

Using a standard IMAC protocol (see methods) only ~1/3 of the available hexa-His tagged PDIp binds to the Ni^{2+} column (see figure 3.6). As a result of this a considerable amount of protein is lost via the flow through. Losses are not due to column overloading as regeneration was shown not to significantly improve total

protein binding (figure 3.6). Clearly, the interaction between the His-tag of PDIp and the Ni^{2+} sepharose is weak and therefore protein is lost during washing with low concentrations of imidazole and even during a simple buffer wash to remove salt (figure 3.6). Loss of binding is not caused by choice of metal ion (i.e. Ni^{2+}) as similar protein losses were seen when a Co^{2+} charged column was used instead (data not shown).

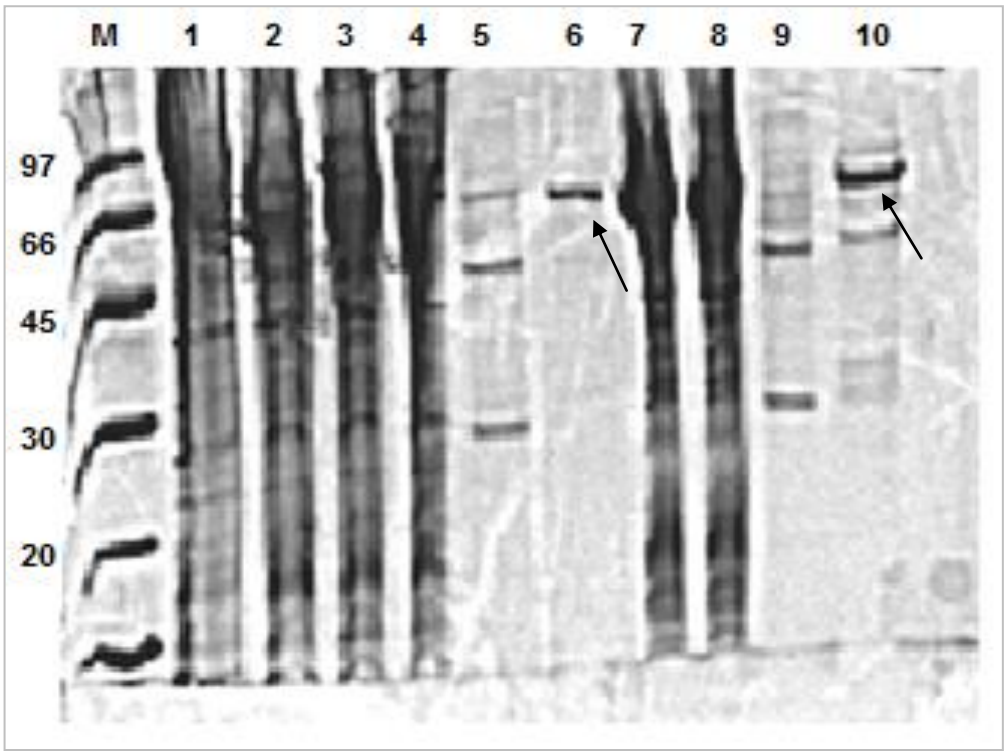

Figure 3.6: SDS-PAGE showing fractions collected by IMAC. M= marker, 1) total cellular protein, 2) supernatant, 3) flow through, 4) wash, 5) loss of salt, 6) elution, 7) flow through(2), 8) wash(2), 9) loss of salt(2) and 10) elution(2). Column was regenerated and the flow through collected during primary IMAC was loaded onto it. Arrows indicates PDIp.

It was suggested that PDIp may be losing the His-tag from the N-terminus as a result of instability issues discussed previously. To try and reduce the likelihood of degradation and subsequent loss of the His-tag, IMAC was repeated at 4°C. Unfortunately, this did not improve binding of PDIp to the Ni^{2+} column (data not shown).

3.4.2. His-tag Western blot of PDIp

A Western blot using antibodies specific to the His-tag showed that it was present on both purified PDIp and also PDIp that had been lost in the flow through (see figure 3.7A). In addition, His-tag staining was also seen for the sample of degraded PDIp (faint band at ~40kDa) implying that degradation occurs at the C-terminus of the molecule in a similar manner to that seen for PDI (Wang *et al.* 2010). These results suggest that reduced binding occurs as a result of the His-tag of PDIp not being solvent-exposed, rather than because it has been lost.

Regrettably, figure 3.7A also shows a small degree of unspecific staining. His-tag staining is particularly susceptible to this as there are a number of *E.coli* proteins that contain multiple His sequences. However despite this, the results are clearly indisputable and demonstrate that the His-tag has not been lost.

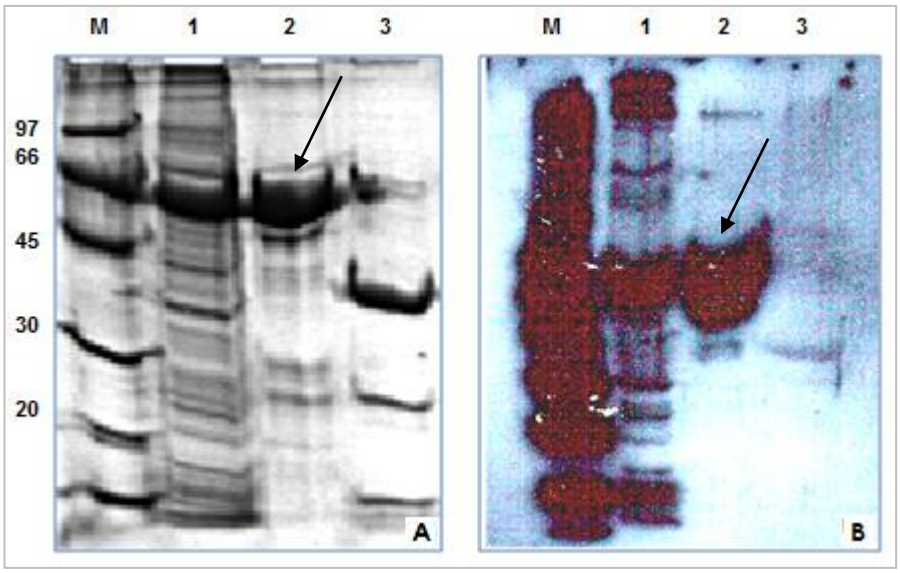

Figure 3.7: His-tag Westen Blot of PDIp. A) SDS-PAGE of his-tag Western blot B) Duplicate His-tag Western blot image**.** M= marker, 1) flow through, 2) pure PDIp and 3) degraded PDIp. (Arrows indicate position of PDIp)

3.4.3. Sequence alignment of the N-terminal region of PDI and PDIp

Sequence alignment of His-tagged PDI and PDIp indicates that the N-terminal region of PDIp (before the 'TRX-fold' domain) is much longer and more negatively charged than the same region in PDI. It can be seen in figure 3.8 that PDIp has 6 negatively charged amino acids at its N-terminus compared to only 3 for PDI. This region is also unstructured. Consequently it is possible that the positively charged His-tag is folding back onto the N-terminus of PDIp. This may explain why the hexa His-tagged PDIp is unavailable and therefore unable to bind to the Ni^{2+} column.

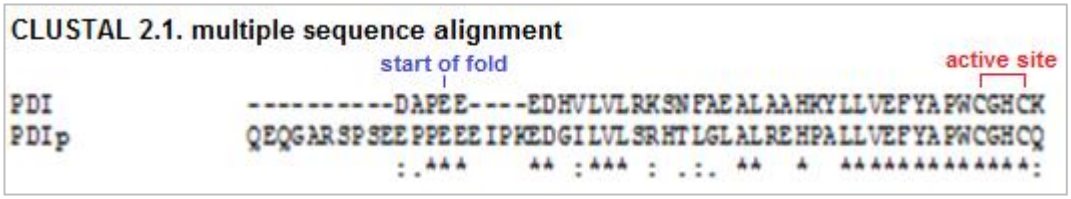

Figure 3.8: CLUSTAL sequence alignment of the N-terminus of PDI and PDIp.

3.4.4. Molecular biology to improve binding of PDIp to the Ni^{2+} column

To determine whether the N-terminus of PDIp interacts with the His-tag and therefore prevents binding, a new clone (pKLW1) with a truncated N-terminus was designed (see figure 3.9).

Figure 3.9: CLUSTAL sequence alignment of the N-terminus of a wild-type PDIp and PDIp truncate (pKLW1).

Regrettably, pKLW1 did not express very well using optimal conditions for wild-type PDIp (described previously) and as such it was difficult to determine its binding properties. Figure 3.10 shows total soluble proteins obtained from expression of

pKLW1 and subsequent IMAC fractions. Total PDIp is minimal in all samples shown.

Poor expression of pKLW1 may indicate that the N-terminal region of PDIp is structured and important for the overall structure of the **a** domain. It may also indicate that the domain boundary of PDIp **a** has been compromised by the truncation. In order to determine whether this is the case, alternate truncation mutants could be made to see if expression can be improved.

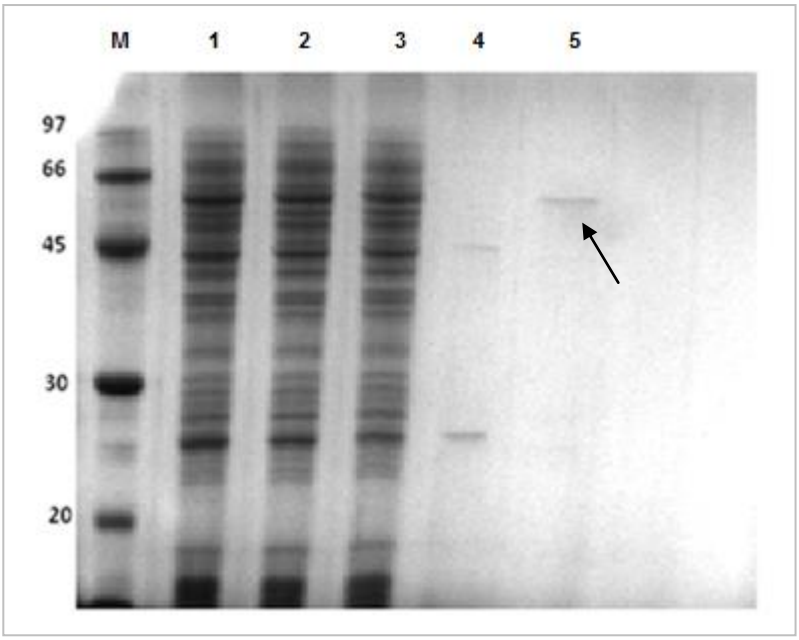

Figure 3.10: N-terminal truncate purification by IMAC. In order as seen on the gel: M = marker, 1) supernatant, 2) flowthrough, 3) 20mM imidazole wash, 4) 50mM imidazole wash and 5) 200mM imidazole elution step. Arrow indicates position of PDIp on the gel.

3.4.5. Ammonium sulphate precipitation

Due to difficulties purifying PDIp via IMAC, an alternative purification technique: ammonium sulphate precipitation was tested. Initial studies showed that PDIp dropped out of solution in 35% saturated ammonium sulphate meaning that it was

possible to significantly reduce the amount of contaminating protein. This method ultimately led to increased precipitation of PDIp in subsequent purification steps and reduced binding to the IEC column. Essentially this meant that a) PDIp losses were high and b) PDIp could not be purified to a high standard (see figure 3. 11).

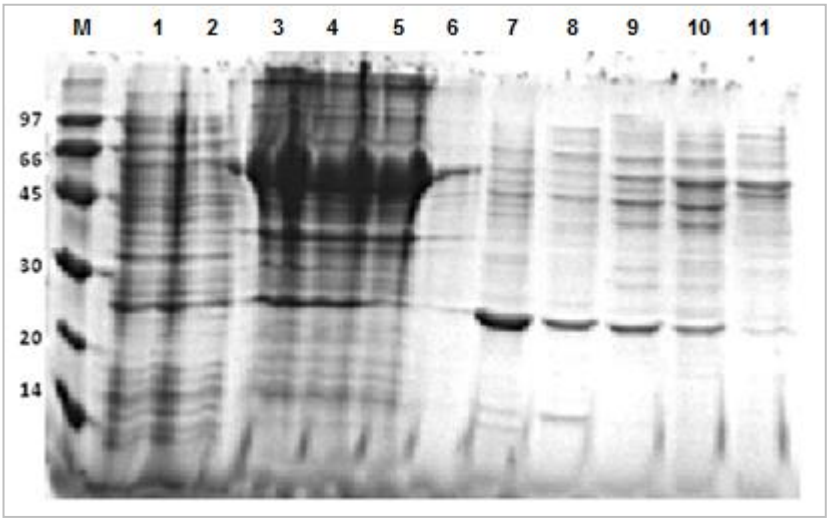

Figure 3.11: IEC of PDIp following salt precipitation. Gel showing fractions collected during IEC. M= marker, 1) supernatant 1, 2) pellet, 3) supernatant 2 (following ammonium suphate precipitation, resuspended protein had a tendency to drop out of solution), 4) wash, 5-11) IEC fractions (arrow shows position of PDIp on the gel)

Figure 3.11 indicates that although the expression yield of PDIp was high, significant losses were observed as a result of an inability to bind to the Source 30Q column. Consequently, a high percentage of PDIp was lost during the purification steps that followed ammonium sulphate precipitation. The reason for this is unclear but it may be that this method reduces the overall stability of PDIp. Furthermore only one IEC fraction, (shown in lane 5, figure 3.11) was shown to contain a considerable amount of PDIp but unfortunately it was also significantly contaminated. Yield of PDIp in subsequent fractions was minimal.

To try to improve binding of PDIp to the IEC column, the dialysed protein sample was centrifuged at high speed (20,000 rpm) and IEC was performed using a Hepes

buffer (10mM Hepes, 5mM DTT (pH 8)). In contrast to the standard phosphate buffer, this buffer has an overall positive charge and it was hoped that this might improve the binding affinity of PDIp to the IEC column. This was not the case and there seemed to be no noteworthy difference between elution profiles produced for either buffer (not shown).

3.4.6. Purifying PDIp using a batch IMAC protocol

A new protocol for purification of PDIp published after this work was initiated utilises a long binding step (incubating PDIp and column material for 1hr at 4ºC) and also a batch methodology. However a standard yield for this protocol was not published (Fu and Zhu, 2009a). Figure 3.12 clearly shows that this method of purifying PDIp markedly improves total yield and reduces total losses in the flow through.

The conclusion that can be taken from this is that the N-terminal His-tag of PDIp is dynamic. This means that a long binding step is providing a longer period of time for the His-tag and the Ni^{2+} column to interact. If the N-terminus of PDIp is structured (as postulated previously) its ability to exist in alternate conformations may be indicative of a capping mechanism and may have implications for the catalytic activity of PDIp **a**.

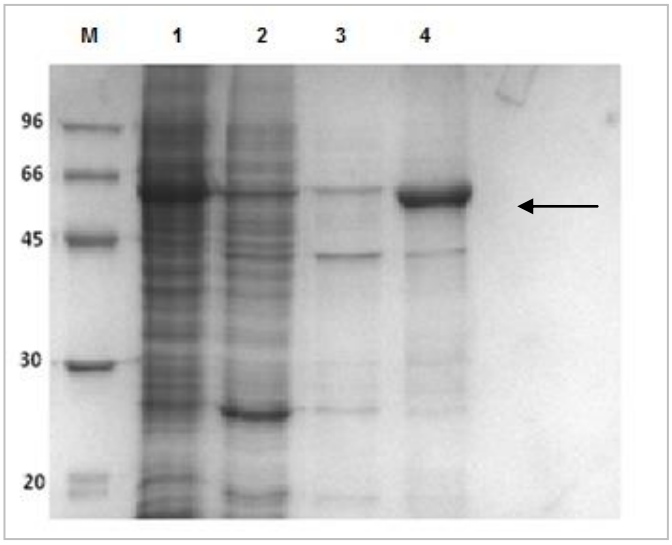

Figure 3.12: Batch purification of PDIp. SDS-PAGE shows that a higher yield of PDIp was obtained when a long binding step was employed (see arrow). M= marker, 1) flow-through, 2) wash 1, 3) wash 2, and 4) elute.

The batch protocol for IMAC gives rise to significantly less contamination than was seen previously for ammonium sulphate precipitation (see figure 3.12) and there were no further problems encountered in subsequent IEC steps. Evidently binding to the Ni^{2+} column remains temperamental even after a long binding step because protein is still lost in the flow through and during both wash steps prior to elution. The small band at ~40kDa (see figure 3.12) is probably caused by degradation of PDIp and is linked to the increase in processing time. Again the size of this fragment suggests loss at the C-terminus and is almost certainly the loss of the **a'** domain (Wang *et al.* 2010).

3.4.7. Ion exchange chromatography (IEC)

Following purification of PDIp by IMAC, the protein is dialysed and purified again by IEC. A typical IEC chromatogram for PDIp is shown in figure 3.13.

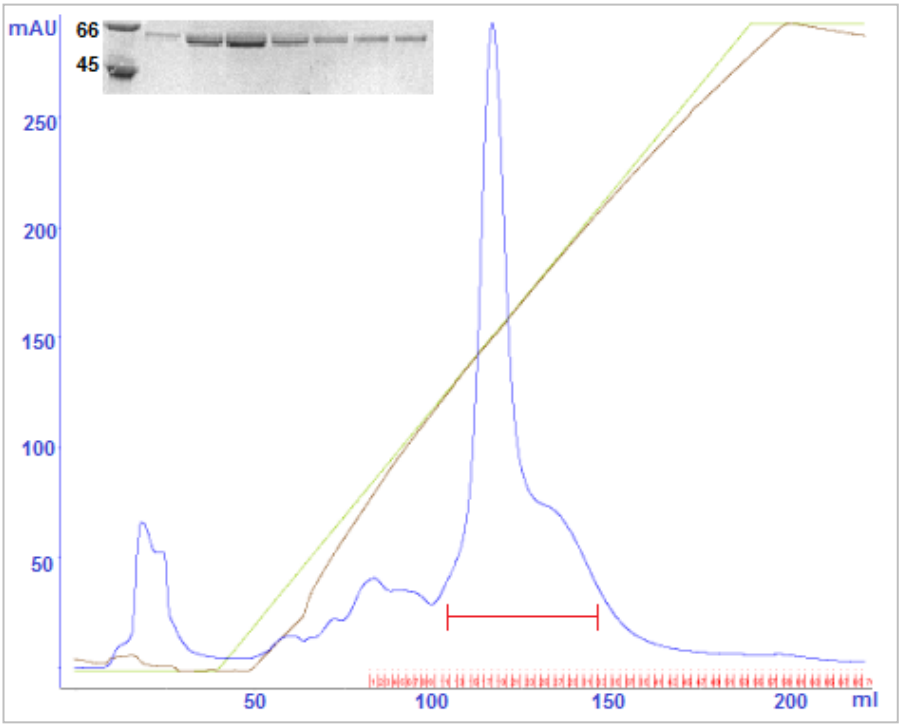

Figure 3.13: IEC chromatogram for PDIp and corresponding SDS-PAGE. Red line shows the region of the elution profile analysed by SDS-PAGE.

It is not dissimilar to that seen for PDI and shows a major elution peak with a clear shoulder. By SDS-PAGE no difference can be seen for samples taken from within the major peak or from the shoulder region but by native-PAGE it is clear that the shoulder peak is made up of dimer (not shown). Again this is similar to what is seen for PDI (Wallis *et. al* 2009). Fractions containing dimer are excluded when protein is pooled and concentrated although this does not prevent dimeric species from forming later.

Figure 3.13 shows a number of minor peaks indicating that although IMAC significantly reduces the number of contaminating proteins in a sample, there are still a lot remaining. IEC is able to remove them and these can be seen at lower salt concentrations than the major peak. It is important to analyse main peak fractions by SDS-PAGE to confirm that contaminants had been removed.

3.5. Stability

3.5.1. Stability studies of PDIp

Given that PDIp had previously been shown to be unstable (see figure 3.1, 3.7, 3.12), it was important to establish the extent of instability in order to arrange suitable storage conditions. Figure 3.14 indicates that after 3 days storage at 4ºC, untreated PDIp (lacking protease inhibitors) exhibits ~80% degradation and ~50% degradation when stored at -20°C or -80°C. At each storage temperature tested degradation could be reduced by the addition of PMSF at cell harvest and sonication (figure 3.14). Furthermore the addition of PMSF, leupeptin and pepstatin during cell harvest and sonication has since been shown to further improve the stability of PDIp and ensure that it can be stored for up to 2 months at -20°C (data not shown).

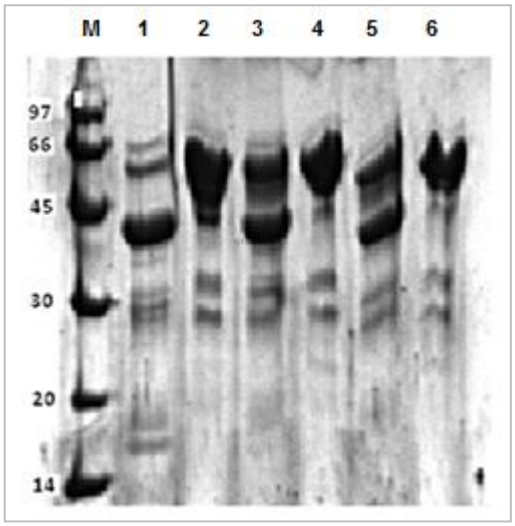

Figure 3.14: Stability of PDIp. Gel shows effect of storage and presence/absence of PMSF on stability of PDIp over a 3 day period. M= marker, 1) 4°C – PMSF, 2) 4°C + PMSF, 3) -20°C – PMSF, 4) -20°C + PMSF, 5) -80°C – PMSF and 6) -80°C + PMSF.

Athough clearly a requirement for this work, the use of PMSF must be controlled as it is possible that it could bind to PDIp. With the substrate binding specificity of PDIp being a hydroxy-aryl group it is likely that the phenolic ring structure of PMSF would fulfil this requirement. Studies of substrate binding in the presence and absence of PMSF would clarify this.

Interestingly, the major degradation product seen at ~40kDa in figure 3.14 correlates with the majority peak seen in the original MS data (see figure 3.1) and also the Western blot figure 3.7. Again, this is likely to be due to the loss of the **a'** domain as in hPDI, the intrinsic flexibility of the x-linker region has been shown to be most susceptible to proteases (Wang *et al*. 2010).

As a final attempt to improve stability, IEC was performed using a water jacket set at 4ºC. This had a negative effect on the binding of PDIp to the IEC column (data not shown) giving rise to a reduced yield. Moreover, the stability of PDIp did not appear to be altered relative to the standard procedure.

3.6. Mass spectrometry of full length PDIp

ESI mass spectrometry was used to confirm that the expressed protein was full length PDIp and that it had not been modified during expression and purification. The M_w of hexa-His tagged PDIp is 56919 Da. The major peak shown in figure 3.15 (peak a) is indicative of un-modified PDIp and has a measured mass of 56915 Da. This difference between actual and measured masses (~4Da) is within the standard error of the machine. It may also be indicative of the oxidised form of the protein (as formation of a disulphide bond at each active site would result in loss of 4 protons).

The difference between peak A and peak D is 178 Da and represents α-N-6-phosphogluconylation of the His-tag (Geoghegan *et al.* 1999). This is a common adduct of N-terminally His-tagged proteins. The exact identity of the adducts corresponding to peaks C and G has not been determined.

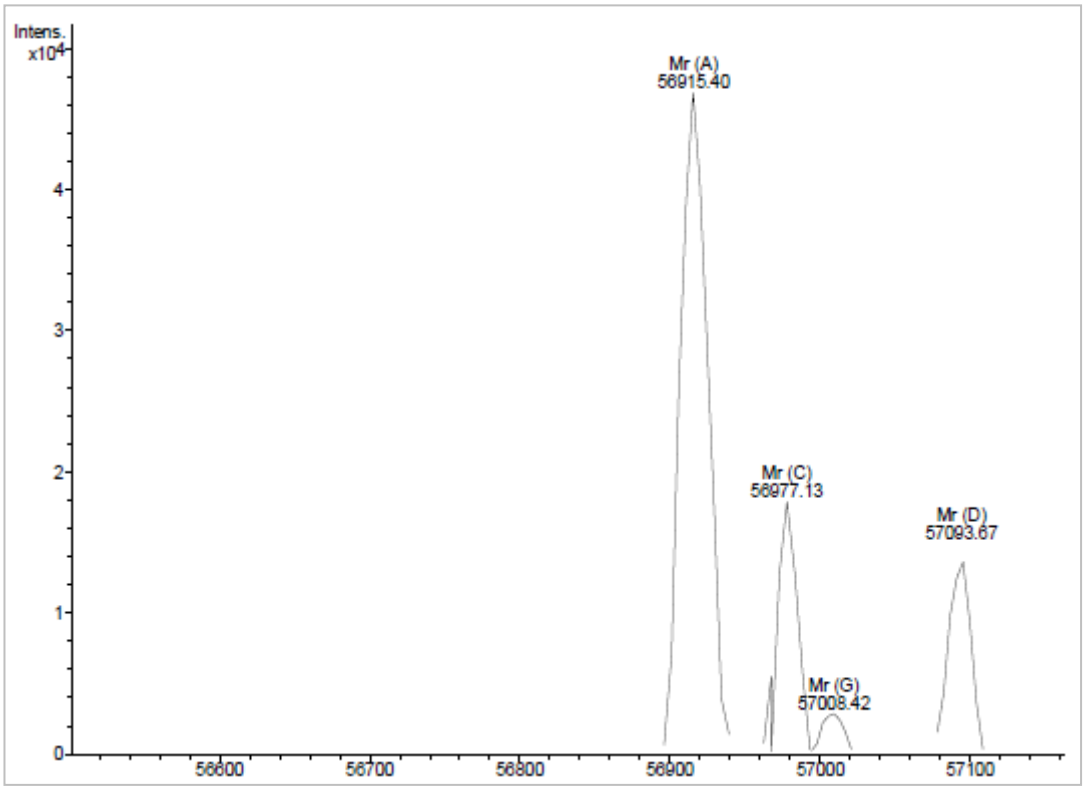

Figure 3.15: Deconvoluted high-resolution ESI MS of full length wild-type PDIp. M_w of hexa-His tagged PDIp is 56919 Da.

3.7. Yield

3.7.1. Improvement in yield due to optimisation of expression and purification

Pre-optimisation, expected yields of PDIp were ~2μg/ml culture. Following optimisation of expression this was more than doubled to ~5μg/ml culture although it was clear that there were losses during IMAC due to limited binding (see previously). Introducing a batch purification method where protein is incubated with Ni^{2+} sepharose for 1 hour has improved yields by 1000%. In addition, studies to improve stability have allowed us to store purified PDIp for up to 2 months if necessary which is also highly advantageous.

3.8. Constructs of PDI and PDIp

3.8.1. Expression and purification of PDI and PDIp constructs

Using the expression, purification and storage protocols developed above, it was possible to express and purify large amounts of WT PDIp, PDIp mutants and also PDI/PDIp chimeras. These are summarised in table 3.1 which also includes standard PDI expression and purification protocols for reference.

The expression of PDIp and PDIp constructs has markedly improved and typically a yield of 20μg/ml of culture can be expected for the full length protein in LB. Although there were issues expressing full length PDIp in EnBase, this system was very successful in improving yields of PDI **a** and PDIp **a** proteins.

Table 3.1: Expression/purification protocols for various PDI/PDIp constructs with expected yield

Protein	Expression/Purification Protocol	Yield (µg/ml culture)
PDI & full length PDI mutants	Growth & expression at 37°C. Expression time: 4hrs. Standard IMAC protocol. IEC at pH 7.3 (phosphate buffers)	24
PDIp & full length PDIp Mutants	Growth at 37ºC & expression at 25°C. Expression time: overnight. Batch IMAC protocol including 1hr binding step at 4°C IEC at pH 7.3 (phosphate buffers)	20
PDIp (N-terminal truncation)	As for PDIp but expression levels very low so purification studies have not been completed.	N/A
PDIp **b'xa'c**	As for PDIp except IEC at pH 8 in 10mM Hepes, 5mM DTT buffer (protein did not bind to column under standard conditions)	4
PDIp (**ab**) PDI (**b'xa'c**)	As for PDIp + size exclusion chromatography (SEC).	15
PDIp (**ab**) PDI (**b'x**) PDIp (**a'c**)	As for PDIp + SEC (if necessary)	29
PDIp (**ab**) PDI (**b'x**) PDIp (**a'c**) T419G	As for PDIp + SEC (if necessary)	17
PDI **a** & PDI **a** Mutants	As for PDI	22
PDI **a** & PDI **a** Mutants	EnBase expression system, following manufacturer's guidelines for expression. IMAC and IEC as for PDI.	150
PDIp **a** & PDIp **a** Mutants	As for PDI	22
PDIp **a** & PDIp **a** Mutants	EnBase expression system, following manufacturer's guidelines for expression. IMAC and IEC as for PDI.	150

3.8.2. Expression of PDIp **b'xa'c**

Like PDIp, initial studies of the expression and purification of PDIp **b'xa'c** were problematic (data not shown). Using a standard protocol for expression (4 hours at 37ºC) poor yields were obtained. Furthermore, PDIp **b'xa'c** did not bind to the Ni^{2+} column making it very difficult to purify by IMAC. This was particularly interesting

because it had been suggested that the N-terminal extension of full length PDIp was the cause of reduced binding. This is lacking in PDIp **b'xa'c** indicating that there must be another contributor to this problem.

Using optimised expression protocols and a long binding step during IMAC improved yield significantly (see figure 3.16). Unfortunately however PDIp **b'xa'c** does not bind to the Source 30Q column in phosphate buffer (pH 7.3) or Tris-HCl buffer (pH 8.3). Its theoretical pI is 5.61 (ExPASy ProtParam) which is not significantly different to the estimated pI of the wild-type protein (5.00). Therefore both proteins should be negatively charged at physiological pH or above and consequently be able to bind to the column (anion exchanger).

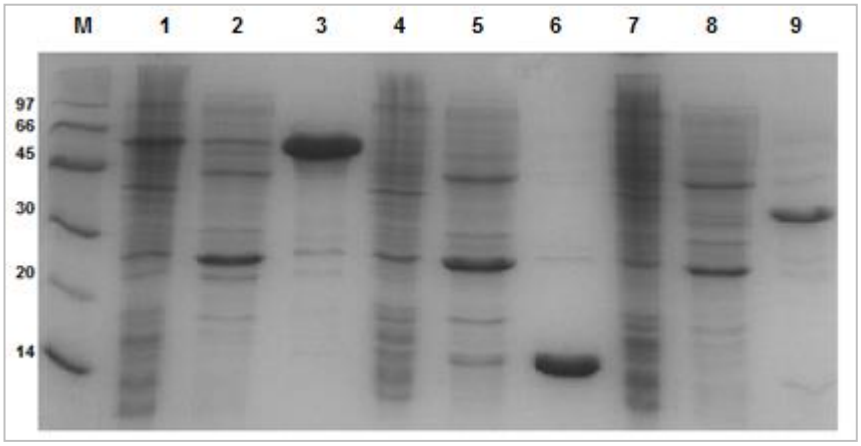

Figure 3.16: IMAC of PDIp, PDIp a' and PDIp b'xa'c. 12% SDS-PAGE gel showing total soluble protein, flow through and elution fractions for IMAC of PDIp (1-3), PDIp **a'** (4-6) and PDIp **b'xa'c** (7-9) respectively. M= marker

Finally, it was possible to purify PDIp **b'xa'c** by IEC using a Hepes buffer (pH 8) which clearly allows binding to the souce 30Q column (data not shown). The reason for this is unknown but it is possible that the negative charges of the PO_4^- ions and Cl^- ions found in the phosphate and tris-HCl buffers respectively were competing with PDIp **b'xa'c** for binding to the column.

Unfortunately having optimised the expression and purification of PDIp **b'xa'c** further study was abandoned because it was very unstable and prone to aggregation. 2 days after purification (storage at -20ºC), a high percentage of PDIp **b'xa'c** is lost to aggregation (data not shown). Instability was not unexpected as similar issues arise during the purification of PDI **b'xa'c.** In addition to being unstable, the exposed hydrophobic surfaces on the **b'** domain of these proteins makes them much more prone to dimerisation. After considerable efforts to improve stability, PDIp **b'xa'c** was removed from further study of structure and function properties *in vitro*.

3.8.3. Expression of PDIp **a'c**

Using the optimised expression protocol for PDIp sufficiently high levels of PDIp **a'c** were obtained. There were no issues in regards to binding of PDIp **a'c** to the Ni^{2+} column and so a long binding step and batch protocol were not required during IMAC (see figure 3.16). Similarly, IEC of PDIp **a'** was also trouble free. During concentration however, PDIp **a'c** rapidly precipitates. As an attempt to reduce precipitation, fractions taken from IEC were pooled and arginine and glutamate were added to a total concentration of 50mM. The protein was then dialysed against decreasing amounts of NaCl (down to 50mM) in the presence of arginine and glutamate. This protocol has been shown to be able to improve protein solubility by up to 8 times on account of arginine and glutamate being effective in improving stability and reducing precipitation (Golovanov *et al*. 2004).

Although this protocol showed some success in improving the solubility of PDIp **a'c,** precipitation readily occurred when lower concentrations of salt, arginine or glutamate were used. This therefore was unfeasible for further work which included NMR and *in vitro* assays. Consequently additional studies of PDIp **a'c** were abandoned.

3.9. Concluding Remarks

The standard yield of PDIp that we can expect per 1ml of culture has been improved from only 2μg/ml to ~20μg/ml. Although expression was optimised, it is clear that the changes made to the purification protocol -specifically a long binding step during IMAC- were the most significant contributing factor. Although this is poorly understood, it is probable that the His-tag on the protein is mobile and therefore between states where it is accessible and where it is not. Based on the results of SDS-PAGE it is likely that only 33% of the protein has an 'accessible' His-tag at any one time. Therefore a long binding step allows the His-tagged protein to be 'trapped' when in the correct conformation thus enabling a greater chance of eventual interaction. This also explains why a His-tag was observed by Western blot (see figure 3.7) even though very little binding was seen.

We have suggested that the acidic N-terminus of PDIp is providing a 'docking' area for the His-tag therefore reducing its solvent accessibility. An N-terminal truncation clone shows very poor expression under conditions optimised for wild-type PDIp suggesting that the N-terminus may exert a more important role than originally anticipated. Therefore, although considerable work is required in order to obtain sound conclusions it is speculated that the N-terminus of PDIp could provide structural features required for the catalytic activity of PDIp **a**.

Chapter 4. Studies of the structure and enzymatic activity of human PDIp

4.1. Introduction

High resolution X-ray structures of oxidised and reduced hPDI (2.9 and 2.5 Å respectively) have recently been published (Wang *et al.* 2012). This and previous work show that hPDI undergoes large redox-mediated conformational changes centred on **b'xa'** which consequently give rise to changes in total cleft volume and also relative exposure of the substrate binding site (Wang *et al.* 2011). With no structure currently available, it has been assumed that hPDIp, which is 45% identical to hPDI in sequence, exhibits a similar 3-dimensional conformation to that of hPDI: its most similar family member.

The enzymatic activity of PDIp is also poorly studied. Using the insulin reduction assay (a classical PDI activity assay) it has been shown that PDIp has ~50% of the activity of PDI (Desilva *et al.* 1996, Fu and Zhu, 2010). Unfortunately these experiments are questionable as the protein being assayed contains 7 amino acids from the signal peptide sequence. In an oxidase assay using the mature protein, PDIp was again found to be less active than PDI but seemed to show an unusual pH dependence that was not further investigated (Alanen *et al.* 2006).

The aims of this work were to test the assumption that PDIp is similar structurally to PDI and also to characterise the oxido-reductase activity of PDIp relative to PDI.

4.2. Redox un-controlled experiments

4.2.1. Intrinsic fluorescence measurements

Phenylalanine, tyrosine and tryptophan are intrinsically fluorescent although the signal emitted from phenylalanine is generally quite low. Typically therefore measurements of protein fluorescence reflect environments of tryptophan and tyrosine only. It is possible to use the intrinsic fluorescence of tryptophan and tyrosine to monitor protein folding because when either residue is buried within a protein (i.e. in the folded state) higher fluorescence intensity is observed than when they are solvent exposed (i.e. in the unfolded state).

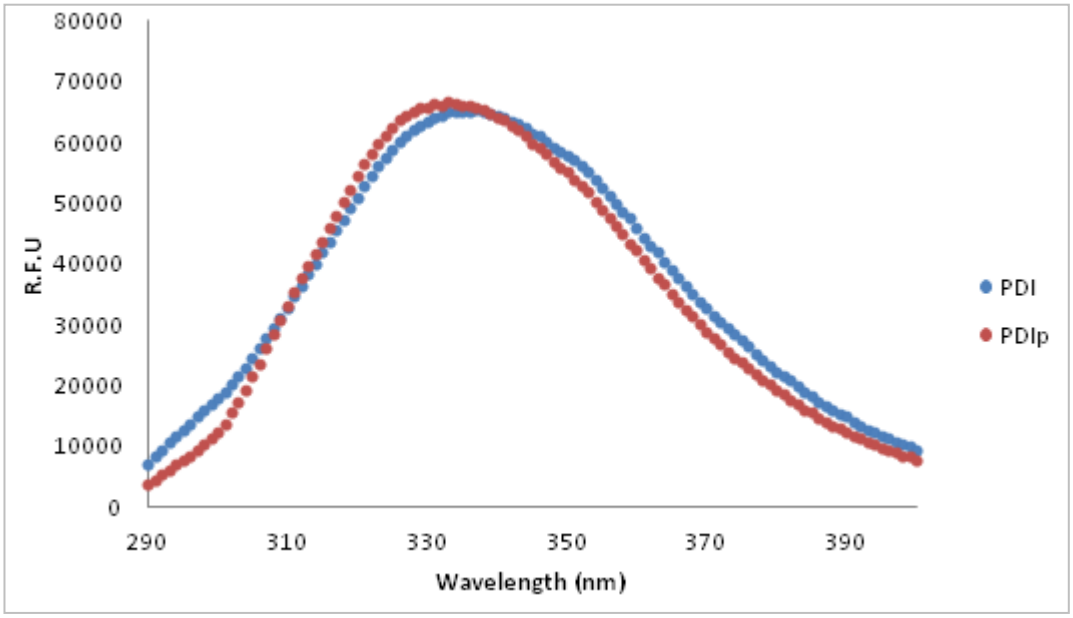

Figure 4.1: Intrinsic fluorescence of PDI and PDIp. Samples containing 10µM PDI/PDIp in 20mM phosphate buffer (pH 7.3) were excited at 280nm and fluorescence emission measured between 290 and 400nm. Slit width = 2nm.

As all 5 PDI tryptophan residues are conserved in PDIp it is possible to compare the two proteins directly using intrinsic fluorescence. Shown in figure 4.1 are emission scans for PDI and PDIp following excitation at 280nm. The emission spectra for PDIp is clearly blue shifted relative to that of PDI. Recent work has indicated that differences between PDI_{red} and PDI_{ox} can be determined by intrinsic protein fluorescence i.e. that PDI_{red} is blue-shifted relative to PDI_{ox} (Wang *et al.* 2011). It is believed that this shift is due to PDI_{ox} being more open and less tightly folded than $PDI_{red.}$ On this basis it is possible that the difference in λ_{max} for PDI and PDIp (see figure 4.1) is indicative of PDIp having a generally more folded structure than PDI. However this conclusion must be treated cautiously as differences in tryptophan environment caused by lack of sequence homology in surrounding regions could also be to blame.

4.2.2. ANS fluorescence

The recent X-ray crystal structure of human PDI (hPDI) has confirmed that like yeast PDI (yPDI), hPDI is arranged in a twisted ‘u’ structure (Wang *et al.* 2012). Along the inside of the ‘u’ are surface exposed hydrophobic amino acids giving rise to a hydrophobic patch associated with substrate binding. ANS is able to probe the hydrophobic surfaces of proteins and so is a suitable probe to investigate the inner surface and substrate binding cleft of PDIp

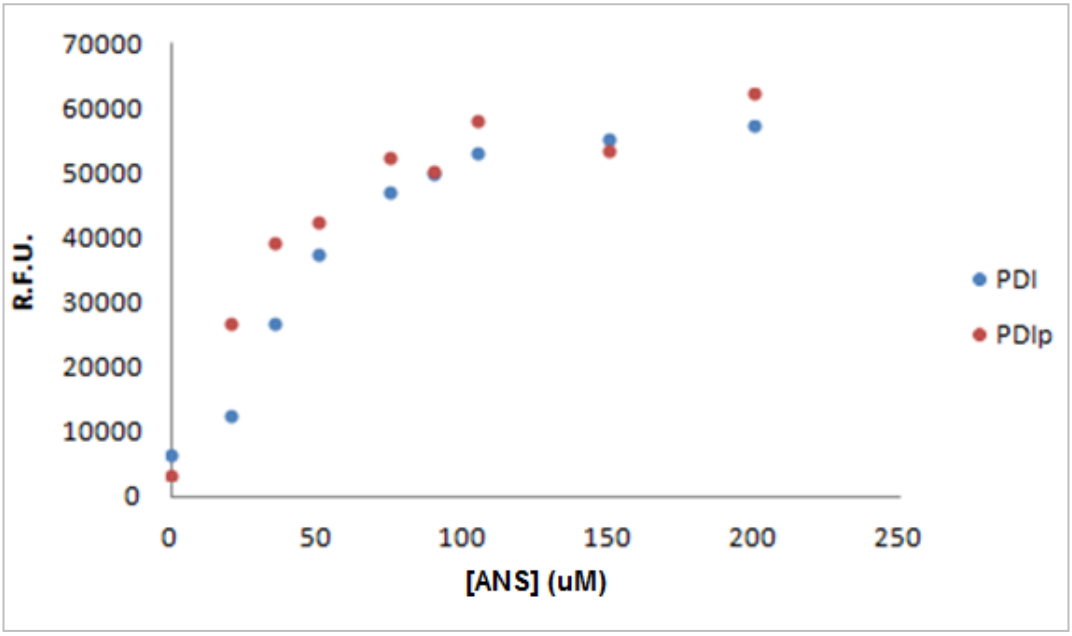

Figure 4.2: ANS saturation curve for PDI and PDIp. The interaction of varying concentrations of ANS with 1μM PDI/PDIp in 20mM phosphate buffer (pH 7.3) was recorded (excitation at 390nm). RFU at λ_{max} is plotted against final ANS concentration.

For both PDI and PDIp, saturation is achieved at ~100μM ANS. Although not an accurate probe of cleft size, figure 4.2 suggests that PDI and PDIp may have roughly the same total hydrophobic surface area. This is in line with the assumption that PDI and PDIp have similar 3-dimensional structure.

4.2.3. Secondary structure analysis by far UV Circular Dichroism (CD)

Far UV CD was used to observe the secondary structure conformations of hPDI and hPDIp (figure 4.3). Unexpectedly this data showed distinct differences between 190 and 200nm: an area representative of α-helical structure. Figure 4.3 therefore suggests that PDIp has a greater proportion of α-helix than PDI.

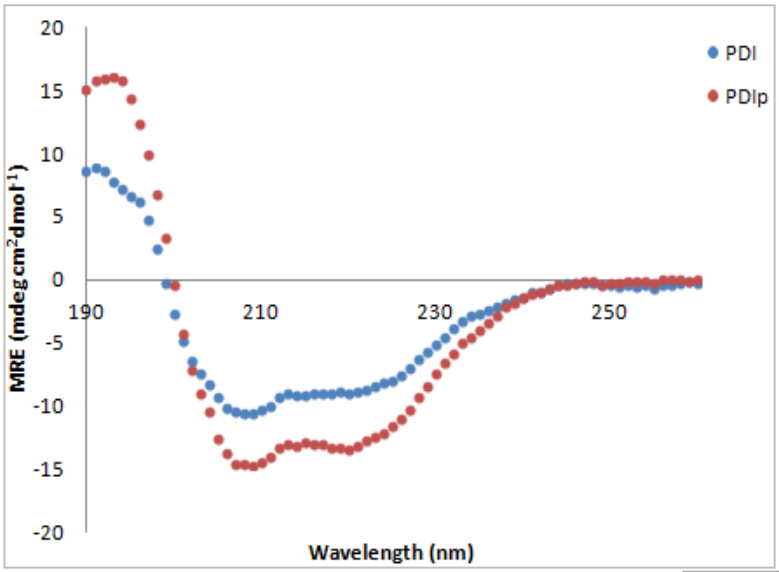

Figure 4.3: Far UV CD of PDI and PDIp at 20ºC. The circular dichroism of each protein (0.1mg/ml) in 5mM phosphate was recorded at wavelengths from 190 to 260nm at 20ºC. The mean residue ellipticity (MRE) was then calculated.

	α-helix	β-sheet	Turns	Unordered
PDI	31%	19%	14%	36%
PDIp	42%	11%	13%	33%

Table 4.1: Results of DichroWeb analysis for PDI and PDIp DichroWeb analysis was performed using the CDSSTR algorithm and reference set SP175. Spectra were collected for 0.1mg/ml samples of each protein in 5mM phosphate at 20ºC.

DichroWeb analysis of the data collected in figure 4.3 estimated that PDIp has 42% α-helical structure and PDI, 31% (see table 4.1). The actual α-helical content of reduced PDI **abb'xa'** (based on crystal structure PDB: 4EKZ) is 28% (UniProt). This small discrepancy between calculated and measured α-helical content of PDI is a disadvantage of using DichroWeb which is biased by user-defined parameters. The quality of the PDI sample is not disputed due to the high reproducibility of the data. This is also true for the obvious differences between PDI and PDIp seen in terms of signal, particularly between 200-240nm. An explanation for this remains unclear.

It is very unlikely that the differences between PDI and PDIp in terms of α-helical structure are due to the two catalytic domains (**a** and **a'**). PDI **a** and **a'** share high sequence identity with the corresponding domains in PDIp (56% and 64% respectively) and also a thioredoxin fold which is highly structurally conserved in PDI family members. It is most probable that the differences in secondary structure observed are due to the N-terminal extension of PDIp or the **b'** domain which shares

relatively low sequence identity with PDI **b'**. Discrepancies in structure between PDI **b'** and PDIp **b'** could explain why PDIp has restricted substrate specificity while PDI is a more general protein folding catalyst.

4.2.4. Thermal denaturation using far UV CD

Figure 4.4 shows the effect of increasing temperature on the secondary structure of PDI and PDIp. Method as described by Wang *et al.* 2010.

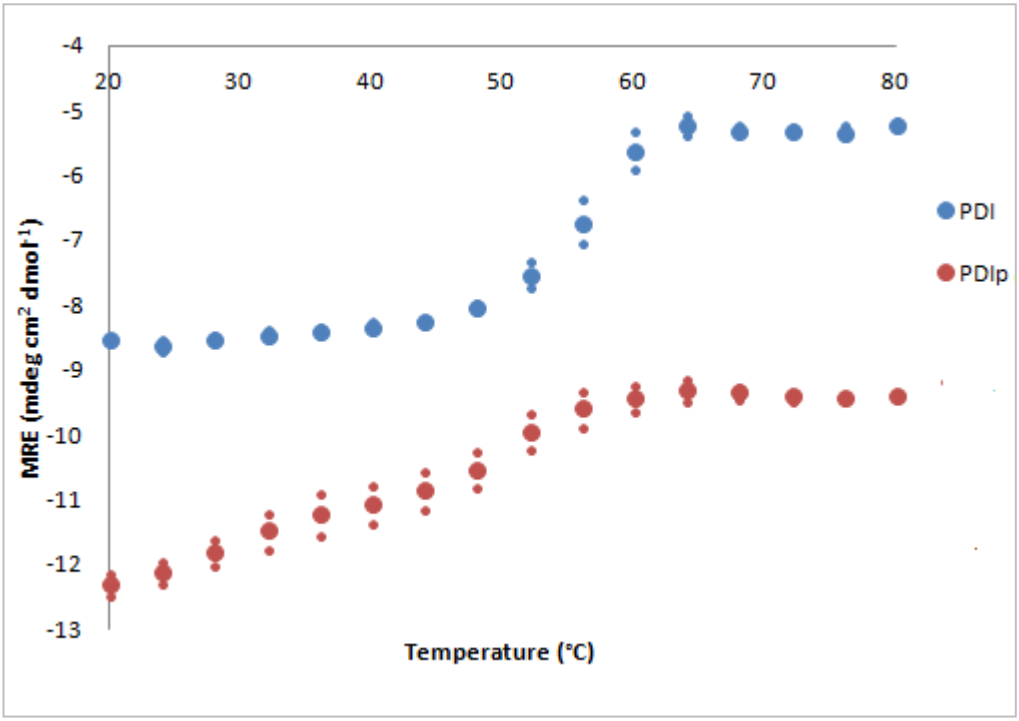

Figure 4.4: Thermal denaturation of PDI and PDIp. The circular dichroism at 222nm was measured for each protein (0.1 mg/ml protein in 5mM phosphate) at 4°C intervals between 20-80°C. Samples were allowed to equilibrate for 10 minutes and then measurements were taken for 2 minutes. The mean CD and MRE for each temperature were then calculated. Method as described by Wang *et al.* 2010.

The thermal denaturation of PDI shows a single transition step with a T_m of ~56ºC and is reproducible (see figure 4.4). In contrast, PDIp loses secondary structure in a continuous fashion between 20-60°C with no definitive T_m. This may indicate that PDIp has a greater degree of intrinsic flexibility than PDI and explains the issues

with stability that had been seen previously in chapter 3. Above 80ºC additional destabilisation events occur but these could not be accurately measured due to limitations of the equipment (data not shown). Similar to that of PDI, the thermal denaturation of PDIp is also reproducible.

When looking at the extent of thermal destabilisation it is clear that of the two proteins, PDIp loses the smallest percentage of secondary structure. Cumulatively this data suggests that PDIp as an entity is not unstable but that there are regions within it that are sensitive to thermal denaturation.

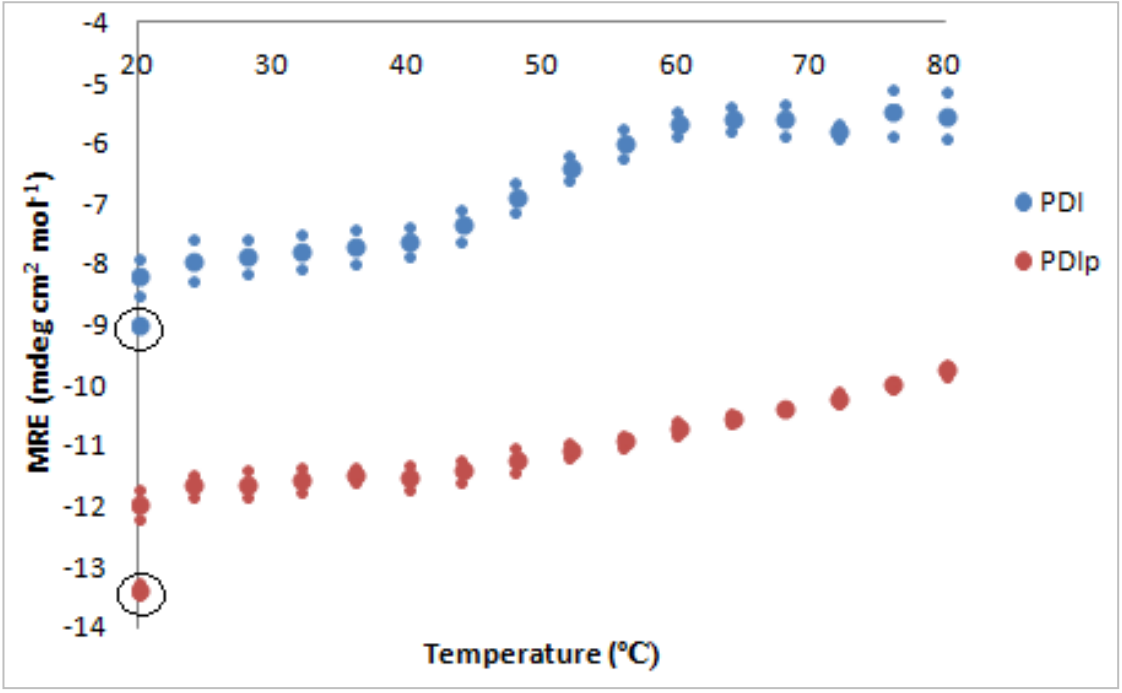

Figure 4.5: Thermal refolding of PDI and PDIp. The circular dichroism at 222nm was measured for each protein (0.1 mg/ml protein in 5mM phosphate) at 4°C intervals between 80-20°C. Samples were allowed to equilibrate for 10 minutes and then measurements were taken for 2 minutes. The mean CD and MRE for each temperature were then calculated. The data points for pre-heated samples are circled.

Refolding of PDI and PDIp can also be measured by far UV CD (see figure 4.5). As temperature is reduced from 80ºC to 20ºC PDI refolds with significant efficiency and

has a clear cut transition step. Refolding of PDIp is continuous over the temperature range tested. For both proteins, refolding is not 100% complete, but occurs via similar transition events (in reverse) to those seen in the initial unfolding experiment.

Interestingly, early work on the purification of PDI from bovine liver included a heat treatment step where the crude sample was incubated at 54ºC (Lambert and Freedman 1983a). Figure 4.4 indicates that this is just below the T_m for PDI and indicates that at this temperature, PDI would be undergoing an unfolding transition. In their protocol the heat treatment is followed by incubation on ice (Lambert and Freedman 1983a). It is likely that almost full recovery of structure would be obtained during cooling because the unfolding transition is reversible (see figure 4.5). Clearly this explains why major issues with reduced protein recovery and aggregate formation are not seen for PDI purification using this protocol.

4.2.5. Analysis of secondary structure by far UV CD after incubation at 80ºC

Both Figure 4.6 and table 4.2 show that after incubation for 10 minutes at 80ºC, PDIp retains significant secondary structure relative to PDI which had seen major losses. This thermal stability is clearly very unusual but is supported by thermal denaturation studies (figures 4.4 and 4.5). This work suggests that PDIp is very stable at high temperatures and loses only a small amount of secondary structure. Again, this may imply that there are regions within PDIp that are dynamic but fewer than within PDI.

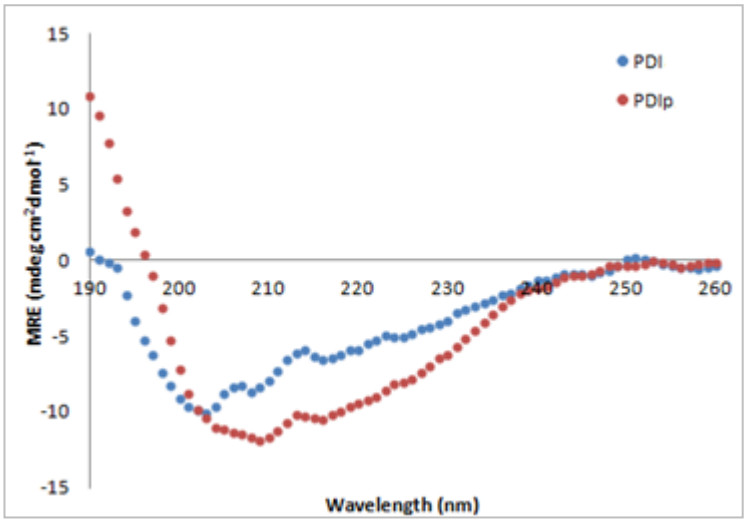

Figure 4.6: Far UV CD of PDI and PDIp at 80ºC. The circular dichroism of each protein (0.1mg/ml) in 5mM phosphate was recorded at wavelengths from 190 to 260nm at 20ºC. The mean residue ellipticity (MRE) was then calculated.

	α-helix	β-sheet	Turns	Unordered
PDI	16%	25%	16%	42%
PDIp	30%	17%	15%	38%

Table 4.2: Results of DichroWeb analysis for PDI and PDIp incubated at 80ºC. DichroWeb analysis was performed using the CDSSTR algorithm and reference set SP175. Spectra were collected for 0.1mg/ml samples of each protein in 5mM phosphate at 80ºC.

Stability to adverse conditions may be a requirement of PDIp *in vivo* and therefore this work may provide clues to possible activities and physiological substrates of PDIp.

4.3. Redox-controlled experiments

4.3.1. Far UV CD of oxidised/reduced protein

Recent work has shown that human PDI undergoes a redox-regulated conformational change centred on **b'xa'** (Wang *et al.* 2011, Wang *et al.* 2012). More specifically, PDI appears to become more 'open' and expose a larger degree of its hydrophobic surfaces when it is in the oxidised state than when it is in the reduced state. In addition oxidised PDI has increased chaperone activity. This is suggested to be

linked to the redox-mediated conformational changes described previously (Wang *et al.* 2011).

Using the same method for thermal denaturation as before, the T_m of PDI_{red} was found to be higher (~56°C) than that of PDI_{ox} (~52°C) i.e. PDI_{ox} is less thermally stable than PDI_{red} (figure 4.7). This result correlates with published data that shows that in its oxidised form PDI exhibits greater surface exposure (Wang *et al.* 2011, Wang *et al*. 2012). There were no significant differences between the thermal stability of $PDIp_{ox}$ and $PDIp_{red}$. This implies that the destabilising effect of oxidation (probably the conformational change discussed previously) that is seen for PDI is not mirrored in PDIp (see figure 4.7).

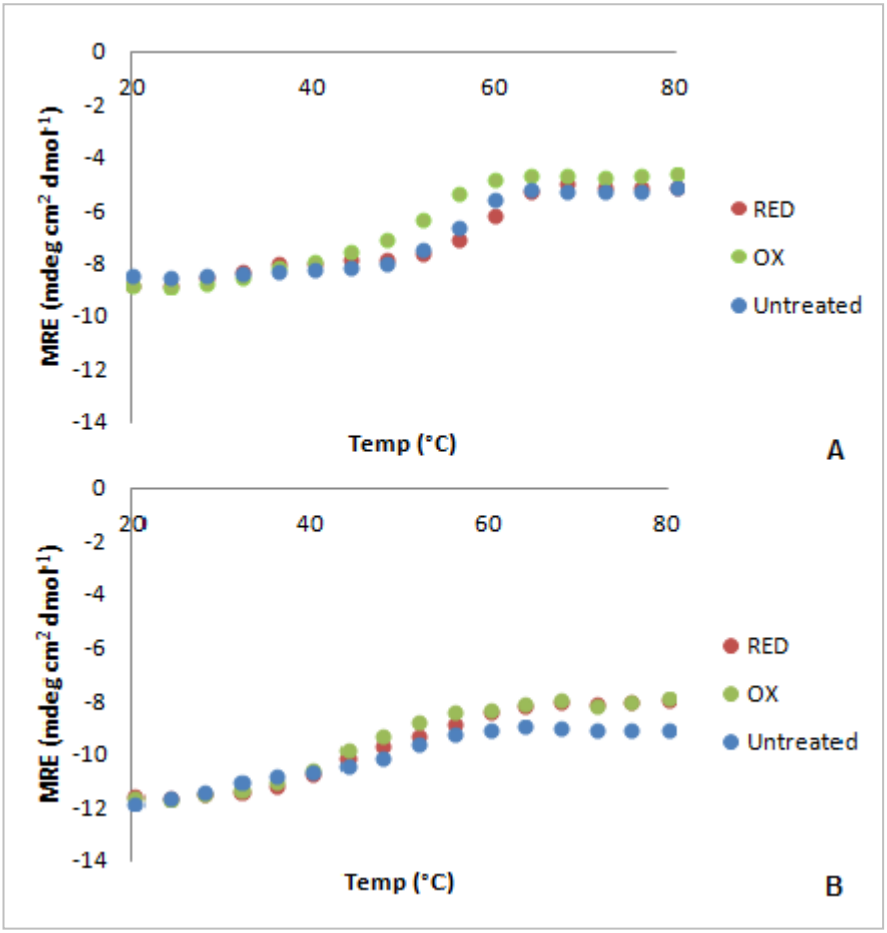

Figure 4.7: Thermal denaturation of A) PDI and B) PDIp in reduced and oxidised states. 1mg/ml protein was prepared in 5mM phosphate buffer containing 5mM DTT or diamide. Desalting was then performed using a PD10 column. The circular dichroism at 222nm for 0.1mg/ml samples of each protein was then measured at 4°C intervals between 20-80°C. Samples were allowed to equilibrate for 10 minutes and then measurements were taken for 2 minutes. The mean CD and MRE for each temperature were then calculated.

4.3.2. Limited proteolysis experiments

In order to investigate the effect of redox state further, limited proteolysis experiments were performed (see figure 4.8). Historically, limited proteolysis has been used to determine the domain boundaries of PDI because regions of structure are known to be less susceptible to proteolysis than linker regions (found between domains). It was expected that changes in conformation associated with the oxidation of PDI would give rise to increased exposure to proteases.

Interestingly, PDIp has fewer potential cleavage sites for trypsin and proteinase K than PDI. It is likely that PDIp has evolved in this way due to its location in the acinar cells of the exocrine pancreas i.e. the cells responsible for the secretion of zymogens. This may therefore be a clue to its physiological function which currently remains unknown. In this experiment, chymotrypsin (another pancreatic protease) was used.

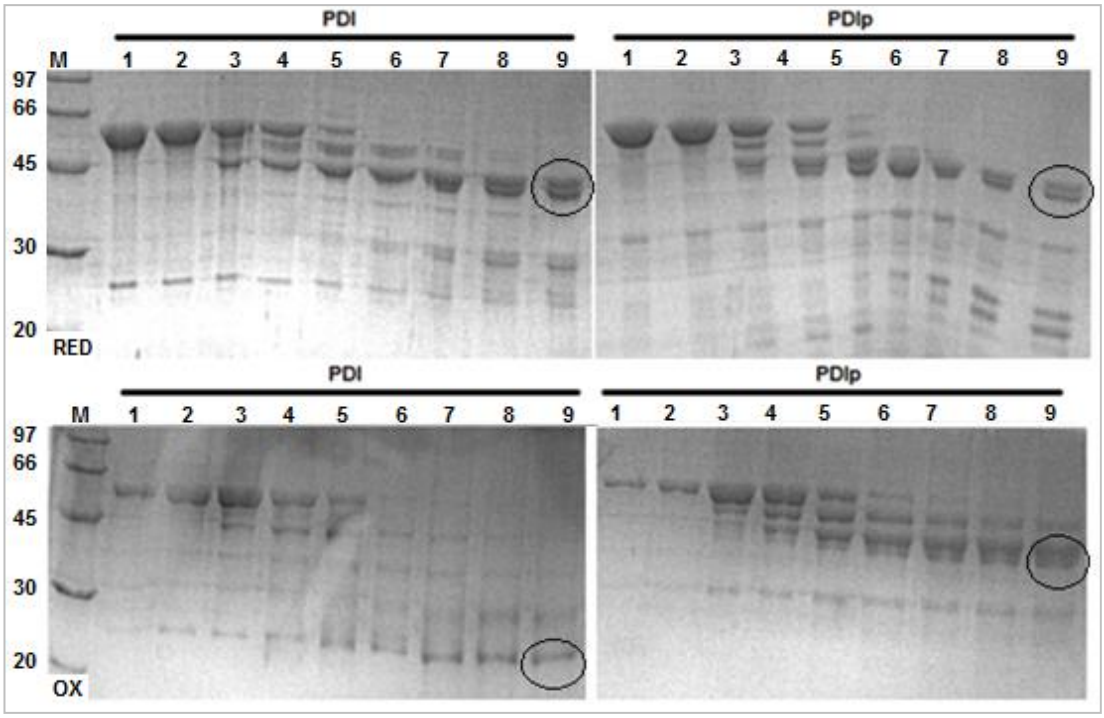

Figure 4.8: Limited proteolysis of PDI and PDIp in reduced and oxidised states. Protein samples (15μM) were incubated with chymotrypsin (75nM) for up to 2 hours in the presence of 5mM DTT or diamide in 50mM Tris HCl buffer pH 7.6. 1) Untreated, 2) 0 mins, 3) 5 mins, 4) 10 mins, 5) 20 mins, 6) 40 mins, 7) 60 mins, 8) 90 mins and 9) 120 mins. The reaction was stopped with the addition of SDS-loading dye and boiling for 5 minutes. Circles indicate gel bands sent for peptide mass fingerprinting analysis.

As expected, figure 4.8 shows that PDI_{ox} is much more susceptible to limited proteolysis than PDI_{red}. PDI_{ox} is almost completely digested after 2 hours incubation with chymotrypsin but for PDI_{red} a major product of ~40kDa can be seen. This correlates with previous data (see chapter 3) and is indicative of intrinsic flexibility at the x-linker region and the subsequent loss of **a'**. In contrast to this, both $PDIp_{ox}$ and

$PDIp_{red}$ are similarly susceptible to chymotrypsin with major fragments in both cases of ~40kDa. This work suggests that like PDI, PDIp has intrinsic flexibility centred on **b'xa'**. Unlike PDI however, susceptibility of PDIp to chymotrypsin does not appear to be increased by oxidation. Therefore this implies that PDIp does not undergo redox-mediated conformational changes similar to PDI. This is also in agreement with thermal denaturation studies shown previously (see figure 4.7).

To identify specific regions within PDI and PDIp that are most susceptible to proteolytic cleavage by chymotrypsin, peptide mass finger-printing analysis was performed (figure 4.9). Bands of interest were cut from the gel, subjected to further proteolysis (trypsin) and then any remaining peptides were detected by MALDI-TOF mass spectrometry. A sequence coverage map is then produced and any missing peptides can be identified (see figure 4.9).

It is clear from peptide mass finger-printing data that proteolytic cleavage occurs preferentially at the C-terminus of both PDI and PDIp (figure 4.9). This was in concordance with previous data that shows that PDI is most susceptible to proteolysis at the x-linker and surrounding area (Wang *et al.* 2010). Overall low sequence coverage meant that it was impossible to identify the exact sites of cleavage. In addition the PDI_{ox} sample which on the gel has a M_w of ~25kDa (see figure 4.9) has peptide coverage of ~60% which is much higher than expected. This suggests that the sample is heterogeneous and is a disadvantage of using peptide mass finger printing. ESI-MS provides exact cleavage sites and therefore is able to identify specific regions with susceptibility to proteases.

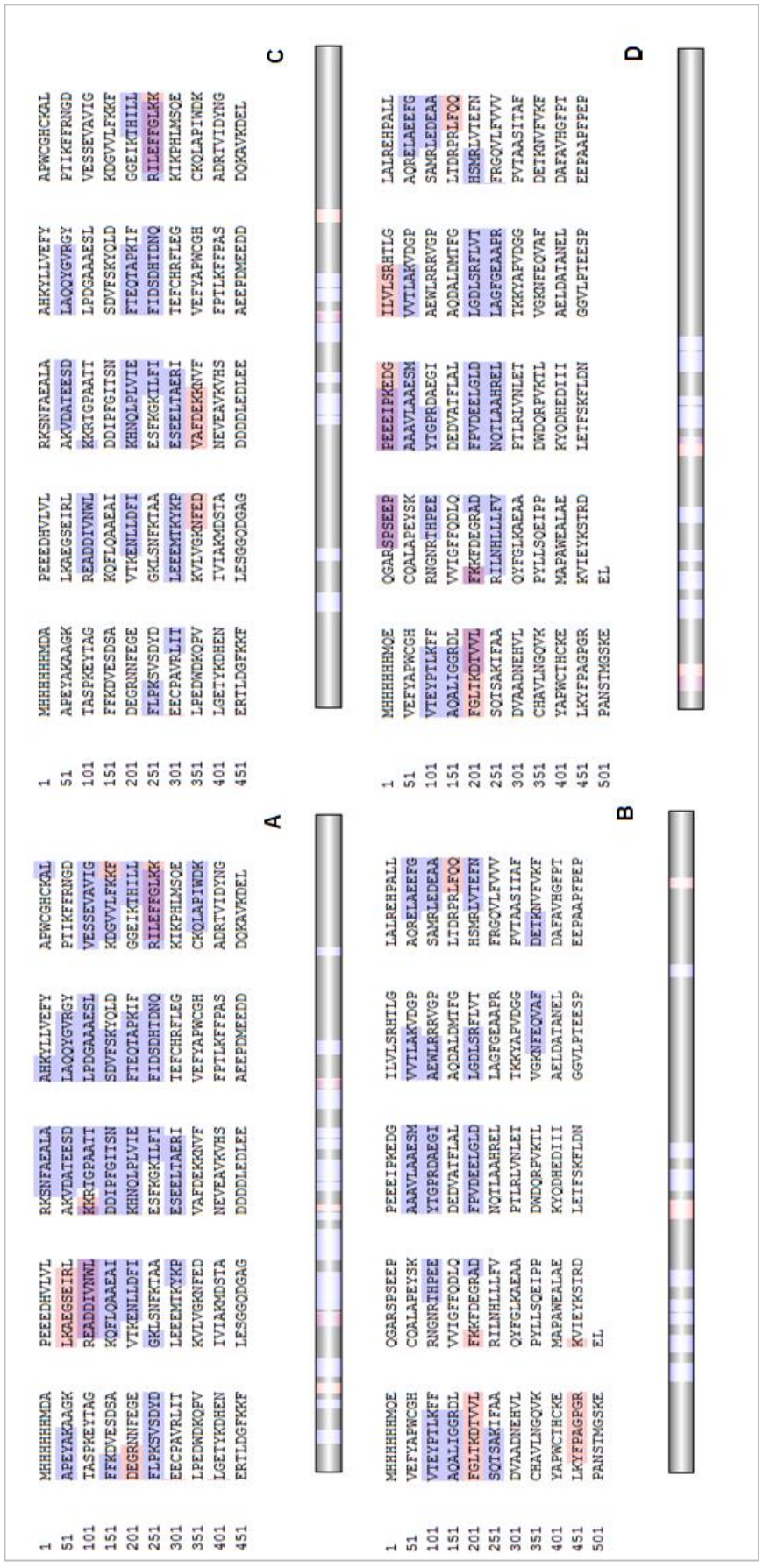

Figure 4.9: Peptide mass finger-printing analysis of limited proteolysis products. Having performed limited proteolysis on PDI and PDIp, (see figure 4.9) digestion products were cut from the gel and sent for peptide mass fingerprinting analysis. Blue shading indicates an abundant peptide while pink shading indicates a less common peptide. A) PDI reduced, B) PDI oxidised, C) PDIp reduced and D) PDIp oxidised.

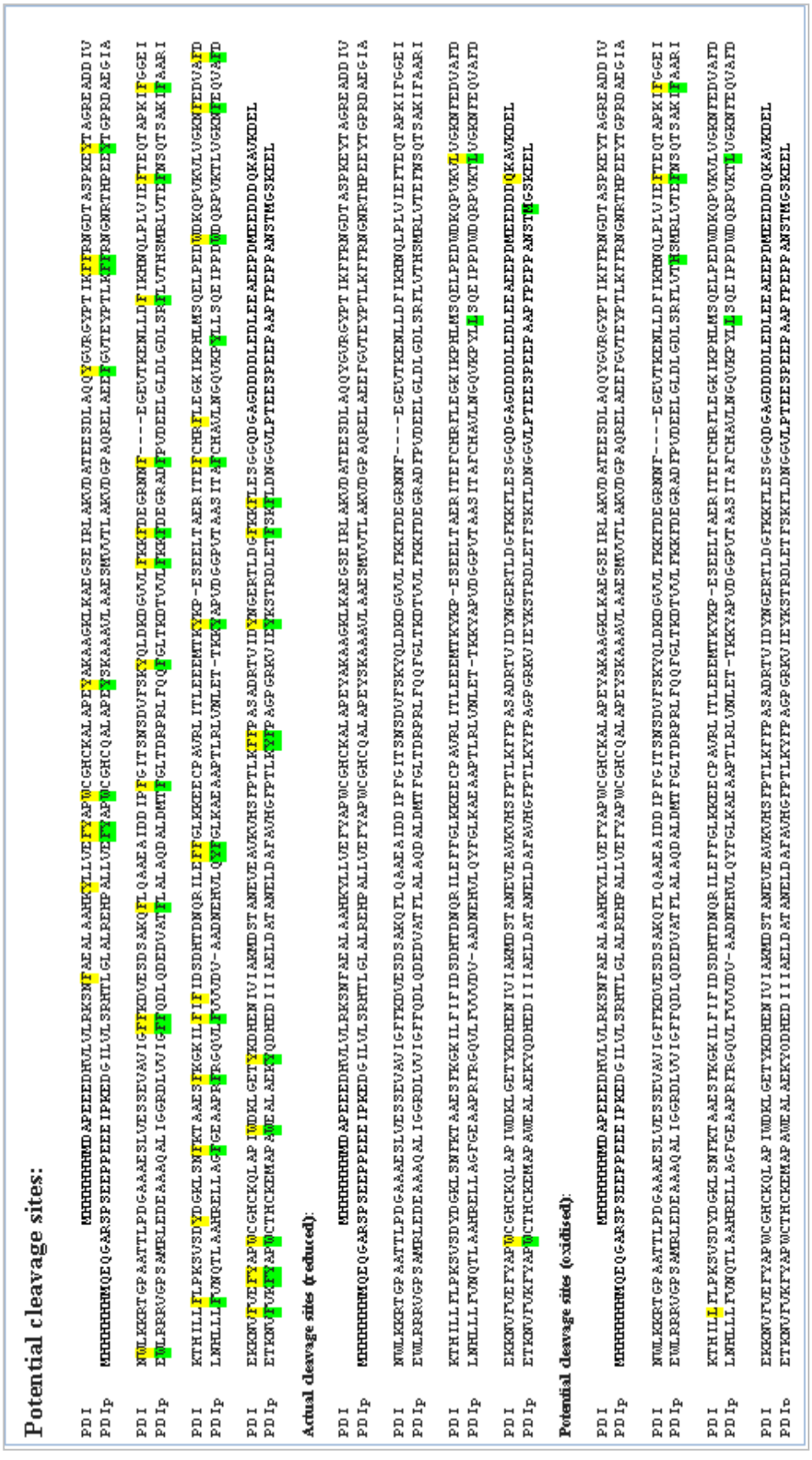

Figure 4.10: Cleavage sites as determined by ESI-MS. Proteins were digested with chymotrypsin for two hours and then the reaction stopped using an excess of PMSF. Samples were then submitted to ESI-MS. The potential and actual cleavage sites (in oxidising and reducing conditions) are shown on an alignment of PDI and PDIp. Potential cleavage sites were calculated using ExPASy PeptideCutter.

Protein	Redox State	Mw from ESI-MS (Da)	Expected Mw (Da)	Mass difference (Da)	Peptide
PDI	N/A	56374	56379	-5	N/A
PDI	Reduced	55589	55596	-7	D18-Q501
PDI	Reduced	43871	43875	-4	D18-W396
PDI	Reduced	41009	41013	-4	D18-L372
PDI	Oxidised	27789	27788	+1	D18-F240
PDI	Oxidised	26727	26726	+1	D18-F249
PDI	Oxidised	25711	25710	+1	D18-L259
PDIp	N/A	56915	56919	-4	N/A
PDIp	Reduced	56271	56276	-5	Q22-M519
PDIp	Reduced	45037	45040	-3	Q22-W417
PDIp	Reduced	42191	42194	-3	Q22-L393
PDIp	Reduced	40074	40077	-3	Q22-Y375
PDIp	Oxidised	42191	42190	+1	Q22-L393
PDIp	Oxidised	40073	40073	0	Q22-Y375
PDIp	Oxidised	28895	28894	+1	Q22-F271
PDIp	Oxidised	27918	27917	+1	Q22-F262
PDIp	Oxidised	26954	26952	+2	Q22-H254

Table 4.3: Peptides identified by ESI-MS: Proteins were digested with chymotrypsin for two hours and then the reaction was stopped using an excess of PMSF. Samples were then submitted to ESI-MS. Peptides corresponding to peaks were identified using ProtParam, ExPASy.

Unlike the results of peptide mass finger-printing, ESI MS (figure 4.10) allowed identification of major cleavage sites. The benefit of using chymotrypsin rather than trypsin or proteinase K was that both PDI and PDIp are similarly susceptible to chymotrypsin based on sequence alone. This means that it is easier to determine potential differences in structure based on differential susceptibility to chymotrypsin. On the basis of possible cleavages alone (see figure 4.10), both proteins showed remarkable resistance especially around the N-terminus. In the reduced state there were 2 conserved cleavage sites for each protein giving rise to 4 peptides of ~42kDa (PDI D18-L372, D18-W396 and PDIp Q22-L393, Q22-L417). Based on the identification of these peptides it is clear that for both proteins flexibility towards the C-terminal end of the molecule leads to the preferential loss of the **a'** domain. This is in agreement with PDI studies by Wang *et al.* (2011).

In the oxidised state however, cleavage of both proteins occurs much earlier on indicating that it is more susceptible to proteolysis than the reduced form. Table 4.4 shows that for PDI, three peptides of ~25kDa were identified corresponding to (PDI D18-F240, D18-F249 and D18-L259). This indicates that the only fully intact domains after proteolysis are the **a** and **b** domains. Again this correlates well with the work of Wang *et al.* (2011) which suggests that PDI **b'xa'** is the major redox-active region of the molecule and that oxidation of PDI gives rise to major conformational changes. Like PDI, oxidised PDIp is more susceptible to digestion by chymotrypsin than its reduced form. Unlike PDI however, peptide fragments of ~40kDa were identified by ESI-MS indicating that oxidised PDIp is far more resistant to proteolysis than oxidised PDI. Smaller peptides of ~25kDa were also identified for oxidised PDIp and these correspond perfectly to those described for PDI previously including having conserved cleavage sites. Clearly the two proteins are very similar in structure but this work may suggest that unlike PDI, PDIp only undergoes minor or limited redox-mediated conformational changes.

4.3.3. ANS fluorescence

ANS binding to PDI and PDIp in both redox states was used as an indicator of cleft size and surface exposure. As binding of ANS to a hydrophobic surface leads to an increase in fluorescence it can also be useful for studying the conformational changes that occur when PDI is oxidised.

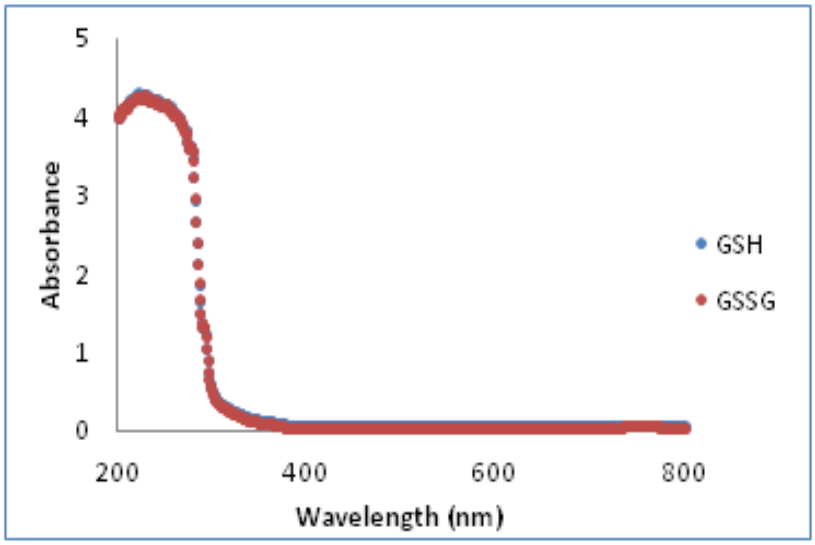

Figure 4.11: Absorbance scan for GSH and GSSG. Samples of 1mM GSSG or 1mM GSH were made up in 20mM phosphate buffer pH7.3

The protocol used by Wang *et al* (2011) to measure ANS binding to PDI in the oxidised and reduced state describes an intial step in which PDI is incubated with ANS followed by a second step where either GSH or GSSG is added. Following addition of GSH or GSSG the sample is incubated again prior to fluorescence measurements being made. However, this method does not take into account the absorbance properties of GSH or GSSG. Figure 4.11 clearly indicates that there may be slight interference at 390nm, the excitation wavelength of ANS. In addition, fluorescence emission was found to be influenced also by presence of DTT or diamide as alternative reductants/oxidants (data not shown). Consequently, it is best practice to desalt reduced or oxidised protein prior to use in this assay.

Using this optimised protocol, preliminary results (shown in figure 4.12) have been obtained.

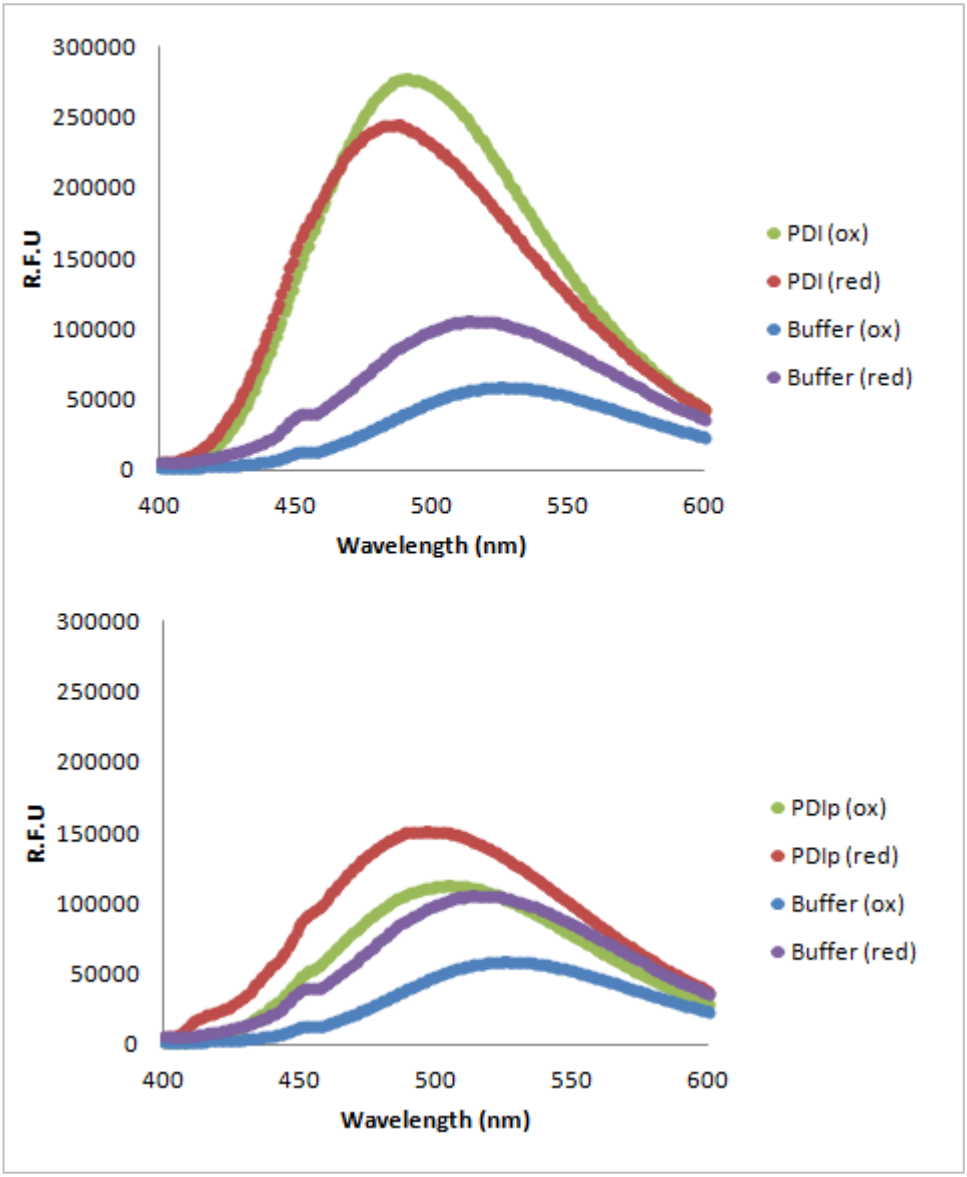

Figure 4.12: ANS binding experiments. The fluorescence emitted when oxidised or reduced protein (10μM) interacted with ANS (100uM) was measured between 400-600nm after excitation at 390nm. The ANS enhancement factor was then calculated for each (ANS enhancement at λ_{max} = ($F_{protein}$ + $_{ANS}$)/F_{ANS}).

Figure 4.12 shows that greater interaction occurs between ANS and PDI_{ox} than ANS and PDI_{red} (ANS enhancement factor 6.83 and 2.84 respectively). This indicates that there is a greater hydrophobic surface available for ANS binding in the oxidised form and this is due to an open conformation (Wang *et al.* 2011). The difference between the interactions of ANS with $PDIp_{ox}$ and $PDIp_{red}$ is much smaller (ANS enhancement factor 2.20 and 1.58 respectively) although like PDI there is greater fluorescence

enhancement when PDIp is in the oxidised state. Again this implies that PDIp may undergo a smaller redox-mediated conformational change. Additional study of these interactions will provide more resolute answers.

4.3.4. Dynamic Light Scattering

In order to try to quantify the extent of conformational change being displayed between the two redox states the associated change in molecular diameter was measured by dynamic light scattering (DLS). Table 4.4 shows that oxidation of PDI gives rise to a 25% increase in diameter compared to the reduced protein. For PDIp this difference is much more subtle: an increase of 8% is observed. Similar to previous work, this may suggest that PDIp undergoes only a minor redox-mediated conformational change.

	Mean Diameter +/- SD	Change in Diameter (%)
PDI(r)	5.15 +/- 1.07	N/A
PDI(o)	6.46 +/- 1.49	+25
PDIp(r)	5.59 +/- 1.02	N/A
PDIp(o)	5.99 +/- 0.85	+8

Table 4.4: Results of DLS for PDI and PDIp. A sample containing 11uM protein and 20mM phosphate were prepared. The protein had been oxidised/reduced with an excess of diamide/DTT and were then desalted before the experiment.

Due to the low replicate number (4) and also the low reproducibility of measurements for mean diameter, the standard deviations calculated for this data are quite high. Furthermore the increase in diameter size for oxidised PDI relative to reduced PDI was found to be not significant using the student's t-test (un-paired). As strict precaution was taken to monitor and reduce polydispersity, the reason behind inconsistencies in diameter is unknown. It could be that different biological samples have natural sample variance or indicate that there are various intermediate

conformations between the reduced and oxidised forms defined by the X-ray crystal structure of PDI (Wang *et al*. 2012).

When observing the effect of redox state on PDI and PDIp by native PAGE, it is clear that the oxidised proteins are retarded more than the reduced proteins (see later, figure 5.9). As expected, the difference in mobility is more striking between redox states for PDI. Again this implies that both PDI and PDIp undergo a redox-mediated conformational change but that the change is much smaller in PDIp than PDI.

4.4. Measuring the enzymatic activity of PDI and PDIp

4.4.1. The Insulin oxido-reductase assay

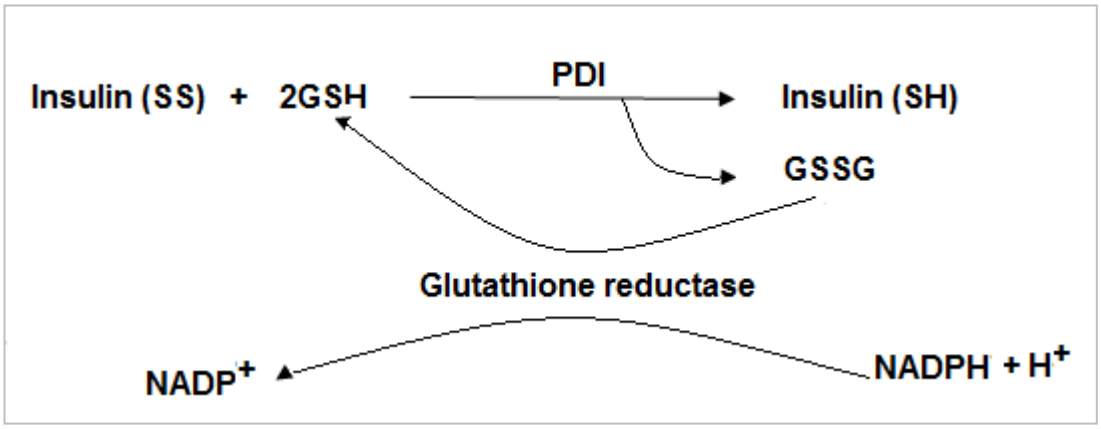

Figure 4.13: Reaction scheme for insulin oxido-reductase assay.

The insulin reduction assay has frequently been used to measure the reductase activity of PDI. By coupling the reduction of insulin with the oxidation of NADPH using glutathione reductase it is possible to measure the oxido-reductase activity of PDI or PDIp (see figure 4.13). Using this assay, PDIp was found to be ~50% as active as PDI (see figure 4.14).

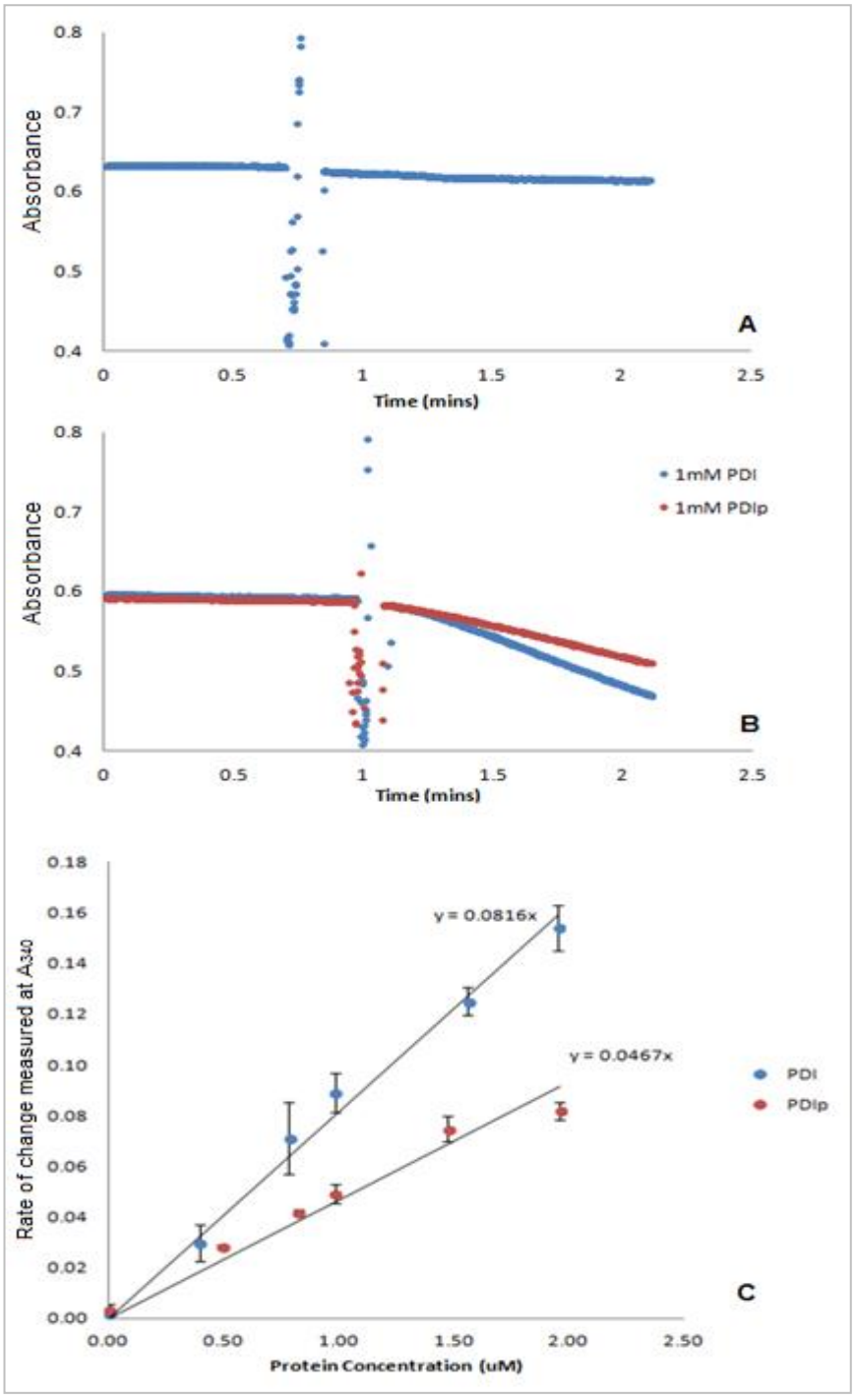

Figure 4.14: Measurements of the oxido-reductase activity of PDI and PDIp. Varying concentrations of protein were added to 200mM phosphate 50mM EDTA buffer (pH 7.5) containing 8mM GSH, 1 unit of glutathione reductase and 120μM NADPH at 37ºC. Reaction was started by adding 15μM insulin and the reaction was monitored by watching the rate of change at A_{340}. 3 relicates were taken for 3 biological samples of each protein in an attempt to reduce error. A) Example trace for control sample (no protein), B) example traces for PDI and PDIp (1mM) and C) Graph showing rate of change (using gradient of line after addition of insulin) vs protein concentration.

The percentage difference in activity for PDI and PDIp (~55%) is remarkably reproducible. The assay however has huge day to day variance. This is largely uncontrollable and is due to the large number of different reactants involved and the high sensitivity of the spectrophotometer. In order to reduce error and standardise the assay the activity of PDIp was always measured relative to the activity of PDI measured on the same day.

4.5. Concluding Remarks

Our work has shown that the 3-dimensional structure of PDIp is not as similar to that of PDI as previously expected. Far UV CD has shown that PDIp has greater α-helical content than PDI and that there are differences in terms of the thermal stability of the two proteins. Unlike PDI, PDIp does not undergo a large redox-mediated conformational change and this is supported by many different lines of evidence including limited proteolysis, mass spectrometry and DLS. At present we do not understand the implications of this but it is feasible that the chaperone activity of PDIp could be affected if the binding surface is not very accessible. It is possible therefore that PDIp undergoes conformational changes that are not redox-regulated but are instead substrate induced.

PDIp has ~50% of the oxido-reductase activity of PDI. Although it is known that PDIp has restricted substrate specificity we expect PDIp to be able to bind insulin as it has a surface exposed tyrosine so it is unlikely that this difference is inability to bind insulin. We also believe that one of the contributors to the low oxido-reductase activity of PDIp is the unusual **a'** active site sequence (CTHC rather than CGHC). It is well known for other PDI family members that the amino acid residues located between active site cysteines are very important for the overall reactivity of the active site. The implications of replacing a glycine residue with a threonine residue are unknown but given the size difference between between the two it is likely that there may be some steric effects.

Chapter 5. Investigation of the contribution of the b'xa'c region to the distinctive properties of PDIp

5.1. Introduction

Our studies have shown that PDI and PDIp are not just different in terms of redox structure but also in terms of catalytic activity. Given that the two share identical domain architecture and ~45% sequence identity these results were surprising. By comparing the structure and activity of PDI, PDIp and two chimera proteins (see figure 5.1) we hope that it will be possible to determine regions of PDIp that contribute to these differences.

We expect that these dissimilarities are due to the **b'xa'c** region because we know that **b'xa'c** is the major region of redox-mediated conformational change in PDI (Wang *et al.* 2011). In addition we also expect that the unusual binding properties (conferred by **b'**) and odd **a'** active site sequence of PDIp (CTHC) are contributing to its low oxido-reductase activity. Consequently plasmids for 2 chimera proteins, PDIp ½ and PDIp ¾ were kindly donated by Dr. Katrine Wallis. Both of these proteins share PDIp **a** and **b** domains but are different in their C-terminal half i.e. **b'xa'c.** Unfortunately up to now our studies of the C-terminus of PDIp have been limited because isolated PDIp **b'xa'c** is unstable (see chapter 3). As a result of this,

comparisons between wild-type PDIp, PDIp ½ and PDIp ¾ were used to study this region.

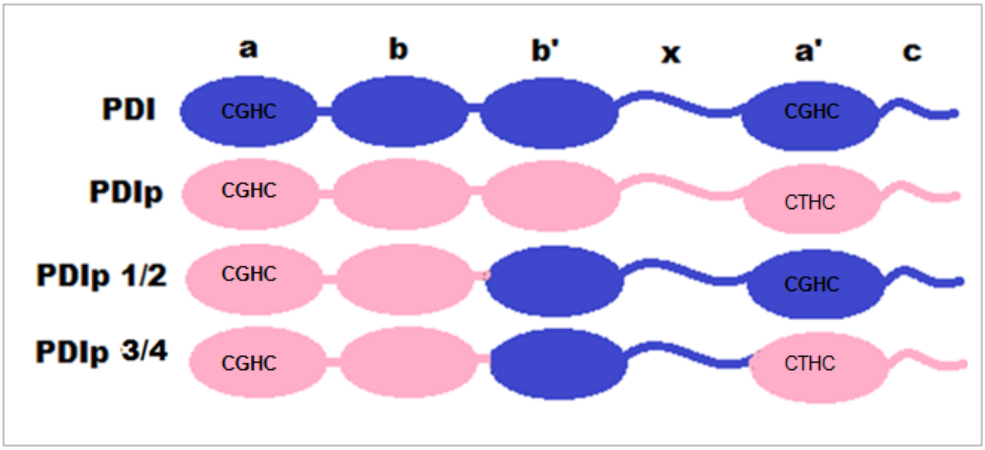

Figure 5.1: Schematic showing domain architecture of PDI, PDIp and two chimera proteins.

Based on our previous work and also published data, we would expect PDIp ½ to have similar redox conformations to PDI because it has PDI **b'xa'c**: the major redox-active region defined by Wang *et al.* 2011. We would also expect it to have similar oxido-reductase activity to PDI because it has two CGHC active site motifs and also the PDI **b'** substrate binding site. However PDIp ¾ will likely exhibit mixed characteristics for both structure and activity because a) it does not have the full redox-active cassette of PDI and b) in having the PDIp **a'** domain (including a CTHC active site) it is probably less active as an oxido-reductase.

5.2. Expression and purification of chimera Proteins

5.2.1. Expression and purification of PDIp ½

PDIp ½ was expressed to a sufficient amount using protocols optimised for expression of wild-type PDIp (see chapter 3). No significant improvement in binding to the Ni^{2+} column was seen when using a long binding step as opposed to the standard IMAC protocol (data not shown). As PDIp ½ shares the same N-terminus as wild-type PDIp this suggests that the problems associated with binding of PDIp to the Ni^{2+} column are not simply caused by this region as originally postulated. This is supported by purification studies of PDIp **b'xa'c** which also saw reduced binding despite not having an **a** domain or an N-terminal extension. To fully understand the issues associated with column binding during IMAC further study must be undertaken.

After IMAC, PDIp ½ was purified by IEC. The chromatogram for PDIp ½ is not dissimilar to wild-type PDI in showing a single peak with a slight shoulder (figure 5.2A). Samples collected from IEC fractions were studied by SDS and native PAGE (see figure 5.2B and 5.2C).

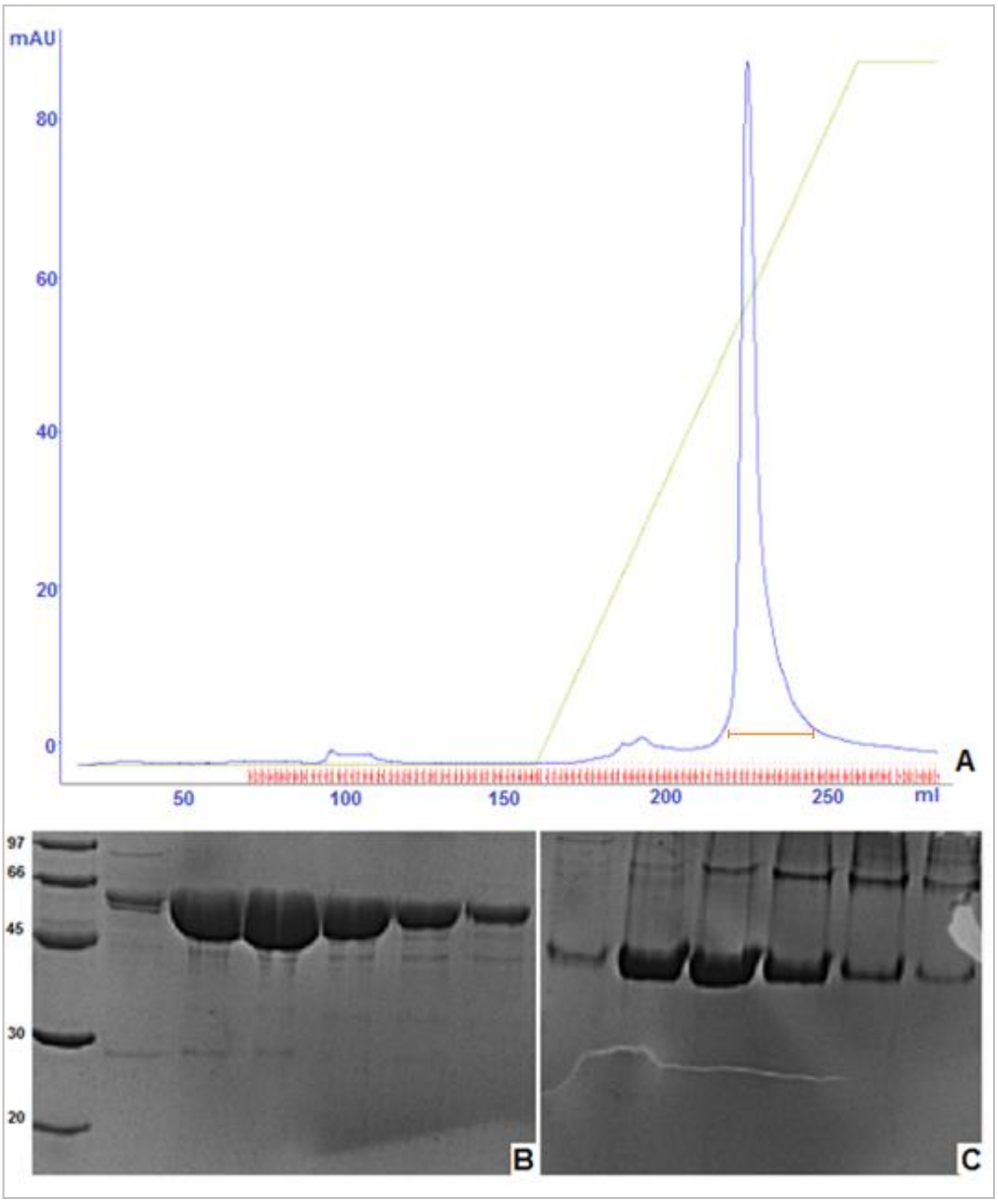

Figure 5.2: IEC of PDIp ½. A) Zoomed IEC chromatogram for PDIp ½. B) 12% SDS-PAGE showing protein collected during IEC of PDIp ½. C) 12% Native-PAGE showing protein collected during IEC of PDIp ½. Fractions were taken from within region shown by the red line.

Figure 5.2B shows that a large yield of PDIp ½ was expressed and purified. Evidently there is a small amount of degradation but this is far outweighed by the full length protein. When duplicate samples were analysed by native PAGE (figure 5.2C), it was clear that PDIp ½ has a natural propensity to dimerise. Like for PDI,

dimer is eluted from the column at a slightly higher salt concentration than the monomer and corresponds to the shoulder seen on the chromatogram (figure 5.2A). In order to separate dimer species from monomer PDIp ½ was purified further by SEC (see figure 5.3).

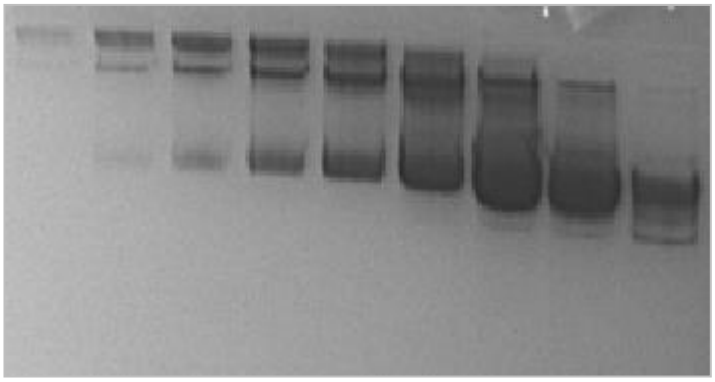

Figure 5.3: Native PAGE showing SEC of PDIp ½. Following dialysis of PDIp ½ from IEC into 20mM phosphate buffer pH 7.3, SEC was performed. SEC was undertaken in 20mM phosphate, 500mM NaCl buffer pH 7.3. Samples were analysed using a 12% native PAGE gel.

Figure 5.3 indicates that it is very difficult to separate monomer and dimer forms of PDIp ½. Therefore only SEC fractions that contain minor dimer contamination were pooled and consequently a significant reduction in total yield was observed. In addition the longer purification time taken to perform IMAC, IEC and SEC leads to increased instability and degradation. Typically greater yields of PDIp ½ are obtained when time taken to express and purify protein is reduced (data not shown).

5.2.2. Expression and purification of PDIp ¾

Similar to PDIp ½, PDIp ¾ is optimally expressed using the conditions determined previously for wild-type PDIp. It can be purified easily using standard PDI protocols and no obvious issues with Ni^{2+} column binding have been seen. Clearly PDIp ¾ also dimerises easily and this is probably caused by PDI **b'x** (see figure 5.4C).

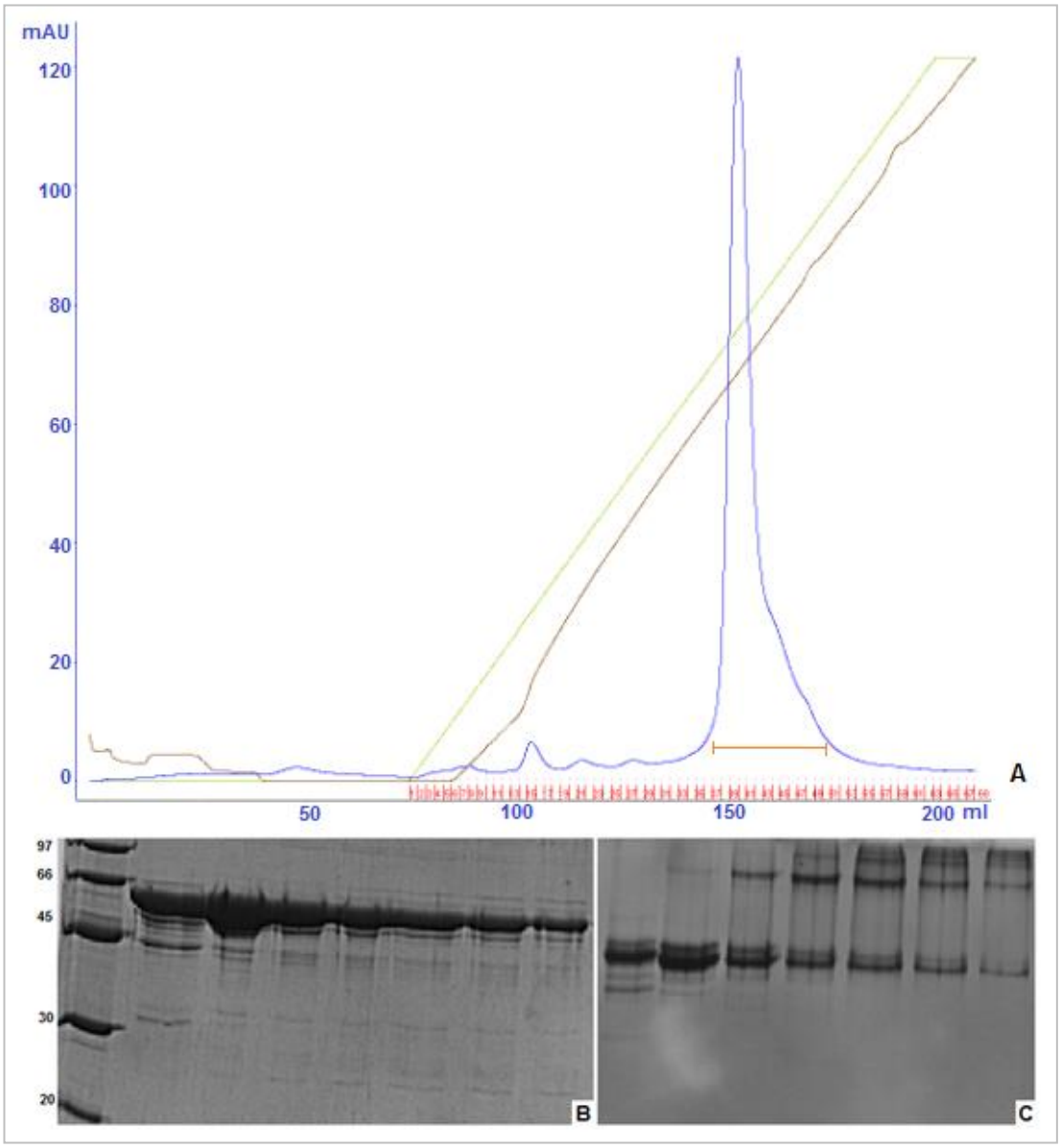

Figure 5.4: IEC of PDIp ¾. A) IEC chromatogram for PDIp ¾. B) 12% SDS-PAGE showing protein collected during IEC of PDIp ¾. C) 12% Native-PAGE showing protein collected during IEC of PDIp ¾. Fractions were taken from within region shown by the red line.

This is in agreement with work from the RBF group that shows that constructs containing PDI **b'x** have a greater propensity to dimerise than those that do not (Wallis *et al*. 2009). Following IEC, SEC is used to remove dimer from the sample of PDIp ¾ (data not shown).

Like for PDIp ½, PDIp ¾ is also quite unstable and minor degradation products can be seen in both figure 5.4B and 5.4C. The accumulative result of losing PDIp ¾ to both degradation and dimer formation is that yield is significantly reduced. By reducing total purification time a huge improvement in yield is observed due to losing less protein to dimer formation or degradation.

5.3. Redox un-controlled experiments

5.3.1. Far UV Circular Dichroism

First and foremost, Figure 5.5 shows that no structural weaknesses were induced by the creation of the chimeras and that they are well folded. The production of chimera proteins with incorrect domain boundaries can give rise to difficulties during protein expression and often the protein is later found to be poorly structured. There is no evidence of this here.

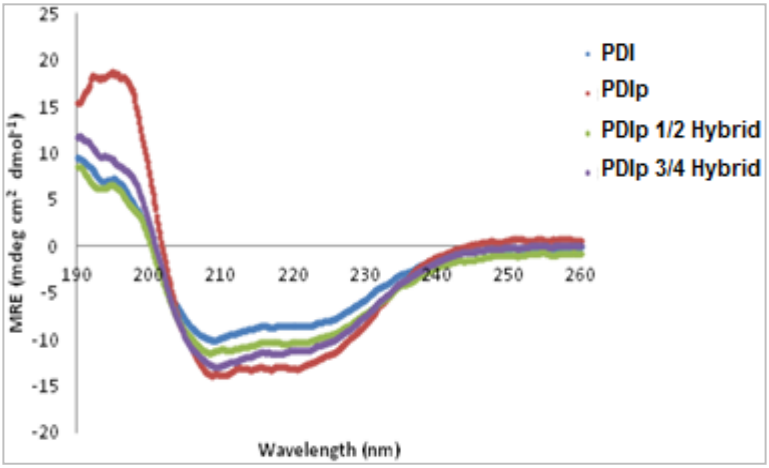

Figure 5.5: Far UV CD of PDI, PDIp and two chimera proteins. The circular dichroism of each protein (0.1mg/ml) in 5mM phosphate was recorded at wavelengths 190 to 260 nm and at 20ºC. The mean residue ellipticity (MRE) was then calculated.

	α-helix	β-sheet	Turns	Unordered
PDI	31%	19%	14%	36%
PDIp	42%	11%	13%	33%
PDIp 1/2	29%	19%	14%	37%
PDIp 3/4	25%	23%	13%	39%

Table 5.1: Results of DichroWeb analysis for chimera proteins. Analysis was performed using the CDSSTR algorithm and reference set SP175. Spectra were collected for 0.1mg/ml samples of each protein in 5mM phosphate at 20ºC.

Scans of the circular dichroism of PDIp ½ and PDIp ¾ show greater resemblance to PDI than PDIp in terms of secondary structure i.e. the chimera proteins also have less α-helical structure than PDIp (see figure 5.5). The most obvious region of difference is between 190-200nm where the chimera proteins clearly resemble PDI. Based on the spectra alone this indicates that PDIp is more α-helical than PDI, PDIp ½ and PDIp ¾. DichroWeb analysis confirms that both chimera protein have similar secondary structure content to PDI (table 5.1).

Differences in secondary structure must be caused by **b'x** because it is the only shared region between PDI and the two hybrid proteins. Additional α-helical structure in this region may contribute to the differences in redox-regulated conformations that were seen previously. Aside from being implicated in redox-dependent conformational change, **b'** is also the substrate binding domain. Structural differences in **b'** may therefore contribute to the limited substrate specificity of PDIp.

5.3.2. Thermal denaturation using far UV CD

Although less distinct, figure 5.6 shows that like PDI, both chimera proteins undergo a single unfolding transition. For PDIp ½ and PDIp ¾ the T_m is ~52ºC which is lower than that seen for PDI indicating a reduction in thermal stability. At present it is uncertain whether this difference is due to PDIp content or whether it is due to disruption of domain interfaces during construct manufacture. It is unlikely to be the latter because no evidence of increased instability has been seen for either chimera during scans of secondary structure.

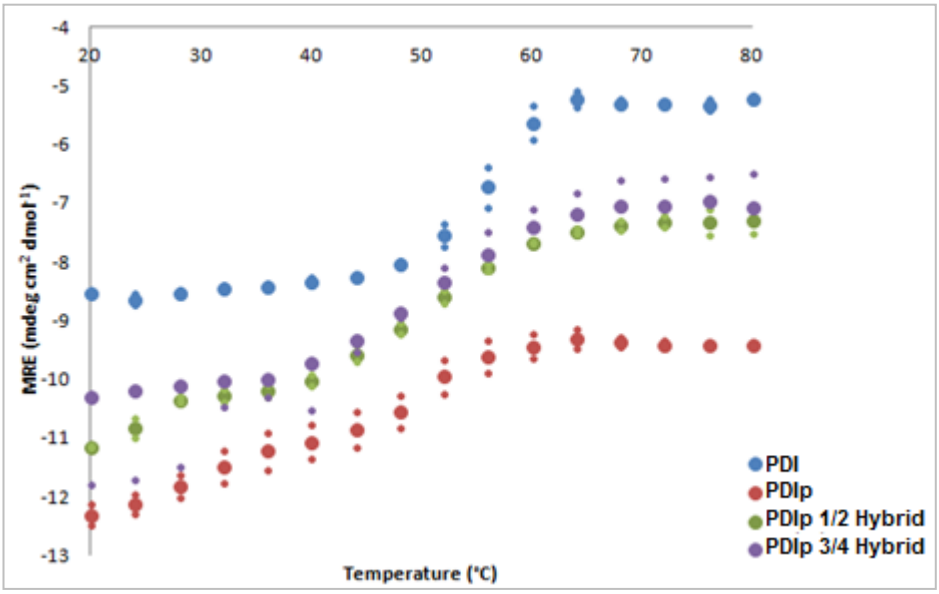

Figure 5.6: Thermal denaturation of PDI, PDIp and two chimera proteins. The circular dichroism at 222nm was measured for each protein (0.1 mg/ml protein in 5mM phosphate) at 4°C intervals between 20-80°C. Samples were allowed to equilibrate for 10 minutes and then measurements were taken for 2 minutes. The mean CD and MRE for each temperature were then calculated.

5.3.3. Analysis of secondary structure by far UV CD after incubation at 80ºC

After incubation at 80ºC both chimera proteins lose significant α-helical structure and gain β-sheet and unordered structure. Unsurprisingly therefore the CD spectra obtained is very similar to that of PDI (see figure 5.7). Clearly PDIp **b'x** is more

stabilising than PDI **b'x**. As the **b'x** region of PDI has been implicated as the site most affected during redox-mediated conformational change (Wang *et al*. 2011) it is possible that the stability of PDIp **b'x** prevents these movements in PDIp.

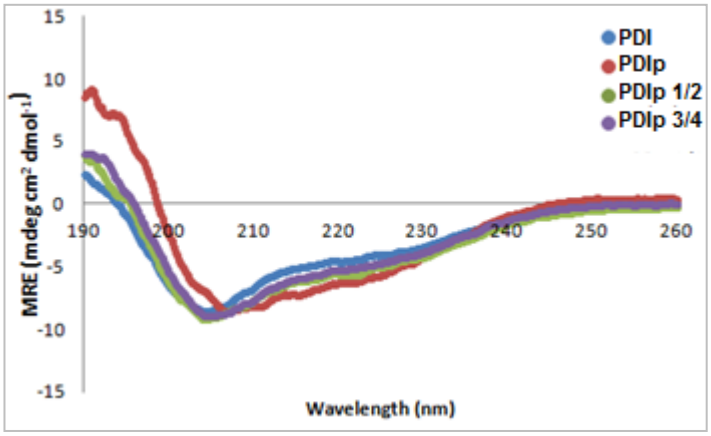

Figure 5.7: Far UV CD of PDIp ½ and PDIp ¾ at 80ºC. The circular dichroism of each protein (0.1mg/ml) in 5mM phosphate was recorded at wavelengths from 190 to 260nm at 80ºC. The mean residue ellipticity (MRE) was then calculated.

	α-helix	β-sheet	Turns	Unordered
PDI	16%	25%	16%	42%
PDIp	30%	17%	15%	38%
PDIp 1/2	18%	27%	15%	40%
PDIp 3/4	7%	34%	15%	41%

Table 5.2: Results of DichroWeb analysis for chimera proteins incubated at 80ºC. Analysis was performed using the CDSSTR algorithm and reference set SP175. Spectra were collected for 0.1mg/ml samples of each protein in 5mM phosphate at 80ºC.

To conclude this work, PDI.PDIp chimeras show greatest resemblance to PDI in terms of secondary structure and thermal stability. PDI, PDIp ½ and PDIp ¾ share the PDI **b'x** region only. Therefore this data indicates that the thermal stability of these proteins is regulated by **b'x** and this is supported by previous work from Wang *et al.* 2010 which defined **b'xa'** as the major flexible element of PDI.

5.4. Redox-controlled experiments

5.4.1. Far UV CD of oxidised/reduced protein

The redox-mediated conformational changes of PDI have been well characterised (Wang *et al*. 2011, Wang *et al*. 2012). Unlike PDI, PDIp only undergoes minor redox-controlled changes. The reason for this is currently unknown. Figure 5.8 indicates that PDIp ½ and PDIp ¾ show no significant difference in thermal stability between redox states. Therefore the chimera proteins are similar to PDIp in that they only experience minor redox-mediated conformational changes.

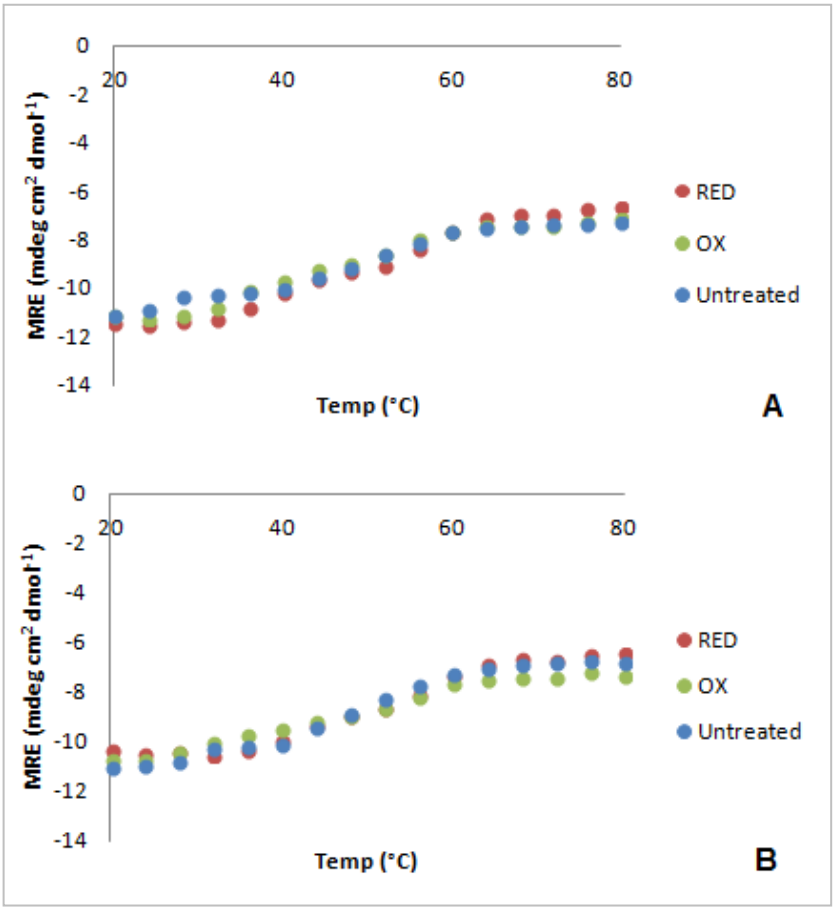

Figure 5.8: Thermal denaturation of PDIp ½ and PDIp ¾ in reduced and oxidised states. 0.1mg/ml protein was prepared in 5mM phosphate buffer also containing 5mM DTT or diamide. Desalting was then performed using a PD10 column. The circular dichroism at 222nm for each protein was measured at 4°C intervals between 20-80°C. Samples were allowed to equilibrate for 10 minutes and then measurements were taken for 2 minutes. The mean CD and MRE for each temperature were then calculated. A) PDIp ½ and B) PDIp ¾.

This data is interesting because figure 5.6 showed that PDIp ½ and PDIp ¾ have similar thermal stability to PDI and this characteristic was attributed to the **b'x** region which is known to have intrinsic flexibility (Wang *et al*. 2010). Figure 5.8 however provides evidence to suggest that the chimera proteins do not undergo redox-mediated conformational changes characteristic of PDI. It is therefore suggested that the **a** and **b** domains of PDIp have a negative effect on the ability to exhibit alternate redox-state conformations. This means that despite the **b'xa'** region of PDI being implicated as the major effector of redox-controlled conformational change (Wang *et al*. 2011, Wang *et al.* 2012) the presence of PDIp **ab** (in PDIp ½) is preventing these structural movements from occurring. Whether this activity is linked to the structure of PDIp **ab** or active-site chemistry is currently unknown.

5.4.2. Dynamic Light Scattering

Table 5.3 shows the percentage change in diameter associated with oxidation for PDI, PDIp and the two chimera proteins. It is clear that oxidised PDI has a much larger diameter than reduced PDI and the conformational changes associated with this have been characterised using X-ray crystallography (Wang *et al.* 2012). The difference in diameter between reduced and oxidised PDIp indicates that it does not undergo such large conformational changes. PDIp ½ and PDIp ¾ resemble PDIp in exhibiting only small differences in diameter upon oxidation demonstrating that they also undergo only minor redox mediated conformational changes. However due to the low replicate number for PDI ½ and PDIp ¾ (3), further accuracy will be gained from repeating this experiment.

Protein	Percentage change in diameter upon oxidation (%)
PDI	+25
PDIp	+8
PDIp 1/2	+6
PDIp 3/4	+6

Table 5.3: Results of DLS for chimera proteins. Samples containing 11μM protein in 20mM phosphate (pH 7.3) were prepared. Protein was oxidised or reduced with an excess of diamide/DTT and then desalted before measurements were taken. The difference in diameter between reduced and oxidised samples is shown.

This work seems to agree with the results shown previously (see figure 5.8) and provides further evidence to support the notion that PDIp exhibits minor redox-mediated movements in a process that is regulated by it's **a** and **b** domain. Again the data is not statistically significant but this may be due to intermediate conformational changes between the open and closed forms.

5.4.3. Analysis of chimera proteins by Native PAGE

Native PAGE analysis can be used to observe the redox-mediated conformational changes of PDI. When oxidised, the increased diameter of PDI causes greater retardation through the gel than the same protein in the reduced state. Figure 5.9 shows that oxidised PDIp is less retarded than oxidised PDI. This is because PDIp undergoes less significant redox-motions and exhibits less considerable differences in molecular diameter upon oxidation.

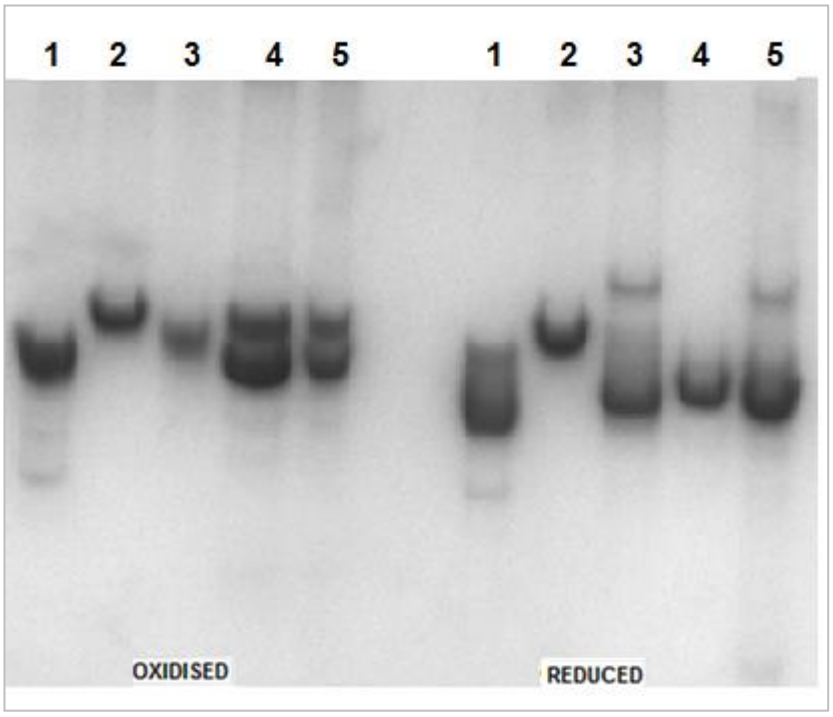

Figure 5.9: Redox state observations by Native PAGE analysis. Samples containing 5µg of protein in 20mM phosphate buffer (pH 7.3) were incubated in the presence of 10mM DTT or diamide for 30 minutes prior to loading into a 12% native gel. Samples shown are: 1) PDI, 2) PDIp, 3) PDIp ½, 4) PDIp ¾ and 5) PDIp T419G.

Unexpectedly, oxidised PDIp ½ is retarded to a greater extent than wild-type PDIp. This contrasts with work described previously and so interpretation requires caution. It may be that PDIp ½ can exist in alternate conformations but that reaching an 'open' conformation is more difficult than for PDI.

In its oxidised form, PDIp ¾ and PDIp ¾ T419G (which will be discussed later) seem to be present in two alternate conformations. Alongside the results of PDIp ½ (described previously) it could be postulated that these species are indicative of equal amounts of oxidant responsive and oxidant unresponsive forms of PDIp ¾ caused by the split nature of chimera proteins. This polymorphism appears to be absent for the reduced form of PDIp ¾ and PDIp ¾ T419G but actually it is likely that this result is due to ~50% of the protein being retarded in the oxidised state and ~50% not.

5.5. Measuring the enzymatic activity of PDIp ½ and PDIp ¾

5.5.1. The Insulin oxido-reductase assay

Figure 5.10 shows that PDIp ½ has ~75% of the oxido-reductase activity of PDI. This is an increase of ~20% relative to wild-type PDIp. Clearly the presence of PDI **b'xa'c** has a positive effect on the ability of PDIp to act as an oxido-reductase. This is probably due to the more general substrate specificity exerted by PDI **b'** and the presence of an intact CGHC catalytic active site motif in PDI **a'**. In PDIp **a'** there is a CTHC active site sequence (rather than CGHC) and this could account for the low oxido-reductase activity measured for wild-type PDIp. Evidently the PDIp **a** and **b** domains have a negative effect on the activity of the PDIp ½ construct. This is interesting because the same region is detrimental to redox-mediated conformational change also.

PDIp ¾ has ~65% oxido-reductase activity relative to PDIp which indicates that PDIp **b'x** is only a minor contributor to the loss of activity. Although *in silico* studies had shown that insulin had a solvent exposed hydroxyl-aryl group suitable for PDIp binding this confirms that the interaction can occur and that reduction in activity seen for PDIp is not simply due to inability to bind insulin.

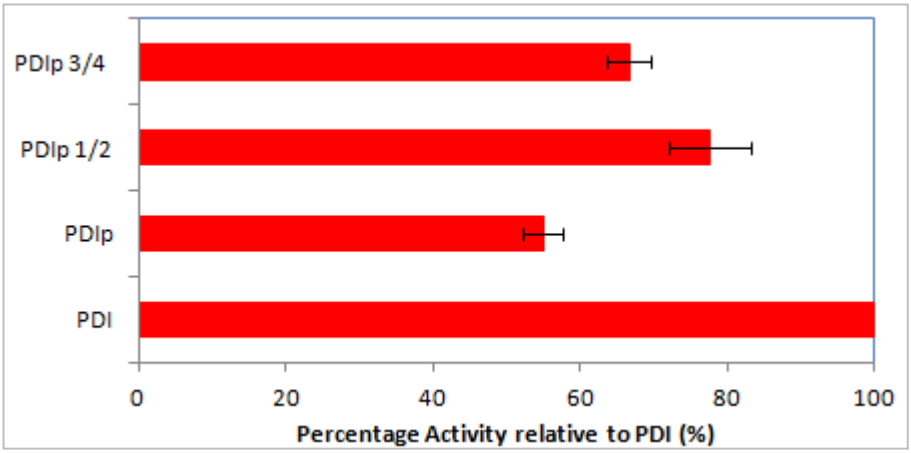

Figure 5.10: Relative oxido-reductase activities of PDIp ½ and PDIp ¾. Varying concentrations of protein were added to 200mM phosphate 50mM EDTA buffer containing 8mM GSH, 1 unit of glutathione reductase and 120µM NADPH at 37ºC. Reaction was started by adding 15µM insulin and the reaction was monitored by watching the rate of change at A_{340}. Activity was calculated from plots of absorbance rate vs concentration of PDI/PDIp (see figure 4.15) as a percentage of the activity of PDI measured on the same day. 3 replicates were taken for 3 biological samples of each protein in an attempt to reduce error.

By measuring the activity of PDIp, PDIp ½ and PDIp ¾ relative to PDI measured on the same day the degree of error is reduced. Figure 5.10 shows that the level of error across 3 replicates is low. The data for PDIp ½ has the greatest amount of error at ~10%.

5.6. Activity studies of PDIp T419G and PDIp ¾ T419G

5.6.1. Expression and purification of PDIp T419G and PDIp ¾ T419G

PDIp T419G and PDIp ¾ T419G were expressed and purified as described previously for wild-type PDIp and PDIp ¾ respectively. Total yields for both proteins were ~20µg/ml of culture. Figure 5.11 shows SDS-PAGE gels of IEC samples taken for each protein. Like PDIp ¾, PDIp ¾ T419G can dimerise easily so following analysis by native-PAGE an SEC step may be required (data not shown).

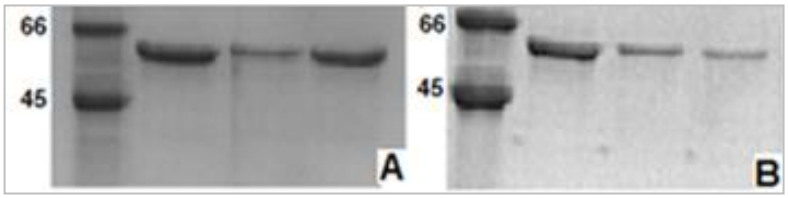

Figure 5.11: IEC of PDIp T419G and PDIp ¾ T419G. A) 12% SDS-PAGE of fractions taken from IEC of PDIp T419G B) 12% SDS-PAGE of fractions taken from IEC of PDIp ¾ T419G

IEC chromatograms of PDIp T419G and PDIp ¾ T419G are similar to those produced for wild-type PDIp and PDIp ¾ respectively (see figures 3.13 and 5.4). Like for wild-type PDIp, PDIp T419G has a distinct second peak. Samples were collected from the major peak only and analysed by SDS-PAGE. There was no indication that this mutant dimerises more readily than the wild-type protein (data not shown). For PDIp ¾ T419G there is only one peak but it has a distinct shoulder probably indicating the presence of dimer. Protein was collected from the peak avoiding this area.

5.6.2. Insulin assay of PDIp T419G and PDIp ¾ T419G

PDIp has ~55% of the oxido-reductase activity of PDI (see figure 5.12). This was assumed to be due to differences in substrate specificity conferred by the **b'** domain and also the unusual **a'** active site sequence of PDIp. Using PDIp ½ it was shown that the **a** and **b** domains of PDIp are also detrimental to the oxido-reductase activity. This was totally unexpected because the catalytic active site motif of PDIp **a** is the same as PDI **a** (i.e. CGHC).

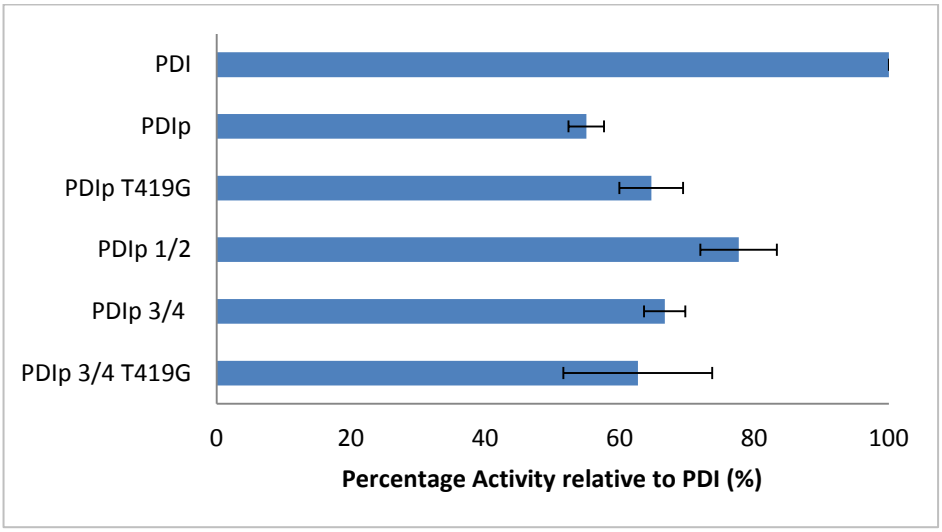

Figure 5.12: Oxido-reductase activity of PDI, PDIp, chimera proteins and mutants. Varying concentrations of protein were added to 200mM phosphate 50mM EDTA buffer (pH 7.5) containing 8mM GSH, 1 unit of glutathione reductase and 120µM NADPH at 37ºC. Reaction was started by adding 15µM insulin and the reaction was monitored by watching the rate of change at A_{340}. Activity was calculated from plots of absorbance rate vs concentration of PDI/PDIp (see figure 4.15) as a percentage of the activity of PDI measured on the same day. 3 relicates were taken for 3 biological samples of each protein in an attempt to reduce error.

As anticipated, PDIp **a'** is less active than PDI **a'** based on the percentage activity measured for PDIp ¾ and PDIp ½ (65% and 75% respectively). Therefore this work has shown that the activity of both active sites of PDIp is impaired relative to those of PDI.

To study PDIp **a'** further, active site mutants PDIp T419G and PDIp ¾ T419G were constructed. This mutation simulates the PDI **a'** domain active site motif. It is necessary to use these mutants because the isolated **a** and **a'** domains cannot be assayed via the insulin assay due to lacking a substrate binding site (**b'**). Figure 5.12 shows that neither PDIp T419G or PDIp ¾ T419G exhibit a significant increase in percentage oxido-reductase activity relative to wild-type PDIp and PDIp ¾ respectively. This is interesting because the presence of threonine in the **a'** active site of PDIp was expected to have a negative effect on its oxido-reductase activity and clearly this does not appear to be the case. This result is surprising because there is evidence to show that the amino acids between catalytic cysteines are important for

conferring the activity of both thioredoxin and DsbA (Krause *et al*. 1991, Lundstrom *et al.* 1992 and Huber-Wunderlich and Glockshuber, 1998).

The main reason that it is difficult to assume differences between PDIp and PDIp T419G is because the error bars are overlapping. Furthermore, for PDIp ¾ T419G, the degree of error is quite large (~20%). This could be caused by air-induced oxidation of NADPH over the course of the total experiment time. Suitable measures were taken to reduce this i.e. by making up fresh NADPH each day and storing it on ice during the experiment but unfortunately these things cannot be fully controlled. In order to improve accuracies further repeats must be undertaken.

5.7. Concluding Remarks

We have previously shown that PDIp is less amenable to redox-mediated conformational changes than PDI. This was unexpected because PDI and PDIp share identical domain architecture, ~45% sequence identity and were assumed to have similar 3-dimensional structure. Construction of PDIp ½ and PDIp ¾ has allowed us to study the domains that are involved in modulating redox change in PDIp.

Far UV CD (figures 5.5 and 5.6) showed that PDIp ½ and PDIp ¾ had similar secondary structure composition to PDI and also a similar unfolding profile consisting of a solitary transition. These proteins share PDI **b'x** and so it is postulated from this work that there are significant differences in terms of stability and possible structure between PDI **b'x** and PDIp **b'x**. This may explain the variance in substrate specificity seen for PDI and PDIp.

Figure 5.8 indicates that the PDIp chimera proteins show similar redox-state effects to wild-type PDIp rather than PDI. This is further confirmed by DLS (table 5.3). We did not expect the chimeras to resemble PDIp in these experiments because we had previously seen similarities conferred by PDI **b'x** and we know from recent work that the major redox-active cassette of PDI is **b'xa'** (Wang *et al*. 2011). The chimera

proteins share PDIp **ab** with PDIp so therefore this region must be more active in redox change than originally suggested. Finally, native PAGE analysis reveals possible polymorphisms for PDIp ½ and PDIp ¾ (see figure 5.9). These were not seen by Far UV CD or DLS because these techniques give average readings for the sample provided. This work requires further study.

PDIp has ~55% of the oxido-reductase activity of PDI. PDIp ½ has ~75% activity (see figure 5.10). This indicates that the **a** and **b** domains of PDIp have a negative effect on activity. PDIp ¾ has ~65% activity and this suggests that the **a'c** region of PDIp also has a negative effect (but to a lesser extent). Given that the catalytic sites of PDIp are **a** and **a'** this work demonstrates that these domains of PDIp are less catalytically active than those of PDI. For PDIp **a** this was unexpected because the active site motif is identical to that seen in PDI **a.**

Interestingly studies of PDIp T419G and PDIp ¾ T419G indicate that the presence of a threonine instead of a glycine residue at the position immediately next to the N-terminal cysteine of the **a'** active site, doesn't have a significant effect on the oxido-reductase activity. This indicates that unexpectedly, the reduced activity of the **a** domain of PDIp is the major contributor to low oxido-reductase activity. The exact mechanism for which is undeciphered.

Chapter 6. Involvement of the active site of the a domain in the distinctive properties of PDIp

6.1. Introduction

We have been unable to identify distinct regions of PDIp responsible for its unusual redox conformations or oxido-reductase activity. Our work has shown that PDIp is more thermally stable than PDI in the **b'x** region and we have suggested that this may explain restricted substrate specificity. In addition the **a** and **b** domains of PDIp seem to be involved in modulating redox-mediated conformational change which is in contrast to work on PDI which implicated **b'xa'** only (Wang *et al.* 2011).

Studies of the oxido-reductase activity of PDIp seem to show that PDIp **a** has a detrimental effect on activity. This was unexpected because unlike PDIp **a'**, PDIp **a** has a normal CGHC motif. Furthermore, the T419G mutant has no significant difference in activity from the wild-type protein implying that the low oxido-reductase activity of PDIp is not caused by the unusual **a'** active site sequence. Therefore our data indicates that the reactivity of PDIp **a** is unexpectedly low.

The reactivity of the active site cysteines can be measured by calculating their pK_a. The pK_a is the pH at which the residue (in this case cysteine) is 50% protonated. The pK_a's of the catalytic cysteines of PDI **a** domain have been determined in a variety

of different ways but have been studied more recently by measuring the pH dependence of the reaction between PDI **a** and DTNB (Karala *et al.* 2010). In this work the N-terminal cysteine of PDI **a** was found to have a pK_a of ~4.8 and the C-terminal cysteine ~8.6. This means that at physiological pH the N-terminal cysteine favours the thiolate state and therefore is more reactive. The reactivity of the C-terminal cysteine is more complex and needs to change according to position in the reactive cycle. In order to enable this, the pK_a of the C-terminal cysteines is modulated by nearby residues (i.e. R120 in PDI **a**). In this way the catalytic cycle is completed (see figure 6.1).

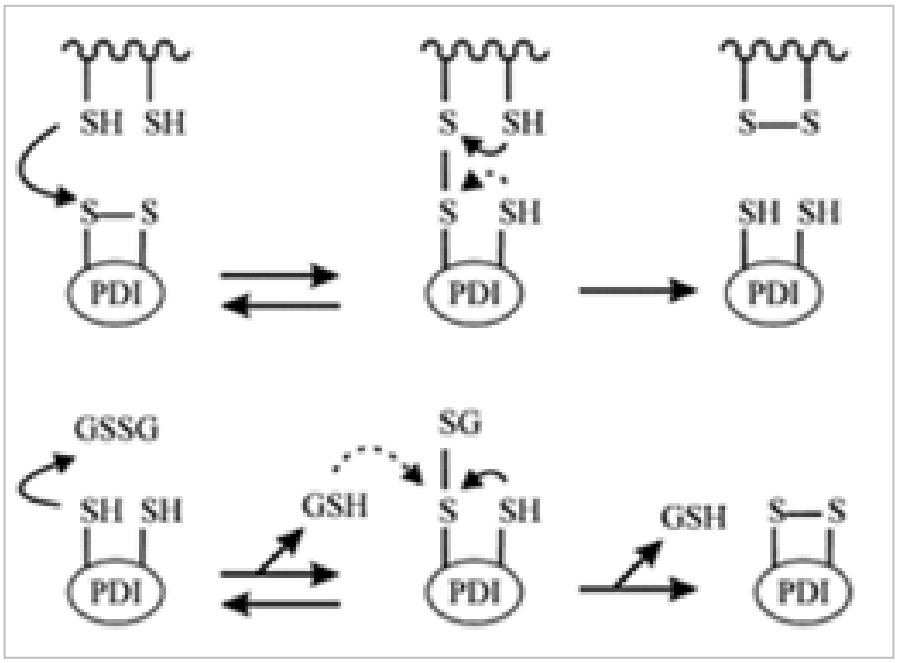

Figure 6.1: Schematic showing reaction schemes of PDI (adapted from Karala *et al.* 2010). Only one active site of PDI is shown for clarity. Nucleophilic attack of the PDI disulphide bond by a substrate protein leads to formation of a mixed disulphide. As the pK_a of the C-terminal cysteine of PDI is high (~8.6), typically this is resolved by the substrate thiol leading to its oxidation. The net result of these reactions is that PDI is in the reduced state. To return to the oxidised state, the N-terminal cysteine of PDI nucleophilically attacks GSSG leading to the formation of a mixed disulphide. To resolve this mixed disulphide, the C-terminal cysteine must have a low pK_a making it reactive enough to nucleophilically attack the N-terminal cysteine and give rise to disulphide bond formation. The pK_a of the C-terminal cysteine therefore is remarkably changeable and this is modulated by a nearby residue, R120 (Karala *et al.* 2010).

6.2. Studies of PDIp a

6.2.1. Expression and purification of PDI a and PDIp a

Using standard expression protocols for full length PDIp, yields of both PDI **a** and PDIp **a** were found to be very high. Figure 6.2 shows that negligible amounts of PDI **a** / PDIp **a** were found in the flow through indicating that there were no issues with binding during IMAC. Consequently a long binding step was not required for purification of PDI **a** or PDIp **a**.

Figure 6.2 shows that PDI **a** exists as a double band on a 12% SDS-PAGE gel. This does not appear to be the case for PDIp **a** but again this is difficult to interpret. The reason for this double banded nature is unexplained but is expected to be due two alternate conformations of PDI **a**. No further information was found from running native gels or analysing this further (data not shown).

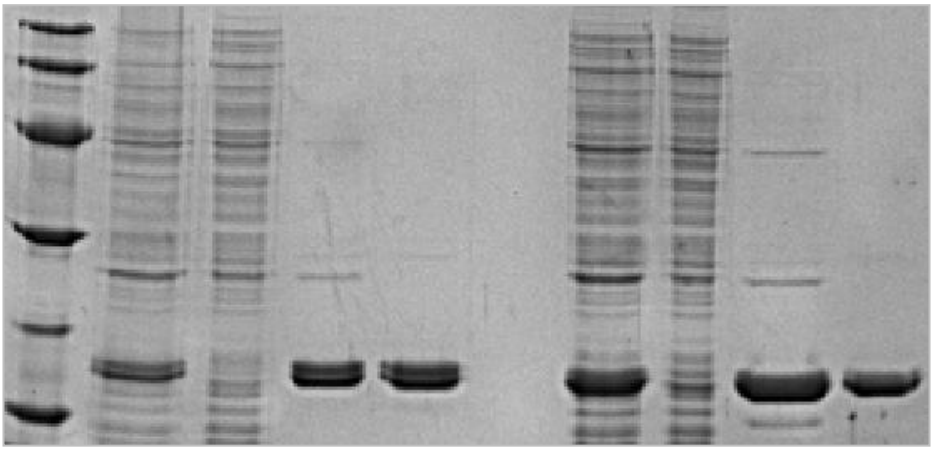

Figure 6.2: 12 % SDS-PAGE showing IMAC fractions and purified protein for PDI a and PDIp a. In order as seen on gel: marker, PDI **a** soluble proteins, PDI **a** flow through, PDI **a** elute, purified PDI **a** (after IEC), PDIp **a** soluble proteins, PDIp **a** flow through, PDIp **a** elute and purified PDIp **a** (after IEC).

IEC of both PDI **a** and PDIp **a** is also unusual in that neither protein binds strongly to the source 30Q column because they have pI's of ~6.49 and 5.9 respectively (ProtParam). Consequently PDI **a** and PDIp **a** can be purified from contaminating

protein by their inability to bind to the source 30Q column and typically elution occurs before a salt gradient is started (see figure 6.3). The purity of the resulting protein is high and can be seen in figure 6.2. In addition both proteins are uniformly monomeric which is in agreement with work suggesting that the presence of **b'** increases dimerisation (Wallis *et al.* 2009).

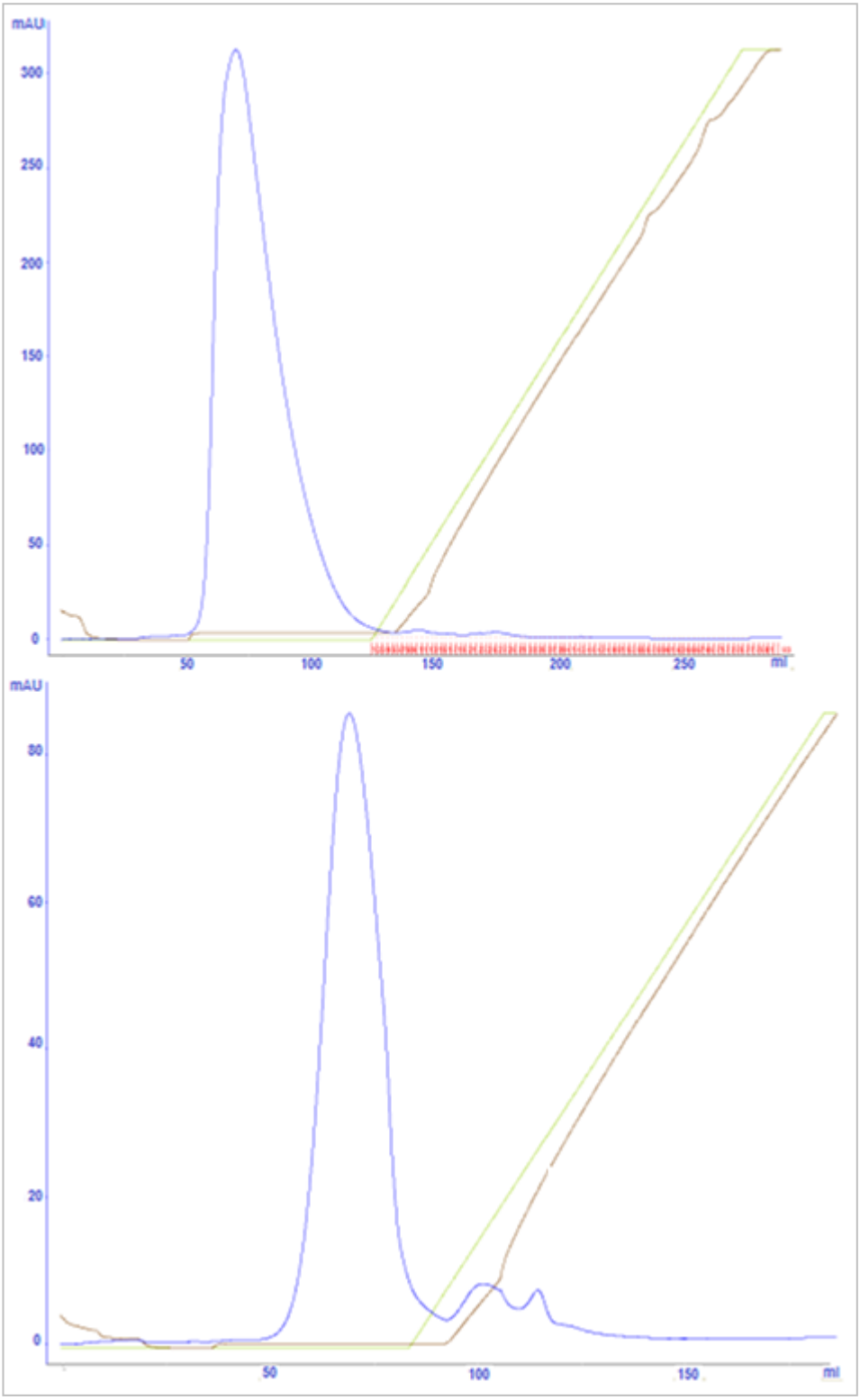

Figure 6.3: IEC of PDI a and PDIp a. A) IEC chromatograph for PDI **a**. B) IEC chromatograph for PDIp **a**.

6.2.2. Far UV CD of PDI a and PDIp a

Together figure 6.4 and table 6.1 show that PDI **a** has slightly greater α-helical content than PDIp **a**. More generally they confirm that both proteins are well folded and indicate that the domain boundaries used for their construct are correct.

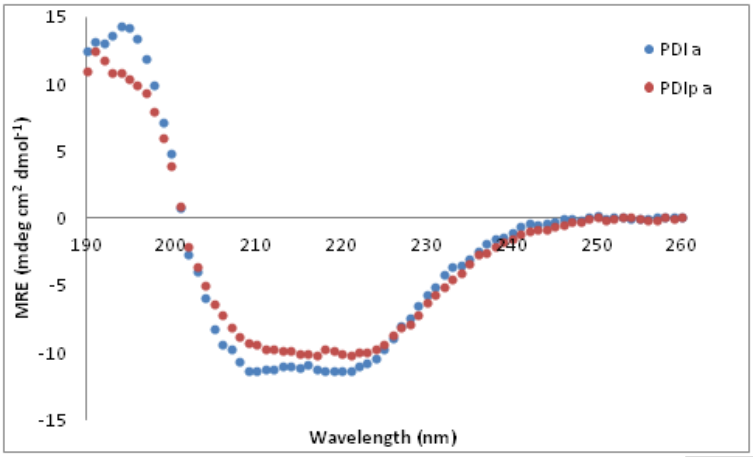

Figure 6.4: Far UV CD of PDI a and PDIp a. The circular dichroism of each protein (0.1mg/ml) in 5mM phosphate was recorded at wavelengths 190 to 260 nm and at 20ºC. The mean residue ellipticity (MRE) was then calculated.

	α-helix	β-sheet	Turns	Unordered
PDI a	34%	20%	20%	28%
PDIp a	31%	20%	21%	30%

Table 6.1: DichroWeb analysis for PDI a and PDIp a. Analysis was performed using the CDSSTR algorithm and reference set SP175. Spectra were collected for 0.1mg/ml samples of each protein in 5mM phosphate at 20ºC.

6.2.3. Molecular modelling of PDIp **a**

Using the amino acid sequence of PDIp **a** and the X-ray crystal structure of PDI **a** from the recent full length structure of human PDI (PDB: 4EKZ), a structural model of PDIp **a** was made (Yasara). Figure 6.5 shows the structural alignment of PDIp **a** and PDI **a** (taken from the X-ray structure of full length PDI). As expected there is significant structural homology between PDI **a** and PDIp **a**. The major region of discrepancy is the N-terminus which in PDIp includes a long acidic extension.

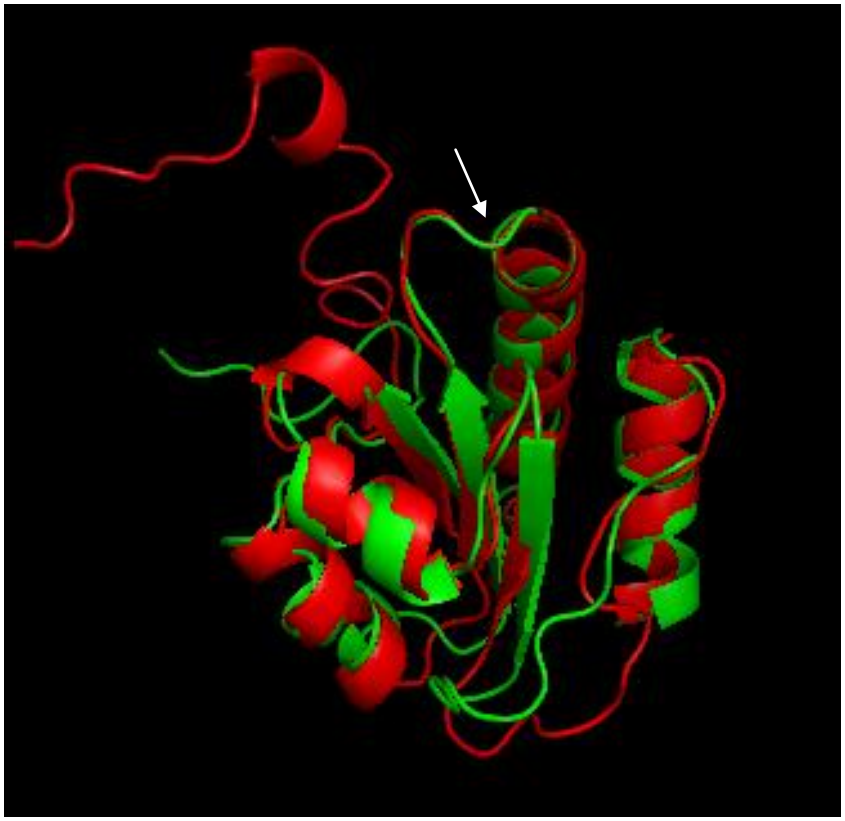

Figure 6.5: PyMOL alignment of PDIp a model and PDI a. Having obtained a model for PDIp **a** using Yasara it was aligned with PDI **a** (from 4EKZ) using PyMOL. PDI **a** is shown in green and PDIp **a** in red. Arrow indicates active site region.

An additional minor difference between the structures of PDI **a** and PDIp **a** is that the 3 core β-strands appear to be longer in PDI **a** than PDIp **a** although this may be an artefact of using a model of PDIp **a** rather than actual structural information. Within the area surrounding the active site (shown in figure 6.5 by an arrow) there appears to be none/negligible differences in structure.

6.2.4. ^{15}N HSQC: oxidised and reduced PDIp a

PDI **a** and PDIp **a** were expressed in minimal media containing ^{15}N-labelled ammonium sulphate. Aside from media, the protocols used for expression and purification were the same as those described previously and gave roughly equivalent yields. Collaborators at the University of Kent performed ^{15}N HSQC on

reduced/oxidised PDI **a** and PDIp **a** in order to observe possible differences in structure caused by change in redox state (see figure 6.6). At this time, observing peak shifts is the extent of analysis. Time has not been taken to try to assign peaks of PDIp **a**.

Figure 6.6A shows HSQC spectra for oxidised and reduced PDI **a**. Clearly oxidation does not give rise to significant peak shifts indicating minor structural differences between redox states. For HSQC spectra of oxidised and reduced PDIp **a** (figure 6.6B) there are more significant differences and clear peak shifts. This indicates that the structural changes associated with the oxidation of PDIp are considerable. This also may explain the differences in redox-mediated conformational change seen for PDIp and chimeras containing PDIp **a**. It is very interesting because published data for PDI suggests that the major redox active cassette for PDI is **b'x'a'**. It is now clear that for PDIp this is not the case.

This experiment will be repeated because pH was not strictly controlled. In order to rule out the possibility that pH is affecting the structure of PDIp **a** rather than redox state this experiment is essential. However, previous work has not implicated pH in structural changes.

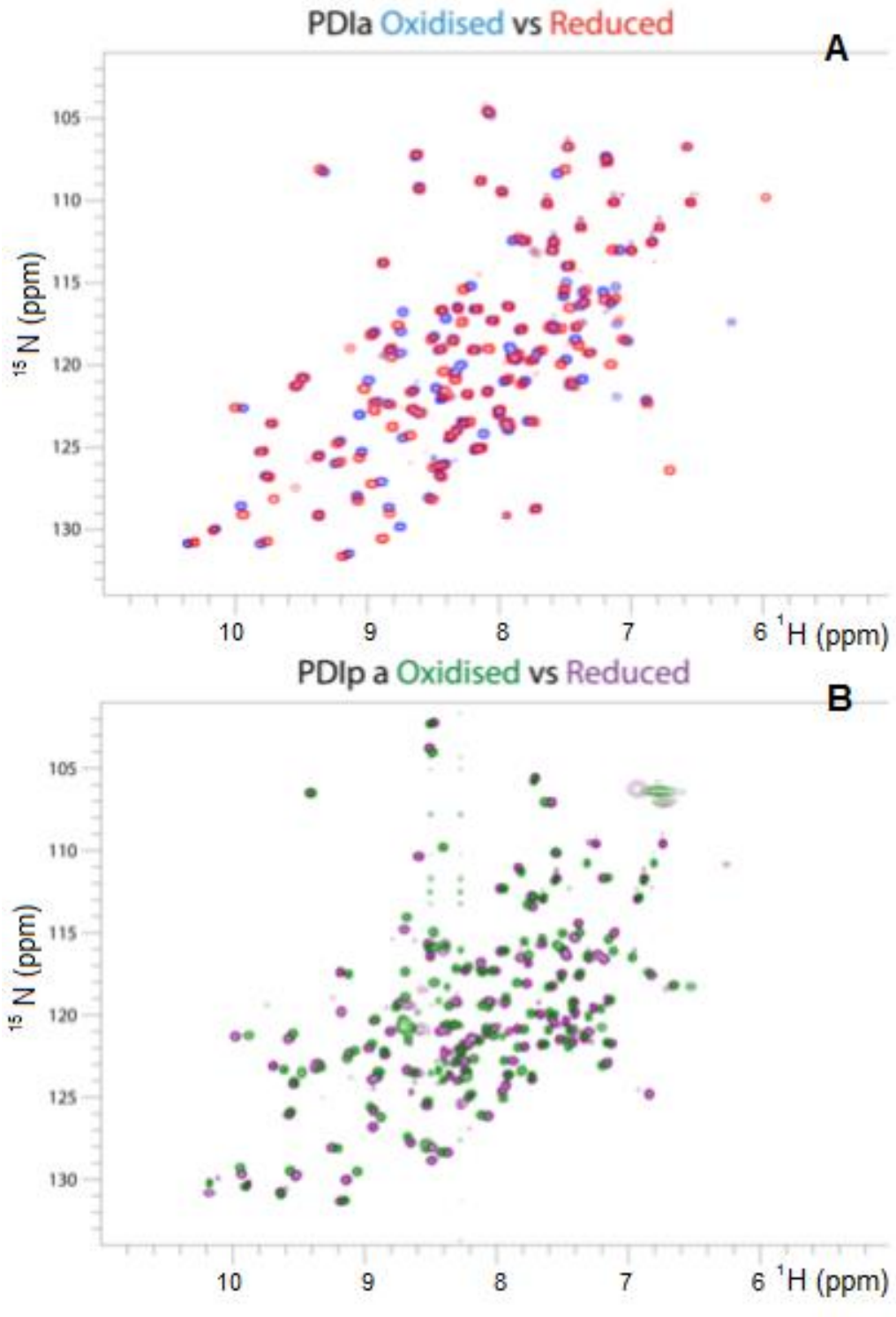

Figure 6.6: ^{15}N HSQC for PDI a and PDIp a in the reduced/oxidised state. 1mM protein in 20mM phosphate buffer (pH 7.3) was reduced or oxidised using 50mM GSH or GSSG. Data was recorded at 25ºC.

6.3. Studying the activity of PDIp a using PDIp a W146F

6.3.1. Molecular biology to make PDIp a W146F mutant

The plasmid encoding PDIp **a** W146F (pKLW14) was made using the protocol described by QuikChange, Agilent. The polymerase used was PFU turbo. Primers were designed to be 33 base pairs in length and were bought from IDT (for primer sequence see methods). PDI **a** W128F (pAKL2), which was used for comparison, was kindly donated by Lloyd Ruddock.

6.3.2. Expression and purification of PDI a W128F and PDIp a W146F

PDI **a** W128F and PDIp **a** W146F were expressed using EnBase. This system makes use of an enzyme which slowly breaks down a synthetic substrate into glucose and in doing so prevents rapid growth and toxicity of the *E. coli* cells. Using this system and the protocol described by manufacturers, a yield of ~150μg/ml of culture was obtained. This is approximately 10x more than typical yields of protein expressed in LB.

As for PDI **a** and PDIp **a**, standard IMAC followed by IEC was sufficient for purification of PDI **a** W128F and PDIp **a** W146F. Far UV CD proved that both proteins were similarly folded to the wild-type and showed that the mutation of W128 and W146 (for PDI and PDIp respectively) had no deteriorating effect on structure (data not shown).

6.3.3. Re-oxidation activity of PDIp a W146F

The activity of PDI **a** and PDIp **a** cannot be studied by the insulin assay as for full length PDI and PDIp because it requires binding at the **b'** substrate binding site. For both proteins, mutating out the second tryptophan (W128 and W146 for PDI and PDIp respectively) leaves only the tryptophan adjacent to the N-terminal cysteines (WCGHC). By measuring the intrinsic fluorescence of both proteins it is possible to

determine redox state because in the oxidised state, the presence of a disulphide bond gives rise to fluorescence quenching.

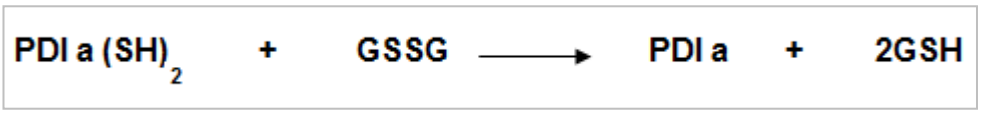

Figure 6.7: Reaction scheme for the reaction of reduced PDI a with GSSG.

Figure 6.8B shows that reduced PDIp **a** W146F is ~4x less easily oxidised than PDI W128F. The re-oxidation activity of both PDI **a** and PDIp **a** is dependent on the nucleophilicity of the N-terminal catalytic cysteine. This means that it is likely that the nucleophilicity of the N-terminal cysteine of PDIp **a** is impaired in some way. This data may also indicate that PDIp **a** was not fully reduced prior to the experiment because relative fluorescence was low compared to PDI **a** even at low concentrations of GSSG (figure 6.8A).

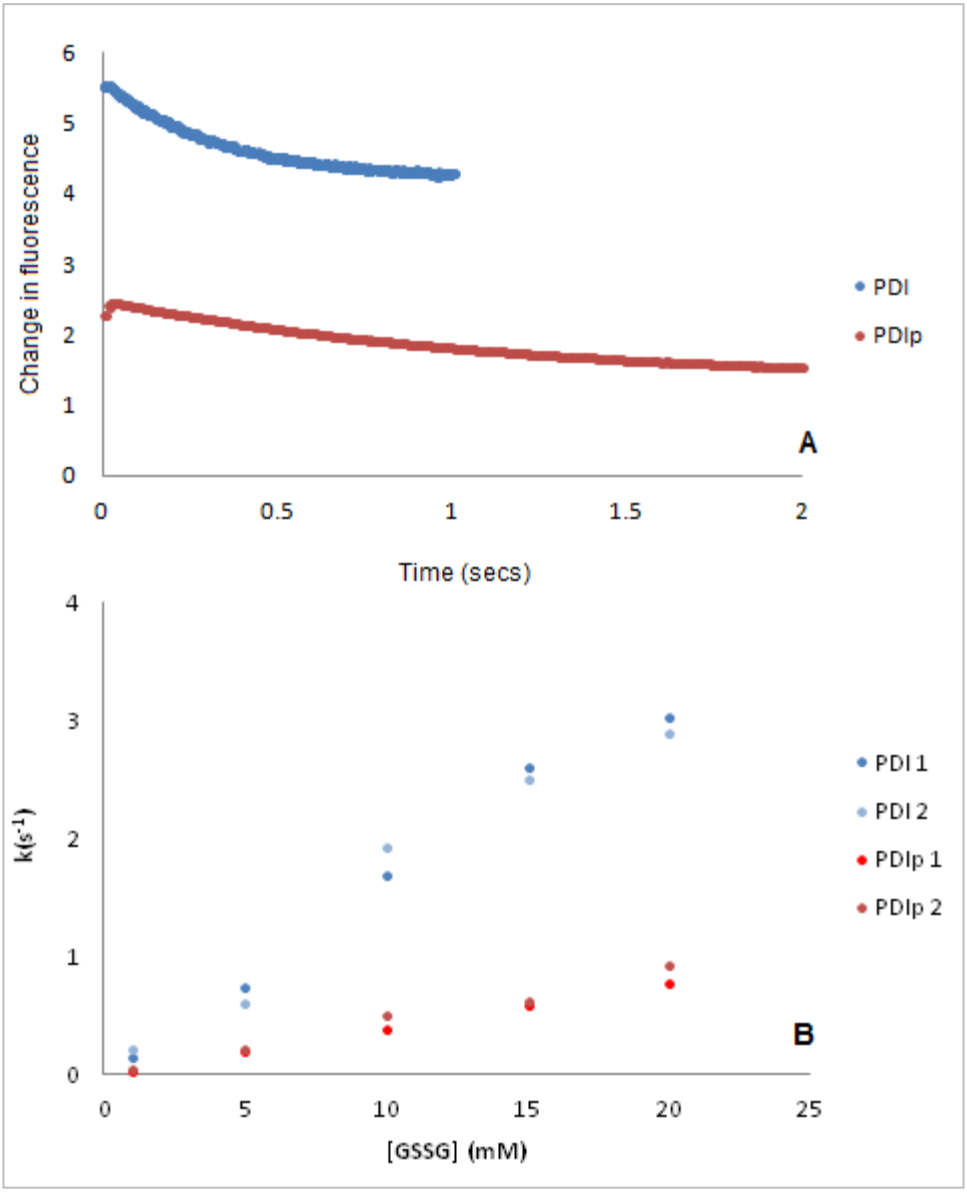

Figure 6.8: Re-oxidation of reduced PDI a W128F and PDIp a W146F. 100µM of PDI **a** W128F and PDIp **a** W146F was reduced using 5mM DTT for 30 minutes at room temperature. Protein was desalted and stored in aliquots at -80ºC prior to use. The reaction of 10µM protein in 0.1M phosphate, 0.1M boric acid buffer pH 7 with varying concentrations of GSSG was measured using a KinTek SF-2004 stopped-flow fluorimeter (excitation: 280nm, bandpass emission >320nm and temperature: 25ºC). A) Raw data for experiment with 20mM GSSG. B) Plot of rate vs [GSSG].

This experiment has only been repeated twice but figure 6.8 shows that relative error is small. In addition, due to the clear differences between PDI and PDIp in re-oxidation activity it is questionable as to whether accuracy could be improved significantly by repeating the experiment further.

6.3.4. Re-reduction activity of PDIp **a** W146F

Similar to the studies of re-oxidation, re-reduction activity can also be determined by measuring the fluorescence of the tryptophan adjacent to the active site. Figure 6.9 shows that PDIp **a** W146F is ~10x less active than PDI **a** W128F in this assay. Clearly the reactivity of the active site cysteines of PDIp **a** is far reduced relative to PDI **a**.

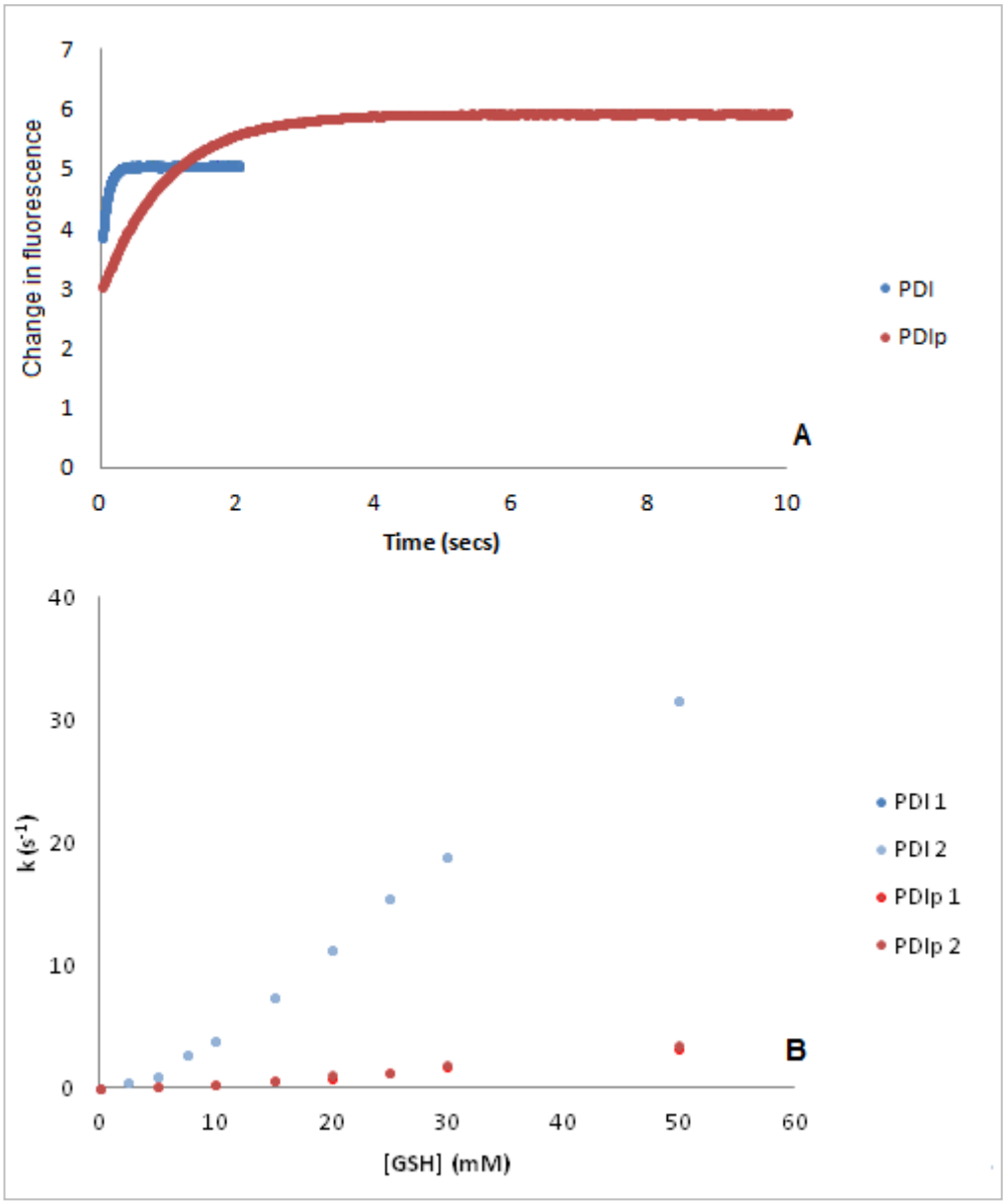

Figure 6.9: Re-reduction of oxidised PDI a W128F and PDIp a W146F. 100µM of PDI **a** W128F and PDIp **a** W146F was reduced using 5mM GSH for 30 minutes at room temperature. Protein was desalted and stored in aliquots at -80ºC prior to use. The reaction of 10µM protein in 0.1M phosphate, 0.1M boric acid buffer pH 7 with varying concentrations of GSH was measured using a KinTek SF-2004 stopped-flow fluorimeter (excitation: 280nm, bandpass emission >320nm and temperature: 25ºC). A) Raw data for experiment with 20mM GSH. B) Plot of rate vs [GSH].

Figure 6.9 shows data collected from two repeats for PDI **a** and PDIp **a**. It is clear that the reproducibility of the assay is very high because data points overlay one

another. Again the difference in re-reduction in activity between PDI **a** and PDIp **a** is clearly distinguishable and so it is not necessary to repeat the experiment further in order to improve accuracy.

For PDI however, figure 6.9 shows that reduction by GSH is negligible until ~5mM GSH. This indicates that spontaneous oxidation of GSH may be occurring. Samples were newly prepared and stored on ice so all precautions to prevent this were taken.

6.4. Determination of pK_a's for the active site cysteines of PDIp a

6.4.1. Molecular biology to make PDIp a C71S and PDIp a C74A

In order to measure the pK_a of the active site cysteines of PDIp **a**, single cysteine mutants needed to be made. As the **a** and **a'** domains of PDIp are like PDI in having high sequence homology being very GC rich they are difficult to mutate in the full length protein. By using the isolated PDIp **a** domain a lot of these difficulties are minimised.

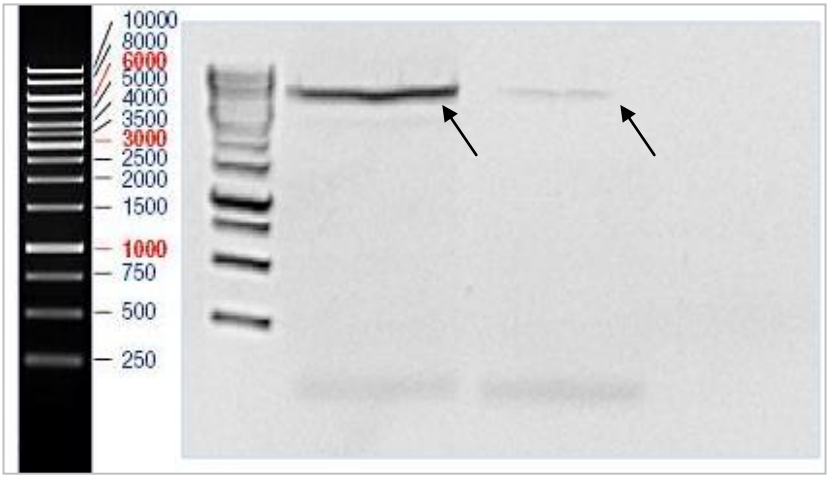

Figure 6.10: DNA gel showing PCR products for PDIp a C71S and PDIp a C74A mutant. Mutagenesis was performed as described by the QuikChange protocol using primers described in methods and PFU ultra (Agilent). DNA was cut from gel and transformed into DH5α super competent cells (NEB). Arrow indicates DNA band cut from gel. A fermentas 1Kb DNA ladder is shown on the left.

Figure 6.10 shows PCR products for QuikChange mutagenesis of plasmid encoding PDIp **a** (pLR1368). Clearly the C71S mutatagenesis reaction was more successful than the C74A mutation as it gives rise to a higher yield of PCR product. These bands were cut from the gel and transformed into super competent cells (for protocol see methods). DNA extraction from these cells confirmed that both mutants had been made.

Previous work has shown that PDIp **a'** and PDIp **b'xa'c** are very unstable (see chapter 3). In order to measure the pK_a of the active site cysteines of PDIp **a'** quadruple cysteine mutants would also need to be made. Work to make these mutants (full length PDIp C71S C74A C364S C418S and PDIp C71S C74A C364S C421A) has already begun. To make these mutants it is necessary to use the BamHI site in the middle of the PDIp DNA sequence because this prevents primers from annealing to the wrong domain as a result of high sequence identity (see methods). By making 4 full length mutants with a single active site cysteine mutated out and 2 full length proteins with the double active site mutation it should be possible to make a full length triple active site cysteine mutant using a restriction digest and ligation based protocol (see figure 6.11). Finally, mutating out C364 gives rise to the quadruple mutant. This work still needs to be completed but 4/6 of the required constructs have already been made.

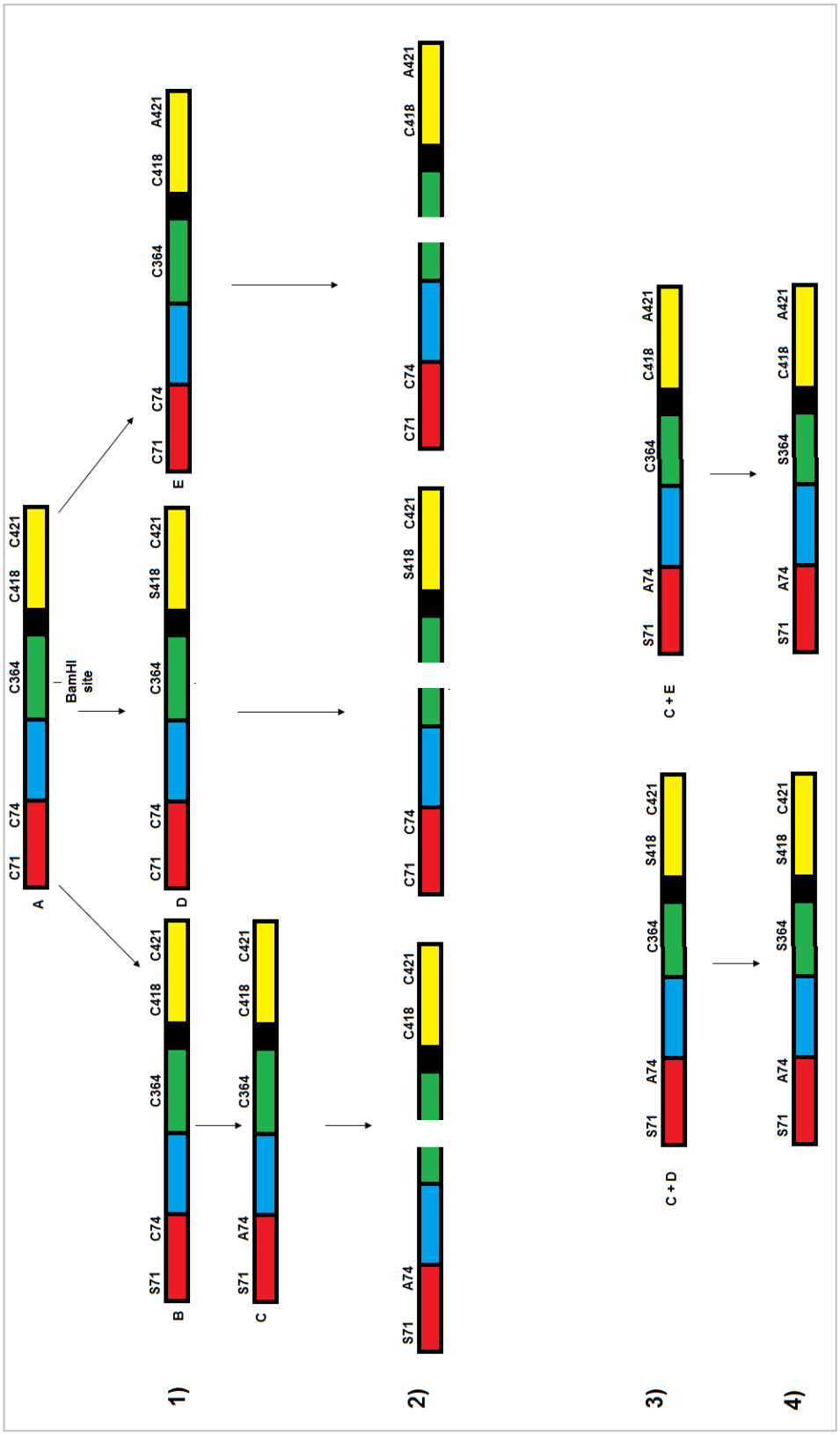

Figure 6.11: Schematic showing construction of PDIp C71S C74A C364S C418S and PDIp C71S C74A C364S C421A. 1) PDIp C71S (B), PDIp C418S (D) and PDIp C421A (E) mutants were made. From (B), (C) can be made (see methods). 2) Restriction digests. 3) Ligation. (C) + (D) and (C) + (E). 4) Site directed mutagenesis of C364 using QuikChange protocol.

6.4.2. Expression and purification of PDIp a C71S and PDIp a C74A

Similar to other PDIp **a** mutants, PDIp **a** C71S and PDIp **a** C74A could be expressed and purified in large amounts using the EnBase system, IMAC and IEC. Far UV CD also confirmed that the active site mutations introduced had no effect on the overall secondary structure of PDIp **a** (data not shown).

6.4.3. Stopped flow pK_a measurements of PDIp a C71S

The pK_a of the C-terminal cysteine was determined by measuring the pH dependence of the rate of reaction between PDIp **a** C71S and DTNB by stopped flow. At pH values above the pK_a of the cysteine it should be in the thiolate (S^-) state. Free thiolates react with DNTB producing the NTB^{2-} ion the concentration of which can be measured spectroscopically at 412nm.

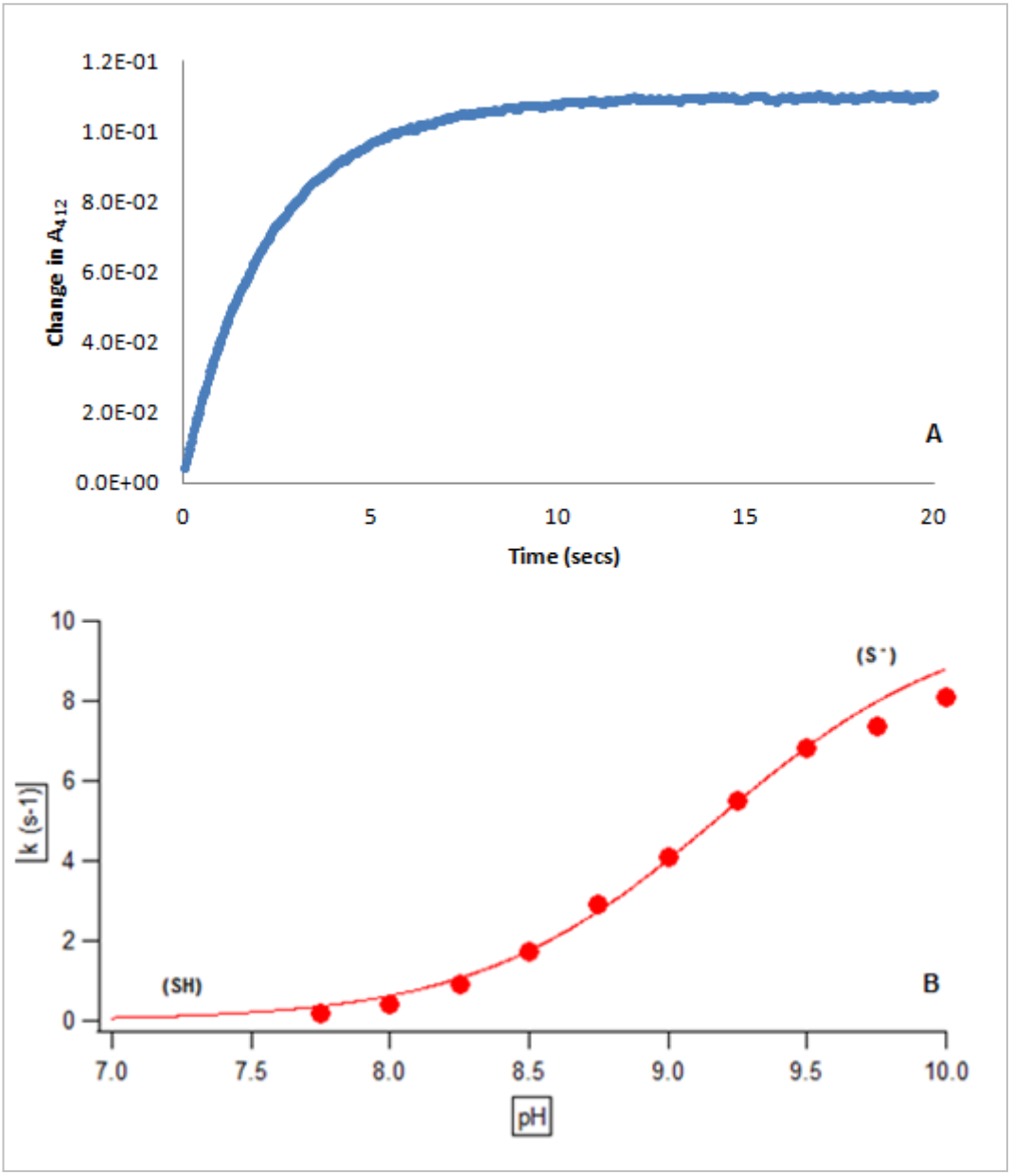

Figure 6.12: pK_a determination of the C-terminal cysteine of PDIp a (C74). The reaction of 25µM PDIp **a** C71S and 0.073 mg/ml DTNB was measured using KinTek SF-2004 stopped flow equipment at 25ºC. The buffer used was 0.1M Na_2HPO_4 and 0.1M boric acid for all pH's (pH 7.5-10). Curve fitting by IGOR Pro software. A) Raw data for pH 8, B) plot of rate vs pH.

Analysis of the data over the pH range 7.5 to 9.5 indicated that the data fitted to a single pKa dependent event with a measured pK_a for PDIp C74 of 9.18 +/- 0.04 (see figure 6.12). This value is slightly higher than for the corresponding cysteine in PDI (C56) which has a pK_a of 8.60 +/- 0.02 (Karala *et al.* 2010). Data taken at > pH 9.5

were excluded from curve-fitting analysis because clear destabilising events had occurred.

6.4.4. Stopped flow pKa measurements of PDIp a C74A

Similar to the data for C71S, the C74A mutant also showed a clear-cut titration.

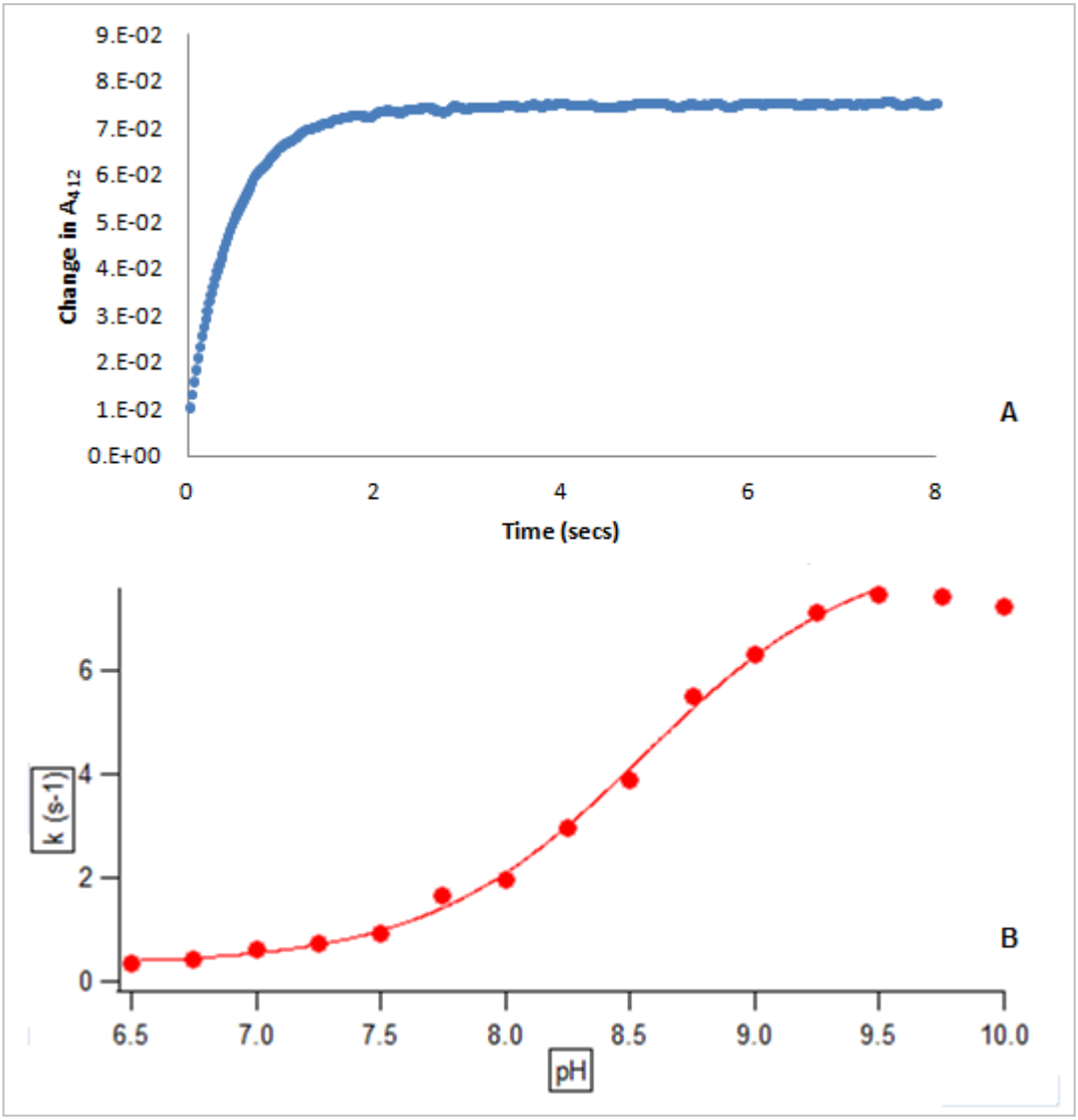

Figure 6.13: pK_a determination of the N-terminal cysteine of PDIp a (C71). The reaction of 25µM PDIp **a** C74A and 0.073 mg/ml DTNB was measured using KinTek SF-2004 stopped flow equipment at 25ºC. The buffer used was 0.1M Na_2HPO_4 and 0.1M boric acid for all pH's (pH 6.5-10). Curve fitting by IGOR Pro software. A) Raw data for pH 8, B) plot of rate vs pH.

Figure 6.13 suggests that the pK_a of C71 is in the region of 8.3-8.5. However, curve-fitting of the data (using IGOR Pro) indicated that there were 2 pK_a dependent events with pK_a's of 8.09 +/- 0.04 and 8.55 +/- 0.04. These are considerably higher than the typical pK_a's calculated for the N-terminal cysteines of PDI family members. Again data taken at >pH 9.5 were excluded from curve fitting analysis.

The high pK_a of the N-terminal cysteine of PDIp **a** explains the poor reactivity that has been seen for PDIp. A high pK_a value means that at physiological pH the N-terminal cysteine is in the unreactive thiol state, while that of PDI which has a pK_a of 4.8 is fully ionised.

6.5. Exploring the potential role of Q75 in modulating the pK_a of C71

6.5.1. Sequence alignment of PDI **a** and PDIp **a** domains

Studies of C71 identified two pK_a dependent events (see figure 6.12) suggesting that the reactivity of the N-terminal cysteine of PDIp **a** was being modulated by nearby residues. In this way the N-terminal cysteine may be slightly less reactive than would be expected for a reduced cysteine. To identify amino acids in PDIp **a** that could potentially contribute to this result, a sequence alignment was performed for PDIp **a** and PDI **a** (see figure 6.14).

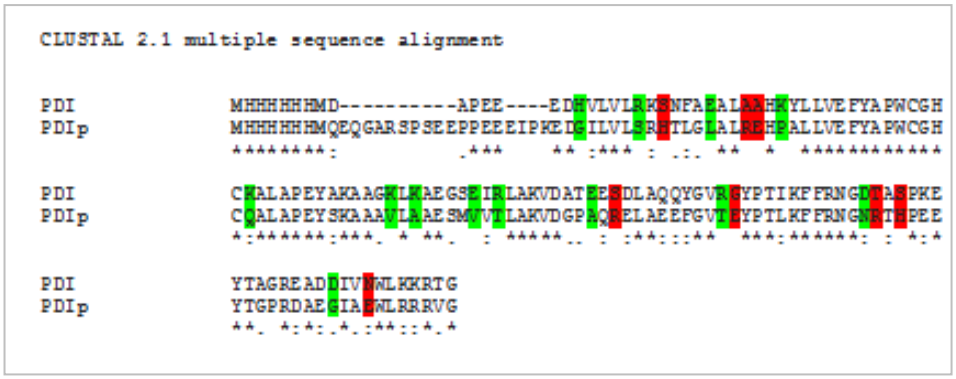

Figure 6.14: Sequence alignment of PDI a and PDIp a (CLUSTAL). Charged residues in PDI that are not conserved in PDIp are shown in green and charged residues in PDIp that are not conserved in PDI are shown in red.

It is clear from figure 6.14 that there are 21 differences in charge for PDI **a** and PDIp **a.** In total there are 13 charged residues in PDI that are not conserved in PDIp and 8 charged residues in PDIp that are not conserved in PDI. However R120, the residue implicated in modulation of PDI **a,** is conserved in PDIp **a** (Karala *et al*. 2010). It remains uncertain which residues are involved in maintaining/modulating the high pK_a of the N-terminal cysteine of PDIp **a** but PDIp Q75 seems like a particularly probable candidate because it is immediately adjacent to the active site in PDIp **a**

(WCGHCQ). Furthermore figure 6.15 shows that in PDI, ERp57 and ERp72, a lysine residue is conserved at this position (WCGHCK).

Figure 6.15: Sequence alignment of PDI, PDIp, ERp57 and ERp72. PDIp Q75 is highlighted in red, typically a lysine residue is conserved at this position (highlighted in green).

In PDI the positive net charge of K57 interacts with the thiolate ion at the N-terminal cysteine stabilising it by electrostatics but for PDIp this is not the case because glutamine is uncharged. However it is possible that the the side group of glutamine could be acting as a hydrogen bond acceptor (see figure 6.16). If a hydrogen bond between Q75 and the unreactive thiol group this may explain why PDIp **a** exhibits some reactivity despite the N-terminal cysteine being in the predominantly unreactive thiol state. Overall this may explain the low oxido-reductase activity seen for wild-type full length PDIp.

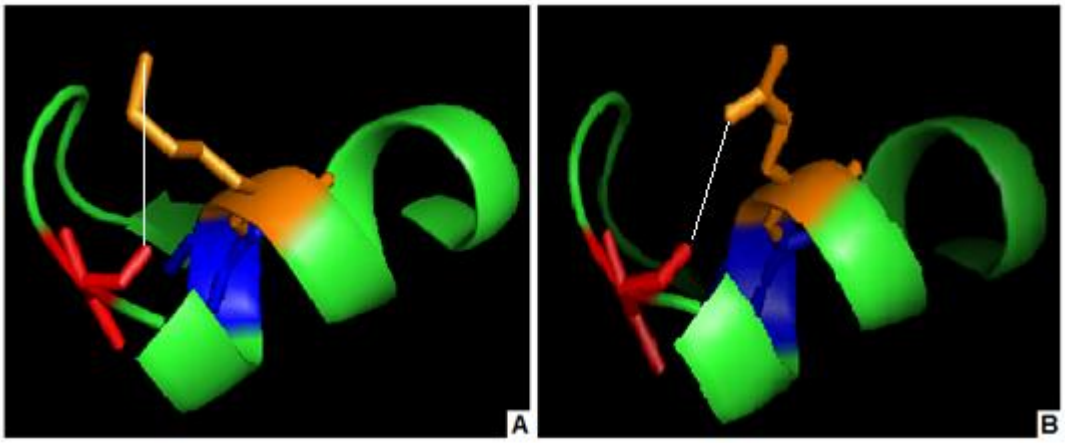

Figure 6.16: PyMOL images of the active site regions of PDI a and PDIp a. The structure of PDI Leu44-Tyr63 was observed using PyMOL and PDB: 4EKZ because this region is conserved in PDI and PDIp (with the exception of Q75 adjacent to active site. For PDIp K57 is mutated to Q using PyMOL mutagenesis function. N-terminal cysteine is shown in red, histidine in blue and either lysine or glutamine in orange (PDI and PDIp respectively). A) Interaction between positive charge of lysine and the negative charge of the thiolate ion on N-terminal cysteine (shown by white line). B) Hydrogen bond between SH group and oxygen on the side chain of glutamine leading to slight negative charge on the donating sulphur atom (shown by white line).

6.6. Concluding Remarks

Previously we showed that PDIp has ~50% of the oxido-reductase activity of PDI. This was expected to be caused by differences in substrate specificity conferred by the **b'** domain and also the unusual **a'** domain active site sequence (CTHC). We have since shown that while the **b'** and **a'** do have a slight negative effect on the activity of PDIp , the effect of PDIp **a** is far more significant.

Stopped flow studies of PDIp **a** that measured the reactivity of the active site with either GSH or GSSG confirmed that it was much less reactive than originally postulated. As PDIp **a** has a normal active site sequence (CGHC) this was unexpected. Additional stopped flow studies to measure the pK_a of the active site cysteines of PDIp **a** showed that the N-terminal cysteine had an exceptionally high pK_a. This means that at physiological pH the N-terminal cysteine is in the unreactive

thiol state and explains the lack of activity seen for PDIp **a** and also the reduced activity of full length PDIp.

Further study identified Q75, an amino acid found immediately adjacent to the PDIp **a** domain active site that is not conserved in other PDI family members (which typically have a lysine residue at this position). Additional work is required to confirm our hypothesis, but we believe that the presence of a glutamine residue at position 75 in PDIp **a** instead of a lysine residue (seen for other PDI family members), leads to overall stabilisation of the thiol state at the N-terminal cysteine. Consequently the N-terminal cysteine of PDIp **a** is not as reactive as that of PDI **a** which is stabilised in the thiolate form by electrostatic interactions with lysine. A PDIp **a** Q75K mutation should therefore stabilise the thiolate state of the N-terminal cysteine and therefore increase the overall reactivity of the active site.

In regards to structure, an unreactive N-terminal cysteine could explain why only minor redox-mediated conformational changes were observed. For example if the N-terminal cysteine is highly unreactive this would mean that it would be very difficult to oxidise PDIp **a**. This means that in our studies of redox structure oxidised PDIp could have a reduced **a** active site and an oxidised **a'** active site and explains the polymorphisms seen by native-PAGE (chapter 5). This does however indicate a role for the **a** domain in the redox conformations of PDIp. This is not the case for PDI for which **b'xa'** is the minimal requirement for redox conformational change. Therefore PDI and PDIp must be different in terms of redox structure. Further work is required to confirm this.

Chapter 7. Discussion

7.1. Expression & purification of PDIp and PDIp constructs

7.1.1. Determining protocols for optimal expression and purification of PDIp

Initial studies of the expression and purification of recombinant PDIp led to attainment of very low yields (~2µg/ml of culture). We attributed this to: a) poor expression , b) limited binding during IMAC and c) reduced stability. While we were able to improve expression yield significantly by increasing induction time, it was clear that the major contributing factor to poor yield was the inefficiency of IMAC.

Typically during IMAC, the hexa-Histidine tag that is artificially added to the protein binds to the immobilised Ni^{2+} of the column material thereby separating it from the crude cell lysate. Protein can then be eluted from the column using a strong chelating agent such as EDTA. In our studies of PDIp binding, we found that this process was inefficient. Furthermore any PDIp that did bind was very easily eluted even in the absence of imidazole or EDTA.

Having aligned the N-terminus of PDIp with that of PDI, we noted that for PDIp, this region was much longer and more negatively charged. Subsequently we suggested that the His-tag might be folding back onto the N-terminus of PDIp via electrostatic interaction, and therefore may not be solvent accessible. This theory has since been supported by the fact that increasing exposure time of the Ni^{2+} column with the hexa-His tagged PDIp led to an increase in total binding. This work therefore suggests that

the His-tag is dynamic and therefore may exist in N-terminus bound and unbound forms.

Although we improved purification yield significantly by increasing column exposure time, we also considered using molecular biology to improve binding efficiency. Plasmid pKLW1 was designed to have a truncated N–terminus that would hopefully prevent the His-tag from binding to it. Unfortunately this clone did not express well and so we were unable to determine whether binding efficiency had improved as a result of the truncation. We now believe that poor expression was caused by the N-terminal **a** domain boundary being compromised by the truncation. This work therefore shows a possible consequence of making mutations close to domain boundaries. It would be useful to re-design this clone to avoid disrupting the **a** domain boundary and so that we could identify differences in column binding associated with a truncated N-terminus.

An additional mutant which could have been made to aid purification is a GST-tagged PDIp construct. Having made this, PDIp could be purified using another form of affinity chromatography which relies on the ability of glutathione-s-transferase to bind to column-bound GSH. Again study of this construct would help us to understand the interaction between the His-tag and the N-terminus of PDIp.

Currently, the physiological role of the negatively charged N-terminus of PDIp is unknown. Furthermore, PDIp also has an acidic C-terminal tail which too has an unknown function. It will be useful to study these regions with the aim to identify their role. An acidic C-terminal tail is fairly typical for PDI family members and for PDI it has been shown to be very flexible, preventing crystallisation (Wang *et al.* 2012). In addition, although the C-terminal tail of PDI was found to be unimportant for isomerase activity, it has been shown to stabilise chaperone activity and may also act as a calcium binding site (Klappa *et al.* 1998a, Tian *et al*. 2004, Macer and Koch, 1988).

7.1.2. Studies to improve the stability of PDIp

We found recombinant PDIp to be very unstable and after just 3 days storage at -20ºC there was significant loss of the full length protein. This is due to the presence of *E.coli* proteases and is easily resolved by adding PMSF, leupeptin and pepstatin during cell harvest and cell lysis. Clearly, recombinant expression of PDIp is toxic to the cell and leads to induction of a stress response. Whether this is simply due to over-expression or whether PDIp is genuinely toxic remains unclear (for review see Gasser *et al.* 2008). Furthermore such cellular toxicity is not seen during the recombinant expression of PDI but this may be on account of a shorter expression period.

This work highlights the importance of balancing recombinant expression with the stress response and we noted for example, that expression times of over 20 hours gave rise to a reduction in yield relative to at 16 hours. This may also explain why we saw negligible yields of PDIp using the EnBase system which uses a 24 hour expression time. The advantage of this media system is that it utilises 'slow glucose feeding' with the aim of increasing cell number without inducing cellular stress. Unfortunately for the expression of PDIp this seems to be futile. It is clear therefore that during expression of recombinant PDIp, the up-regulation of cellular proteases is detrimental to stability and final yield.

Interestingly, unstable PDIp gives to rise to one major product. This protein fragment has a M_w of ~40kDa which corresponds to the approximate M_w of hexa-His tagged PDIp **abb'x** and indicates the loss of the **a'** domain. This shows that similar to PDI, PDIp exhibits intrinsic flexibility and susceptibility to proteases at the **x**-linker region (Wang *et al*. 2010). After the loss of the **a'** domain, PDIp **abb'x** was very stable and did not seem to deteriorate any further in the time tested (data not shown). Again this is indicative of an almost hinge-like region at the C-terminus of PDIp that may give rise to redox-mediated conformational changes similar to those described for PDI (Wang *et al.* 2011, Wang *et al*. 2012).

7.1.3. Studies of the structure and activity of PDIp using PDI.PDIp chimera proteins

Plasmids encoding PDIp ½, PDIp ¾ and PDIp ¾ T419G (pAKW5, pAKW11 and pAKW12 respectively) were kindly donated by Dr. Katrine Wallis. The domain boundaries of these proteins were constructed as described by Alanen *et al*. (2003) and Pirneskoski *et al*. (2004). The disadvantage of using chimera proteins as we have done is that if the domain boundaries are incorrect and/or domain interface interactions are disturbed, then the protein can be unstable or incorrectly folded as we have seen previously for our full length N-terminal truncate. If this were the case, the chimera proteins would not be suitable for further study.

In our work, we were careful to control for the possibility that the chimera proteins were not correctly folded. In PDIp ½ there is one non-native domain boundary (**b-b'**) and in PDIp ¾ and PDIp ¾ T419G there are two (**b-b'** and **x-a'**). The first indicator that these boundaries had been constructed correctly was that we were able to generate significant yields of soluble protein for all 3 chimeras (Alanen *et. al* 2003). In addition, far UV CD of this protein showed that PDIp ½, PDIp ¾ and PDIp ¾ T419G were all well folded with similar overall secondary structure to wild-type PDI and denaturation studies showed that they were no less stable than wild-type PDIp. It is clear from this work that our chimera proteins are well structured. We can therefore conclude that the artificial domain boundaries that have been introduced into these chimeras are at least not detrimental to the overall structure of the protein.

Obviously despite having performed these controls, it is not ideal to use chimera proteins because they are not true representations of either parent protein. Furthermore we cannot assume that 2 domains that have a particular characteristic in one protein will act identically in another. Therefore we must be cautious in the conclusions that are taken from studies of chimera proteins. For our work however, these studies have been essential in our understanding of the structure and activity of PDIp.

7.1.4 Studies of the structure and activity of PDIp using mutant

Similar to our studies of chimera proteins, we must be vigilant when using mutants to ensure that the introduced mutation is not detrimental to the integrity of the protein. Again we used far UV CD to study the effect of any mutations on the secondary structure of the protein. Although for most mutants no significant change in secondary structure was observed, for PDIp H278A and PDI H256A there was a huge loss of α-helical structure relative to the wild-type proteins (data not shown). These mutants were designed to probe the role of H278 and H256 (PDIp and PDI respectively) in substrate binding. In published work on PDIp H278A, the change in secondary structure described here is not commented upon (Fu *et al.* 2011). Authors focus instead on the loss of oestradiol binding activity which may in fact be caused by structural changes in the substrate binding site. On account of these structural observations we ceased further study on PDI H256A and PDIp H278A.

7.2. Redox-mediated conformational changes of PDIp

7.2.1. The 3-dimensional structure of PDIp

Currently there is very limited structural information for PDIp but we have assumed that its 3-dimensional structure is similar to the recently published X-ray crystal structure of hPDI (Wang *et al.* 2012). Unfortunately however, initial structural work indicated that this may be an over-simplification and far UV CD data clearly shows that PDIp has more α-helical structure than PDI. Furthermore, additional study using chimera proteins, PDIp ½ and PDIp ¾ (PDIp **ab** PDI **b'xa'c** and PDIp **ab** PDI **b'x** PDIp **a'c** respectively), attributed this difference to the **b'x** region. This is particularly interesting because we know that PDI **b'** harbours the substrate binding site (Klappa *et al.* 1998a). Consequently it is possible that physical differences between PDI and PDIp in this area may contribute to their contrasting substrate binding properties. Further study of the structure of PDIp **b'x** will be essential for clarification.

The **b'x** region of PDI is also important for redox-mediated conformational change and is part of the larger redox-active cassette, **b'xa'c** (Wang *et al.* 2011, Wang *et al.* 2012). If PDIp **b'x** has a larger percentage of α-helical content than PDI **b'x** this may mean that it is also more stable. Although this hasn't been studied directly, we have shown by far UV CD that PDIp has remarkable thermal stability and retains significant secondary structure after incubation at 80ºC. The implications of increased stability for PDIp could be that unlike PDI, PDIp does not undergo large redox-mediated conformational changes. Furthermore this characteristic could help protect PDIp from the harsh environment of the exocrine pancreas.

7.2.2. Studies of the redox-mediated conformational changes of PDIp

The recent X-ray crystal structures of reduced and oxidised hPDI show the structural changes associated with the two redox states (Wang *et al.* 2012). For example in reduced PDI, the **a'** domain is tightly packed against **b'** via numerous inter-domain interactions but in the non-reduced structure these are broken and the **b'** and **a'** domains are distinct. The net effect of this is that upon oxidation, PDI exhibits a more open conformation which increases exposure of hydrophobic surfaces and promotes substrate binding (Wang *et al*. 2012). In this way the redox-mediated conformational changes of PDI have a significant effect on modulating its activities and recent work has shown that for its chaperone activity, PDI is most efficient in its oxidised form (Wang *et al.* 2011).

Our studies show that unlike PDI, PDIp undergoes only minor redox-mediated conformational changes. For example we showed that the thermal stability of PDIp is unaffected by redox state, whereas for PDI a reduction in T_m of ~4ºC was seen for the oxidised protein. Surprisingly, the thermal stability of PDIp ½ and PDIp ¾ which are similar to PDIp in having PDIp **a** and **b** domains, also appears to be unaffected by redox state. Therefore contradicting our original hypothesis, differences between PDI and PDIp in response to redox state do not seem to be caused by PDIp **b'x** but instead may be due to PDIp **ab**.

In agreement with this work, dynamic light scattering (DLS) experiments show that the chimera proteins are more similar to PDIp than PDI in terms of redox-mediated conformational change. More specifically, the diameters of PDIp, PDIp ½ and PDIp ¾ are increased by ~8% in the oxidised form rather than ~25% which is the percentage change in diameter seen for oxidised PDI. Unfortunately however, the difference in diameter for reduced and oxidised PDI (25%) was found to be not significant using the student's t-test. This was not unexpected because standard deviation was high and replicate number was low. Therefore increasing the number of measurements should reduce variance and as a consequence also improve significance.

The role of PDIp **ab** in influencing redox-mediated conformational change was completely unexpected because recent studies have shown that for PDI, **b'xa'c** is the minimum redox-active cassette (Wang *et al.* 2011, Wang *et al.* 2012). In contrast, our work shows that that for PDIp ½, the presence of PDI **b'xa'c** is not sufficient for redox-mediated conformational change and therefore indicates that PDIp **ab** may be preventing this from occurring. Further study is required to understand how PDIp **ab** exerts this effect and it would be useful to observe the thermal stability of PDI ½ and PDI ¾ (PDI **ab** PDIp **b'xa'c** and PDI **ab** PDIp **b'x** PDI **a'c** respectively) in order to see how their redox-conformations differ compared to wild-type PDI. In this way we could identify whether this moderating activity is unique to PDIp **ab** or whether it has simply been overlooked in PDI **ab**.

An additional concern is that the process of making chimera proteins has artificially implicated **ab** as a modulator of redox-conformational change. This is a possibility because we have disrupted the domain boundaries between **b** and **b'**. Having studied the secondary structure and intrinsic flexibility of both PDIp ½ and PDIp ¾ by far UV CD and limited proteolysis respectively (for the latter, data is not shown), we believe that this is not the case. Both chimera proteins are well folded and do not show increased susceptibility to proteolysis compared to the wild-type. We conclude that the implied role of **ab** in redox-mediated change is real and not an artefact caused by using chimera proteins.

7.2.3. Limited proteolysis experiments to examine intrinsic flexibility

In light of the significant contribution made by PDIp **ab** in moderating redox-regulated conformational change, we decided to use limited proteolysis to examine regions of flexibility that may or may not be linked to redox state. These experiments have traditionally been very useful for domain boundaries determination and have more recently been used to identify **b'x** as the site of greatest plasticity in PDI (Darby *et al.* 1996, Wang *et al*. 2010). Limited proteolysis of yPDI however shows that the linker between **a** and **bb'** is the most flexible region and thus exhibits the greatest degree of conformational change (Tian *et al.* 2008). It was important to study PDIp by limited proteolysis in order to rule out the slight possibility that it may have an alternative mechanism of conformational change that may or may not be similar to yPDI.

As anticipated, limited proteolysis experiments show that like hPDI, PDIp is most susceptible to chymotrypsin at its C-terminus and preferentially loses the **a'** domain (Wang *et al.* 2010). In addition, PDIp shows remarkable resistance to proteolysis at its N-terminus indicating that it does not exhibit conformational changes similar to yPDI (Tian *et al.*2008). In regards to redox-linked conformational changes, these limited proteolysis experiments show that although PDIp has increased susceptibility to chymotrypsin in its oxidised state (relative to the reduced form), this is less significant than for hPDI. Furthermore, 2 distinct populations of peptides could be seen following the digestion period: those with M_w <30kDa (similar to oxidised hPDI) and those with M_w >30kDa. This could be indicative of 2 different start species (i.e. diamide sensitive/insensitive) or may indicate that due to accessibility limitations, the full cleavage reaction requires a longer incubation time than 2 hours. Reduced sensitivity to chymotrypsin, an enzyme produced by the acinar cells of the pancreas for example, may provide protection for a protein catalyst exclusively expressed there.

7.2.4. Molecular mechanisms for conformational change in PDIp

We have shown that PDIp undergoes less significant redox-mediated conformational change than PDI but have not yet determined an exact mechanism to explain this. Our studies have however shown that: a) PDIp is more thermally stable than PDI and that this property is probably due to **b'x**, b) the limited redox change seen for PDIp is mediated by its **a** and **b** domains and c) that PDI and PDIp exhibit almost identical regions of susceptibility to chymotrypsin indicating that they probably have quite similar tertiary structure. However we have not yet discussed the possible role of inter-domain interactions.

In their paper, Wang *et al.* (2011) describe several inter-domain reactions that occur between PDI **b'** and PDI **a'** in the reduced protein and that are broken when in its oxidised state. Consequently they can be described as 'tethering' interactions. One such interaction seen in reduced PDI, is a cation-π interaction between R300 in **b'** and W396 in **a'**. Research shows that when the **a'** active site is oxidised, due to the proximity of W396 (WCGHC), steric hindrance leads to the breakage of the R300: W396 interaction. When this bond is broken, the PDI **a'** domain rotates ~45^{o} around the x-linker and toward the hydrophobic surface of **b'** (Wang *et al.* 2011, Wang *et al.* 2012). In support of the importance of R300: W396 in tethering the reduced conformation, mutating either residue led to increased susceptibility to proteolysis and therefore suggested presence of the open conformation (Wang *et al.* 2011, Wang *et al*. 2012).

Interestingly, R300 is not conserved in PDIp and instead there is a His residue at this position. We postulated that the H321:W417 interaction could be stronger than that of R300:W396 because His and Trp could interact via a parallel stacking interaction (Samanta, 1999). Consequently the H321:W417 interaction would be a major contributing factor in the limited redox-mediated conformational changes of PDIp. In order to test this hypothesis we made PDIp H321R mutants but no significant difference in redox-linked conformation was seen relative to wild-type PDIp (data not shown). Furthermore for PDIp ¾, which has PDI **b'x** (and so PDI R300) and PDIp **a'** (W396) there was also no sign of redox-mediated change. This preliminary work may therefore give rise to several conclusions: a) that the H321: W417 is not

stronger than R300:W396 and/or b) the tethering interactions of PDIp are not the sole cause of limited redox-mediated conformational change. Further data is needed to fully understand the role of this interaction in the redox-linked conformational changes of PDI and PDIp.

7.2.5. Implications of a limited redox-mediated conformational change

In the X-ray crystal structure of reduced PDI, the cleft diameter is ~15 Å and therefore is significantly limited in its potential interaction targets being only able to accommodate small peptides. The active site of the **a'** domain is also largely shielded suggesting that the catalytic activity may also be limited. In the oxidised crystal structure however, the cleft diameter is ~ 30 Å and both the hydrophobic surfaces and the **a'** active site are exposed (Wang *et al.* 2012). Therefore having been oxidised, PDI has greater ability to interact with much larger protein substrates i.e. non-native protein structures. In support of this, oxidised PDI exhibits greater chaperone activity than the reduced form (Wang *et al.* 2011).

Due to sharing identical domain architecture and ~45% sequence identity we have assumed that PDI and PDIp share similar 3-dimensional structure. If this is the case, reduced PDIp will have a similarly small cleft size. The implication here however is, that if PDIp does not undergo large redox-mediated conformational change as we have shown to be the case, then how does it accommodate substrate?

We know that PDIp is able to interact with large protein substrates as we have been able to study its activity in the insulin oxido-reductase assay (discussed in more detail later). In addition, we also know that the **b** and **b'** domains are capable of chaperone activity (Fu *et al.* 2010). Therefore on account of this, PDIp must undergo conformational changes that lead to exposure of its inner hydrophobic surfaces.

One possible mechanism for non redox-mediated conformational change is substrate binding induced conformational change. This would mean that PDIp is less likely to exhibit an open conformation in an environment where potential substrates are limited. This could be a protective mechanism because if PDIp exhibited redox-mediated conformational change like PDI, its chaperone activity could be affected by

non-specific substrate competition. It would also prevent PDIp from exposing its most susceptible areas to the harsh environment of the exocrine pancreas if there was a limited substrate pool.

7.2.6. The redox conformation debate

There is an on-going debate about the use of organic oxidant/reductants for studies of structural conformation such as those described here (for review see Hatahet and Ruddock, 2009). As noted previously, recent work has shown that oxidation of PDI by GSSG leads to conformational change associated with increasing cleft size (Wang *et al.* 2011). However, the disadvantage of using GSSG in these studies is that it is able to bind to PDI and has been shown to inhibit the association of PDI with the α-subunit of prolyl-4-hydroxylase (Lumb and Bulleid, 2002). Unfortunately this is not limited to GSSG, and the X-ray crystal structure of PDI **bb'xa'** shows a molecule of oxidised DTT trapped at the **b'** domain (Wang *et al.* 2011). It has therefore been suggested that the conformational changes that have been presented for PDI, are not oxidation induced, but instead are caused by ligand binding.

If conformational change is found to be associated with substrate binding rather than oxidation state, this will be in agreement with our studies of PDIp. It is easy to suggest that the reason PDIp exhibits limited redox-mediated conformational change is because unlike PDI, it has more restricted substrate specificity and therefore is unable to bind GSSG or DTT. Certainly it is known that GSSG can inhibit binding of PDI to the α-subunit of prolyl-4-hydroxylase (Lumb and Bulleid, 2002). In our studies of redox-conformation we have used diamide and DTT as our oxidant/reductant of choice. At this time it is unknown whether these molecules are also able to bind PDI/PDIp. Consequently we are still unable to determine whether these structural changes are associated with redox-state or ligand binding.

The suggestion that ligand binding may be inducing conformational change is in direct contrast with the recent X-ray crystal structure of untreated PDI (Wang *et al.* 2012). Compared to DTT-treated PDI, this structure has a significantly larger cleft diameter indicating that even in the absence of oxidant, PDI has an open

conformation. This therefore implies that redox-state does dictate conformation. Although not reduced, this structure is not a true representation of the oxidised form as the **a** domain is only ~70% oxidised (Wang *et al*. 2012). Consequently the true extent of conformational change may still be unknown.

In order to determine whether conformational change is associated with ligand binding or redox-state, we could replace GSSG and DTT with non-organic oxidant/reductants such as H_2O_2 and Tris-2-carboxyethyl phosphine (TCEP). Performing several of the experiments described earlier e.g. thermal denaturation, limited proteolysis etc, in the presence of H_2O_2 or TCEP will establish their effect on redox structure and finally identify the true reason for conformational change.

7.3. The oxido-reductase activity of PDIp

7.3.1. Historical measurements of activity for PDIp

Prior to this work the catalytic activities of PDIp were poorly characterised. Published studies on the oxido-reductase activity of PDIp are tainted by their use of a PDIp construct termed Pa-1 PDIA2 which has an incorrect N-terminus (Desilva *et al*. 1996). Unfortunately this construct has been routinely used in studies of recombinant PDIp and there is now a significant amount of published data that is irrelevant to the wild-type protein. An example of this is seen in work published by Fu and Zhu (2009a) which identifies an inter-subunit disulphide bond centred on an aberrant cysteine residue in the Pa-1 PDIA2 construct. This issue has now been formally resolved with publication of the correct construct (Walker *et al*. 2012). Furthermore authors suggest that Pa-1 PDIA2 is the product of an unusual recombination event that ultimately led to insertion of an incorrect start codon.

7.3.2. Measurements of the oxido-reductase activity of full length wild-type PDIp

We have shown that PDIp has ~55% of the oxido-reductase activity of PDI (see figure 4.14) and this is not dissimilar to the measured activity of Pa-1 PDIA2 (Desilva *et. al* 1996). This result was expected because the catalytic active sites are

not affected by the discrepancy at the N-terminus. It was important to confirm this because we know that the Pa-1 PDIA2 construct dimerises readily and this may have affected the reported activity (Fu and Zhu, 2009a).

Initially we proposed that differences between the oxido-reductase activity of PDI and PDIp were caused by a) differences in substrate specificity and b) the unusual **a'** domain active site motif for PDIp (CTHC instead of CGHC).

7.3.3. The role of the **b'** domain in the oxido-reductase activity of PDI and PDIp

We know that in our assay, substrate binding at the **b'** domain is essential for oxido-reductase activity because negligible activity is seen for the isolated PDI/PDIp **a** and **a'** domains (data not shown). This is consistent with work by Darby *et al.* (1998) which showed significantly increased oxidase/reductase activity for constructs containing the PDI **b'** domain compared to those that did not. Like PDI, PDIp clearly requires large substrates/ligands to be bound at **b'** before the catalytic domains are able to act upon them.

Despite having restricted substrate specificity, our studies show that PDIp is able to bind insulin although it is unclear whether this process is the same or less efficient than for PDI. *In silico* studies show that insulin (porcine) has at least one exposed hydroxy-aryl group (PDB ID: 4INS) and this satisfies the minimal requirement for PDIp binding. Insulin is highly conserved in vertebrates: human and porcine insulin differ by one amino acid and human and bovine insulin differ by 3 amino acids.

In order to study the role of insulin binding in our oxido-reductase assay a PDI/PDIp chimera was made. PDIp ¾ has PDIp **ab**, PDI **b'x** and PDIp **a'c**. Figure 5.10 shows that the effect of replacing PDIp **b'x** with PDI **b'x** is positive and gives rise to an increase in activity of ~12% i.e. that PDIp ¾ has ~67% of the activity of PDI. This therefore indicates that in our assay, the measured activity of wild-type PDIp is limited to a small extent by its inefficiency in binding insulin. It also implies that there are additional requirements for ligand binding that are not linked to the presence/absence of a hydroxy-aryl group. Further studies of the ligand binding properties of PDIp will be essential in order to resolve this.

One such study would include measuring the activity of a PDI ¾ chimera (PDI **ab,** PDIp **b'x** and PDI **a'c**). This would determine definitively the effect of PDIp **b'x** (i.e. the role of substrate binding) on the oxido-reductase activity of PDI. It would also be interesting to identify conserved residues between PDI and PDIp that are implicated in the binding site of PDI (Byrne *et. al* 2010). Mutating out these residues one at a time should allow us to recognise those that are directly involved in binding insulin to PDI or PDIp.

Similar to this, Fu *et al.* (2011) have shown that for the interaction of 17-β-oestradiol with PDIp, His278 (found in the **b'** domain) is essential. This residue supposedly forms a hydrogen bond with estradiol-3-hydroxyl group and when mutated out leads to negligible/no binding. We are cautious of this work for two main reasons: a) the incorrect Pa-1 PDIA2 clone was used and b) our studies of PDIp H278A and PDI H256A indicate that the secondary structure of these mutants is compromised relative to the wild-type proteins (data not shown). Although further work is required to fully interpret this result it is possible that these structural changes are the real cause of reduced binding. No evidence of these structure controls are shown in the paper of Fu *et al*. (2011).

7.3.4. The effect of the **a'** domain on the oxido-reductase activity of PDIp

Unlike PDI and ERp57, its closest family members, PDIp has a CTHC active site motif instead of CGHC. The implications of this are currently unknown but it is likely that this contributes to the reduced oxido-reductase activity of PDIp. In PDI it is thought that the positive charge of the imidazole ring of the histidine residue at position 3 in the CXXC motif plays a role in stabilising the low pK_a of the N-terminal cysteine (Ferrari and Söling, 1999). If this is true it is likely that the presence of a much larger amino acid side chain at position 2 in the **a'** domain of PDIp (threonine instead of glycine) will sterically block the interaction between the histidine side chain and the N-terminal cysteine. The consequence of this may be that the N-terminal cysteine is unstable as a thiolate ion and a less potent nucleophile.

In order to study this further a PDIp T419G mutation was made. This protein has an **a'** domain active site that mimics that of PDI. Our studies of the oxido-reductase activity of PDIp T419G show that it is ~65% as active as PDI (see figure 5.12). This means that this construct has roughly equivalent activity to the PDIp ¾ mutant and is ~10% more active than the wild-type protein. Clearly PDIp **a'** has a much lesser effect on the low oxido-reductase activity than initially postulated.

Additional studies showed that PDIp ¾ T419G was ~63% as active as an oxido-reductase as PDI (see figure 5.12). Based on previous results we had expected a cumulative effect of the two mutations but this indicates that the PDIp ¾ T419G mutant was similarly active to both PDIp ¾ and PDIp T419G mutants. Unfortunately the high standard deviation (11.06) means that it is difficult to interpret the actual activity of the PDIp ¾ T419G mutant. In order to resolve this additional repeats should be performed to reduce variance.

This work indicates that the unusual PDIp **a'** domain catalytic motif has a much less significant effect on the oxido-reductase activity of PDIp than originally postulated. We have not studied the oxido-reductase activity of PDI G398T or PDI ½ (PDI **abb'x**, PDIp **a'c**) but these mutants would provide greater insight into the molecular mechanisms determining the activity of PDI and PDIp. Measuring the activity of PDI G398T for example would allow us to directly observe the negative effect of this mutation within a PDI background. In PDIp there are so many unknown variables governing activity that it would be useful to see the effect of this mutation in PDI which has been better characterised. This work could be supplemented by molecular modelling studies which are able to predict the orientation of the threonine residue within the active site and the possible consequences for activity.

The benefit of studying the PDI ½ chimera is that it would be possible to observe the effect of the complete PDIp **a'** domain on the oxido-reductase activity of PDI. We have assumed that the major cause of the low activity observed for PDIp is due to the **a**' active site rather than the whole domain because PDIp **a'** shares ~65% sequence identity with PDI **a'**. However this may not be the case and other regions within PDIp **a'** may be exerting a negative effect.

7.3.5. Studies of PDIp **b'xa'c**

We have shown that both the reduced substrate binding capacity of PDIp and the unusual PDIp **a'** domain catalytic motif have a negative effect on the oxido-reductase activity of PDIp relative to PDI. Unexpectedly however the cumulative effect of both of these does not equal the sum of the loss of activity. Furthermore the PDIp ¾ T419G mutant only exhibits ~65% of the oxido-reductase activity of PDI despite sharing **b'x** with PDI and having a CGHC **a'** domain catalytic active site. Clearly there are still factors involved in the oxido-reductase activity of PDIp that have not yet been identified.

Unfortunately our studies of PDIp **b'xa'c** were thwarted by instability issues and consequently a reproducible value for its oxido-reductase activity was not recorded. Using the PDIp ½ chimera (PDIp **ab** PDI **b'xa'c**) it was possible to infer the effect that PDIp **b'xa'c** has on the activity of PDIp. We showed that this chimera has ~78% of the oxido-reductase activity of PDI. This is an improvement in activity of ~23% but indicates that PDIp ½ is still 22% less active than wild-type PDI. The implications of this work are that a) PDIp **b'xa'c** accounts for approximately half of the difference in oxido-reductase activity between wild-type PDI and PDIp and b) PDIp **ab** must also have impeded activity relative to the same region in PDI. Additional study of PDIp **ab** is therefore required to elucidate this.

The activity of PDIp ½ also shows the importance of repeating activity studies for PDIp ¾ T419G. Clearly the discrepancy between these proteins could be due to differences in the **a'** domain but it could also be linked to the high standard deviation seen for activity measurements of PDIp ¾ T419G. Repeating the experiment will clarify this, as it is possible that PDIp ¾ T419G has a higher percentage oxido-reductase activity than previously measured.

7.3.6. Studies of the activity of PDIp **a**

PDIp **a** shares ~55% sequence identity with PDI **a** and unlike PDIp **a'** has an intact CGHC active site motif. Furthermore residues adjacent to and surrounding the catalytic active site of PDIp **a** are almost fully conserved in PDI. For these reasons it was not anticipated that PDIp **a** would exhibit significantly different oxido-reductase

activity to PDI **a.** As a result of increasing evidence from chimera studies that implicated PDIp **a** as a contributor to the low oxido-reductase activity of PDIp we decided to study the catalytic activity of isolated PDIp **a** relative to PDI **a.**

Unfortunately it is impossible to measure the oxido-reductase activity of the individual catalytic domains of PDI and PDIp using the insulin assay described previously. This is because for ligands as large as insulin the **b'** substrate binding domain is also required. Consequently a fluorescence based assay was used. Our studies of the re-oxidation of reduced PDI **a** W128F and PDIp **a** W146F show that PDI **a** is ~4x more active than PDIp **a** (see figure 6.8). In addition, re-reduction of oxidised PDI **a** W128F and PDIp **a** W146F indicates that PDI **a** is ~10x more active than PDIp **a** (see figure 6.9). Clearly the PDIp **a** domain catalytic active site has impaired oxido-reductase activity relative to PDI **a**.

The low reduction activity of oxidised PDIp **a** implies that the N-terminal cysteine is incapable of accepting electrons. Typically we would expect GSH to nucleophilically attack the N-terminal cysteine of oxidised PDIp **a** breaking the disulphide bond and leading to formation of a mixed disulphide. Clearly this is not the case. This work therefore suggests that for the most part the N-terminal cysteine of PDIp **a** is in an un-reactive thiol state despite being treated with GSSG. Clearly this state is stable at the pH of this experiment ~pH 7.3 indicating that the pK_a of the N-terminal cysteine is much higher than anticipated.

7.3.7. Determination of pK_a values for PDIp C71 and C74

For PDI and many other PDI family members, catalytic activity relies on the unusually low pK_a of the N-terminal cysteine. For PDI **a** this is ~4.8 (Karala *et al.* 2010) and leads to stabilisation of the thiolate state at physiological pH. Consequently PDI **a** is a potent catalyst of oxidation. The C-terminal cysteine of PDI **a** has multiple roles in the catalytic cycle and therefore requires that its pK_a is modulated by surrounding residues according to the activity in hand. The measured pK_a of the C-terminal cysteine of PDI **a** is ~8.6 and is significantly increased in

R120Q and R120D mutants indicating a role for R120 in modulating the catalytic activity of PDI **a** (Karala *et al.* 2010).

Our studies show that the N-terminal cysteine of PDIp **a** has an unusually high pK_a (~8.09). This is typical for free cysteines in aqueous solution but is completely atypical for the N-terminal cysteine of PDI family members. Such a high pK_a explains the low reactivity of PDIp **a** in our previous studies of oxidation and reduction activities as it suggests that for the most part the N-terminal cysteine of PDIp **a** is in an unreactive thiol state.

We have postulated that Q75, which is immediately adjacent to the C-terminal cysteine of PDIp **a** and is not conserved in PDI family members, is modulating the pK_a of the N-terminal cysteine. By acting as a hydrogen bond donor to the side chain of Q75, the unreactive thiol group of the N-terminal cysteine is made slightly more reactive. The consequence of this is that PDIp **a** maintains some/low level activity and this correlates with our studies described previously. Obviously further study including mutagenesis of Q75 is very important to justify these assumptions. We have already made a series of mutants and hope to continue study of this residue using NMR and a stopped flow kinetics assay.

It is also possible that other amino acids close to the substrate thiol have a role in modulating the pK_a of PDIp **a**. This correlates well with our understanding that PDIp has very limited substrate specificity. Therefore PDIp may confer specificity in its catalytic domains (**a** domain at least) and also the **b'** domain as described previously. If this is the case we would speculate that the N-terminal cysteine of PDIp would be most active towards thiols with a nearby positive charge (i.e. an adjacent arginine, histidine or lysine residue) which may help to stabilise the thiolate state. Similar modulation by a positively charged residue is seen for PDI C53 and R120 (Karala *et al.* 2010).

7.3.8. DsbD: comparisons to PDIp

DsbD is a prokaryotic transmembrane protein with 3 domains. Its most C-terminal domain has a typical thioredoxin fold and a catalytic CXXC active site motif. The main function of DsbD is to transfer electrons from thioredoxin in the cytoplasm via

a disulphide cascade involving cysteine residues in each of its 3 domains. Interestingly the N-terminal cysteine of the catalytic motif of cDsbD (C-terminal domain of DsbD) has an unusually high pK_a ~10.5 (Mavridou *et al*. 2007). This means that like PDIp, cDsbD is relatively unreactive towards substrate thiols.

In cDsbD the high pK_a of C461 is maintained by two nearby adjacent negatively charged acids: D455 and E468. In addition when cDsbD forms a complex with the N-terminal domain (nDsbD) the nucleophilicity of its N-terminal cysteine is markedly improved (Mavridou *et al.* 2008). In this way the activity of cDsbD has evolved to be environment sensitive and therefore it protects itself from non-specific re-oxidation.

Currently we do not know how PDIp interacts with its binding partners. We have postulated that the high pK_a of the N-terminal cysteine is modulated by a nearby glutamine residue (Q75) and also that the binding interaction is specific to ensure improved nucleophilicity. Therefore PDIp may be very similar to cDsbD in its reaction mechanisms and clearly is not alone in being an oxido-reductase with a seemingly inactive active site.

7.3.9. Alternative methods to determine pK_a

Studying pK_a by monitoring the rate of alkylation as a function of pH (as used in this work) has been very successful for members of the Trx superfamily. For the most part this success is down to the fact that the cysteine of interest is chemically reactive and solvent exposed. Unfortunately however, when cysteine side chains are protected by the protein structure the rate of alkylation can be quite significantly affected. There are many alternate experimental approaches that could have been used for these calculations but due to lack of structural information unfortunately computational methods such as PROPKA were unsuitable.

One such alternative, more traditional method for pK_a determination makes use of UV absorption spectroscopy. The basis of this assay is that the thiolate exhibits greater absorption of UV light at 240nm than the thiol, so that it is possible to monitor the change in absorbance as pH is varied. Perhaps the biggest disadvantage

of this method is that the side chains of Phe, Tyr and Trp also absorb at 240nm. Consequently if their molecular environment changes during the titration process, this can affect their absorption properties. This interference can significantly reduce the accuracy of these pK_a measurements but can be counteracted by comparing spectra to an identical control protein only differing in lacking a thiol group.

The protocol described above was used for early measurements of the pK_a of PDI **a** catalytic cysteines (Kortemme *et al*. 1996). Similar to more recent work which shows that the N-terminal cysteine of PDI **a** has a pK_a of ~4.8 (Karala *et al.* 2010), this group showed that the pK_a of the N-terminal cysteine of PDI **a** was ~4.5. Clearly despite obvious technical issues this protocol remains an accurate and useful tool to study pK_a.

7.4. Implications of our studies of PDIp

7.4.1. Implications of the low catalytic activity of PDIp **a**

PDIp is a pancreas-specific homolog of PDI with unusual substrate specificity. Its physiological role is unknown but it is highly expressed alongside PDI in the acinar cells of the pancreas. We believe that it is highly unlikely that a protein folding catalyst with such limited activity as an oxido-reductase would be conserved when a significantly more active general folding catalyst such as PDI is co-expressed in the same location. Consequently PDIp must have been conserved in order to act on a unique substrate set.

Although this seems a reasonable explanation, work by Rutkevich *et al*. (2010) has shown that PDI family members are capable of compensating for one another to a much greater extent than originally expected. For example depletion of PDI in HepG2 cells had only a modest impact on the capability of the ER secretory pathway (Rutkevich *et al*. 2010). If the PDI family members are able to compensate for one another why has PDIp been conserved with exclusivity to the pancreatic acinar cells?

Particular emphasis has been put on the ability of PDIp to bind 17-β-oestradiol. This interaction is highly specific (17-α-oestradiol cannot bind, Klappa *et al*. 2001) and has a K_d of ~170nM (Fu and Zhu, 2009b). It is unlikely to be an essential physiological interaction however because a) physiological concentrations of oestradiol in a fertile female are <1.5nM (Akerlund *et al*. 1981) and b) PDIp has been shown to be expressed similarly in both male and female rats (Fu *et al*. 2009). Whether this interaction is important for modulation of substrate binding and/or catalytic activity is currently unknown. Furthermore it has been suggested that the role of PDIp may be to catalyse folding of pancreatic zymogens. Modulation of this activity by 17-β-oestradiol may be a contributor to digestive malfunctions such as hyperemesis (Baron *et al*. 1993).

7.4.2. The structural and catalytic significance of PDIp **ab**

We have shown that PDIp **ab** is able to act as a modulator of redox-mediated conformational change. This is in contrast to recent work which shows that PDI **b'xa'c** is the minimal requirement for redox-linked activity (Wang *et al*. 2011). This is clearly an oversimplification as our studies of PDIp ½ show that the presence of PDIp **ab** can prevent conformational change from occurring in the seemingly redox-active, PDI **b'xa'c**. Therefore for both PDI and PDIp, the **a** and **b** domains are more influential in redox-mediated conformational change than originally anticipated.

For PDIp **a**, we have shown that the pK_a of both active site cysteines is high and for the N-terminal cysteine, this was entirely unexpected. The implication of this is that at physiological pH, the PDIp **a** domain will have a predominantly reduced active site. Furthermore the PDIp **a** active site thiols will be hard to oxidise. Consequently, the limited redox-mediated conformational change exerted by diamide treated PDIp may be due to the fact that PDIp **a** remains in a mostly reduced state indicating that in contrast to published data, the **a** domain is important for redox-mediated conformational change.

Unfortunately until pK_a measurements were taken for PDIp **a** its inability to be oxidised went unnoticed. This was because we assumed that the pK_a of the PDIp **a**

domain cysteines would be similar to those of PDI **a**, and that using an excess of oxidant or reductant would sufficiently control redox state. This was not an irrational assumption because PDI **a** and PDIp **a** share significant sequence identity and have identical CGHC active site motifs. Furthermore given the unusual active site motif in PDIp **a'**, we anticipated that the low oxido-reductase activity measured for PDIp would be caused by the **a'** domain and not the catalytic activity of **a.**

The effect exerted by the redox state of PDI **a** on redox-mediated conformational change, has not been studied although clearly it has been assumed that there is no effect (Wang *et al.* 2011). In recent work, Wang *et al.* (2011) attempted to study the effect of PDI **a** and **a'** on the redox-mediated conformational changes of PDI. To do this they made two, double active site mutants which they described as PDI**a**SS**a'**CC and PDI**a**CC**a'**SS. Interestingly, they found that only the PDI**a**CC**a'**SS mutant showed increased susceptibility to proteolysis leading to the conclusion that oxidation of the **a'** domain only, was sufficient for redox-mediated conformational change. However as the redox state of the remaining cysteines was not controlled, we can assume that they were ~50% reduced and ~50% oxidised. Therefore this work does not indicate the implications on redox mediated conformational change that occurs if PDI **a** is trapped in a reduced state (as is seen in PDIp). We have shown previously that for PDIp ½, which almost certainly has a reduced PDIp **a** active site, redox-mediated conformational change does not occur despite having an oxidised PDI **a'** active site.

In this work and in published work by Wang *et al.* (2011, 2012) the redox state of both PDI active sites is manipulated by using an excess of oxidant or reductant. Clearly this is not physiological and *in vivo* there will be times when the two active sites of PDI are in different redox states i.e. PDI **a** will be reduced and PDI **a'** oxidised. The implication of this on redox-linked conformation is unknown (Wang *et al.* 2011, 2012) but our work suggests that if the active site of PDI **a** is in the reduced state, then major redox-mediated conformational changes may not occur.

In the recent X-ray crystal structure of oxidised PDI however, the active site of the **a'** domain is shown to be oxidised (as expected) but the **a** domain is shown as a mixture of oxidised (70%) and reduced (30%) forms (Wang *et al*. 2012). Despite

this, the structure of 'oxidised' PDI exhibits a significantly more open conformation than reduced PDI. We can speculate therefore, based on our understanding of the role of PDI **a** in redox-mediated conformational change, that in this structure the molecule is not fully open i.e. that complete oxidation will give rise to an even more open conformation. In addition it is also possible that unlike PDIp **a,** the redox state of PDI **a** has no effect on the redox conformations of PDI. Further study to identify/nullify the function of PDI **a** in the redox-mediated changes of PDI are required.

7.4.3. Does PDIp display asymmetrical oxidase activity similar to PDI?

Our data shows that PDIp has an unusually unreactive **a** domain active site. This was unexpected because unlike the **a'** domain, PDIp **a** contains an active site motif identical to that seen for PDI (CGHC). Although the **b'** and **a'** domains of PDIp clearly make some contribution to its low oxido-reductase activity (~50% relative to PDI), we now know that the major factor is the high pK_a of the **a** domain N-terminal cysteine. The benefits for PDIp in having an inactive thioredoxin domain at its N-terminus are currently unknown.

Interestingly, in Ero1-Lα mediated oxidative folding, the **a'** domain of PDI is much more active than the **a** domain (Wang *et al*. 2009). This means that the **a'** domain is preferentially oxidised by Ero1-Lα over the **a** domain. This is also true for yPDI and the Ero1-Lα yeast homolog, Ero1p (Kulp *et al.* 2006). In both cases, the ability to bind Ero1 has been shown to be position dependent rather than **a** or **a'** dependent and consequently PDI **bb'xa** has been found to be more active than PDI **a'bb'x**. Furthermore it has been suggested that binding of Ero1-Lα to hPDI at the **b'** domain, inhibits the oxido-reductase activity of PDI **a.** Authors therefore suggest that the PDI **a'** domain may be responsible for oxido-reductase activity and PDI **a** domain, isomerase activity. In this way PDI is able to synchronise isomerase activity with oxido-reductase activity potentially making it more efficient as a protein folding catalyst (Wang *et al.* 2009).

This work provides a possible explanation for the asymmetric oxido-reductase activity of PDIp. Alongside PDI, PDIp is the only other PDI family member that has been shown to bind Ero1β and has a rate of oxidation of ~50% of that seen for PDI (Wang *et al*. 2011). This in itself is unexpected because it implies that the activity of PDIp **a'** is still far lower than that of PDI **a'** and is not in agreement with our work described here. It would be useful to measure the oxido-reductase activity of PDIp C71S C74A and PDIp C417S C420A to explore this further. Additionally, pK_a data for the active site cysteines of PDIp **a'** would also help to elucidate this problem.

Therefore like PDI, the **a'** domain of PDIp may exhibit functional activity as an oxido-reductase while the **a** domain operates as an isomerase. Certainly we have shown that PDIp **a** is inefficient as an oxido-reductase. Although it is unlikely that the low activity of PDIp **a** is position dependent, this may explain why PDIp **a'**, which is at the C-terminus of PDIp next to x, has retained oxido-reductase activity. In this way PDIp **a** may direct oxido-reductase activity to the **a'** active site while simultaneously performing complex isomerisation reactions.

7.4.4. The role of glycosylation in the activities of PDIp *in vivo*

In contrast to all other PDI family members, *in vivo* PDIp has 3 glycosylation sites: one in each of the **a** and **b'** domains and one in **c** (Desilva *et al*. 1996, Walker *et al*. 2012). Our work describes the *in vitro* activity of recombinant PDIp (*E. coli)* and so fails to consider the potential effect of glycosylation on activity. Currently this has been very poorly studied, but it has recently been shown that all 3 sites are glycosylated. Furthermore, the glycan on the **b'** domain (N284) prevents dimerisation and so it would be expected that it would also interfere with substrate binding (Walker *et al.* 2012). This is probably not the case however, because we know from early cross-linking studies, that PDIp derived from sheep pancreas microsomes could effectively bind many of the different ligands tested (Klappa *et al*. 1998b).

As PDIp is unique (as a PDI family member) in being glycosylated, it is likely that glycosylation is important for either its structure or function within the cell.

Therefore it is essential that it is studied further. Obviously the difficulty with this at the moment is that no pancreatic, PDIp-expressing cell line has currently been identified and therefore as a consequence, we are limited to *in vitro* studies. Hopefully this is something that will be rectified in the future.

7.5. Further work

7.5.1. NMR studies of PDIp a

There are no published structures of PDIp. Based on the work presented here it is deemed important to obtain a structure for PDIp **a** so that residues that may interact with and enable the reactivity of the active site can be determined. Due to the equipment and expertise available to us, we will use solution state NMR. The advantage of this is that unlike in X-ray crystallography, the molecule is not fixed in its structure. Nevertheless, following full assignment of PDIp **a** a molecular model can be made and we can start to make predictions about possible interactions that may help to improve/reduce the activity of the active site. Furthermore, NMR can also be used to study the effect of single point mutations (e.g. Q75K) on the overall structure of PDIp **a (**by measuring changes in peak width).

Recent work has shown that redox potentials can be measured using NMR (Taylor *et al.* 2013). Therefore the redox potential of PDIp **a** could also be measured. Having already created a full length PDIp C71S C74A mutant with an intact **a'** domain, it would be useful to determine its redox potential because it is difficult to stabilise the PDIp **a'** domain in its isolated form. This information would supplement the pK_a studies (described previously).

7.5.2. Studies of the effect of Q75 on the reactivity of PDIp a

In order to study the effect of Q75 on the reactivity of PDIp **a** a number of mutants need to be made:

1. PDIp **a** Q75K (made)

2. PDIp **a** Q75A
3. PDIp **a** Q75K W146F (made)
4. PDIp **a** Q75A W146F
5. PDIp **a** C71S Q75K (made)
6. PDIp **a** C71S Q75A
7. PDIp **a** C74A Q75K (made)
8. PDIp **a** C74A Q75A
9. PDIp Q75K
10. PDIp Q75A
11. PDI **a** K57Q
12. PDI **a** K57A
13. PDI **a** K57Q W128F
14. PDI **a** K57A W128F
15. PDI K57Q
16. PDI K57A

By studying the reactivity of these mutants via stopped flow experiments and the insulin assay (full length proteins only) it should be possible to determine the role of Q75 and K57 in modulating the reactivity of the N-terminal cysteine of PDI **a** and PDIp **a** respectively. It is expected that the Q75K PDIp mutation will have a positive effect on the activity of PDIp **a** and also the molecule as a whole. Similarly the K57Q mutation should be detrimental to the activity of PDI **a** and the overall activity of PDI.

7.5.3. Studies of the catalytic cysteines of PDIp **a'**

Up to now the catalytic activity of PDIp **a'** has not been studied. For the most part this is because PDIp **b'xa'c** and PDIp **a'** are unstable and therefore very difficult to work with. It would be useful to determine the activity of PDIp **a'** and this could be done using the insulin assay and the PDIp C71S C74A mutant that has already been made.

In order to measure the pK_a for both PDIp **a'** domain catalytic cysteines, quadruple mutants need to be made : PDIp C71S C74A C364A C418S and PDIp C71S C74A C364A C421A. Although we expect that the N-terminal cysteine of PDIp **a'** will be characteristic of normal PDI family members in having a very low pK_a this needs to be confirmed. Mutating the active site threonine to glycine in these mutants will also indicate the effect of this residue (if any) on the pK_a of the catalytic cysteines.

7.6. Concluding Remarks

This work represents the first study to characterise the *in vitro* oxido-reductase activity of PDIp. Despite having an unusual **a'** active site sequence (CTHC), we found that the abnormally high pK_a of the **a** domain N-terminal cysteine was the major contributor to the low oxido-reductase activity of PDIp.

In regards to structure, we found that unlike PDI, PDIp undergoes only minor redox-mediated change. Using chimera proteins we concluded that this may be due to modulation by the **a** and **b** domains, probably as a result of the low reactivity of the **a** domain catalytic site. Furthermore we also saw that the minimum redox-active cassette of PDI, **b'xa'c**, could also be modulated by PDIp **ab** and so led to the loss of redox-mediated conformational change. Therefore this work is in contrast to recent work by Wang *et al*. (2011) which suggests that the **a** and **b** domains are unimportant for redox-mediated structure.

References

Afelik, S., Chen, Y. and Pieler, T. (2004) Pancreatic protein disulphide isomerase (XPDIp) is an early marker for the exocrine lineage of the developing pancreas in *Xenopus Laevis* embryos. *Gene Expression Patterns* **4 (1)** 71 - 76

Akerlund, M., Batra, S. and Helm, G. (1980) Comparison of plasma and myometrial tissue concentrationsof estradiol-17β and progesterone in non-pregnant women. *Contraception* **23 (4)** 447 – 455

Alanen, H.I., Raykhel, I.B., Luukas, M.J., Salo, K.E.H., Ruddock, L.W. (2011) Beyond KDEL: The role of positions 5 and 6 in determining ER localisation. *Journal of Molecular Biology* **409** 291 – 297

Alanen, H.I., Salo, K.E.H., Pekkala, M., Siekkinen, H.M., Pirneskoski, A. and Ruddocl. L.W. (2004) Defining the domain boundaries of the human protein disulphide isomerases. *Antioxidants and Redox Signaling* **5 (4)** 367 - 374

Alanen, H.I., Salo, K.E.H., Pirneskoski, A. and Ruddock, L. (2006) pH dependence of the peptide thiol-disulphide oxidase activity of six members of the human protein disulphide isomerase family. *Antioxidants and Redox Signalling* **8 (3)** 283 -291

Anfinsen, C.B. (1973) Principles that govern folding of protein chains. *Science* **181 (4096)** 223 – 230

Anfinsen, C.B., Haber, E., Sela, M., White, F.H. (1961) The kinetics of formation of native ribonuclease during oxidation of the reduced polypeptide chain. *Proceedings of the National Academy of Sciences* **47 (9)** 1309 – 1314

Anrtfield, M. and Van der Kooy, D. (2011) β-cell evolution: How the pancreas borrowed from the brain. *Bioessays* **33** 582 - 587

Appenzeller-Herzog, C. and Ellgaard, L. (2008) The human PDI family: versatility packed into a single fold. *Biochemica et Biophysica Acta* **1783** 535 – 548

Appenzellor-Herzog, C. (2011) Glutathione and non-glutathione-based oxidant control in the endoplasmic reticulum. *Journal of Cell Science* **124** 847 – 855

Appenzellor-Herzog, C., Riemer, J., Zito, E., Chin, K., Ron, D., Spiess, M. and Ellgaard, L. (2010) Disulphide production by Ero1α-PDI relay is rapid and effectively regulated. *The EMBO Journal* **29 (19)** 3318 -3329

Araki, K. and Inabi, K. (2012) Structure, mechanism, and Evolution of Ero1 family enzymes. *Antioxidants & Redox Signalling* **16 (8)** 790 - 799

Araki, K. and Nagata, K. (2011) Functional *In vitro* analysis of Ero1 and protein disulphide isomerase (PDI) pathway. *Journal of Biological Chemistry* **286** 32705 – 32712

Arduino, D.M., Esteves, A.R., Cardoso, S.M. and Oliveira, C.R. (2009) Endoplasmic and mitochondrial interplay mediates apoptotic cell death: relevance to Parkinson's disease. *Neurochemistry International* **55** 341 – 348

Aslund, F., Berndt, K. and Holmgren, A. (1997) Redox potentials of glutaredoxins and other thiol-disulfide oxidoreductases of the thioredoxin superfamily determined by direct protein-protein redox equilibria. *The Journal of Biological Chemistry* **272 (49)** 30780 - 30786

Bandopadhya, R. and Belleroche, J. (2009) Pathogenesis of Parkinson's disease: emerging role of molecular chaperones. *Trends in Molecular Medicine* **16 (1)** 27 – 36

Banghegyi, G, Margittai, E., Szarka, A., Mandl, J. and Csala, M. (2012) Cross talk and barriers between the electron carriers of the endoplasmic reticulum. *Antioxidants & Redox Signalling* **16 (8)** 772 -780

Bardwell, J.C.A. and Beckwith, J. (1993) The bonds that tie: catalysed disulphide bond formation. *Cell.* **74.** 769 -771

Bardwell, J.C.A., McGovern, K. and Beckwith, J. (1991) Identification of a protein required for disulfide bond formation In Vivo. *Cell Press.* **67** 581 – 589

Benham, A. M. (2012) The protein disulfide isomerase family: key players in health and disease. *Antioxidants & Redox Signalling* **16 (8)** 781 - 789

Bouvier, M. (2003) Accessory proteins and the assembly of human class I MHC molecules: a molecular and structural perspective. *Molecular Immunology* **39** 697 – 706

Braakman, I. and Bulleid, N. (2011) Protein folding and modification in the mammalian endoplasmic reticulum. *Annual Review of Biochemistry* **80** 71 – 99

Burns, J.A., Butler, J.C., Moran, J. and Whitesides, G.M. (1991) Selective reduction of disulfides by Tris(2-carboxyethyl)phosphine. *Journal of Organic Chemistry* **56** 2648 – 2650

Byrne, L.J., Sidhu, A., Wallis, K., Ruddock, L., Freedman, R.B., Howard, M.J. and Williamson, R.A. (2009) Mapping of the ligand-binding site on the b' domain of human PDI: interaction with peptide ligands and the x-linker region. *Biochemical Journal* **423** 209 - 217

Cai, H., Wang, C. and Tsuo, C. (1994) Chaperone-like activity of protein disulfide isomerase in the refolding of a protein with no disulfide bonds. *The Journal of Biological Chemistry* **269 (40)** 24550 – 24552

Cao, Z., Tavender, T.J., Roszak, A. W., Cogdell, R.J. and Bulleid, N.J. (2011) Crystal structure of reduced and of oxidised peroxiredoxin IV reveals a stable oxidised decamer and a non-disulphide bonded intermediate in the catalytic cycle. *Journal of Biological Chemistry* **286 (49)** 42257 - 42266

Caves, M.S., Derham, B.K., Jezek, J. and Freedman, R.B. (2011) The mechanism of Inactivation of glucose oxidase from *Penicillium amagasakiense* under ambient storage conditions. *Enzyme and Microbial Technology* **49 (1)** 79 - 87

Chakravarthi, S. and Bulleid, N.J. (2004) Glutathione is required to regulate the formation of native disulfide bonds within proteins entering the secretory pathway. *The Journal of Biological Chemistry* **279** 39872 – 39879

Chakravarthi, S., Jessop, C.E. and Bulleid, N.J. (2006) The role of glutathione in disulfide bond formation and endoplasmic-reticulum-generated oxidative stress. *EMBO Reports* **7 (3)** 271 – 275

Chambers, J.E., Tavender, T.J., Oka, O.B.V., Warwood, S., Knight, D. and Bulleid, N.J. (2010) The reduction potential of the active site disulphides of human protein disulphide isomerase limits oxidation of the enzyme by Ero1α. *The Journal of Biological Chemistry* **285 (38)** 29200 – 29207

Chang, L., Wen, E. and Chang, C. (1996) The essentiality of His-47 and the N-terminal region for the binding of 8-anilinonaphthalene-1-sulfonate with Taiwan cobra phospholipase A_2. *Journal of Protein Chemistry* **15 (3)** 255 - 260

Chen, H., Wang, L. and Chen, C. (2009) Domain a' of protein disulphide isomerase plays key role in inhibiting α-synuclein fibril formation. *Cell Stress and Chaperones* **15 (4)** 415 - 421

Chen, X., Walker, A.K., Strahler, J.R., Simon, E.S., Tomanicek-Volk, S.L., Nelson, B.B., Hurley, M.C., Ernst, S.A., Williams, J.A. and Andrews, P.C. (2006) Organellar proteomics. Analysis of pancreatic zymogen granule membranes. *Molecular and Cellular Proteomics* **5 (2)** 306 – 312

Colla, E., Coune, P., Liu, Y., Pletnikova, O., Troncoso, J.C., Iwatsumbo, T., Schneider, B.L. and Lee, M.K. (2012) Endoplasmic reticulum stress is important for the manifestations of α-synucleinopathy *In vivo. The Journal of Neuroscience* **32 (10)** 3306 – 3320

Conn, K.J., Gao, W., McKee, A., Lan, M.S., Ullman, M.D., Eisenhauer, P.B., Fine, R.E. and Wells, J.M. (2004) Identification of the protein disulphide isomerase family PDIp in experimental Parkinson's disease and Lewy body pathology. *Brain Research.* **1022** 164 – 172

Creighton, T.E., Zapun, A. and Darby, N.J. (1995) Mechanisms and catalysts of disulphide bond formation in proteins. *TIBTECH* **13** 18 – 23

Crowley, P. B. and Golovin, A. (2005) Cation-π interations in protein-protein interfaces. *PROTEINS: Structure, Function & Bioinformatics* **59** 231 – 239

Csala, M., Kereszturi, E., Mandl, J. and Banhegyi, G. (2012) The endoplasmic reticulum as the extracellular space inside the cell: role in protein folding and glycosylation. *Antioxidants & Redox Signalling* **16 (10)** 1100 - 1108

Daar, A.S., Fuggle, S.V., Fabre, J.W., Ting, A. and Morris, P.J. (1984) The detailed distribution of HLA-A, B, C antigens in normal human organs. *Transplantation* **38 (3)** 287 – 292

Daniels, R., Kurowski, B., Johnson, A.E. and Hebert, D.N. (2003) N-linked glycans direct the cotranslational folding pathway of *Influenza* Hemagglutinin. *Molecular Cell* **11** 79 – 90

Daniels, R.J., Peden, J.F., Lloyd, C., Horsley, S.W., Clark, K., Tufarelli, C., Kearney, L., Buckle, V.J., Doggett, N.A., Flint, J. and Higgs, D.R. (2001) Sequence, structure and pathology of the fully annotated terminal 2 Mb of the short arm of human chromosome 16. *Human Molecular Genetics* **10 (4)** 339 – 352

Darby, N.J. and Creighton, T.E. (1995) Functional properties of the individual thioredoxin-like domains of protein disulfide isomerase. *Biochemistry* **34** 11725 - 11735

Darby, N.J., Freedman, R.B. and Creighton, T.E. (1994) Dissecting the mechanism of protein disulphide isomerase: catalysis of disulphide bond formation in a model peptide. *Biochemistry* **33** 7937 – 7947

Darby, N.J., Kemmink, J. and Creighton, T.E. (1996) Indentifying and characterising a structural domain of protein disulphide isomerase. *Biochemistry* **35** 10517 – 10528

Darby, N.J., Penka, E. and Vincentelli, R. (1998) The multi-domain structure of protein disulfide isomerase is essential for high catalytic efficiency. *Journal of Molecular Biology* **276** 239 – 247

Darby, N.J., Straaten, M., Penka, E., Vincentelli, R. and Kemmink, J. (1999) Indentifying and charactersing a second structural domain of protein disulphide isomerase. *FEBS Letters* **448** 167 – 172

Debas, H.T. (1997) Molecular insights into pancreas development. *The American Journal of Surgery* **174** 227 – 231

Denisov, A., Määtänen, P., Dabrowski, C., Kozlov, G., Thomas, D.Y. and Gehring, K. (2008) Solution structure of the bb' domains of human protein disulphide isomerase. *The FEBS Journal* **276** 1440 – 1449

Denisov, A.Y., Maattanen, P., Sprules, T., Thomas, D.Y. and Gehring, K. (2007) ^{1}H, ^{13}C and ^{15}N resonance assignments of the bb' domains of human protein disulphide isomerase. *Biomolecular NMR assignments.* **1** 129 – 130

Dias-Gunasekara, S., Gubbens, J., Van Lith, M., Dunne, C., Williams, J.A.G., Kataky, R., Scoones, D., Lapthorn, A., Bulleid, N.J. and Benham, A.M. (2005) Tissue-specific expression and dimerization of the endoplasmic reticulum oxidoreductase Ero1β. *The Journal of Biological Chemistry* **280 (38)** 33066 – 33075

Dickerhof, N., Kleffmann, T., Jack, R. and McCormick, S. (2011) Bacitracin inhibits the reductive activity of protein disulfide isomerase by disulfide bond formation with free cysteines in the substrate-binding domain. *The FEBS Journal* **278 (12)** 2034 - 2043

Dobson, C.M. (2003) Protein folding and misfolding. *Nature* **426** 884 - 890

Dong, G., Wearsch, P.A., Peaper, D.R., Cresswell, P. and Reinisch, K, M. (2009) Insights into MHC class I peptide loading from the structure of the Tapasin-ERp57 thiol oxidoreductase heterodimer. *Immunity* **30** 21 – 32

Duckworth, W.C., Bennett, R.G. and Hamel, F.G. (1998) Insulin degradation: progress and potential. *Endocrine Reviews* **19 (5)** 608 – 624

Ellgaard, L. and Frickel, E. (2003) Calnexin, Calreticulin, and ERp57. *Cell Biochemistry and Biophysics* **39** 223 – 247

Elliott, J.G., Oliver, J.D., Volkmer, J., Zimmermann, R. and High, S. (1998) In *vitro* characterisation of the interaction between newly synthesised proteins and a pancreatic isoform of protein disulphide isomerase. *European Journal of Biochemistry* **252** 372 -377

Ferrari, D.M. and Söling (1999) The protein disulphide-isomerase family: unravelling a string of folds. *Biochemical Journal* **339** 1 – 10

Flohé, L. (2012) The fairytale of the GSSG/GSH potential. *Biochemica et Biophysica Acta* **1830 (5)** 3139 - 3142

Flohé, R. and Maiorino, M. (2013) Glutathione peroxidases. *Biochemica et Biophysica Acta* **1830 (5)** 3289 - 3303

Forman-Kay, J.D., Clore, G.M. and Gronenborn, A.M. (1992) Relationship between electrostatics and redox function in human thioredoxin: Charaterization of pH titration shifts using two-dimensional homo- and heteronuclear NMR. *Biochemistry* **31** 3442 – 3452

Freedman, R.B. (2009) A non-catalytic disulphide bond regulating redox flux in the ER oxidative folding pathway. *The EMBO journal* **28** 169 -170

Freedman, R.B., Gane, P.J., Hawkins, M.C., Hlodan, R., McLaughlin, H. and Parry, J.W.L. (1998) Experimental and theoretical analyses of the domain architecture of mammalian protein disulphide isomerase. *Biological Chemistry* **379** 321 – 328

Freedman, R.B., Klappa, P. and Ruddock, L.W. (2001) Protein disulphide isomerases exploit synergy between catalytic and specific binding domains. *EMBO Reports.* **31 (21)** 136 – 140

Fu, X. and Zhu, B.T. (2009a) Human pancreas-specific protein disulphide isomerase homolog (PDIp) is redox-regulated through formation of an inter-subunit disulphide isomerase. *Archives of Biochemistry and Biophysics* **485** 1 – 9

Fu, X. and Zhu, B.T. (2009b) Human pancreas-specific protein disulphide isomerase homology (PDIp) is an intracellular estrogen-binding protein that modulates estrogen

levels and actions in target cells. *Journal of Steroid Biochemistry and Molecular Biology* **115** 20 – 29

Fu, X. and Zhu, B.T. (2010) Human pancreas-specific protein disulfide-isomerase (PDIp) can function as a chaperone independently of its enzymatic activity by forming stable complexes with denatured substrate proteins. *Biochemical Journal* **429** 157 - 169

Fu, X. and Zhu, B.T. (2011) Both PDI and PDIp can attack the native disulphide bonds in thermally-unfolded RNase and form stable disulphide-linked complexes. *Biochemica et Biophysica Acta: Proteins and Proteomics* **1814** 487 - 495

Fu, X., Dai, X, Ding, J. and Zhum B.T. (2009) Pancreas-specific protein disulphide isomerase has a cell type-specific expression in various mouse tissues and is absent in human pancreatic adenocarcinoma cells: implications for its functions. *Journal of Molecular Histology* **40 (3)** 189 – 199

Fu, X., Wang, P. and Zhu, B.T. (2011) Characterisation of the estradiol-binding site structure of human pancreas-specific protein disulphide isomerase: indispensable role of the hydrogen bond between His278 and the estradiol 30-hydroxyl group. *Biochemistry* **50** 106 -115

Fu, X., Wang, P., Fukui, M., Long, C., Yin, L., Choi, H.J. AND Shu, B.T. (2012) PDIp is a major intracellular estrogen-storage protein that modulates the tissue levels of estrogen in the pancreas. *Biochemical Journal* **447** 115 – 123

Gailit, J. (1993) Restoring free sulphydryl groups in synthetic peptides. *Analytical Biochemistry* **214** 334 – 335

Galligan, J.J. and Peterson, D.R. (2012) The human protein disulfide isomerase gene family. *Human Genomics* **6 (6)** doi:10.1186/1479-7364-6-6

Gane, P.J., Freedman, R.B. and Warwicker, J. (1995) A molecular model for the redox potential difference between Thioredoxin and DsbA, based on electrostatics calculations. **249** 376 – 387

Gasser, B., Saloheimo, M., Rinas, U., Dragosits, M., Rodriguez-Carmona, E., Baumann, K., Giuliani, M., Parrilli, E., Branduardi, P., Lang, C., Porro, D., Ferrer, P., Tutino, M.L., Mattanovich, D. and Villaverde, A. (2008) Protein folding and conformational stress in microbial cells producing recombinant proteins: a host comparative overview. *Microbial Cell Factories* **7 (11)** 1 – 18

Geoghegan, K.F., Dixon, H.B.F., Rosner, P.J., Hoth, L.R., Lanzetti, A.J., Borzilleri, K.A., Marr, E.S., Pezzullo, L.H., Martin, L.B., LeMotte, P.K., McColl, A.S., Kamith, A.V. and Stroh, J.G. (1999) Spotaneous α-N-6-Phosphogluconoylation of a 'His-Tag' in *Escherichia coli*: The cause of extra mass of 258 or 178 Da in fusion proteins. *Analytical Biochemistry* **267** 169 – 184

Gething, M. (1999) Role and regulation of the ER chaperone BiP. *Cell & Developmental Biology* **10** 465 – 472

Gething, M. and Sambrook, J. (1992) Protein folding in the cell. *Nature* **355** 33 – 45

Golovanov, A.P., Hautbergue, G.M., Wilson, S.A. and Lian, L. (2004) A simple method for improving protein solubility and long-term stability. *JACS* **126** 8933 - 8939

Gonzalez, V., Pal, R. and Narayan, M. (2010) The oxidoreductase behaviour of protein disulphide isomerase impedes fold maturation of endoplasmic reticulum-processed proteins in the pivotal structure-coupled step of oxidative folding: implications for subcellular protein trafficking. *Biochemistry* **49 (29)** 6282 – 6289

Gorelick, F.S., Modlin, I.M., Leach, S.D., Carangelo, R. and Katz, M. (1992) Intracellular proteolysis of pancreatic zymogens. *The Yale Journal of Biology and Medicine* **65** 407 – 420

Grauschopf, U., Winther, J.R., Korber, P., Zander, T., Dallinger, P. and Bardwell, J.C.A. (1995) Why is DsbA such an oxidising disulfide catalyst. *Cell* **83** 947 – 955

Greenfield, N.J. (2006) Using circular dichroism collected as a function of temperature to determine the thermodynamics of protein unfolding and binding interactions. *Nature Protocols* **1 (6)** 2527 - 2535

Gruber, C.W., Čemažar, M., Heras, B., Martin, J.L. and Craik, D.J. (2006) Protein disulphide isomerase: the structure of oxidative folding. *TRENDS in Biochemical Sciences* **31 (8)** 455 – 464

Guttman, R.P. and Powell, T.J. (2012) Redox regulation of cysteine-dependent enzymes in neurodegeneration. *International Journal of Cell Biology* **2012** doi:10.1155/2012/703164

Hagiwara, M and Nagata, K. (2012) Redox-dependent protein quality control in the endoplasmic reticulum: folding to degradation. *Antioxidants & Redox Signalling* **16 (10)** 1119 – 1128

Hashimoto, S., Shiomoto, K., Okada, K. and Imaoka, S. (2011) The binding site of bisphenol A to protein disulphide isomerase. *Journal of Biochemistry* **151 (1)** 35 - 45

Hatahet, F. and Ruddock, L.W. (2007) Substrate recognition by the protein disulphide isomerases. *The FEBS Journal* **274** 5223 – 5234

Hatahet, F. and Ruddock, L.W. (2009) Protein disulphide isomerase: a critical evaluation of its function in disulphide bond formation. *Antioxidants and redox signalling* **11** 2807 - 2850

Hawkins, H.C., Nardo, M.D. and Freedman, R.B. (1991) Redox properties and cross-linking of the dithiol/disulphide active sites of mammalian protein disulphide-isomerase. *Biochemical Journal* **275** 341 - 348

Hayes, N.V.L., Smales, C.M. and Klappa, P. (2009) Protein disulphide isomerase does not control recombinant IgG4 productivity in mammalian cell lines. *Cellular and metabolic engineering* **105 (4)** 770 - 779

Haze, K., Yoshida, H., Yanagi, H., Yura, T. and Mori, K. (1999) Mammalian transcription factor ATF6 is synthesised as a transmembrane protein and activated by proteolysis in response to endoplasmic reticulum stress. *Molecular Biology of the Cell* **10** 3787 – 3799

Hendershot, L., Wei, J., Gaut, J., Melnick, J., Aviel, S. and Argon, Y. (1996) Inhibition of immunoglobulin folding and secretion by dominant negative BiP ATPase mutants. *Proceedings of the National Academy of Sciences* **93** 5269 – 5274

Heras, B., Kurz, M., Shouldice, S.R. and Martin, J.L. (2007) The name's bond.....disulphide bond. *Current Opinion in Structural Biology* **17** 691 – 698

Higa, A. and Chevet, E. (2012) Redox signalling loops in the unfolded stress response. *Cellular Signalling* **24 (2012)** 1548 - 1555

Hirsch, C., Gauss, R., Horn, S.C., Neuber, O. and Sommer, T. (2009) The ubiquitylation machinery of the endoplasmic reticulum. *Nature* **458** 453 – 460

Honjo, Y., Ito, H., Horibe, T., Takahashi, R. and Kawakami, K. (2010) Protein disulphide isomerase- immunopositive inclusions in patients with Alzheimer's disease. *Brain Research* **19 (1349)** 90 – 96

Horibe, T., Kikuchi, M. and Kawakami, K. (2008) Interaction of human protein disulphide isomerase and human P5 with drug compounds: analysis using biosensor technology. *Process Biochemistry* **43** 1330 - 1337

Huber-Wunderlich, M. and Glockshuber, R. (1998) A single dipeptide sequence modulates the redox properties of a whole enzyme family. *Current Biology* **3 (3)** 161 – 171

Ibbetson, A.L. and Freedman, R.B. (1976) Thiol-protein disulphide oxidoreductases-Assay of microsomal membrane-bound glutathione-insulin transhydrogenase and comparison with protein disulphide-isomerase. *Biochemical Journal* **159** 377 – 384

Jalleh, R.P., Gilbertson, J.A., Williamson, R.C.N., Slater, S.D. and Foster, C.S. (1993) Expression of major histocompatibility antigens in human chronic pancreatitis. *Gut* **34** 1452 – 1457

Jansen, G., Maatanen, P., Denisov, A.Y., Scarffe, L., Schade, B., Balghi, H., Dejgaard, K., Chen, L.Y., Muller, W.J., Gehring, K. and Thomas, D.Y. (2012) An interaction map of ER chaperones and foldases. *Molecular Cell Proteomics* **11 (9)** 710 - 723

Jessop, C.E. and Bulleid, N.J. (2004) Glutathione directly reduces an oxidoreductase in the endoplasmic reticulum of mammalian cells. *The Journal of Biological Chemistry* **279 (53)** 55341 – 55347

Jessop, C.E., Chakravarthi, S., Watkins, R.H. and Bulleid, N.J. (2004) Oxidative protein folding in the mammalian endoplasmic reticulum. *Biochemical Society Transactions* **32 (5)** 655 – 658

Jiang, N., Ryan, R.J. and Albert, A. (1973) Radioimmunoassay of serum estrogen. *Clinical Chemistry* **19 (7)** 740 – 747

Karala, A, Lappi, A., Saaranen, M.J. and Ruddock, L.W. (2009) Efficient peroxide-mediated oxidative refolding of a protein at physiological pH and implications for oxidative folding in the endoplasmic reticulum. *Antioxidants & Redox Signalling* **11 (5)** 963 – 970

Karala, A., Lappi. A. and Ruddock, L.W. (2010) Modulation of an active-site cysteine pK_a allows PDI to act as a catalyst of both disulfide bond formation and isomerisation. *Journal of Molecular Biology* **396** 883 – 892

Kardos, J., Bodi, A., Zavodszky, P., Venekei, I and Graf, L. (1990) Disulfide-linked propetides stabilise the the structure of zymogens and mature pancreatic serine proteases. *Biochemistry* **38** 12248 - 12257

Katti, S.K., LeMaster, D.M. and Eklund, H. (1990) Cystal structure of thioredoxin from *Escherichia coli* at 1.68 Å resolution. *Journal of Molecular Biology* **212** 167 – 184

Katzen, H.M. and Tietze, F. (1966) Studies on the specificity of mechanism of action of hepatic glutathione-insulin transhydrogenase. *The Journal of Biological Chemistry* **241 (15)** 3561 – 3570

Kelly, S.M., Jess, T.J. and Price, N.C. (2005) How to study proteins by circular dichroism. *Biochimica et Biophysica Acta* **1751** 119 – 139

Kemmink, J., Darby, N.J., Dijkstra, K, Scheek, R.M. and Creighton, T.E. (1995) Nuclear magnetic resonance characterization of the N-terminal thioredoxin-like domain of protein disulfide isomerase. *Protein Science* **4** 2587 – 2593

Kemmink, J., Darby, N.J., Dijkstra, K., Nilges, M. and Creighton, T.E. (1997) The folding catalyst protein disulphide isomerase is constructed of active and inactive Thioredoxin modules. *Current Biology* **7** 239 : 245

Kemmink, J., Darby, N.J., Dijkstra, K., Nilges, M. and Creighton, T.E. (1996) Structure determination of the N-terminal thioredoxin-like domain of protein disulfide isomerase using multidimensional hetronuclear C^{13}/N^{15} NMR Spectroscopy. *Biochemistry* **35** 7684 – 7691

Kemmink, J., Dijkstra, K., Mariani, M., Scheek, R.M., Penka, E., Nilges, M. and Darby, N.J. (1999) The structure in solution of the b domain of protein disulfide isomerase. *Journal of Biomolecular NMR* **13** 357 – 368

Kikuchi, M., Doi, E., Tsujimoto, I., Horibe, T. and Tsujimoto, Y. (2002) Functional analysis of human P5, a protein disulfide isomerase homologue. *Journal of Biochemistry* **132** 451 – 455

Klappa, P., Freedman, R.B., Langenbuch, M., Lan, M.S., Robinson, G.K., Ruddock, L.W. (2001) The pancreas-specific protein disulphide-isomerase PDIp interacts with a hydroxyaryl group in ligands. *Biochemical Journal* **354 (3)** 553 -559

Klappa, P., Koivunen, P., Pirneskoski, A., Karvonen, P., Ruddock, L.W., Kivirikko, K.I. and Freedman, R.B. (2000) Mutations that destabilise the a' domain of human protein disulfide-isomerase directly affect peptide binding. *The Journal of Biological Chemistry* **275 (18)** 13213 – 13218

Klappa, P., Ruddock, L.W., Darby, N.J. and Freedman, R.B. (1998a) The b' domain provides the principal peptide-binding site of protein disulfide isomerase but all domains contribute to binding of misfolded proteins. *The EMBO Journal* **17 (4)** 927 – 935

Klappa, P., Stromer, T., Zimmermann, R., Ruddock. L. W. and Freedman, R.B. (1998b) A pancreas-specific glycosylated protein disulphide-isomerase binds to misfolded proteins and peptides with an interaction inhibited by oestrogens. *European Journal of Biochemistry* **254** 63 – 69

Klessen, C. (1972) Histochemical staining of zymogen granules of pancreatic acinar cells using permanganate-HID-Technique. *Histochemie* **30** 365 – 366

Kolb, V.A. Cotranslational protein folding. *Molecular Biology* **35 4** 584 – 590

Kortemme, T. Darby, N.J. and Creighton, T.E. (1996) Electrostatic interactions in the active site of the N-terminal thioredoxin-like domain of protein disulfide isomerase. *Biochemistry* **35** 14503 - 14511

Koslov, G., Määtänen, P., Schrag, J.D., Hura, G.L., Gabrielli, L., Cygler, M., Thomas, D.Y. and Gehring, K. (2009) Structure of the noncatalytic domains and global fold of the protein disulfide isomerase ERp72. *Structure* **17** 651 – 659

Koslov, G., Maatanen, P., Thomas, D.Y. and Gehring, K. (2010) A structural overview of the PDI family of proteins. *The FEBS Journal* **277 (19)** 3924 - 3936

Kosuri, P., Alegre-Cebollada, J., Feng, J., Kaplan, A., Ingles-Prieto, A., Badilla, C. L., Stockwell, B.R., Sanchez-Ruiz, J.M., Holmgren, A. and Fernandez, J.M. (2012) Protein folding drives disulfide formation. *Cell* **151** 794 – 806

Krause, G., Lundström, J., Barea, J.L., Pueyo de la Cuesta, C. and Holmgren, A. (1991) Mimicking the active site of protein disulfide-isomerase by substitution of proline 34 in *Escherichia coli* Thioredoxin. *The Journal of Biological Chemistry* **266 (15)** 9494 – 9500

Kulp, M.S., Frickel, E., Ellgaard, L. and Weissman, J.S. (2006) Domain architecture of protein-disulfide isomerase facilitates its dual role as an oxidase and as an isomerase in Ero1p-mediated disulfide mediation. *The Journal of Biological Chemistry* **281 (2)** 876 - 884

Lambert, N. and Freedman, R.B. (1983a) Structural properties of homogeneous protein disulphide-isomerase from bovine liver purified by a rapid high-yielding procedure. *Biochemical Journal* **213** 225 -234

Lambert, N. and Freedman, R.B. (1983b) Kinetics and specificity of homogeneous protein disulphide-isomerase in protein disulphide isomerisation and in thiol-protein-disulphide oxidoreduction. *Biochemical Journal* **213** 235 -243

Lappi, A. and Ruddock, L.W. (2011) Reexamination of the role of interplay between glutathione and protein disulphide isomerase. *Journal of Molecular Biology* **409** 238 - 249

Lappi, A.K., Lensink, M.F., Alanen, H.I., Salo, K.E.H., Lobell, M., Juffer, A.H. and Ruddock, L.W. (2004) A conserved arginine plays a role in the catalytic cycle of the protein disulphide isomerases. *Journal of Molecular Biology* **335** 283 – 295

Lee, A., Chu, G.C., Iwakoshi, N.N. and Glimcher, L.H. (2005) XBP-1 is required for biogenesis of cellular secretory machinery of exocrine glands. *The EMBO Journal* **24** 4368 – 4380

Lee, A., Iwakoshi, N.N. and Glimcher, L.H. (2003) XBP-1 regulates a subset of endoplasmic reticulum resident chaperone genes in the unfolded protein response. *Molecular and Cellular Biology* **23 (21)** 7448 - 7459

Li, S., Hong, X., Shi, Y., Li, H. and Wang, C. (2005) Annular arrangement and collaborative actions of four domains of protein-disulphide isomerase. *The Journal of Biological Chemistry* **281** 6581 – 6588

Lin, J.H., Walter, P. and Yen, T.S.B. (2008) Endoplasmic reticulum stress in disease pathogenesis. *The Annual Review of Pathology* **3** 399 - 425

Lin, T. (2010) Protein-protein interaction as a powering source of oxidoreductase activity. *Molecular Biosystems* **6** 1454 – 1462

Lith, M., Hartigan, N., Hatch, J. and Benham, A.M. (2005) PDILT, a divergent testis-specific protein disulfide isomerase with a non-classical SXXC motif that

engages in disulfide-dependent interactions in the endoplasmic reticulum. *The Journal of Biological Chemistry* **280 (2)** 1376 - 1383

Lith, M.V., Tiwari, S., Pediani, J., Milligan, G. And Bulleid, N.J. (2011) Real-time monitoring of redox changes in the mammalian endoplasmic reticulum. *Journal of Cell Science* **124** 2349 – 2356

Loewenthal, R., Sancho, J. and Fersht, A.R. (1992) Histidine-aromatic interactions in Barnase elevation of histidine pK_a and contribution to protein stability. *Journal of Molecular Biology* **224** 759 – 770

Lovat, P.E., Corazzari, M. and Armstrong, J.L. (2008) Increasing melanoma cell death using inhibitors of protein disulfide isomerases to abrogate survival responses to endoplasmic reticulum stress. *Cancer Research* DOI:10.1158/0008-5472.CAN-08-0035

Ludström, J. and Holgren, A. (1990) Protein-disulphide isomerase is a substrate for thioredoxin reductase and has thioredoxin-like activity. *The Journal of Biological Chemistry* **265 (16)** 9114 – 9120

Lumb, R.A. and Bulleid, N.J. (2002) Is protein disulfide isomerase a redox-dependent molecular chaperone? *The EMBO Journal* **21 (24)** 6763 - 6770

Lundström, J., Krause, G. and Holmgren, A., (1992) A Pro to His mutation in active site of Thioredoxin increases its disulfide-isomerase activity 10-fold. *The Journal of Biological Chemistry* **267 (13)** 9047 – 9052

Lyles, M.M. and Gilbert, H.F. (1994) Mutations in the thioredoxin sites of protein disulphide isomerases reveal functional non-equivalence of the N- and C-terminal domains. *The Journal of Biological Chemistry* **269 (49)** 30946 – 30952

Ma, Y. and Hendershot, L. (2004) The role of the unfolded protein response in tumour development: friend or foe? *Nature Reviews Cancer* **4** 966 – 977

Maeda, R., Ado, K., Takeda, N. and Taniguchi, Y. (2007) Promotion of insulin aggregation by protein disulphide isomerase. *Biochemica et Biophysica Acta* **1774** 1619 – 1627

Margittai, E. and Banhegyi, G. (2010) Oxidative folding in the endoplasmic reticulum: towards a multiple oxidant hypothesis? *FEBS Letters* **584** 2995 – 2998

Margittai, E., Low, P., Stiller, I., Greco, A., Garcia-Manteiga, J., Pengo, N., Benedetti, A., Sitia, R. and Banhegyi, G. (2012) Production of H_2O_2 in the endoplasmic reticulum promotes *In vivo* disulfide bond formation. *Antioxidants & Redox Signalling* **16 (10)** 1088 - 1099

Matulis, D., Baumann, C.G., Bloomfield, V.A. and Lovrien, R.E. (1998) 1-anilino-8-naphthalene sulfonate as a protein conformational tightening agent. *Biopolymers* **49** 451 – 458

Mavridou, D.A.I., Stevens, J.M., Ferguson, S.J. and Redfield, C. (2007) Active-site properties of the oxidized and reduced C-terminal domain of DsbD obtained by NMR spectroscopy. *Journal of Molecular Biology* **370** 643 – 658

Mayer, M., Reinstein, J. and Buchner, J., (2003) Modulations of the ATPase cycle of BiP by peptides and proteins. *Journal of Molecular Biology* **330** 137 – 144

Mehnert, M., Sommer, T. and Jarosch, E. (2010) ERAD ubiquitin ligases. *Bioessays* **32** 905 – 913

Merulla, J., Fasana, E., Soldà, T. and Molinari, M. (2013) Specificity and regulation of the endplasmic reticulum-associated degradation machinery. *Traffic* **14** 767 – 777

Meusser, B., Hirsch, C., Jarosch, E. and Sommer, T. (2005) ERAD: the long road to destruction. *Nature Cell Biology* **7 (8)** 766 – 772

Nakamura, T. and Lipton, S. (2009) Cell death: protein misfolding and neurodegenerative diseases. *Apoptosis* **14 (4)** 455- 468

Nakamura, T. and Lipton, S. (2010) Preventing Ca^{2+} mediated nitrosative stress in neurodegenerative diseases: possible pharmacological strategies. *Cell Calcium* **47 (2)** 190 -197

Nakasako, M., Maeno, A., Kurimoto, E., Harada, T., Yamaguchi, Y., Oka, T., Takayama, Y., Iwata, A. and Kato, K. (2010) Redox-dependent domain

rearrangement of protein disulphide isomerase from a thermophillic fungus. *Biochemistry* **49** 6953 – 6962

Nardo, G., Pozzi, S., Pignataro, M., Lauranzano, E., Spano, G., Garbelli, S., Mantovani, S., Marinou, K., Papetti, L., Monteforte, M., Torri, V., Paris, L., Bazzoni, G., Lunetta, C., Corbo, M., Mora, G., Bendotti, C and Bonetto, V. (2011) Amylotrophic lateral sclerosis multiprotein markers in peripheral blood mononuclear cells. *PLoS One* **6 (10)** e25545

Nguyen, V.D., Saaranen, M.J., Karala, A., Lappi, A., Wang, L., Raykhel, I.B., Alanen, H. I., Salo, K.E.H., Wang, C. And Ruddock, L.W. (2011) Two endoplasmic reticulum PDI peroxidises increase the efficiency of the use of peroxide during disulfide bond formation. *Journal of Molecular Biology* **406 (3)** 503 – 515

Nguyen, V.D., Wallis, K., Howard, M.J., Haapalainen, A.M., Salo, K.E.H., Saaranen, M.J., Sidhu, A., Wierenga, R.K., Freedman, R.B., Ruddock, L.W. and Williamson, R.A. (2008) Alternative conformations of the x region of human protein disulphide-isomerase modulate exposure of the substrate binding b' domain. *Journal of Molecular Biology* **383** 1144 – 1155

Niki, S., Oshikawa, K., Mouri, Y., Hirota, F., Matsushima, A., Yano, M., Han, H., Bando, Y., Izumi, K., Matsumoto, M., Nakayama, K.I., Kuroda, N. and Matsumoto, M. (2006) Alteration of intra-pancreatic target-organ specificity by abrogation of Aire in NOD mice. *The Journal of Clinical Investigation* **116 (5)** 1292 – 1301

Novoa, I., Zeng, H., Harding, H.P. and Ron, D. (2001) Feedback inhibition of the unfolded protein response by GADD34-mediated dephosphorylation of eIF2α. *The Journal of Cell Biology* **153 (5)** 1011 – 1021

Novy, R., Drott, D. Yaeger, K. and Mierendorf, R. (2001) Overcoming the codon bias of *E.coli* for enhanced expression. *InNOVAtions* **12** 1 – 3

Odenlund, M., Ekblad, E. and Nilsson, B. (2008) Stimulation of oestrogen receptor-expressing endothelial cells with oestrogen reduces proliferation of co-cultured vascular smooth muscle cells. *Clinical and Experimental Pharmacology and Physiology* **35** 245 -248

Ohsugi, M., Cras-Méneur, C., Zhou, Y., Bernal-Mizrachi, E., Johnson, J.D., Luciani, D.S., Polonsky, K.S. and Permutt, M.A. (2005) Reduced expression of the insulin receptor in Mouse Insulinoma (MIN6) cells reveals multiple roles of insulin signalling in gene expression, proliferation, insulin content and secretion. *The Journal of Biological Chemistry* **280 (6)** 4992 – 5003

Oka, O.B.V. and Bulleid, N.J. (2013) Forming disulfides in the endoplasmic reticulum. *Biochemica et Biophysica Acta* doi: 1016/j.bbamcr.2013.02.007

Okumura, K., Miyake, Y., Taguchi, H. and Shimabayashi Y. (1992) Estimation of protein disulphide-isomerase activity based on protein refolding. *Bulletin of the Faculty of Bioresources: Mie University* **8** 59 – 63

Oliver, J.D., Roderick, H.L., Llwellyn, D.H. and High, S. (1999) ERp57 functions as a subunit of specific complexes formed with the ER lectins calreticulin and calnexin. *Molecular Biology of the Cell* **10** 2573 – 2582

Oommen, A.M., Narayanan, U. and Jagannath, M.R. (2012) An intergrative network biology approach to evaluate the role of endoplasmic reticulum stress response in obese type 2 diabetes. *Cell Biology* doi: 10.5402/2012/278636

Pagani, M., Fabbri, M., Benedetti, C., Fassio, A., Pilati, S., Bulleid, N.J., Cabibbo, A. and Sitia, R. (2000) Endoplasmic reticulum oxidoreductin 1-L β (ERO1-Lβ), a human gene induced in the course of the unfolded protein response. *The Journal of Biological Chemistry* **275 (31)** 23685 – 23692

Pihlajaniemi, T., Helaakoski, T, Tasanen, K., Myllya, R., Huhtala, M., Koivu, J. and Kivirikko, K.I. (1987) Molecular cloning of the β-subunit of human prolyl 4-hydroxylase. This subunit and protein disulphide isomerase are products of the same gene. *The EMBO Journal* **6 (3)** 643 - 649

Pirneskoski, A., Klappa, P., Lobell, M., Williamson, R.A., Byrne, L., Alanen, H.I., Salo, K.E.H., Kivirikko, K.I., Freedman, R.B. and Ruddock, L.W. (2004) Molecular characterisation of the principal substrate binding site of the ubiquitous folding catalyst protein disulphide isomerase. *The Journal of Biological Chemistry* **279 (11)** 10374 – 10381

Primm, T.P. and Gilbert, H.F. (2001) Hormone binding by protein disulfide isomerase, a high capacity hormone reservoir of the endoplasmic reticulum. *The Journal of Biological Chemistry* **276 (1)** 281 - 286

Ramming, T. and Appenzellor-Herzog, A. (2012) The physiological functions of mammalian endoplasmic oxidoreductin 1: on disulfides and more. *Antioxidants & Redox Signalling* **16 (10)** 1109 - 1118

Raturi, A. and Mutus, B. (2007) Characterization of redox state and reductase activity of protein disulfide isomerase under different redox environments using a sensitive fluorescent assay. *Free Radical Biology & Medicine* **43** 62 – 70

Raturi, A., Vacratsis, P.O., Seslija, D, Lee, L. and Mutus, B. (2005) A direct, continuous, sensitive assay for protein disulphide-isomerase based on fluorescence self-quenching. *Biochemical Journal* **391** 351 – 357

Ritz, D. and Beckwith, J. (2001) Roles of thiol-redox pathways in bacteria. *Annual Review of Microbiology* **55** 21 – 48

Roos, G., Foloppe, N. and Messens, J. (2013) Understanding the pK_a of redox cysteines: the key role of hydrogen bonding. *Antioxidants & Redox Signalling* **18 (1)** 94 – 127

Ruddock, L.W. (2012) Low molecular-weight oxidants involved in disulfide bond formation. *Antioxidants & Redox Signalling* **16 (10)** 1129 - 1138

Ruddock, L.W., Freedman, R.B. and Klappa, P. (2000) Specificity in substrate binding by protein folding catalysts: tyrosine and tryptophan residues are the recognition motifs for the binding of peptides to the pamcreas-specific protein disulfide isomerase PDIp. *Protein Science* **9** 758 – 764

Rutkevich, L.A., Cohen-Doyle, M.F., Brockmeier, U and Williams, D.B. (2010) Functional relationship beween protein disulphide isomerase family members during the oxidative folding of human secretory proteins. *Molecular Biology of the Cell* **21** 3093 – 3105

Samanta, U., Pal, D. and Chakrabatti, P. (1999) Packing of aromatic rings against tryptophan residues in proteins. *Acta Crystallographica* **D55** 1421 - 1427

Santanam, N., Shern-Brewer, R., McClatchey, R., Castellano, P.Z., Murphy, A.A., Voelkel, S. and Parthasarathy, S. (1998) Estradiol as an antioxidant: incompatible with its physiological concentrations and function. *Journal of Lipid Research* **39** 2111 – 2118

Satoh, M., Shimada, A., Keino, H., Kashiwai, A., Nagai, N., Saga, S. and Hosokawa, M. (2005) Functional characterization of 3 thioredoxin homology domains of ERp72. *Cell Stress & Chaperones* **10 (4)** 278 – 284

Schroder, M. and Kaufmann, R.J. (2005) ER stress and the unfolded protein response. *Mutation Research* **569** 29 - 63

Serve, O., Kamiya, Y., Maeno, A., Nakano, M., Murakami, C., Sasakawa, H., Yamaguchi, Y., Harada, T., Kurimoto, E., Yagi-Utsumi, M., Iguchi, T., Inaba, K., Kikuchi, J., Asami, O., Kajino, T., Oka, T., Nakasako, M. and Kato, K. (2010) Redox-dependent domain rearrangement of protein disulfide isomerase coupled with exposure of its substrate-binding hydrophobic surface. *Journal of Molecular Biology* **396** 361 – 374

Sevastsyanovich, Y., Alfasi, S., Overton, T., Hall, R., Jones, J., Hewitt, C. and Cole, J. (2009) Exploitation of the GFP fusion proteins and stress avoidance as a generic strategy for the production of high-quality recombinant proteins. *FEMS Microbiology Letters* **299** 86 -94

Sevier, C. S. (2012) Erv2 and quiescin sulfhydryl oxidases: Erv-domain enzymes associated with the secretory pathway. *Antioxidants & Redox Signalling* **16 (8)** 800 - 808

Sharp, P.M. and Li, W. (1986) Codon useage in regulatory genes in *Escherichia coli* does not reflect selection for 'rare' codons. *Nucleic Acids Research* **14 (19)** 7737 – 7749

Shen, J., Person, M.D., Zhu, J., Abbruzzese, J.L. and Li, D. (2004) Protein expression profiles in pancreatic adenocarcinoma compared with normal pancreatic tissue and tissue affected by pancreatitis as detected by two-dimensional gel electrophoresis and mass spectroscopy. *Cancer Research* **64** 9018 – 9026

Sogame, A., Hayata, T. and Asashima, M. (2003) Screening for novel pancreatic genes from *in vitro*-induced pancreas in Xenopus. *Development, Growth and Differentiation* **45** 143 – 152

Soldà, T., Garbi, N., Hämmerling, J.G. and Molinari, M. (2006) Consequences of ERp57 deletion on oxidative folding of obligate and facultative clients of the calnexin cycle. *Journal of Biological Chemistry* **281** 6219 – 6226

Stryer, L. (1965) The interaction of naphthalene dye with apomyoglobin and apohemoglobin a fluorescent probe of non-polar binding sites. *Journal of Molecular Biology* **13** 482 - 495

Sun, X., Dai, Y., Liu, H, Chen, S. and Wang, C. (2000) Contributions of protein disulphide isomerase domains to its chaperone activity. *Biochemica et Biophysica Acta* **1481** 45 – 54

Tasanen, K., Parkkonen, T., Chow, L.T., Kivirikko, K.I. and Pihlajaniemi, T. (1988) Characterization of the human gene for a polypeptide that acts both as the β-subunit of prolyl 4-hydroxylase and as protein disulfide isomerase. *The Journal of Biological Chemistry* **263 (31)** 16218 – 16224

Tavender, T.J., Springate, J.J. and Bulleid, N.J. (2010) Recycling of peroxiredoxin VI provides a novel pathway for disulphide formation in the endoplasmic reticulum. *The EMBO Journal* **29** 4185 – 4197

Taylor, M., Banerjee, T., Ray, S., Tatulian, S.A. and Teter, K. (2011) Protein-disulfide isomerase displaces the cholera toxin A1 subunit from the holotoxin without unfolding the A1 subunit. *The Journal of Biological Chemistry* **286 (25)** 22090 - 22100

Thiede, B., Hohenwarter, W., Krah, A., Mattow, J., Schmid, M., Schmidt, F. and Jungblut, P.R. (2005) Peptide mass fingerprinting. *Methods* **35** 237 - 247

Tian, G., Kober, F., Lewandrowski, U., Sickmann, A., Lennarz, W.J. and Schindlin, H. (2008) The catalytic activity of protein disulphide isomerase requires a conformationally flexible molecule. The *Journal of Biological Chemistry* **283(48)** 33630 – 33640

Tian, G., Xiang, S., Noiva, R., Lennarz, W.J. and Schindelin, H. (2006) The crystal structure of yeast protein disulphide isomerase suggests cooperativity between its active sites. *Cell* **124** 61 – 73

Tian, R., Li, S., Wang, D., Zhao, Z., Lin, Y. and He, R. (2004) The acidic C-terminal domain stabilizes the chaperone function of protein disulfide isomerase. *The Journal of Biological Chemistry* **279** 48830 – 48835

Tokuhiro, K., Ikawa, M., Benham, A.M. and Okabe, M. (2011) Protein disulfide isomerase homolog PDILT is required for quality control of sperm membrane protein ADAM3 and male fertility. *PNAS* **109 (10)** 3850 – 3855

Tsai, B, Rodighiero, C., Lencer, W.I. and Rappoport, T. (2001) Protein disulfide isomerase acts as a redox-dependent chaperone to unfold cholera toxin. *Cell* **104** 937 - 948

Tsai, B. and Rappoport, T. (2002) Unfolded cholera toxin is transferred to the ER membrane and released from protein disulfide isomerase upon oxidation by Ero1. *The Journal of Cell Biology* **159 (2)** 207 - 215

Tsai, Y. and Weissman, A.M. (2011) Ubiquitylation in ERAD: Reversing to go forward? *PLoS Biology* **9 (3)** 1 – 5

Tsibris, J.C.M., Hunt, L.T., Ballejo, G., Barker, W.C., Toney, L.J. and Spellacy, W.N. (1989) Selective inhibition of protein disulfide isomerase by estrogens. *The Journal of Biological Chemistry* **264 (24)** 13967 – 13970

Turano, C., Coppari, S., Altieri, F. and Ferraro, A. (2002) Proteins of the PDI family: unpredicted non-ER locations and functions. *Journal of Cellular Physiology* **193** 154 – 163

Urano, F., Wang, X., Bertolotti, A., Zhang, Y., Chung, P., Harding, H.P. and Ron, D. (2000) Coupling of stress in the ER to activation of JNK protein kinases by transmembrane protein kinase IRE1. *Science* **287** 664 – 666

Vembar, S.S. and Brodsky, J.L. (2008) One step at a time: endoplasmic reticulum-associated degradation. *Nature Reviews: Molecular Cell Biology* **9** 944 – 957

Vivian, J.T. and Callis, P.R. (2001) Mechanisms of tryptophan fluorescence shifts in proteins. *Biophysical Journal* **80** 2093 – 2109

Volkmer, J., Guth, S., Nastainczyk, W., Knippel, P., Klappa, P, Gnau, V. and Zimmermann, R. (1997) Pancreas specific protein disulphide isomerase, PDIp, is in transient contact with secretory proteins during late stages translocation. *FEBS Letters* **406** 291 – 295

Walczak, C.P., Bernardi, K.M. and Tsai, T. (2012) Endoplasmic reticulum-dependent redox reactions control endoplasmic reticulum-associated degradation and pathogen entry. *Antioxidants & Redox Signalling* **16 (8)** 809 - 818

Walker, A.K. (2010) Protein disulfide isomerase and the endoplasmic reticulum in amyotrophic lateral sclerosis. *The Journal of Neuroscience* **30 (11)** 3865 – 3867

Walker, A.K., Farg, M.A., Bye, C.R., McLean, C.A., Horner, M.K. and Atkin, J.D. (2010) Protein disulphide isomerase protects against protein aggregation and is S-nitrosylated in amyotrophic lateral sclerosis. *Brain* **133** 105 – 116

Walker, A.K., Soo, K.Y., Levina, V., Talbo, G.H. and Atkin, J.D. (2013) N-linked glycosylation modulates dimerization of protein disulfide isomerase A member 2 (PDIA2). *The FEBS Journal* **280** 233 – 243

Wallis, A.K., Sidhu, A., Byrne, L.J., Howard, M.J., Ruddock, L.W., Williamson, R.A. and Freedman, R.B. (2009) The ligand-binding **b'** domain of human protein disulphide-isomerase mediates homodimerization. *Protein Science* **18** 2569 – 2577

Wang, C., Chen, S., Wang, X., Wang, L., Wallis, A.K. and Freedman, R.B. (2010) Plasticity of human protein disulfide isomerase. Evidence for mobility around the x-linker region and its functional significance. *The Journal of Biological Chemistry.* **285 (35)** 26788 – 26797

Wang, C., Li, W., Ren, J., Fang, J., Ke, H., Gong, W., Feng, W. and Wang, C. (2012) Structural insights into the redox-regulated dynamic conformations of human protein disulfide isomerase. *Antioxidants & Redox Signalling* DOI: 10.1089/ars.2012.4630

Wang, C., Yu, J., Huo, L., Wang, L., Feng, W., and Wang, C. (2011) Human protein disulfide isomerase is a redox-regulated chaperone activated by oxidation of domain a'. *Journal of Biological Chemistry* **287** 1139 - 1149

Wang, L., Li, S., Sidhu, A., Zhu, L., Liang, Y., Freedman, R.B. and Wang, C. (2009) Reconstitution of human Ero1-Lα/ protein-disulfide isomerase oxidative folding pathway *in vitro*: position dependent differences in role between the a and a' domains of protein-disulfide isomerase. *The Journal of Biological Chemistry* **284 (1)** 199 - 206

Wang, L., Wang, L., Vavassori, S., Li, S., Ke, H., Anelli, T., Degano, M., Ronzoni, R., Sitia, R., Sun, F. and Wang, C. (2008) Crystal structure of human ERp44 shows a dynamic functional modulation by its carboxy-terminal tail. *EMBO Reports* **9 (7)** 642 - 647

Wang, L., Zhu, L. and Wang, C. (2011) The endoplasmic reticulum sulfhydryl oxidase Ero1β drives efficient oxidative protein folding with loose regulation. *Biochemical Journal* **434** 113 – 121

Wang, T. and Hebert, D.N. (2003) EDEM an ER control receptor. *Nature Structural Biology* **10 (5)** 319 – 321

Westphal, V., Darby, N.J. and Winther, J.R. (1999) Functional properties of the Two redox-active sites in Yeast Protein Disulphide Isomerase *in vitro* and *in vivo. Journal of Molecular Biology* **286** 1229 – 1239

Wilkinson, B. and Gilbert, H.F. (2004) Protein disulfide isomerase. *Biochemica et Biophysica Acta* **1699** 34 -44

Winter, J., Gleiter, S., Klappa, P. and Lilie, H. (2011) Protein disulphide isomerase (PDI) isomerizes non-native disulphide bonds in human proinsulin independent of its peptide binding activity. *Protein Science* **20 (3)** 588 -596

Woehlbier, U. and Hetz, C. (2011) Modulating stress responses by the UPRosome: a matter of life and death. *Trends in Biochemical Sciences* **36 (6)** 329 – 337

Woycechowsky, K.J. and Raines, R.T. (2003) CXC motif: a functional mimic of protein disulfide isomerase. *Biochemistry* **42 (18)** doi:10.1021/bi026993q

Yao, Y., Zhou, Y. and Wang, C. (1997) Both the isomerase and chaperone activities of protein disulphide isomerase are required for the reactivation of reduced and denatured acidic phospholipase A_2. *The EMBO journal* **16 (3)** 651 – 658

Yoshida, H. (2006) ER stress and disease. *The FEBS Journal* **274** 630 – 658

Zito, E. (2012) PRDX4, an ER-localised peroxiredoxin at the crossroads between enzymatic oxidative protein folding and non-enzymatic protein oxidation and non-enzymatic protein oxidation. *Antioxidants & Redox Signalling* doi: 10.1089/ars.2012.4966

Zito, E., Melo, E.P., Yang, Y., Wahlander, A, Neubert, T.A. and Ron, D. (2010) Oxidative protein folding by an endoplasmic reticulum-localized peroxiredoxin. *Molecular Cell* **40** 787 – 797